ACOUSTIC THERMOMETRY IN THE RANGE 2 - 20 K.

A thesis submitted for the degree of

Doctor of Philosophy.

by

A. R. Colclough B. Sc.

Imperial College of Science and Technology
The University of London
March 1972

ABSTRACT

The reader is referred to the list of contents for a detailed abstract of this thesis. Following the introductory first chapter, Chapters II, III and IV contain a detailed analysis of the systematic errors in high and low frequency acoustic thermometry. By "high" and "low" frequency thermometry we mean thermometry where the operating frequencies are respectively above (usually far above) and below the lowest characteristic cut off frequency of the resonant cavity used to measure the velocity of sound. A case is developed for using the low frequency approach although in the past it has led to apparently inferior results. Attention is drawn, in particular, to Sections 2.2.3 and 2.3 where two important difficulties for the high frequency approach are discussed. In the former section it is shown that it is impossible to tell from the positions of the observed cavity resonances whether or not there are errors in the measured velocity due to the presence of unresolved high order resonances (although as is shown in the following section these are likely to be small in the work done hitherto). In Section 2.3 an account of the errors to be expected from bad cavity geometry is given. This applies only to low frequency devices, the extension of the analysis to higher frequencies being very difficult. Thus, at the moment, there also remains an unanalysed source of error in the high frequency technique.

Neither of these two problems arise at low frequencies where the predominant systematic error is due to the acoustic boundary layer. The theoretical corrections for this effect are discussed at length in Chapter III where it is also argued that past criticisms of the theory are in error. It is, in any case, possible to measure the boundary layer corrections relying only on a restricted set of theoretical assumptions.

Chapters IV, V and VI discuss in detail the design, testing and use of such a low frequency acoustic thermometer. Measurements have shown that the systematic errors characteristic of this technique function exactly as expected and it has been used to measure the normal boiling points of helium-4 and equilibrium hydrogen and the triple point of equilibrium hydrogen.

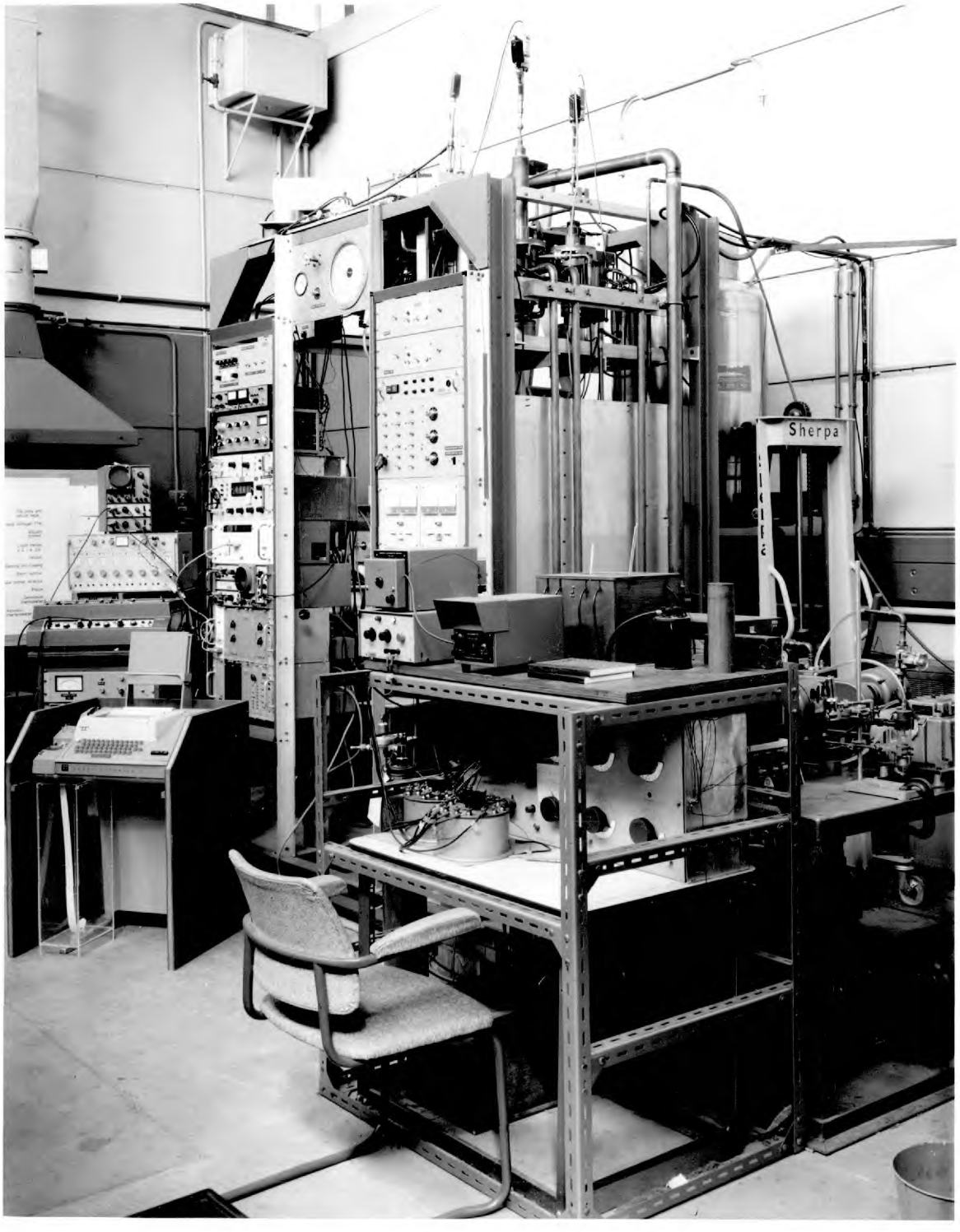

The NPL's Acoustic Thermometer.

CONTENTS

ABSTRACT 2

FRONTISPIECE 3

CHAPTER I INTRODUCTION. 6

1.1 Primary and Secondary Thermometry in the Range 2-20K. 7
1.2 The Velocity of Sound as a Function of Thermodynamic Temperature. 13
1.3 The Velocity of Sound and the Virial Coefficients of the Equation of State for a Real Gas. 19
1.4 The Velocity of Sound and the Principal Specific Heats of a Real Gas. 23
1.5 Existing Acoustic Thermometry. 25

CHAPTER II THE THEORY OF THE ACOUSTIC INTERFEROMETER WITH IDEAL BOUNDARY CONDITIONS. 28

2.1 The Ideal Interferometer. 29
2.2 The Effect of Practical Transducers. 43
2.2.1 The Form of the Normal Modes. 43
2.2.2 The General Solution and the Amplitudes of the Normal Modes. 51
2.2.3 Velocity Errors Due to Higher Modes. 55
2.2.4 Some Practical Cases. 65
2.3 The Effect of Geometrical Misalignment of the Cavity End Faces. 74
2.3.1 Bad Geometry and Velocity Errors. 74
2.3.2 Tilted End Faces. 79
2.3.3 The Flatness of the End Faces. 81

CHAPTER III THE PROBLEM OF THE BOUNDARY LAYER. 83

3.1 The Theory of the Boundary Layer. 83
3.1.1 Towards a Simple Statement of the Problem. 86
3.1.2 The Existence of an Acoustic Boundary Layer and its Properties. 94
3.1.3 Boundary Layer Corrections Associated with the Radial Boundary Condition. 99
3.1.4 The Boundary Layer Correction for the End Faces of an Interferometer. 110
3.2 Objections to the Boundary Layer Corrections. 114

CHAPTER IV PRACTICAL DESIGN CONSIDERATIONS FOR AN ACOUSTIC THERMOMETER. 119

4.1 High Frequencies vs. Low Frequencies. 120
4.2 Variable Path vs. Variable Frequency Interferometry. 130
4.3 The Excitation of the Cavity and the Detection of Resonance. 133
4.4 Some Remaining Systematic Errors of Acoustic Origin. 141
4.4.1 The Effect of Finite Sound Amplitudes. 141
4.4.2 The Effect of Frequency Dispersion. 142
4.4.3 Approximations in the Radial Boundary Conditions. 143
4.4.4 Parametric Oscillation. 145

CHAPTER V THE PRACTICAL INSTRUMENT AND TESTS ON THE SYSTEM. 146

5.1 The Acoustic Interferometer. 146
5.1.1 The Cavity, its Dimensions and Alignment. 149
5.1.2 The Transducer and the Accelerometer. 153
5.1.3 The Optical Interferometer. 155
5.2 Control and Measurement of Temperature and Pressure. 159
5.2.1 The Cryostat. 159
5.2.2 Temperature Measurement and Control. 165
5.2.3 Pressure Measurement and Control. 167
5.3 The Modus Operandi and Tests on the System. 169
5.3.1 The Measurement of Velocity. 169
5.3.2 Tests on the Accelerometer. 173
5.3.3 Tests on the Boundary Layer Corrections. 182
5.3.4 Tests on the Measured Diameters of the Impedance Circles. 195
5.3.5 Testing the Coupling of the Transducer to the Cavity. 198

CHAPTER VI EXPERIMENTAL RESULTS. 201

6.1 The Normal Boiling Point of Helium-4. 201
6.1.1 Reproduction of the Isotherm Temperature. 203
6.1.2 The Boundary Layer Corrections at the NBP of Helium-4. 207
6.1.3 The Isotherm at the NBP of Helium-4. 209
6.2 The Triple Point of Hydrogen. 215
6.2.1 Reproduction of the Isotherm Temperature. 215
6.2.2 The Boundary Layer Corrections at the Triple Point of Hydrogen. 217
6.2.3 The Isotherm at the Triple Point of Hydrogen. 217
6.3 The Normal Boiling Point of Equilibrium Hydrogen. 221
6.3.1 Reproduction of the Isotherm Temperature. 223
6.3.2 The Boundary Layer Corrections at the NBP of Equilibrium Hydrogen. 223
6.3.3 The Isotherm at the NBP of Equilibrium Hydrogen. 225
6.4 The Second Virial Coefficient. 228
6.5 The Principal Specific Heats of Helium-4 and their Ratio. 231
6.6 Conclusions 232

APPENDIX 1.1 238
APPENDIX 1.2 240
APPENDIX 1.3 241
APPENDIX 1.4 245
APPENDIX 2.1 246
APPENDIX 2.2 248

REFERENCES 256

SUPPLEMENTARY MATERIAL I 259
Report of Preliminary Work to the 9th Meeting of the CCT, Paris (1971). Also submitted to the 5th Symposium on Temperature Measurement, Washington D.C., U.S.A. (1971).
SUPPLEMENTARY MATERIAL II 277
"Higher Modes in Acoustic Interferometry" (1970).

ACKNOWLEDGEMENTS 285

NOTATIONAL GLOSSARY 286

CHAPTER I

INTRODUCTION

In 1967 the National Physical Laboratory (NPL) instigated an investigation into the possibilities and limitations of measuring true thermodynamic temperatures in the range 2-20K by means of acoustic thermometry. As a result of this study a low frequency variable-path acoustic thermometer was designed and constructed which appears to have met the requirements of a primary thermometer with some measure of success. The burden of this thesis is to review the various sources of systematic error in this and other comparable acoustic techniques of primary thermometry, and to report the results of an experimental investigation of the practical instrument. By way of an introduction to the subject the relation between primary and secondary thermometry in the range of interest will be discussed, followed by an account of the dependence of various thermodynamic parameters - in particular the thermodynanic temperature - on the velocity of sound. It will be understood throughout that the thermometric medium under discussion is always helium-4 gas. Nothing else apart from the lighter isotope of helium, helium-3, remains uncondensed over the whole range. Earlier acoustic thermometry is also discussed.

1.1 Primary and Secondary Thermometry in the Range 2-20K.

Since the conception of this project the relationship between primary and secondary thermometry from 2 to 20K has changed somewhat. It was not until 1968 that the definition of the International Practical Temperature Scale (IPTS) was extended down to cover part of this range. The previous version of this scale, IPTS-48, defined by the Comite Consultatif de Thermometrie (CCT) of the Comite Internationale des Poids et Mesures (CIPM) in 1948, [1] terminated at the normal boiling point of liquid oxygen (then assigned a value of 90.18K). This was superceded by IPTS-68 [2,3,4] whose lowest point is the triple point of equilibrium hydrogen to which the value 13.81K is assigned. The extension of the IPTS below 90K enabled the confused situation which existed previously to be rationalised. It used to be the case that a large number of secondary practical temperature scales carried on platinum resistance thermometers were in use. [5] These scales were defined mainly by the various national standards laboratories of the world and were related to their own gas thermometry. Published comparisons of the scales enabled temperature measurements (and other measurements based on temperature measurements) to be reinterpreted in terms of the scale to which any individual worker happened to be committed. Now any new work in this range may simply be referred to IPTS-68 as may any previous work through published comparisons of IPTS-68 with the old scales.

The extent to which the old scales disagreed can be seen clearly from figure 1.1 which is taken from reference 5. At the triple point of equilibrium hydrogen PRMI-54 (defined by the Physicotechnical and Radiotechnical Measurements Institute of the USSR in 1954) differed by as much as 57mK from PSU-54 (Pennsylvania State University - 1954). The other two scales represented in figure 1.1 are those of the National Physical Laboratory, NPL-61, and of the National Bureau of

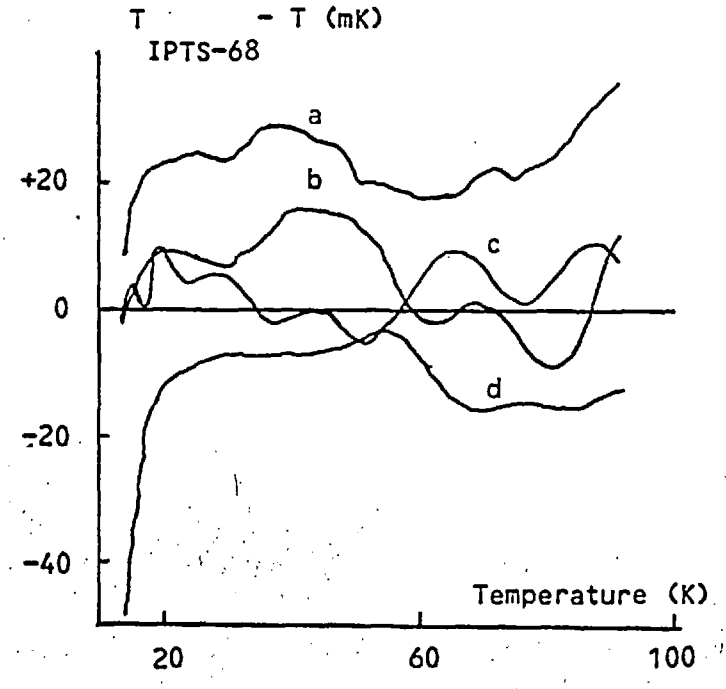

FIGURE 1.1

The Differences between some of the More Common Platinum Resistance Thermometer Scales and IPTS-68.

(a) PSU-54
(b) NBS-55
(c) NPL-61
(d) PRMI-54

Standards (USA), NBS-55.

The IPTS-68 is defined by assigning carefully chosen values of thermodynamic temperature to the various reproducible fixed points in the range of interest (see Table 1.1). A convention is then stated for interpolation using the specified interpolation device calibrated at the fixed points so that any intermediate temperature may be measured. From 13.81K up to 903.90K the interpolation instrument is the platinum resistance thermometer. It is the loss of sensitivity of pure platinum which limits its use as a thermometric element below about 14K. In this region its residual resistance (largely attributable to impurities and lattice imperfections) begins to mask the thermal resistance arising from the scattering of electrons by phonons. Thus, in the absence of a new interpolating instrument, the IPTS-68 cannot be extended far below the triple point of hydrogen.

However, the CCT of the CIPM has recommended the use of practical helium vapour pressure scales between 0.2 and 5.2K. The helium-4 vapour pressure scale of 1958, T-58, is defined by a set of published tables relating saturated vapour pressure to temperature from 0.5 to 5.2K. [6,7] These values are derived from the integrated Clausius-Clapeyron equation for a first order phase change. Since the thermodynamic temperature appears in this equation it might be asked why it should not form the basis for a primary thermometer - an exceptionally simple one to use by the standards of other primary thermometers. Unfortunately the basic relationship involves certain temperature-dependent thermodynamic quantities such as the latent heat of evaporation and the molar volumes of the two phases present at any given temperature. The determination of these will therefore presuppose some independently defined temperature scale. In fact the CCT evaluated them on the basis of several sets of gas thermometry measurements. A similar secondary vapour pressure scale, T-62, was

TABLE 1.1

Fixed Points in the Range 2-20K.

Practical Scale	Status of Point	Assigned Temperature (K)	Fixed Point
IPTS-68	Secondary	20.397	n.b.p. of normal hydrogen.
IPTS-68	Primary	20.28	n.b.p. of equilibrium hydrogen.
IPTS-68	Primary	17.042	b.p. of equilibrium hydrogen at 33 330.6 N/m^2.
IPTS-68	Secondary	13.956	triple point of normal hydrogen.
IPTS-68	Primary	13.81	triple point of equilibrium hydrogen.
T-58 and T-62	Tabulated Value	4.215	n.b.p. of helium-4.
T-58 and T-62	Tabulated Value	3.190	n.b.p. of helium-3.

Primary fixed points are the defining fixed points of IPTS-68. Secondary fixed points are additional fixed points whose temperatures are given on IPTS-68 as defined by the primary points. Thus the secondary temperatures are ultimately traceable to the temperatures assigned to the primary points rather than to direct thermodynamic measurements.

The n.b.ps. of the two isotopes of helium are not properly called fixed points of the scales T-58 and T-62 since they are tabulated values of equal status to any other value in the tables. However they are widely used as fixed points in the calibration of many simple secondary thermometers such as carbon resistors or thermocouples. The values assigned are usually those shown.

defined in 1962 relating temperature to the vapour pressure of helium-3. [8,9] The upper limits of T-58 and T-62 are set by the critical temperatures of the two isotopes of helium and the lower by the diminution of their vapour pressures. These three secondary scales, IPTS-68, T-58 and T-62, still leave a gap from 5.22K up to 13.81K in the present range of interest for which no established secondary practical scale exists. At the moment workers may use various thermocouples relying on such information as is available for their calibration or calibrate them themselves at several fixed points. Some electronic circuit devices have also been used as temperature sensors with varying degrees of success. [10,11] However, none of these methods can easily offer the precision, thermodynamic accuracy and, in particular, the reproducibility of the three approved secondary scales. They do, on the other hand, have the advantage of simplicity which is always important in secondary practical thermometry. Fortunately, for more demanding requirements, there remains the doped germanium (or, occasionally, silicon) resistance thermometer. [10] Over the last ten years this has been developed to the point where its reproducibility on thermal cycling is good enough for it to function as the calibrated carrier of a primary scale. Its range and sensitivity are widely controllable through adjustment of the doping impurities. But, unlike the platinum resistance thermometer or the first order phase transition of a pure substance, there is no sufficiently accurate theoretical description of its resistance-temperature dependence to enable it to function as a conventional secondary thermometer. Instead of determining a few constants in a simple theoretical relationship, it is necessary to calibrate it against a primary thermometer at many points over its whole range (typically twenty points between 2 and 20K) and to fit, for example, a high order polynomial to the points for the purposes of

interpolation. [12]

It is clear, therefore, that primary thermometry plays a dual role in this region. It provides, as at higher temperatures, values of thermodynamic temperatures for the readily accessible fixed points of conventional convenient secondary thermometry. In addition, in the absence of a simple interpolating secondary device for part of the range, it provides direct closely spaced thermodynamic calibrations.

There also remains the possibility of using an instrument conventionally operated as a primary thermometer - that is an independent thermometer measuring accurate thermodynamic temperatures in the usual sense - as a secondary thermometer. It could be calibrated at one or more fixed points or it could be self-calibrating. Subsequently it could be used as an interpolating thermometer over the whole range of interest. Hitherto no acoustic thermometer has been used in this way, but it has become commonplace to calibrate a gas thermometer at a single or a few temperatures rather than to plot a full pressure-volume isotherm at any temperature to be measured. If such thermometers are self calibrating they still do not merit the title of primary in the strong sense, however, since they will not measure thermodynamic temperatures entirely independently. This arises because corrections for the non-ideality of the thermometric substance will generally be required from another instrument. For example virial coefficients will be needed for this type of gas or acoustic thermometry.

Mention should also be made of the unique status of magnetic thermometry in this range. Too complex a technique for general use as a secondary scale, it does however cover the whole range 2-20K (remaining useful down to much lower temperatures as well). And, like vapour pressure thermometry, it is based on a theoretical relationship, the Curie-Weiss law, in which the thermodynamic

temperature appears as a function of the magnetic susceptibility of a paramagnetic salt. But again, it is unsuitable for use as a primary thermometer since it depends on the independent evaluation of several (three or four) constants in the basic equation. Nevertheless, it has been found worthwhile to use magnetic thermometers in the past to check the internal consistency of the purportedly thermodynamic temperatures of other primary thermometers and of the three approved secondary scales. [13,14] They are also used at lower temperatures (as low as 0.006K using cerium magnesium nitrate as the thermometric salt) where the choice of thermometers, primary or secondary, is very narrow.

1.2 The Velocity of Sound as a Function of Thermodynamic Temperature.

For a wide range of frequencies the propagation of sound in a gas is almost perfectly adiabatic so that the velocity of sound, c, in the unbounded medium will be given by:

$$c^2 = B_s / \rho \qquad (1.2.1)$$

where B_s is the adiabatic bulk modulus of the gas and ρ is the density. Since

$$B_s \equiv -V\left(\frac{\partial P}{\partial V}\right)_S \qquad (1.2.2)$$

where P and V are the pressure and volume of the gas respectively, and since for n moles of gas

$$\rho = nM/V \qquad (1.2.3)$$

where M is its molecular weight, we obtain for an ideal gas

$$c^2 = \gamma RT/M \qquad (1.2.4)$$

Here γ is the ratio of the principal specific heats, C_p/C_v, R is the gas constant and T the thermodynamic temperature. Conversely

$$T = \frac{M}{\gamma R} c^2 \qquad (1.2.5)$$

thus enabling the thermodynamic temperature to be established in terms of the velocity of sound in an unbounded ideal gas. This is the basic principle of acoustic thermometry in gases.

The claim to measure true thermodynamic temperatures will stand or fall in the first place on the justification for our interpretation of T in this equation. We take as the fundamental definition of thermodynamic temperature that conventionally given in terms of ideal Carnot cycles in most formulations of thermodynamics. That the temperature appearing in the equation of state for an ideal gas (Boyle's law) is the same thermodynamic temperature of the fundamental

definition follows from an elementary theorem of thermodynamics. Thus, given the basic widely confirmed relation, 1.2.1, of fluid dynamics, we may interpret the variable, T, of equation 1.2.5 as the thermodynamic temperature with full confidence. The same interpretation holds even more directly for primary gas thermometry where Boyle's law is applied without the intermediation of equation 1.2.1.

As with primary gas thermometry, however, allowance must be made for the non-ideality of the gas available for use as a thermometric fluid. Expressing the square of the acoustic velocity as a virial expansion of pressure terms we obtain:

$$c^2 = A_0(T) + A_1(T)P + A_2(T)P^2 + \cdots \qquad (1.2.6)$$

where

$$A_0(T) = \frac{\sigma R}{M} T \qquad (1.2.7)$$

Equation 1.2.7 follows from the increasingly ideal behaviour of real gases at progressively lower pressures where equation 1.2.6 must ultimately conform with equation 1.2.4.

From equation 1.2.6 it can be seen that the value of A_0 (and so of the thermodynamic temperature) may be obtained by plotting isotherms of c^2 as a function of pressure and obtaining its value, c_0^2, at the intercept with the line P=0. At sufficiently low pressures when the

quadratic term of the virial expansion is negligible, the slope of the isotherm gives the second acoustic virial coefficient, A_1.

In principle a "density" expansion:

$$c^2 = A_0'(T) + A_1'(T)\left(\frac{n}{V}\right) + A_2'(T)\left(\frac{n}{V}\right)^2 + \cdots \qquad (1.2.8)$$

could be used instead of equation 1.2.6 and the corresponding isotherm plotted as a function of reciprocal molar volume. But in practice the pressure expansion is always used since molar volume is far harder to measure than pressure. In primary gas thermometry on the other hand, both expansions are found . But there the molar volume has to be determined in any case. It is the avoidance of this measurement with its necessity of estimating satisfactory dead-space and adsorption corrections which is deemed to be a major advantage of acoustic thermometry. However, it sometimes appears that these errors are not markedly more difficult to deal with than the systematic errors characteristic of the latter method which will be discussed at length in the following chapters.

In order to determine the thermodynamic temperature from an acoustic isotherm two procedures may be adopted. Firstly, and more simply, it may be calculated from equation 1.2.5 where the value, c_0, is substituted for c and accepted values for M and R are used, σ taking the exact theoretical value for an ideal gas (5/3 for monatomic helium-4). The constant of proportionality, $\sigma R/M$, between c^2 and T plays the same role as the constant nR in primary gas thermometry which relates the directly measured quantity PV to T. This quantity, nR, is usually evaluated experimentally by measuring pressure and

volume at the triple point of water where the thermodynamic temperature is defined to be 273.16K - a convention which determines the Kelvin. Thus there is an essential difference between primary gas and acoustic thermometry here. The former is unable to function without a calibration at the triple point of water. Knowledge of the gas constant is of no use in this respect since, to apply it, one needs to know how many moles of gas, n, one has in the thermometer. But to determine this requires either an application of Boyle's law at the triple point of water in any case, or an even more difficult measurement of the mass of the gas used. (*1) Acoustic thermometry, on the other hand, does not require this triple point calibration since it is independent of the amount of gas used. This is because the velocity of sound is an intensive thermodynamic quantity whereas PV is not since V is extensive (Cf respectively, the quantities α-RT/M and nRT).

However, this is not to say that an acoustic thermometer may not be directly calibrated at the triple point of water - this being the second operating procedure mentioned above. Since α and M are independently known to a high degree of accuracy this would in fact offer a new method of determining the gas constant. (*2) It may easily be shown that the fractional error in measured temperature, T, associated with an acoustic calibration error at the triple point of

---

(1) The combination of these two measurements enables the gas constant to be measured. It is, in fact, the basis of the conventional technique of limiting density (See, for example, T. Batuecas, Proc. Sec. Intl. Conf. on Nuclidic Masses, Vienna (1963), Ed. W. H. Johnson (Springer-Verlag, 1964))

(2) Such an acoustic determination of the gas constant is about to be undertaken at the NPL.

water is

$$\frac{\Delta T}{T} = \frac{\Delta T_c}{273.16} - 2\frac{\Delta c_c}{c_c} \qquad (1.2.9)$$

where the subscript, c, refers to the calibration values. ΔT_c may be expected to be less than .01K and $\Delta c_c / c_c$ one or two parts in 10^4. Thus the second term is the predominant one. The comparable error arising from using the existing value of the gas constant is a little less being equal to the fractional error in the gas constant itself since σ and M are known much more accurately. The standard error usually quoted for R is 45 parts in 10^6. Taking the previous figure of one or two parts in 10^4 to be three standard errors it can be seen that there is a marginal advantage (based only on rough figures) in using the existing value of R. This is further recommended by the experimental simplification brought about by adopting the orthodox value. In particular, operation of an acoustic thermometer at the triple point of water would entail rigorous precautions against gaseous impurities in the thermometric helium which are not necessary at very low temperatures.

1.3 The Velocity of Sound and the Virial Coefficients of the Equation of State for a Real Gas

The aforementioned virial expansions of gas thermometry are the pressure and density expansions of the product PV which form the most familiar alternative statements of the equation of state of a real gas:

$$PV = nRT\left\{1 + B(T)\left(\frac{n}{V}\right) + C(T)\left(\frac{n}{V}\right)^2 + \cdots\right\} \qquad (1.3.1)$$

and

$$PV = nRT\left\{1 + B'(T)P + C'(T)P^2 + \cdots\right\} \qquad (1.3.2)$$

The virial coefficients and the thermodynamic temperature may be obtained by plotting pressure-volume isotherms in the usual way and extrapolating to zero pressure or density. Values of virial coefficients obtained from the different expansions may be compared through the following relations:

$$B'(T) = B(T)/RT \qquad (1.3.3)$$

and

$$C'(T) = \left\{ C(T) - B^2(T) \right\} \Big/ R^2 T^2 \qquad (1.3.4)$$

(See Appendices 1.1 and 1.2 respectively).

Values of acoustic and pressure-volume virial coefficients may be compared as well:

$$A_1(T) = \frac{\sigma}{M} \left\{ 2B(T) + \frac{4}{3} \frac{dB(T)}{dT} + \frac{4}{15} T^2 \frac{d^2B(T)}{dT^2} \right\} \qquad (1.3.5)$$

and

$$A_2(T) = \frac{\sigma}{MRT} \left\{ \frac{13}{5} C(T) + \frac{16}{5} T \frac{dC(T)}{dT} + \frac{2}{15} T^2 \frac{d^2C(T)}{dT^2} + \frac{2}{5} B^2(T) + \frac{98}{45} T^2 \left(\frac{d^2B(T)}{dT^2} \right)^2 + \frac{8}{45} T^4 \left(\frac{d^2B(T)}{dT^2} \right)^2 + \frac{28}{15} TB(T) \frac{dB(T)}{dT} + \frac{8}{15} T^2 B(T) \left(\frac{d^2B(T)}{dT^2} \right) + \frac{56}{45} T^3 \left(\frac{dB(T)}{dT} \right) \left(\frac{d^2B(T)}{dT^2} \right) \right\} \qquad (1.3.6)$$

(See Appendices 1.3 and 1.4 respectively)

Since it is unnecessary for the purposes of primary thermometry - gas or acoustic - to work at pressures high enough for the third

virial term to become important, there is very little information on the form of $A_2(T)$ or $C(T)$. $B(T)$ on the other hand may be roughly represented by the form:

$$B(T) = a + b/T \qquad (1.3.7)$$

which is suggested by the Van der Waals two constant equation of state. Since this equation has only the simplest of theoretical justifications the limitations of equation 1.3.7 are not surprising. Experimentally measured values of $B(T)$ may be represented to within several per cent in our present range of interest which is somewhat less than the disagreement found in the results of different workers. The exact form of the temperature variation of B depends upon the form of the intermolecular potential of helium-4. It is usual to postulate a plausible form for this potential and to derive a relation between $B(T)$ and the chosen function. Measured values of $B(T)$ may subsequently be used to evaluate constants in the intermolecular potential. The successive terms in the virial equation of state are then seen to correspond to interactions of increasingly higher order between molecules. However, whilst this procedure constitutes an important theoretical justification for the virial equation of state, it will be appreciated that it cannot offer a theoretical description of the form of $B(T)$ in the absence of a prior and independent definition of the intermolecular potential. It is therefore necessary to approach the problem experimentally and to obtain $B(T)$ from such data as is available. Since the disagreement between the various measured values of B is as large as it is, it is felt that there is little point in

attempting to represent B(T) with a many-constant numerical approximation so that pressure-volume and acoustic virial coefficients may be compared accurately. Taking equation 1.3.7 and substituting for B(T) in equation 1.3.5 we obtain

$$A_1(T) = \frac{\alpha}{M}\left\{2a + \frac{6b}{5T}\right\} \qquad (1.3.8)$$

or

$$A_1(T) = d + e/T \qquad (1.3.9)$$

where

$$d = \frac{2\alpha}{M}a \quad \text{and} \quad e = \frac{6\alpha}{5M}b \qquad (1.3.10)$$

thus deriving a similar functional dependence on temperature for the second acoustic virial coefficient.

1.4 The Velocity of Sound and the Principal Specific Heats of a Real Gas

Expressing equation 1.2.1 in terms of the isothermal bulk modulus, $B_T = B_S/\sigma$, we obtain

$$c^2 = -\sigma \left(\frac{\partial P}{\partial V}\right)_T \frac{V^2}{Mn} \qquad (1.4.1)$$

which is easily evaluated from the virial equation of state, 1.3.1, to give

$$\sigma \equiv C_p/C_v = \frac{Mc^2}{RT}\left\{1 - 2B(T)\left(\frac{n}{V}\right) + \left(2B^2(T) - 3C(T)\right)\frac{P^2}{R^2T^2}\right\} \qquad (1.4.2)$$

A second relationship between C_p and C_v may be obtained from the familiar equation

$$C_p = C_v + T\left(\frac{\partial P}{\partial T}\right)_v \left(\frac{\partial V}{\partial T}\right)_p \qquad (1.4.3)$$

whence

$$C_p - C_v =$$

$$R\left\{1 + \frac{2}{R}\frac{dB(T)}{dT}P + \left(B^2(T) - 4TB(T)\frac{dB(T)}{dT}\right.\right.$$

$$\left.\left. + T^2\frac{d^2B(T)}{dT^2} - C(T) + 2T\frac{dC(T)}{dT}\right)\frac{P^2}{R^2T^2}\right\} \qquad (1.4.4)$$

Equations 1.4.2 and 1.4.4 enable σ, C_p and C_v to be calculated from a knowledge of the virial coefficients and the thermodynamic temperature. To measure the latter acoustically it will be necessary to assume that $\sigma = \sigma_0 = 5/3$, the ideal gas value, at vanishingly small pressures. Given this, values of σ, C_p and C_v may be calculated at higher pressures.

It would, however, be useful to check that $\sigma_0 = 5/3$ at limitingly low pressures. Such a check could in principle be made if an independent measurement of temperature was available. This value might then be substituted into the limiting form of equation 1.4.2:

$$\sigma_0 = \frac{Mc^2}{RT} \qquad (1.4.5)$$

to give σ_0. In the range 2-20K this would require a primary gas thermometry determination of T which needs make no assumption as to the value of σ_0. However, the experimental error in such a value would exceed the error expected in the assumed theoretical value of σ_0. Thus, in practice, the suggestion is not very helpful. Moreover, the status of acoustic thermometry as a technique of primary thermometry

hangs upon the independence of its measurements. To use a measured value of σ_0 would be tantamount to doing secondary (but hardly practical) acoustic thermometry. In any case, systematic errors in acoustically measured temperatures attributable to σ_0 should become apparent in direct comparison with temperatures measured by primary gas thermometry provided that they can be disentangled from other sources of error. This would not be made any easier by the above approach.

1.5 Existing Acoustic Thermometry

In recent years several interferometric investigations have been made into the propagation of sound in helium gas in the range 2-20K. These have been directed mainly at measuring thermodynamic temperatures, but have also served to evaluate the other thermodynamic parameters dealt with in the previous two sections. Standing wave techniques of sound velocity measurement have invariably been used since it is far simpler to house resonant cavities in a liquid helium cryostat than any conceivable time of flight device of comparable accuracy. Due largely to a naive approach to the design of acoustic interferometers the earlier measurements fell far below what could be currently achieved by conventional gas thermometry. Accordingly our attention will be directed to more recent measurements [15-25] of greater metrological usefulness.

Two different approaches seem to have emerged in acoustic interferometry in general (and in acoustic thermometry in particular). Firstly there are high frequency methods with the attendant risk of an ill-defined wave field in the resonant cavity [15,16,21-24] and secondly low frequency methods [17-19,25] where this problem is avoided at the expense of incurring difficulties with boundary layer effects for which reliable theoretical corrections may not easily be made. These two different types of systematic error will be dealt with

in detail in the following two chapters. It suffices to point out here that in the event of agreement being reached between high and low frequency acoustic thermometry it would be difficult not to conclude that their characteristic systematic errors were accounted for correctly and that, all other things being equal, true thermodynamic temperatures were being measured. Moreover, should both methods then agree with the results of primary gas thermometry then we might say that all primary thermometry in the range 2-20K was basically sound and reliable. The internal consistency of the measured temperatures (but not their absolute values) could be further checked by magnetic thermometry.

There exist two important sets of low frequency measurements due to De Laet [19] (following earlier work at Leiden [15-17]) and to Grimsrud and Werntz. [25] De Laet used a cavity of fixed length and determined sound velocities from measurements of its resonant frequencies. Grimsrud and Werntz used a cavity of variable path excited at some constant frequency and measured the separation of the positions of resonance. With the exception of a measurement close to the boiling point of hydrogen from De Laet neither of these investigations extended beyond the region between 2 and 4.3K in the present range of interest. Temperatures determined by De Laet were higher than temperatures measured on the helium- 4 vapour pressure scale, T-58, by as much as 22mK at 3.2K and 12mK at the normal boiling point of helium-4 . This last figure compared with a 32mK discrepancy found in the earlier Leiden work using ultrasonic techniques. The acoustic temperatures of Grimsrud and Werntz determined using both helium-3 and helium-4 as the thermometric gas exceeded temperatures measured in the T-58 scale by between 1 and 7mK over the range 1.2 to 3.8K.

These results of Grimsrud and Werntz are in general agreement with

the ultrasonic thermometry of Plumb and Cataland [21-24] in the region in which they may be compared. The temperatures determined by the latter using a variable-path interferometer excited at a frequency of 1MHz were higher than T-58 temperatures by between 5 and 12mK in the region 2 to 5K with a 10mK difference at the normal boiling point of helium-4. However, the results of Plumb and Cataland extend over the whole range 2-20K at intervals of roughly 1K thus forming a detailed ultrasonic temperature scale over a wider range than has yet been achieved with low frequency acoustic thermometry. This was a major factor in our deciding to pursue low frequency acoustic thermometry rather than the high frequency method.

CHAPTER II

THE THEORY OF THE ACOUSTIC INTERFEROMETER WITH IDEAL BOUNDARY CONDITIONS

There are many possible forms of acoustic interferometer which might be adopted for the measurement of wavelength and hence acoustic velocity. The most familiar devices are those where the sound propagates axially in a cavity of rectangular or circular cross section between two reflecting end faces. But in principle any cavity might be used where reflected waves have a constant phase relationship with incident waves and where the wavefronts are coextensive thus allowing interference to take place. For example a sphere excited at its centre or the region between two concentric spheres would suffice. In practice, however, only the two familiar cavities mentioned above have been widely used. This arises firstly because the wave equation for an inviscid fluid is easily stated and solved in the appropriate coordinate systems, and secondly because, unlike the spherical interferometers, they are easy to construct with a high degree of accuracy. Here only the cylindrical resonator is discussed since it is universally used for low temperature acoustic thermometry. It is not feasible to manufacture a rectangular cavity with truly squared vertices other than by assembling four separate flat walls. These have then to be effectively and reliably sealed and to remain so at the lowest temperatures. Such practical cryogenic problems are less acute with the cylindrical cavity and so it has always been the preferred

alternative.

The cylindrical interferometer may be used in several ways. It can be excited at one end by a suitable transducer which may also serve to monitor the resonances in the cavity. Alternatively a separate receiver, commonly the opposite end reflector, may be employed as well. Wavelengths may then be determined either by measuring the resonant frequencies of a cavity of fixed length, or by measuring the lengths at which a variable-path cavity resonates at some constant frequency. The results about to be derived will apply equally to variable-path and variable frequency instruments. But for the most part we shall restrict our investigation to interferometers where a single transducer is used both to excite the cavity and to monitor the sound. This better suits the type of experimental instrument ultimately adopted for our measurements . Generally the extension of the theory to the other case will be obvious.

2.1 The Ideal Interferometer

In the absence of viscosity and of effects attributable to the thermal conductivity of the boundaries of the cavity, the general problem of deriving the acoustic field within the cavity (Figure 2.1) becomes very simple. Following Hubbard [26,27] we assume that the transducer at z=l vibrates like a perfect piston, i.e. the amplitude of its vibration at any instant, t, is the same over the whole radiating face:

$$\xi(r,\theta) = \xi_0 e^{i\omega t} \qquad (2.1.1)$$

where ω is the angular frequency of the vibration and i is the imaginary unit.

It is assumed that plane waves travel in both directions in the cavity suffering attenuation on reflection at the transducer, T, and

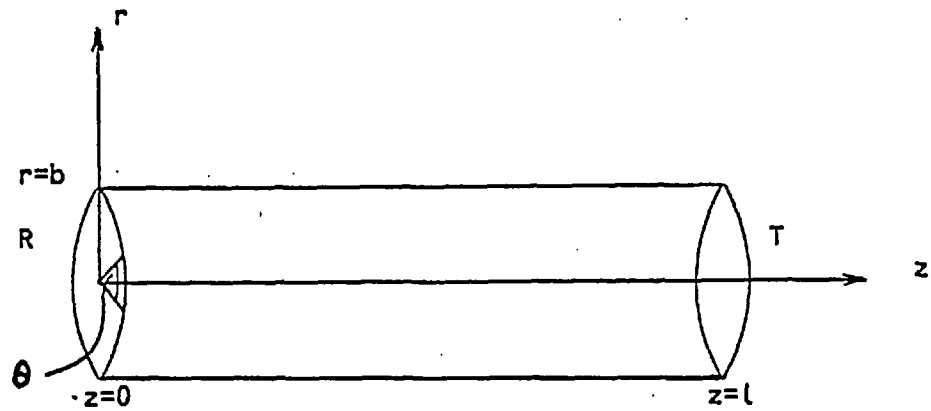

FIGURE 2.1

The Acoustic Interferometer Cavity.

the reflector, R, and in the body of the gas itself due to the usual mechanisms of acoustic absorption. The respective reflection coefficients, R_R and R_T, are taken to be real and only slightly less than one so that $1-R_{R,T} \ll 1$. If $1-R_{R,T} \doteq \alpha l$ where α is the acoustic absorption coefficient and l the length of the cavity then we may say that losses by reflection and absorption are comparable. Practical values will be discussed at the end of this section.

Summing the negative and positive going waves we obtain

$$\xi(z) = \xi_0 e^{i\omega t} \left\{ \sum_{n=0}^{\infty} R_R^n R_T^n e^{-(\alpha+ik)([2n+1]l-z)} - \sum_{n=0}^{\infty} R_R^{n+1} R_T^n e^{-(\alpha+ik)([2n+1]l+z)} \right\}$$

$$= \xi_0 e^{i\omega t} \frac{e^{-(\alpha+ik)(l-z)} - R_R e^{-(\alpha+ik)(l+z)}}{1 - R_R R_T e^{-2(\alpha+ik)l}} \qquad (2.1.2)$$

where $k=2\pi/\lambda \gg \alpha$ is the wavenumber, λ being the wavelength of the sound. This equation enables us to calculate the acoustic reaction on the transducer from the following relation for the acoustic (i.e. excess) pressure in the cavity:

$$p(z) = -\rho c^2 \partial\xi(z)/\partial z$$

$$\doteq i\rho c^2 k \frac{e^{-(\alpha+ik)(l-z)} + R_R e^{-(\alpha+ik)(l+z)}}{1 - R_R R_T e^{-2(\alpha+ik)l}} \qquad (2.1.3)$$

where ρ is the density of the gas, c the velocity of sound and where we have made the approximation ik for the factor $(\alpha+ik)$. Thus at the

face of the transducer (z=l) this becomes

$$p(l) = i\rho c^2 k \frac{1 + R_R e^{-2(\alpha+ik)l}}{1 - R_R R_T e^{-2(\alpha+ik)l}} \qquad (2.1.4)$$

or

$$p(l) = i\rho c^2 k \left\{ R_G(l) - i X_G(l) \right\} \qquad (2.1.5)$$

where

$$R_G(l) = \frac{1 - R_R^2 R_T e^{-4\alpha l} + R_R(1-R_T) e^{-2\alpha l} \cos 2kl}{1 - 2R_R R_T e^{-2\alpha l} \cos 2kl + R_R^2 R_T^2 e^{-4\alpha l}} \qquad (2.1.6)$$

and

$$X_G(l) = \frac{R_R(1+R_T) e^{-2\alpha l} \sin 2kl}{1 - 2R_R R_T e^{-2\alpha l} \cos 2kl + R_R^2 R_T^2 e^{-4\alpha l}} \qquad (2.1.7)$$

Since over the face of the transducer both transducer and gas have the same particle velocity their respective mechanical impedances, $\underline{Z}_T$ and $\underline{Z}_G(l)$, may be added to give the total mechanical impedance

$$\underline{Z}(l) = \underline{Z}_T + \underline{Z}_G(l) \qquad (2.1.8)$$

where

$$\underline{Z}_G(l) = A\frac{\underline{P}(l)}{\dot{\underline{\xi}}(l)} = A\rho c \left\{ R_G(l) - i X_G(l) \right\} \qquad (2.1.9)$$

and A is the area of the radiating face of the transducer.

Equations 2.1.6 and 2.1.7 are in agreement with the relevant results of Hubbard if we substitute $\gamma = R_R = R_T = (R_R + R_T)/2$ for R_R and R_T. Our expressions have the advantage that R_R and R_T have not been assumed to be equal - an important consideration when one or both of the coefficients is very low. However, with the current assumption that $1-R_{R,T} \ll 1$ Hubbard's approximation can be seen to be very accurate in the vicinity of a resonance when $R_G(l)$ takes its maximum value and $X_G(l)$ is zero. This arises because $\cos(2kl) \doteq 1$ near resonance and because the (identical) denominators of $R_G(l)$ and $X_G(l)$ are symmetrical in R_R and R_T which appear only in powers of the product $R_R R_T$. Since they appear as a factor $R_R(1+R_T) \doteq 2$ in the numerator of $X_G(l), X_G(l)$ may be regarded as well represented by Hubbard's approximation for all values of kl and αl. It is exact both at resonance and antiresonance. $R_G(l)$, on the other hand, has an approximate minimum value of $l+(1-R_R)/2$ at antiresonance which, depending only on R_R, may not necessarily be equal to Hubbard's corresponding approximation, $l+(1-\gamma)/2$. However, it is nearly always possible to regard this quantity as being negligible in the measurement of the velocity of sound in the present context. Thus for our purposes we shall consider any interferometer with which we may be concerned as having end faces with equal reflection coefficients, γ. Then with Hubbard we have

$$R_q(l) = \frac{1 - \gamma^3 e^{-4\alpha l} + \gamma(1-\gamma) e^{-2\alpha l} \cos 2kl}{1 - 2\gamma^2 e^{-2\alpha l} \cos 2kl + \gamma^4 e^{-4\alpha l}} \qquad (2.1.10)$$

and

$$X_G(l) = \frac{\gamma(\gamma+1)\sin 2kl}{1 - 2\gamma^2 e^{-2\alpha l}\cos 2kl + \gamma^4 e^{-4\alpha l}} \qquad (2.1.11)$$

Figure 2.2 shows the form of the functions $R_G(l)$ and $X_G(l)$ and that the locus of $\underline{Z}_G(l)$ is a series of circles in the complex plane which are approximately touching when $\underline{Z}_G(l)=0$ if $1-\gamma \ll 1$ and $\alpha l \ll 1$. The ratios of the diameters of the impedance circles are shown as being 1 : 1/2 : 1/3 : 1/4 : ... diminishing as the order of resonance, N, increases. This is characteristic of the situation where reflection losses are negligible ($1-\gamma \ll \alpha l$). In this case equations 2.1.10 and 11 simplify to give

$$R_G(l) = \frac{\sinh 2\alpha l}{\cosh 2\alpha l - \cos 2kl} \qquad (2.1.12)$$

and

$$X_G(l) = \frac{\sin 2kl}{\cosh 2\alpha l - \cos 2kl} \qquad (2.1.13)$$

From equation 2.1.8 it can be seen that the point $\underline{Z}_G(l)=0$ on the impedance circles will be located at $\underline{Z}_T$ in the complex plane and that $\underline{Z}(l)$ will be the vectorial resultant at $\underline{Z}_T + \underline{Z}_G(l)$. For the familiar case of an ultrasonic quartz crystal transducer driven at resonance $\underline{Z}_T \doteq 0$, and the circles $\underline{Z}_G(l)$ would lie symmetrically about the posative real axis touching the origin. In that case $Z(l)$, the experimental function generally measured, would have the approximate form of $R_G(l)$ with exact agreement at resonance and antiresonance i.e. when $l=N\lambda/2$ or $(2N-1)\lambda/4$ ($N=1,2,3, \ldots$). The form of $Z(l)$ for the example of

figure 2.2 is shown in figure 2.3.

It can easily be seen that if an experimental plot of Z(l) such as this is obtained, then one has all the information necessary to draw the impedance circles of figure 2.2. The diameter, D_N, of the Nth impedance circle is obtainable from the difference between the maximum and minimum values of Z for the resonance. Thus all the impedance circles may be drawn on collinear diameters touching at one point on their circumferences. It is then only necessary to locate the origin of the complex plane. It will lie at a distance Z_T from the point of contact of the circles. It will also lie at that distance from the centre of any one circle given by the mean, Z_{AV}, of the maximum and minimum values of Z for that circle. Thus, having drawn the circles, one may draw two arcs to locate the origin - or rather the two possible positions of the origin. Which is the true position is easily determined by seeing from one's experimental Z(l) curve whether Z(l) must increase or decrease as the circles are traversed in a clockwise direction from antiresonance to resonance.

Having drawn the complete figure from the measured function, Z(l), the values, Z_{RES}, of Z at resonance may be taken by measuring the distance from the origin of the extreme points on the circles for which $\underline{Z}_G(l)$ is entirely real. The corresponding values, l_{RES} of l at resonance may then be read from the original experimental curve. As can be seen from figure 2.2 the functions $R_G(l)$ and $X_G(l)$ are changing very rapidly at resonance in such a way that nearly the whole circumference of a circle is traversed for only a small change in l. It should be possible using this type of instrument to measure velocities to several parts in 10^4 and so, all other things being equal, to measure temperature to within twice this fractional error.

Some idea of the relative importance of the expected absorption and reflection losses may be obtained from Tables 2.1 and 2.2. The

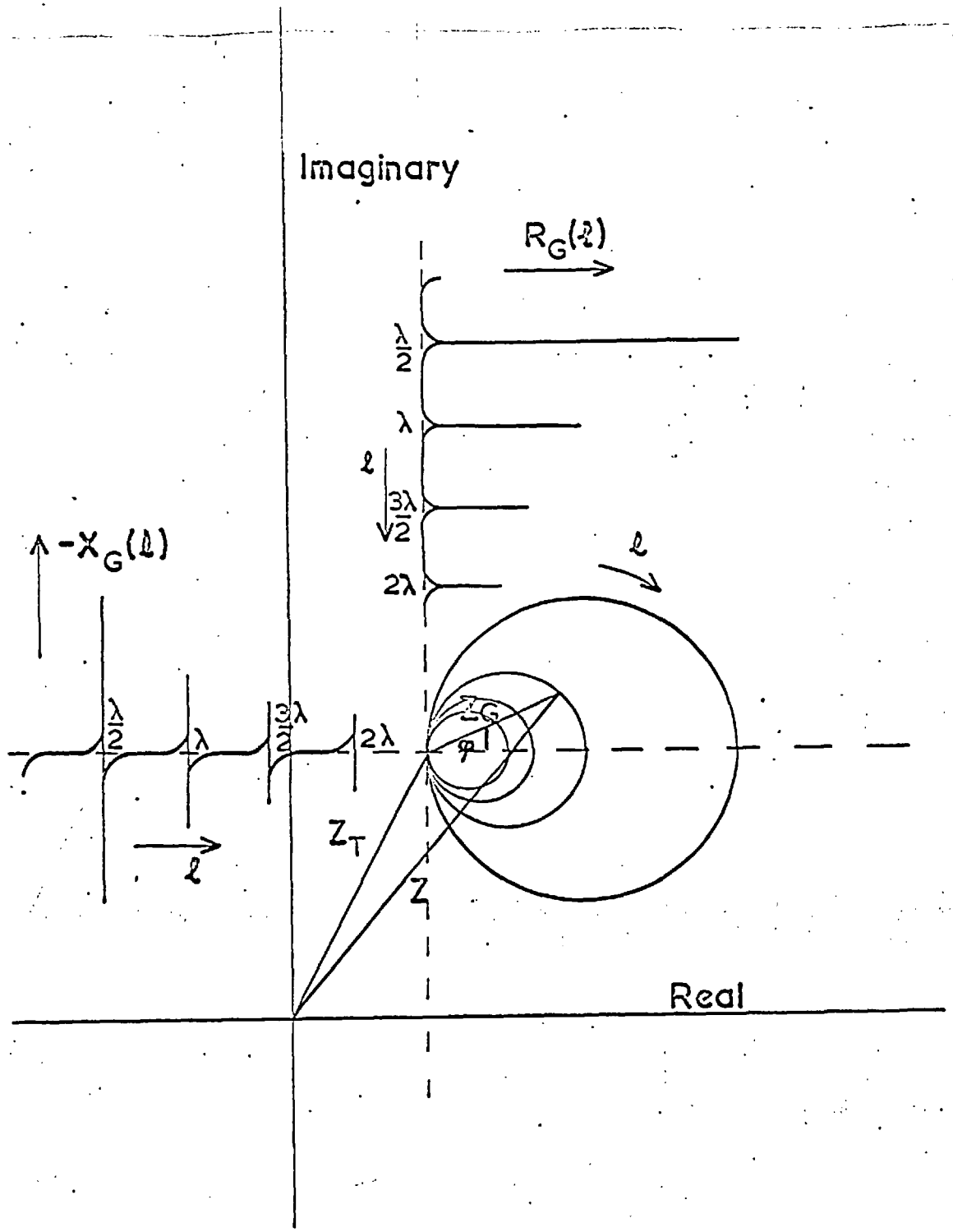

FIGURE 2.2

Showing the Combined Complex Mechanical Impedance Z of Transducer and Gas Loading.

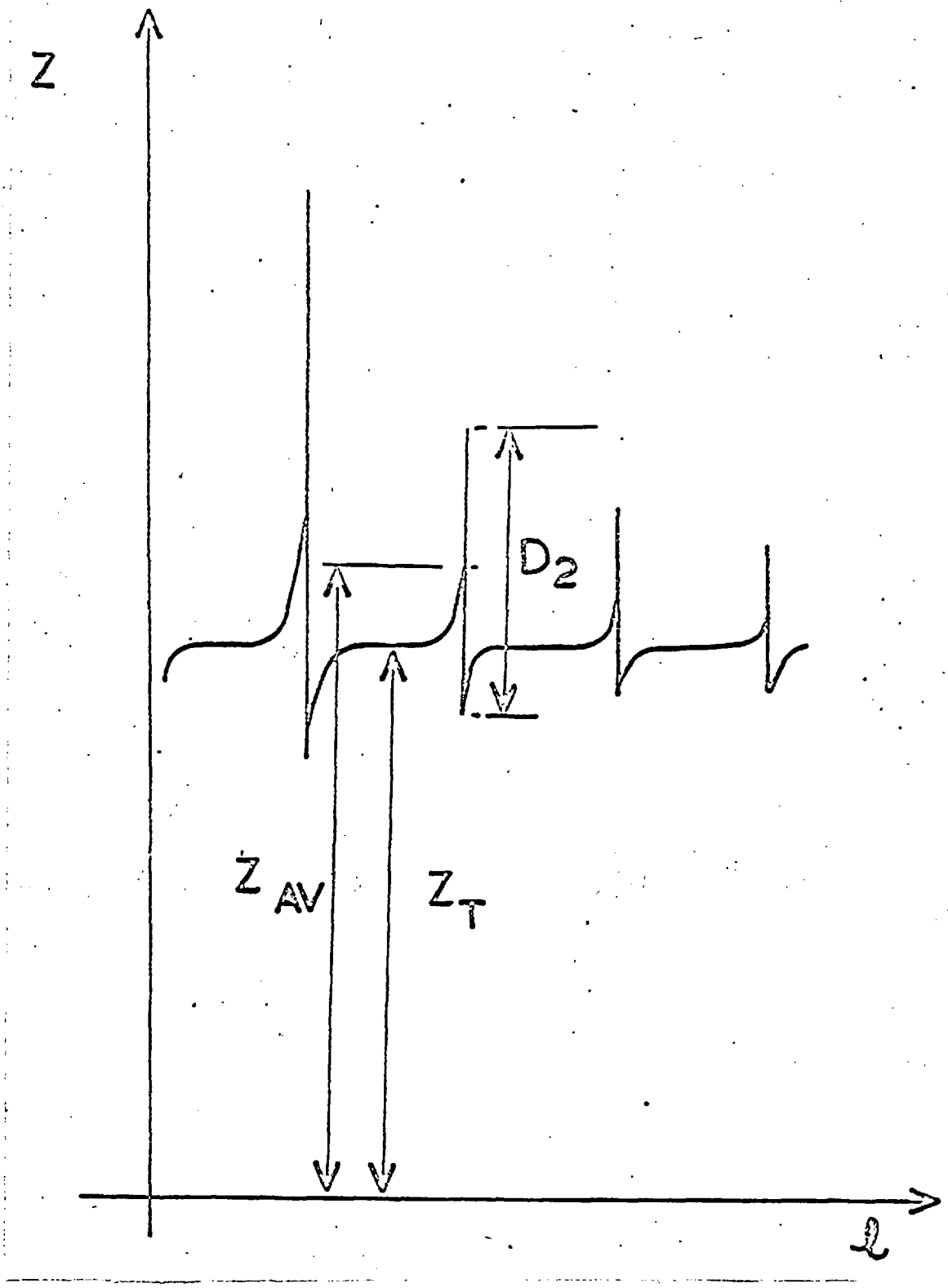

FIGURE 2.3

The Experimental Trace of Z(l) from which Figure 2.2 may be Constructed.

reflection losses have been calculated from a formula due to Herzfeld [28] which allows for the losses arising from the existence of a "temperature" wave which occurs in the gaseous medium when a compressional adiabatic wave is reflected from a solid reflector. The combined temperature wave amplitude and the normal reflected wave amplitude must equal the amplitude of the incident acoustic wave. i.e. the particle velocity must be zero at the boundary. Thus the reflected acoustic wave must be diminished to an extent beyond that to be expected solely from the impedance mismatch of gas and wall. The loss does not arise from the propagation of heat into the wall since it periodically flows in and out of the wall, but is due to the temperature wave causing the excess temperature of the gas to be slightly out of phase with the acoustic pressure. Only when they are in phase will the work integral per cycle vanish.

In the derivation of Herzfeld's formula, which we prefer to write

$$1 - \gamma = \frac{\sigma - 1}{c}\left(\frac{K}{\rho c_p}\right)^{\frac{1}{2}}(2\omega)^{\frac{1}{2}} \qquad (2.1.14)$$

where K is the thermal conductivity of the gas and c_p the specific heat per unit mass at constant pressure, it is assumed (entirely justifiably) that the thermal conductivity of the solid reflector may be regarded as being infinite in comparison to that of the gas. Thus γ should depend only upon the transport properties of the gas in the interferometer cavity and not upon those of the end faces. This is fortunate in that the opposite ends of an interferometer cavity often require to be made of different metals (e.g. when one end is to be the diaphragm of a transducer and the other a movable reflector of the same metal as that of the cylindrical bore). Thus if Herzfeld's mechanism of reflection loss could be guaranteed to be the only one

TABLE 2.1

Reflection Losses and Absorption Losses.

Frequency (Hz)	$1-\gamma$	$b\alpha_{KH}$	α cm^{-1}
10^2	4.8×10^{-5}	9.2×10^{-5}	4.2×10^{-10}
10^3	1.5×10^{-4}	2.9×10^{-4}	4.2×10^{-8}
10^4	4.8×10^{-4}	9.2×10^{-4}	4.2×10^{-6}
10^5	1.5×10^{-3}	2.9×10^{-3}	4.2×10^{-4}
10^6	4.8×10^{-3}	9.2×10^{-3}	4.2×10^{-2}
10^7	1.5×10^{-2}	2.9×10^{-2}	4.2×10^{0}

The rough values of $1-\gamma$, $b\alpha_{KH}$ and α at a pressure of one atmosphere and a temperature of 4.2K are shown. They have been calculated from equations 2.1.14, 15 and 16 using the following values for helium-4 gas:

$R=2.079\times10^{3}$ J/K.kg

$C_p=3.917\times10^{3}$ J/K.kg

$\sigma=2.05$

$c=120.8$m/s

$\eta=1.27\times10^{-6}$ Pa.s

$K=0.009$W/K.m

$\rho=11.9$kg/m^3

TABLE 2.2

Reflection Losses and Absorption Losses.

Frequency (Hz)	$1-\gamma$	$b\alpha_{KH}$	α cm^{-1}
10^2	3.0×10^{-4}	3.3×10^{-4}	5.1×10^{-10}
10^3	9.5×10^{-4}	1.0×10^{-3}	5.1×10^{-8}
10^4	3.0×10^{-3}	3.3×10^{-3}	5.1×10^{-6}
10^5	9.5×10^{-3}	1.0×10^{-2}	5.1×10^{-4}
10^6	3.0×10^{-2}	3.3×10^{-2}	5.1×10^{-2}
10^7	9.5×10^{-2}	1.0×10^{-1}	5.1×10^{0}

The rough values of $1-\gamma$, $b\alpha_{KH}$ and α at a pressure of one atmosphere and a temperature of 273K are shown. They have been calculated from equations 2.1.14, 15 and 16 using the following values for helium-4 gas:

$R=2.079\times10^{3}$ J/K.kg

$C_p=5.297\times10^{3}$ J/K.kg

$\gamma=1.63$

$c=971.9$m/s

$\eta=1.86\times10^{-9}$ Pa.s

$K=14.15\times10^{-2}$ J/K.m

$\rho=0.1785$kg/m^3

present, then there would be a sound theoretical justification for adopting Hubbard's approximation.

Two absorption coefficients are shown. The first, α_{KH}, is calculated from the formula for the absorption coefficient for sound in an infinite tube which was derived by Kirchhoff and Helmholtz [29,30]:

$$\alpha_{KH} = \frac{1}{bc}\left\{\nu^{\frac{1}{2}} + (\sigma-1)\left(\frac{K}{\rho c_p}\right)^{\frac{1}{2}}\right\}\left\{\frac{\omega}{2}\right\}^{\frac{1}{2}} \qquad (2.1.15)$$

where ν is the kinematic viscosity and b the radius of the interferometer cavity. Some obvious points of comparison with Herzfeld's formula for reflection losses are apparent here, notably the dependence on the square root of the frequency of the sound. Such a dependence on frequency commonly occurs with boundary layer corrections to a first order analysis of an acoustic problem based on the assumptions that all propagation is both adiabatic and frictionless. It is not suggested here that this formula is anything other than a device for rough approximation in this situation. A fuller discussion on the problem of boundary layer corrections will follow in the next chapter. It does, however, give some indication of the relative importance of this mechanism of absorption compared to losses by reflection.

The second absorption coefficient, α, is calculated from the familiar equation [31] for the effects of viscosity and thermal conduction within the body of the gas itself:

$$\alpha = \frac{1}{2c^3}\left\{\frac{4}{3}\nu + (\sigma-1)\frac{K}{\rho c_p}\right\}\omega^2 \qquad (2.1.16)$$

This mechanism depends on the square of the frequency of the sound and so may be expected to predominate over both the aforementioned boundary loss mechanisms at sufficiently high frequencies. Tables 2.1 and 2.2 show this. The values used for the various parameters occuring in equations 2.1.14 to 2.1.16 are also given. Since they are only roughly known the values of α , α_{KH} and $1-\gamma$ should be regarded as being comparative rather than absolute.

In the equations for $\underline{Z}_G$, R_G and X_G the argument of the functions has been the length of the cavity, l. It is equally valid to regard k ($=2\pi/\lambda=\omega/c$) as the variable and to apply the equations to the aforementioned fixed path interferometers operated at variable frequency. There is, however, one practical problem which arises in the latter case when drawing the impedance circle diagrams. For the fixed path cavity it is possible to assume that $\underline{Z}_T$ is a complex constant whereas this is unlikely when the frequency is varied. It would be expected that $\underline{Z}_T$ might remain approximately constant over the narrow bandwidth of a single resonance, but not that it would be the same at successive orders of resonance. This would result in the corresponding impedance circles of figure 2.2 ceasing to lie on collinear diameters so that for each circle a new determination of $\underline{Z}_T$ would need to be made. More important, however, it would be impossible to infer anything about the relative magnitudes of the absorption and reflection losses since these, too, change with frequency and require at least two circles to be taken at any one frequency for their determination. The full significance of this will be discussed at length in Chapter IV where practical designs are considered.

2.2 The Effect of Practical Transducers

The assumption of section 2.1 that a transducer behaves like a perfect piston vibrator is obviously implausible in practice. At low frequencies driven diaphragms of stiff metal sheet are frequently employed. These diaphragms are clamped at their edges and so must flex if they are to vibrate at their centres. The conventional quartz crystals of ultrasonic interferometry may also fail to approximate to the ideal in many cases.

The effect of such vibrations is to excite the higher modes of propagation in the cavity which are, in addition to the zero order (plane wave) mode, allowed solutions of the wave equation. Each of these higher modes can be shown to have a unique phase velocity which is higher than that of the plane wave mode, and a characteristic cut-off frequency below which it is severely attenuated. Often workers with the acoustic interferometer have operated at frequencies well above many of these cut-off frequencies and have observed "satellite" (sic) peaks corresponding to resonances of the higher modes. [32-34] When unresolved these parasitic resonances can lead to errors in measuring the velocity of sound due to the increased phase velocities of their parent modes. Measured values of absorption coefficients are also too high because of interference between the plane wave resonances and those of the higher modes.

The purpose of this section is to show how the amplitudes of the higher modes may be calculated from the way in which the transducer vibrates. Knowing this it should be possible to decide in advance the suitability of various possible designs of transducer for working at high frequencies.

2.2.1. The Form of the Normal Modes

In order to establish the form of the normal modes we follow a similar method to that used by Krasnooshkin[35] except that we shall allow for the angular dependence of the modes as well as for their radial dependence. It is assumed that a velocity potential

$$\varphi'(r,\theta,z,t) = \varphi(r,\theta,z)\, e^{i\omega t} \qquad (2.2.1)$$

exists such that

$$\nabla^2 \varphi(r,\theta,z) + q_{00}^2 \varphi(r,\theta,z) = 0 \qquad (2.2.2)$$

where $q_{00} = k_{00} - i\alpha_{00}$ is the complex wavenumber for propagation in the unbounded medium. Thus α_{00} is the free gas absorption coefficient and k_{00} the corresponding wavenumber (previously α and k respectively).

Expressing equation 2.2.2 in cylindrical coordinates it becomes

$$\left\{\frac{\partial^2}{\partial r^2} + \frac{1}{r}\frac{\partial}{\partial r} + \frac{1}{r^2}\frac{\partial^2}{\partial \theta^2} + \frac{\partial^2}{\partial z^2}\right\}\varphi + q_{00}^2 \varphi = 0 \qquad (2.2.3)$$

Assuming a solution of the form

$$\varphi(r,\theta,z) = R(r)\,\Theta(\theta)\,Z(z) \qquad (2.2.4)$$

this separates into the three equations

$$\frac{d^2Z}{dz^2} + q^2 Z = 0 \qquad (2.2.5)$$

$$\frac{d^2\Theta}{d\theta^2} + m^2\Theta = 0 \qquad (2.2.6)$$

and

$$\frac{d^2R}{dr^2} + \frac{1}{r}\frac{dR}{dr} + \left(q_{oo}^2 - q^2 - \frac{m^2}{r^2}\right)R = 0 \qquad (2.2.7)$$

where $-q^2$ and $-m^2$ are the respective z and θ separation constants.

Solving 2.2.5 we obtain

$$Z(z) \propto J e^{iqz} + K e^{-iqz} \qquad (2.2.8)$$

where J and K are constants. Assuming perfect reflection at z=0 (i.e. $\gamma = 1$) we have

$$\left.\frac{\partial \varphi}{\partial z}\right|_{z=0} = 0 \qquad (2.2.9)$$

so that

$$K = J \qquad (2.2.10)$$

and

$$Z(z) \propto \cos q_z z \qquad (2.2.11)$$

We prefer to write the solution of equation 2.2.6 in the form

$$\Theta(\theta) \propto A \cos m\theta + B \sin m\theta \qquad (2.2.12)$$

m will be restricted to integer values so that

$$\varphi(r, \theta, z) = \varphi(r, \theta + 2\pi, z) \qquad (2.2.13)$$

Equation 2.2.7 is Bessel's equation with solutions

$$R(r) \propto L J_m(r\sqrt{q_{oo}^2 - q_r^2}) + M Y_m(r\sqrt{q_{oo}^2 - q_r^2}) \qquad (2.2.14)$$

where L and M are constants and J_m and Y_m are Bessel functions of order m of the first and second kind respectively. Since

$$Y_m(0) = -\infty \qquad (2.2.15)$$

we require that M=0 giving

$$R(r) \propto J_m(r\sqrt{q_{oo}^2 - q_r^2}) \qquad (2.2.16)$$

We shall assume that the wall of the cylinder is perfectly rigid so that the radial component of the particle velocity must vanish i.e.

$$\left.\frac{\partial}{\partial r} J_m(r\sqrt{q_{oo}^2 - q_r^2})\right|_{r=b} = 0 \qquad (2.2.17)$$

for a cavity of radius b, or

$$\left.\frac{d}{dX} J_m(X)\right|_{X = b\sqrt{q_{r00}^2 - q_r^2}} = 0 \qquad (2.2.18)$$

where $X = r(q_{00}^2 - q^2)^{1/2}$.

The (n+1)th solution of this equation is given by

$$X = X_{mn} = b\sqrt{q_{r00}^2 - q_r^2} \qquad (2.2.19)$$

Some values of X_{mn} which are always real (see Appendix 2.1) are given in Table 2.3. It will be noticed that since b and q_{00} are constants, equation 2.2.18 gives rise to a series of complex wavenumbers, $q = q_{mn}$, for the modes corresponding to the various values of X_{mn}. q_{mn} may be calculated from

$$q_{rmn} = \left\{ q_{r00}^2 - \left(\frac{X_{mn}}{b}\right)^2 \right\}^{\frac{1}{2}} \qquad (2.2.20)$$

whose real and imaginary parts, k_{mn} and $-\alpha_{mn}$ respectively, are given by

$$k_{mn} = \frac{1}{\sqrt{2}} \left\{ k_{00}^2 - \alpha_{00}^2 - \left(\frac{X_{mn}}{b}\right)^2 + \left\{ \left[k_{00}^2 - \alpha_{00}^2 - \left(\frac{X_{mn}}{b}\right)^2 \right]^2 + 4\alpha_{00}^2 k_{00}^2 \right\}^{\frac{1}{2}} \right\}^{\frac{1}{2}}$$

$$(2.2.21)$$

and

$$\alpha_{mn} = \alpha_{00} k_{00} / k_{mn} \qquad (2.2.22)$$

k_{mn}/k_{00} and α_{mn}/α_{00} are plotted in figure 2.4 as a function of

TABLE 2.3

Some Values of X_{mn}.

	n =	0	1	2	3	4	5
m =	0	0	3.83	7.01	10.17	13.32	16.47
	1	1.84	5.33	8.54	11.71		
	2	3.05	6.70	9.97	13.17		
	3	4.20	8.01	11.37	14.54		

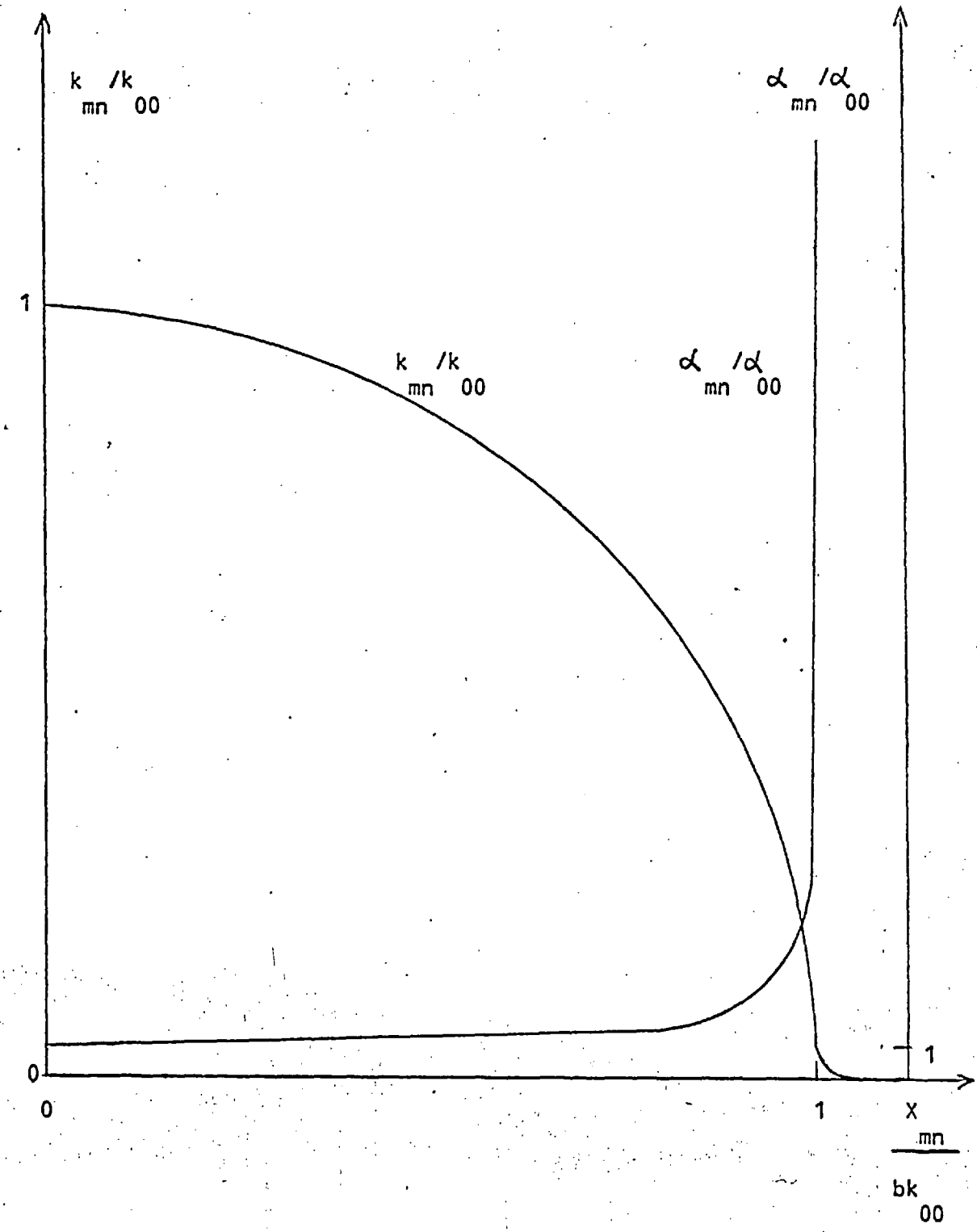

FIGURE 2.4

The Dependence of the Wavenumber and Absorption Coefficient upon the Order of the Mode.

The cut off condition for the mnth mode is seen to be $k_{00} = X_{mn}/b$.

X_{mn}/bk_{00}. Although full curves are drawn it will be appreciated that they represent the general distribution of discrete points each corresponding to a value of X_{mn}. At $X_{mn}=bk_{00}=2\pi b/\lambda_{00}$ (where b/λ_{00}, like l/λ_{00}, is to be considered as a fundamental scaling parameter of the interferometer) it can be seen that the wavelengths, $\lambda_{mn}=2\pi/k_{mn}$, of the higher modes become very large as do the corresponding absorption coefficients, α_{mn}. This gives the cut-off condition for a high order mode. The larger b/λ_{00}, the larger is the value of X_{mn} at this point and the greater the number of higher modes which can propagate in the cavity.

The dependence of the phase velocity of the mnth mode upon m and n arises from the z and θ separation constants of the wave equation remaining in the radial equation 2.2.7. The necessary imposition of the radial boundary condition 2.2.17 then puts the constraint 2.2.20 upon the wavenumber, q, requiring it to take only the values, q_{mn}. Consequently the phase velocity of the mnth mode will be

$$c_{mn} = \omega / k_{mn}$$

which must also take a set of discrete characteristic values different from $c_{00}=\omega/k_{00}$. Combining the expressions for R(r), Θ(θ) and Z(z) we obtain

$$\varphi_{mn} = J_m\left(\frac{X_{mn}r}{b}\right)(A_{mn}\cos m\theta + B_{mn}\sin m\theta)\cos q_{mn}z \qquad (2.2.23)$$

for the form of the mnth mode. Its amplitude will be $|A_{mn}+B_{mn}| = (A_{mn}^2+B_{mn}^2)^{1/2}$ with a "phase lag" on θ of $\tan^{-1}(B_{mn}/A_{mn})$.

2.2.2. The General Solution and the Amplitudes of the Normal Modes.

The general solution, $\Phi(r,\theta,z)$, of the wave equation in the cavity will be a superposition of the normal modes, $\varphi_{mn}(r,\theta,z)$:

$$\Phi(r,\theta,z) = \sum_{m=0}^{\infty}\sum_{n=0}^{\infty} J_m\left(\frac{X_{mn}r}{b}\right)(A_{mn}\cos m\theta + B_{mn}\sin m\theta)\cos q_{mn}z \qquad (2.2.24)$$

Applying the one remaining boundary condition

$$-\left.\frac{\partial\Phi}{\partial z}\right|_{z=l} = \frac{\partial}{\partial t}\left(\xi_0(r,\theta)\,e^{i\omega t}\right) \qquad (2.2.25)$$

we obtain

$$\xi_0(r,\theta) = \frac{1}{i\omega}\sum_m\sum_n q_{mn} J_m\left(\frac{X_{mn}r}{b}\right)(A_{mn}\cos m\theta + B_{mn}\sin m\theta)\sin q_{mn}l \qquad (2.2.26)$$

where $\xi_0(r,\theta)$ is the amplitude of vibration at (r,θ) on the face of the transducer. Equation 2.2.5 thus asserts the continuity of particle velocity at the transducer (assuming that no temperature wave is present i.e. that $\gamma=1$).

The amplitudes A_{mn} and B_{mn} where $m>0$ are simply obtained from the orthogonality relations for circular functions and Bessel functions. Multiplying equation 2.2.26 by $\cos j\theta$ or $(\sin j\theta)$ where $j=1,2,\ldots$ and integrating from $\theta=0$ to $\theta=2\pi$ it becomes

$$\int_0^{2\pi} \begin{matrix}\cos\\ \sin\end{matrix} j\theta\,\xi_0(r,\theta)\,d\theta = \frac{\pi}{i\omega}\sum_n q_{jn} J_j\left(\frac{X_{jn}r}{b}\right)\begin{matrix}A_{jn}\\ B_{jn}\end{matrix}\sin q_{jn}l \qquad (2.2.27)$$

since

$$\int_0^{2\pi} \begin{matrix} \cos j\theta \cos m\theta \\ \cos j\theta \sin m\theta \\ \sin j\theta \cos m\theta \\ \sin j\theta \sin m\theta \end{matrix} d\theta = \begin{matrix} \pi\,\delta_{jm} \\ 0 \\ 0 \\ \pi\,\delta_{jm} \end{matrix}$$

where δ_{jm} is the Kronecker δ.

Now multiplying by $rJ_j(X_{jk}\,r/b)$ where k= ,1,2,... and integrating from r=0 to r=b we obtain for m>0

$$\begin{matrix} A_{mn} \\ B_{mn} \end{matrix} = \frac{2i\omega}{\pi b^2 q_{mn}\left(1-m^2/X_{mn}^2\right) J_m^2(X_{mn}) \sin q_{mn} l} \times \int_0^b \int_0^{2\pi} r\, J_m\left(\frac{X_{mn} r}{b}\right) \begin{matrix} \cos \\ \sin \end{matrix} m\theta\, \xi_o(r,\theta)\, dr\, d\theta \qquad (2.2.28)$$

Here the following relations for Bessel functions have been used prior to changing the subscripts j and k back to m and n respectively:

$$\int_0^b r\, J_j\left(\frac{X_{jn} r}{b}\right) J_j\left(\frac{X_{jk} r}{b}\right) dr = \delta_{kn} \int_0^b r\, J_j^2\left(\frac{X_{jk} r}{b}\right) dr$$

$$= \delta_{kn} \frac{b^2}{2}\left(1-j^2/X_{jk}^2\right) J_j^2(X_{jk}) \qquad (2.2.29)$$

For the case where m=0 the answer is only slightly different.

Integrating equation 2.2.26 from $\theta=0$ to $\theta=2\pi$ one obtains

$$\int_0^{2\pi} \xi_0(r,\theta)\,d\theta = \frac{2\pi}{i\omega} \sum_n q_{on} \bar{J}_0\left(\frac{X_{on} r}{b}\right) A_{on} \sin q_{on} l \qquad (2.2.30)$$

and from the relations 2.2.29

$$A_{on} = \frac{i\omega}{\pi b^2 q_{on} J_0^2(X_{on}) \sin q_{on} l} \int_0^b \int_0^{2\pi} r \bar{J}_0\left(\frac{X_{on} r}{b}\right) \xi_0(r,\theta)\,dr\,d\theta \qquad (2.2.31)$$

In particular, since $J_0(X_{00})=J_0(0)=1$, the amplitude of the plane wave mode will be

$$A_{oo} = \frac{i\omega}{\pi b^2 q_{oo} \sin q_{oo} l} \int_0^b \int_0^{2\pi} r\, \xi_0(r,\theta)\,dr\,d\theta \qquad (2.2.32)$$

The amplitudes B_{0n} cannot be derived, but are not required since when $m=0$, $\sin m\theta=0$ and the second term in the expression for φ_{0n} vanishes.

We prefer to restate these results in the following form so that the amplitudes A_{mn} and B_{mn} cease to be functions of l, and so that an obvious analogy may be drawn with the analysis of the ideal case of section 2.1:

$$\Phi(r,\theta,l) = \sum_m \sum_n \left\{ (R_{mn} + i\alpha_{mn}) \times \right.$$

$$J_m\left(\frac{X_{mn}r}{b}\right)(C_{mn}\cos m\theta + D_{mn}\sin m\theta)$$

$$\left. \times \left(R_{mn}(l) - i\,X_{mn}(l)\right) \right\} \qquad (2.2.33)$$

where generally

$$\begin{matrix} C_{mn} \\ D_{mn} \end{matrix} = \frac{2i\omega}{\pi b^2 (k_{mn}^2 + \alpha_{mn}^2)(1 - m^2/X_{mn}^2)\, J_m^2(X_{mn})}$$

$$\times \int_0^b \int_0^{2\pi} r\, J_m\left(\frac{X_{mn}r}{b}\right) \begin{matrix} \cos m\theta \\ \sin m\theta \end{matrix} \xi_o(r,\theta)\, dr d\theta$$

$$(2.2.34)$$

(2 being replaced by 1 if m=0 where $m^2/X_{0n}^2 = 0$ also),

$$R_{mn}(l) = \frac{\sinh 2\alpha_{mn} l}{\cosh 2\alpha_{mn} l - \cos 2k_{mn} l} \qquad (2.2.35)$$

and

$$X_{mn}(l) = \frac{\sin 2k_{mn} l}{\cosh 2\alpha_{mn} l - \cos 2k_{mn} l} \qquad (2.2.36)$$

The functions $R_{mn}(l)$ and $X_{mn}(l)$ are of the same form as $R_G(l)$ and $X_G(l)$ defined by equations 2.1.12 and 2.1.13 in the ideal case. (The latter now become $R_{00}(l)$ and $X_{00}(l)$.). Since $k_{mn} < k_{00}$ when $m,n>0$ the maxima of $R_{00}(l)$ will be more widely spaced as will the corresponding points on $X_{mn}(l)$ and the increase in the absorption coefficients will cause both functions to decay more rapidly with increasing order. For

evanescent modes $\alpha_{mn} >> k_{mn}$ and the functions R_{mn} and X_{mn} are of negligible value even at resonance ($l=N\lambda_{mn}/2$, $N=1,2,3,\ldots$). It is then only necessary to perform the summations of equation 2.2.33 over those modes whose cut-off frequencies are not exceeded. For transducers of good design the amplitudes C_{mn} and D_{mn} of the higher modes are in any case only significantly large for the lower values of m and n as will be shown. In practice, therefore, it may only be necessary to take the first few modes into consideration even if others may propagate in the cavity. For such modes α_{mn} may still be small in comparison to k_{mn} and so may be removed from equations 2.2.33 and 2.2.34.

2.2.3. Velocity Errors Due to Higher Modes

The effect of the higher modes on the measured impedance of the transducer may now be calculated. The power dissipated in the interferometer cavity will be given by:

$$\dot{W}_q(l) = \int_0^b \int_0^{2\pi} r \, \mathrm{Re}\{p(l)\} \, \mathrm{Re}\{\dot{\xi}(l)\} \, dr\,d\theta \qquad (2.2.37)$$

From

$$p(l) = \rho \frac{\partial}{\partial t}\left\{ \Phi(r,\theta,l)\, e^{i\omega t} \right\}$$

we have

$$\mathrm{Re}\{p(l)\} = -\sum_m \sum_n \left\{ \rho\omega k_{mn} \times J_m\left(\frac{X_{mn} r}{b}\right)\left(C_{mn}\cos m\theta + D_{mn}\sin m\theta\right) \times \left(R_{mn}(l)\sin\omega t - X_{mn}(l)\cos\omega t\right)\right\}$$

and from

$$\dot{\xi}(\ell) = i\omega \xi_o(r,\theta)\, e^{i\omega t}$$

we obtain

$$Re\left\{\dot{\xi}(\ell)\right\} = -\omega \xi_o(r,\theta) \sin\omega t$$

Thus, substituting these expressions into equation 2.2.37, it becomes

$$\dot{W}_q(\ell) = \sum_m \sum_n F_{mn}\left\{R_{mn}(\ell)\sin^2\omega t - X_{mn}(\ell)\sin\omega t\cos\omega t\right\} \qquad (2.2.38)$$

where

$$F_{mn} = \left\{2\rho c_{mn}\omega^2 \Big/ \left(\pi b^2(1-m^2/X_{mn}^2)\,J_m^2(X_{mn})\right)\right\}$$

$$\times\left[\left\{\int_0^b\int_0^{2\pi} r\,J_m\left(\frac{X_{mn}r}{b}\right)\cos m\theta\,\xi_o(r,\theta)\,dr\,d\theta\right\}^2\right.$$

$$\left.+\left\{\int_0^b\int_0^{2\pi} r\,J_m\left(\frac{X_{mn}r}{b}\right)\sin m\theta\,\xi_o(r,\theta)\,dr\,d\theta\right\}^2\right] \qquad (2.2.39)$$

if $m>0$ and half this if $m=0$ (where $m^2/X_{mn}^2=0$).

We now suppose that we may write $\xi_{0mn}(r,\theta)$ in the form

$$\xi_o(r,\theta) = \xi_o\, g(r,\theta) \qquad (2.2.40)$$

where ξ_0 is the amplitude of vibration of that point on the radiating

face of the transducer at which the amplitude is measured - usually the centre. This is always possible in practice and would only cease to be so were different parts of a transducer able to vibrate entirely independently. Since such devices are not used to excite acoustic interferometers the treatment remains entirely general for all practical purposes.

We prefer to write equation 2.2.38 in the form

$$\dot{W}_G(\ell) = \omega^2 \xi_o^2 \left\{ \left(\sum_m \sum_n G_{mn} R_{mn}(\ell) \right) \sin^2 \omega t + \left(\sum_m \sum_n G_{mn} X_{mn}(\ell) \right) \sin \omega t \cos \omega t \right\} \qquad (2.2.41)$$

where

$$G_{mn} = F_{mn} / \omega^2 \xi_o^2$$

Given equation 2.2.40 it may easily be seen from equation 2.2.39 that G_{mn} is independent of ξ_0. Thus the right hand side of equation 2.2.41 has the familiar form for the power dissipated on a damped harmonic system of impedance $\underline{Z}=R-iX$:

$$\dot{W} = \omega^2 \xi_o^2 \left\{ R \sin^2 \omega t - X \sin \omega t \cos \omega t \right\}$$

We may therefore assign some effective impedance

$$\underline{Z}_G(\ell) = R_G(\ell) - i X_G(\ell)$$

$$= \sum_m \sum_n G_{mn} R_{mn}(\ell) - i \sum_m \sum_n G_{mn} X_{mn}(\ell) \qquad (2.2.42)$$

to the gas loading which may be conceived of as an impedance associated with a vibrating system which has the same velocity as the centre of the transducer, $-\omega\xi_0 \sin\omega t$.

Some power, $\dot{W}_T$, will also be expended on the transducer itself. If we regard this too as a system to which the same unique velocity may be assigned then we may write

$$\dot{W}_T = \omega^2 \xi_0^2 \left\{ R_T \sin^2\omega t + X_T \sin\omega t \cos\omega t \right\}$$

where R_T and X_T are constants chosen to give the correct value for $\dot{W}_T$.

The total power dissipated will then be

$$\dot{W}(l) = \dot{W}_T + \dot{W}_G(l)$$

$$= \omega^2 \xi_0^2 \left\{ (R_T + R_G(l)) \sin^2\omega t + (X_T - X_G(l)) \sin\omega t \cos\omega t \right\}$$

which enables us to regard the combined system as a system having a resistance $R=R_T+R_G(l)$ and a reactance $X=X_T-X_G(l)$ vibrating with a single easily measurable velocity, $-\omega\xi_0 \sin\omega t$. At constant driving force this combined impedance could be measured in arbitrary units from the reciprocal of the velocity or displacement amplitude at the centre of the transducer.

This recourse to first principles for a definition of the combined mechanical impedance is forced upon us because the particle velocity and acoustic pressure are, ex hypothesi, no longer constant over the face of the transducer. Consequently a simple application of the electroacoustic analogy cannot be made here as in section 2.1. Reduction of a system, electrical or acoustic, to a lumped circuit

has to be possible if the electroacoustic analogy is to function, and this presupposes that currents or particle velocities may be considered to be constant over the cross sections of the circuit elements.

It is possible to define the state of resonance of the gas in several ways which, *prima facie*, may not be equivalent when higher modes are present in the cavity. The cavity might be said to resonate when the impedance $\underline{Z}_G(l)$, is entirely real or, alternatively, when the real part of $\underline{Z}_G(l)$ is greatest (that is when the maximum time averaged power is dissipated in the cavity at constant amplitude). These alternative definitions are, however, shown to be equivalent in Appendix 2.2 provided that the frequency is high enough to ensure that the higher mode resonances are far from being resolved. Consideration of some practical cases in the next section will indicate that it is generally only the lower modes (small m and n) that have amplitudes comparable to that of the plane wave mode. Where calculation shows this not to be the case it is assumed that the transducer design in question would not be adopted. Furthermore, if such higher modes as are present in strength have their cut-off frequencies exceeded to a large degree then, as may be confirmed from equations 2.2.21 and 2.2.22, k_{mn} and α_{mn} will vary only slowly with m and n thus leading to the "bunching" of these major resonances responsible for the poor resolution at high frequencies. In this situation the derivation of an expression for errors in measured velocity is comparatively simple. At somewhat lower frequencies where one or more of the higher modes may be almost resolved, a correction to the simple case may be derived. However, the form of this correction will be slightly different for the two definitions of resonance. We shall pursue an analysis in terms of the second criterion for resonance, and, should it be required, the other case may be dealt with in an exactly analogous way. Such

differences as will be found are briefly outlined in Appendix 2.2 and do not in any way affect the validity of the general conclusions which the expressions for the velocity errors lead us to.

It is thus possible to make a general analysis of the effect of practical transducers on the measurement of the velocity of sound by considering only the simplest definition in terms of the maximum average power dissipation. Taking a time average of equation 2.2.38 we have

$$\dot{W}_G(l) = \frac{\omega^2 \xi_o^2}{2} \sum_m \sum_n G_{mn} R_{mn}(l) \qquad (2.2.43)$$

for the power dissipated in a cavity of length, l. It is clear from this that an experimental measurement of $\dot{W}_G(l)$ would produce a superposition of resonance curves each of the form $R_{mn}(l)$ corresponding to each of the modes present in the cavity. The situation is shown in figure 2.5. Two effects are apparent. Firstly, because the higher modes have increased phase velocities their resonances become increasingly displaced from those of the plane wave mode as the order of resonance, N, is raised. This results in the maximum of the resultant (group) resonance being increasingly displaced from that of the plane wave, so that the measured separation of the resonances is too large. Wavelengths and velocities are consequently overestimated. Secondly the group maxima appear to die away more rapidly than they should because of the increasing separation of the phase maxima. It may be seen from figure 2.5 that this comes about because the decay of the group maxima is larger than that of the plane wave maxima. Thus measured values of the plane wave absorption coefficient, α_{00}, will be too great like the measured velocity. An estimate of the magnitude of the effect may be obtained by differentiating equation 2.2.43. We have:

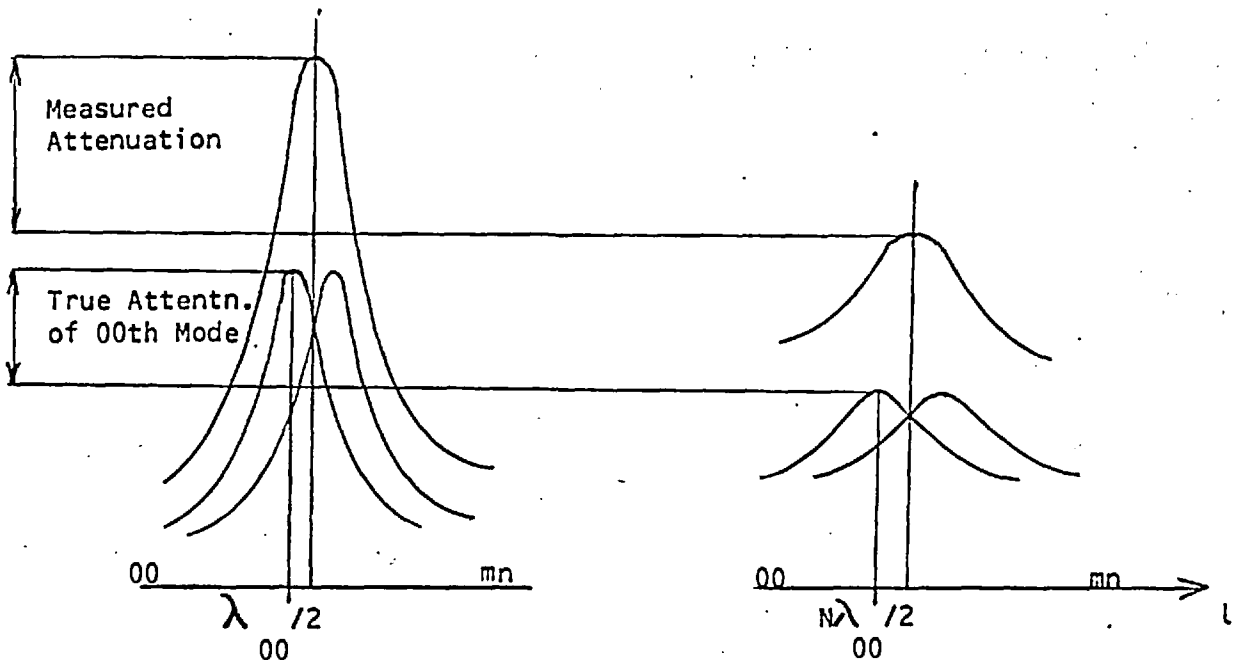

FIGURE 2.5

Showing the Effect of a Single Higher Mode

on the Measured

Positions of Resonance and the Measured Attenuation.

$$R_{mn}(\ell) \equiv \frac{\sinh 2\alpha_{mn}\ell}{\cosh 2\alpha_{mn}\ell - \cos 2k_{mn}\ell}$$

$$\doteq \frac{\alpha_{mn}\ell}{\alpha_{mn}^2\ell^2 + k_{mn}^2(\ell-\ell_{mn})^2} \qquad (2.2.44)$$

in the vicinity of a resonance where $\alpha_{mn} \doteq \alpha_{00} \ll 1$, $k_{mn} \doteq k_{00}$ and $l_{mn} = N\lambda_{mn}/2$. We require that

$$\frac{d}{d\ell}\sum_m\sum_n G_{mn} R_{mn}(\ell) = \sum_m\sum_n G_{mn}\frac{d}{d\ell} R_{mn}(\ell) = 0 \qquad (2.2.45)$$

which to a good approximation gives

$$\sum_m\sum_n G_{mn}\frac{(\ell-\ell_{mn})}{\left\{\Delta_{mn}^2 + (\ell-\ell_{mn})^2\right\}^2} \qquad (2.2.46)$$

where $\Delta_{mn} = \alpha_{mn}\, l/k_{mn}$ is the half-width of the mnth mode resonance at half the height of the resonance. Δ_{mn} will be roughly constant and equal to Δ_{00} for cases of interest since $\alpha_{mn} \doteq \alpha_{00}$ and $k_{mn} \doteq k_{00}$. At sufficiently high frequencies it becomes unlikely that any modes of significent strength will be resolved since

$$\Delta_{mn}^2 \gg (\ell-\ell_{mn})^2 \qquad (2.2.47)$$

Then, since the Δ_{mn} are constant, we have

$$\sum_m\sum_n G_{mn}(\ell-\ell_{mn}) = 0 \qquad (2.2.48)$$

so that

$$l = \frac{\sum_m \sum_n G_{mn} l_{mn}}{\sum\sum G_{mn}} = \frac{N}{2} \frac{\sum_m \sum_n G_{mn} \lambda_{mn}}{\sum_m \sum_n G_{mn}} \quad (2.2.49)$$

leading to a fractional error in measured velocity of

$$\frac{\Delta c}{c} = \frac{\sum_m \sum_n G_{mn}(\lambda_{mn}-\lambda_{oo})}{\sum_m \sum_n G_{mn}} = \frac{\sum\sum G_{mn} X_{mn}^2}{2b^2 k_{oo}^2 \sum_m \sum_n G_{mn}} \quad (2.2.50)$$

It may be seen from 2.2.49 that l at resonance depends only on the order of resonance, N, as would be the case if only the plane wave mode were present. Thus for situations such as these there can be no check from the observed separation of the resonances that errors resulting from parasitic modes are not occurring. Only if an examination of the symmetry of a resonance is made may such a situation become apparent, but even then it is uncertain since sets of amplitudes, G_{mn}, may easily occur which preserve the symmetry of the peak whilst still causing it to be displaced. For example, if a single unresolved mnth mode is present in the same strength as the 00th mode, resonances would remain almost perfectly symmetrical.

The range of applicability of the approximations 2.2.48 and 49 depends upon the validity of the inequality 2.2.47. If $(l_{00}-l_{mn})/2 = l(X_{mn}^2/bk_{00}^2)/4$ is taken as a rough estimate for $(l-l_{mn})$ then the requirement 2.2.47 becomes

$$l_{oo}^2 k_{oo}^2 \gg X_{mn}^2 / 16b^2 \quad (2.2.51)$$

The values presented in and with Tables 2.1 and 2.2 enable the quantity $\alpha_{00}^{2} k_{00}^{2}$ to be evaluated for various different frequencies. At a frequency of 1MHz in a cavity of 2cm diameter the approximation 2.2.48 is valid for modes where $X_{mn}^{4} \ll 10.3^{4}$ at the normal boiling point of helium-4 and where $X_{mn}^{4} \ll 8.2^{4}$ at NPT. Should higher modes be present in comparable strength to those satisfying these conditions a better way of estimating the error is required. Rather than attempt a solution of equation 2.2.46 it would be preferable to calculate a first excessive approximate value of l from 2.2.49 and use it to recalculate a new set of amplitudes, G'_{mn}, thus

$$G'_{mn} = G_{mn} \Big/ \left\{ 1 + \left(\frac{l - l_{mn}}{\Delta_{mn}} \right)^2 \right\}^2$$

$$= G_{mn} \Big/ \left\{ 1 + \frac{1}{4\alpha_{00}^2 k_{00}^2 b^4} \left(\frac{\sum_j \sum_k G_{jk} (X_{jk}^2 - X_{mn}^2)}{\sum_j \sum_k G_{jk}} \right)^2 \right\}^2 \qquad (2.2.52)$$

which could again be used in equation 2.2.48. This could be repeated until the values of the amplitudes converged. However, it is not anticipated that more than one recalculation would be necessary in most practical cases.

Inspection of the denominator in equation 2.2.52 reveals that the corrected amplitudes, G'_{mn}, will very rapidly become negligible once the order of the mode is high enough to ensure that $(l - l_{mn})^2 > \Delta_{mn}^2$. Thus it is possible to ignore these modes which, in any case, may be expected to be resolved. It is the case, therefore, that the above procedure offers a method of assessing errors due to higher modes whether they are far from being resolved or are, in fact, virtually resolved. The recalculated amplitudes, G'_{mn}, are not dependent on the value of l or the order of resonance, N so that our previous remarks on the impossibility of ensuring that higher modes were absent are

still valid when modes are present which are nearly resolved. The difficulty is thus seen to be entirely general at all frequencies where it is possible for at least one higher mode to be present. In particular, it applies to the instrument used by Plumb and Cataland [21-24] for their acoustic thermometry. If this is correct then it would appear they were mistaken in arguing that the constant separation of the resonances in their instrument as the order of resonance increased proved that only a single wavelength (assumed to be λ_{00}) was present. However, examination of the amplitudes, G_{mn}, which could be expected with their type of instrument at a frequency of 1 MHz will show that errors from this source are likely to be negligible. The possibility of detecting higher modes from the increase in absorption coefficient is dealt with in Appendix 2.2, but is found to be unreliable also.

2.2.4. Some Practical Cases

The first case to be considered is that of an ideal transducer executing perfect piston-like vibrations. Values of G_{mn} will be calculated for various diameters of transducer up to and including the cavity diameter, 2b. In the latter case we would expect to obtain the result of section 2.1 where only the 00 order mode is propagated. Initially it might be expected that any transducer executing such vibrations could excite only plane waves in the cavity. However it should be remembered that only modes characteristic of the cavity which satisfy the wave equation enter into the expansion of $\xi_0(r,\theta)$, and that if the transducer has a radius a<b there will be a discontinuity at r=a which cannot easily be approximated to with a plane wave. This is one more manifestation of a general feature of approximation by orthogonal functions - namely that when there are discontinuities present in the function to be represented, the higher terms in the expansion are required in greater strength. It is the

increasing number of maxima and minima usually found in the range of definition of the higher order functions which enables them to represent discontinuities more readily than the lower order members of the set.

The present case is shown in figure 2.6. From the definition of piston-like vibrations we have

$$\xi_0(r,\theta) = 0 \qquad (r \geq a)$$

$$\xi_0(r,\theta) = \xi_0 \qquad (r < a) \qquad (2.2.54)$$

From 2.2.39 and 2.2.42

$$G_{mn} = \left(2\rho c_{mn} \left\{ \pi b^2 (1-m^2/X_{mn}^2) J_m^2(X_{mn}) \right\} \right) \times \left(\int_0^a r J_m\left(\frac{X_{mn} r}{b}\right) dr \right)^2$$

$$\times \left\{ \left(\int_0^{2\pi} \cos m\theta \, d\theta \right)^2 + \left(\int_0^{2\pi} \sin m\theta \, d\theta \right)^2 \right\} \qquad (2.2.55)$$

or half this if m=0. Thus

$$G_{mn} = 0 \qquad (m > 0) \qquad (2.2.56)$$

$$G_{on} = \frac{4\pi\rho c_{on}}{b^2 J_o^2(X_{on})} \left(\int_0^a r J_o\left(\frac{X_{on} r}{b}\right) dr \right)^2$$

$$= 4\pi a^2 \rho c_{on} \left(\frac{J_1(X_{on} a\, b)}{X_{on} J_o(X_{on})} \right)^2 \qquad (2.2.57)$$

where n>0, and

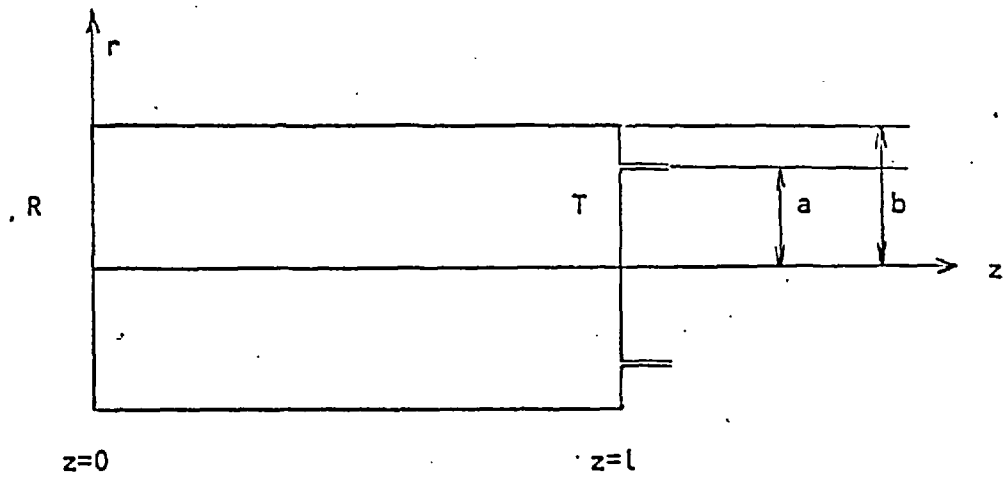

FIGURE 2.6

Showing an Ideal Transducer of Radius a Less than b.

$$G_{00} = 4\pi a^2 \rho c_{00} \cdot \frac{1}{4} \cdot \frac{a^2}{b^2} \qquad (2.2.58)$$

Several points of interest arise from these results. Firstly, as expected, $G_{mn} = 0$ if $m>0$ or $n>0$ and $a=b$. All amplitudes are zero if $m>0$ due to the θ-integrals of equation 2.2.55 and our not having specified any θ-dependence for the transducer vibrations. $G_{0n} = 0$ for $n>0$ when $a=b$ because $J_1(X_{0n}\, a/b) = J_1(X_{0n})$ is $dJ_0(X_{0n})/dX$ which is identically zero by definition of X_{0n}. Thus only plane waves may propagate in the cavity when $a=b$ concurring with the results of section 2.1. We have from equation 2.2.42

$$Z_{G_1}(\ell) = \pi b^2 c_{00} \left\{ R_{00}(\ell) - i X_{00}(\ell) \right\} \qquad (2.2.59)$$

in exact agreement with equation 2.1.9. If the plane wave amplitude, G_{00}, is expressed in terms of its value when $a=b$ we find

$$\frac{G_{00}(a \leq b)}{G_{00}(a = b)} = \frac{a^4}{b^4} \qquad (2.2.60)$$

showing that the amplitude of the plane wave falls off very rapidly as the diameter of the transducer decreases. This is attributable to two causes - the decrease in the power radiated due to the diminishing area of the transducer and the loss of that power which goes to excite the higher modes of vibration. The former effect applies equally to all modes of course, but nevertheless represents a practical difficulty in that the overall sensitivity of the interferometer is reduced. Expressing the 0nth amplitudes in the same units we have

$$\frac{G_{on}\,(a \leq b)}{G_{oo}\,(a = b)} = 4\,\frac{a^2}{b^2}\left(\frac{J_1(X_{on}\,a\,b)}{X_{on}\,J_o(X_{on})}\right)^2 \qquad (2.2.61)$$

The amplitudes G_{00} to G_{05} are shown in Table 2.4 for a/b=1, 3/4, 1/2 and 1/4. The fractional errors to be expected in a velocity of sound measurement have been calculated from equation 2.2.50 and are also included together with the resulting error in a temperature measurement made at 4.2K at a frequency of 1 MHz in a cavity of 2cm diameter. It can be seen that they are tolerably small even when a/b=1/4. When a/b is small the transducer behaves something like a point source in the cavity and the plane wave mode is barely excited at all. This situation is representative of interferometers where the cavity is excited by entering the sound through a small circular central port in one end face. Both De Laet [19] and Grimsrud and Werntz [25] used such a technique, but since both instruments were operated below the first cut-off frequency, f_{10}, they would not have led to experimental errors. However the value of G_{00} for a/b=1/4 shows how very inefficient a method of exciting plane waves this must be.

The second model to be considered is perhaps of more general application. Many transducers are unable to vibrate at their perimeter, but may flex to provide a useful amplitude at their centres. At frequencies below about 100KHz stiff metal diaphragms clamped at their perimeter and driven by a moving coil are frequently employed whilst at ultrasonic frequencies the conventional quartz crystal is often mounted in such a way as to restrict vibration at r=b. Some typical cases are shown in figure 2.7. In order to estimate the consequences of using such transducers we shall assume the following form for $\xi_0(r,\theta)$:

TABLE 2.4

Amplitudes G_{mn} for an Ideal Transducer.

n	a/b	G_{0n}	$2b^2 k_{00}^2 \Delta c/c$	ΔT at 4.2K (mK)
0	1	1.000 *	0	0
1		0.000		
2		0.000		
3		0.000		
4		0.000		
5		0.000		
0	3/4	0.317	16.8	0.26
1		0.249		
2		0.061		
3		0.010		
4		0.006		
5		0.008		
0	1/2	0.063	29.5	0.45
1		0.164		
2		0.061		
3		0.017		
4		0.001		
5		0.007		
0	1/4	0.004	46.2	0.71
1		0.019		
2		0.019		
3		0.009		
4		0.001		
5		0.000		

* By Definition

All amplitudes G_{mn} where m is greater than zero are zero.

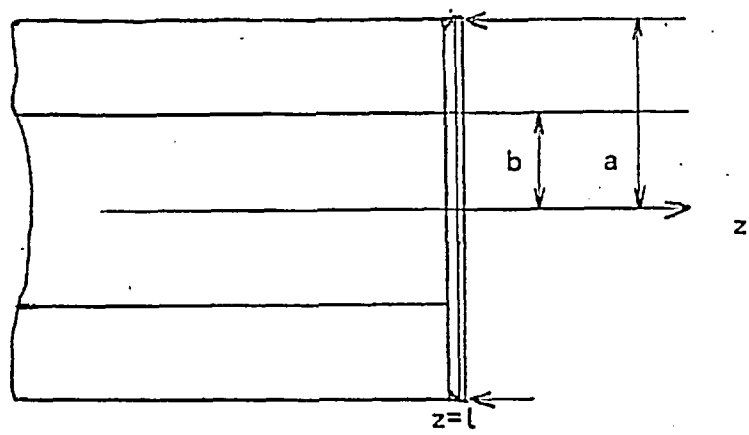

(a) Stiff Metal Diaphragm with Radius a Greater than the Cavity Radius b.

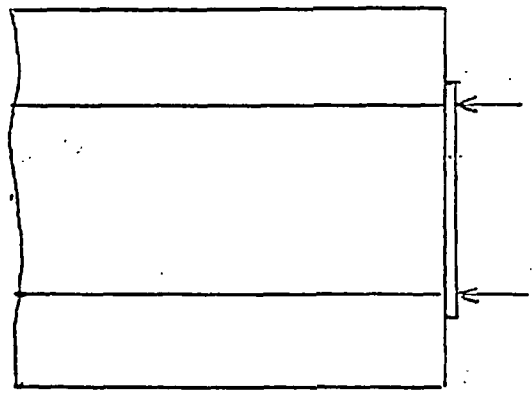

(b) Stiff Metal Diaphragm Clamped against Mouth of Cavity.

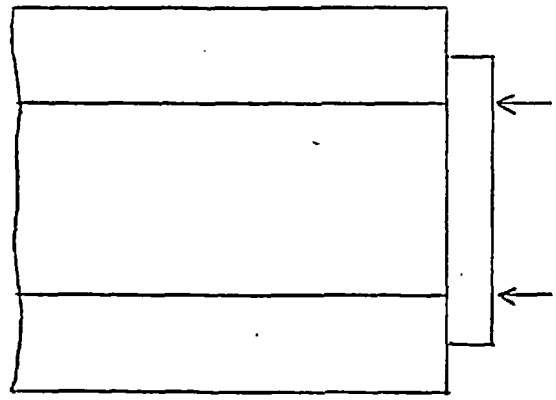

(c) Quartz Crystal Transducer Clamped against Mouth of Cavity.

FIGURE 2.7

Three Common Transducer Mountings

Where no Motion is Possible at the Perimeter of the Transducer.

$$\xi_o(r,\theta) = 0 \qquad (r \geq a)$$

$$\xi_o(r,\theta) = \xi_o e^{-r^2/(a^2-r^2)} \qquad (r > a)$$

(2.2.62)

Thus away from its equilibrium position the face of the transducer is conceived of as being bell-shaped with a maximum displacement, ξ_0, at its centre. Calculating the amplitudes, G_{mn}, as before we have:

$$G_{mn} = 0 \qquad (m > 0),$$

$$G_{on} = \frac{4\pi\rho c_{on}}{J_o^2(X_{on})} \cdot \frac{a^4}{b^2} \left(\int_0^L s\, e^{-s^2/(1-s^2)}\, J_o\left(\frac{X_{on}\, as}{b}\right) ds \right)^2$$

(2.2.63)

and

$$G_{oo} = 4\pi\rho c_{oo} \frac{a^4}{b^2} \left(\int_0^L s\, e^{-s^2/(1-s^2)}\, ds \right)^2 \quad (2.2.64)$$

where L=b/a if a>b and L=1 if a<b. The variable s has been substituted for r/a. The integrals have been evaluated numerically and the results are shown in Table 2.5 as before.

TABLE 2.5

Amplitudes G_{mn} for a Clamped Transducer.

n	a/b	G_{on}	$2b_{00}^2k^2$	$\Delta c/c$	ΔT at 4.2K (mK)
					7.8×10^{-4}
0	4	5.752	0.005		
1		0.002			
2		0.000			
3		0.000			
4		0.000			
5		0.000			
					2.5×10^{-2}
0	2	4.582	0.160		
1		0.037			
2		0.004			
3		0.000			
4		0.000			
5		0.000			
					1.1×10^{-1}
0	1	1.000 *	7.030		
1		0.658			
2		0.043			
3		0.002			
4		0.000			
5		0.000			
					1.9×10^{-1}
0	3/4	0.316	12.192		
1		0.609			
2		0.012			
3		0.018			
4		0.000			
5		0.001			
					4.1×10^{-1}
0	1/2	0.063	26.466		
1		0.235			
2		0.113			
3		0.007			
4		0.004			
5		0.003			
0	1/4	0.004	88.932		1.4
1		0.021			
2		0.029			
3		0.026			
4		0.016			
5		0.007			

* By Definition

All amplitudes G_{mn} where m is greater than zero are zero.

2.3 The Effect of Geometrical Misalignment of the Cavity End Faces.

Very often, when reporting values for sound velocities and absorption coefficients measured with acoustic interferometers, workers have omitted to mention what errors are attributable to mechanical misalignments in their instruments. In general it is tacitly assumed that if errors in geometry are small compared to the wavelength of sound in the medium under investigation, then any resulting acoustic errors will be negligible. At low frequencies this condition is easily achieved and often it has been thought unnecessary to state the tolerances to which an instrument has been built. At very high frequencies, on the other hand, when wavelengths can approach orders of smallness not far removed from what are normally considered to be fine engineering tolerances, it has occasionally been the practice to quote the accuracy to which transducers and reflectors have been aligned. But, again, no assessment of the errors to be expected is offered. Neither is it shown that the tolerances achieved are sufficient to make the errors negligible.

2.3.1 Bad Geometry and Velocity Errors.

Unfortunately, to solve the problem of evaluating the wave field at any point within a cavity whose end faces may be described by the equations

$$z = z_R(r,\theta) \ll \lambda, \ell \qquad (2.3.1)$$

and

$$z = z_T(r,\theta) + \ell \qquad (z_T(r,\theta) \ll \lambda, \ell) \quad (2.3.2)$$

is not easy because the solution to the wave equation fails to separate as in the case of perfect geometry. However, we may attempt

an approximate treatment of the problem which yields a separable solution at frequencies below the lowest cut-off frequency of the cavity.

It is supposed that normal modes, φ_{mn}, of the form

$$\varphi_{mn} = J_m\left(\frac{X_{mn}r}{b}\right)\left(A_{mn}\cos m\theta + B_{mn}\sin m\theta\right)e^{i(\omega t \pm q_{mn}z)} \qquad (2.3.3)$$

propagate in the interferometer. For values of m and n greater than zero, however, the modes will be evanescent and will only travel extremely short distances before becoming severely attenuated. Thus it is only necessary to consider such modes in the immediate vicinity of the end faces where they arise from the incidence of the plane wave mode which is the principal constituent of the wave field in the cavity. It is also assumed that because the errors in geometry are small, the amplitudes of the higher modes are small even in the neighbourhood of the end faces. And for the same reason we write

$$-\nabla\varphi\Big|_{z=z_R(r,\theta)} \doteq -\frac{\partial\varphi}{\partial z}\Big|_{z=z_R(r,\theta)} = 0 \qquad (2.3.4)$$

for an approximate boundary condition on the end face. Thus for a plane wave

$$\varphi = A\, e^{i(\omega t + q_{00}z)} \qquad (2.3.5)$$

incident upon an end face we have

$$q_{oo} A e^{iq_{oo} z_R(r,\theta)} =$$

$$- \sum_m \sum_n \left\{ q_{mn} (A_{mn} \cos m\theta + B_{mn} \sin m\theta) \right.$$

$$\left. \times J_m\left(\frac{X_{mn} r}{b}\right) e^{-iq_{mn} z_R(r,\theta)} \right\} \qquad (2.3.6)$$

Multiplying both sides by $\exp(iq_{00} z(r,\theta))$ this becomes

$$q_{oo} A e^{2iq_{oo} z_R(r,\theta)} =$$

$$-\sum_m \sum_n q_{mn} (A_{mn} \cos m\theta + B_{mn} \sin m\theta) J_m\left(\frac{X_{mn} r}{b}\right) e^{i(q_{oo} - q_{mn}) z_R(r,\theta)}$$

$$\doteq - \sum_m \sum_n q_{mn} (A_{mn} \cos m\theta + B_{mn} \sin m\theta) J_m\left(\frac{X_{mn} r}{b}\right).$$

The approximation follows because $z(r,\theta)$ is very small as are A_{mn} and B_{mn} when $m,n>0$ and because when $m,n=0$ the index in the exponential term on the right hand side vanishes. Integration from $\theta=0$ to 2π and from $r=0$ to b now yields

$$R_R = \frac{A_{00}}{A} = \frac{1}{\pi b^2}\int_0^b \int_0^{2\pi} r e^{2iq_{00} z_R(r,\theta)} dr d\theta$$

$$\doteq \frac{1}{\pi b^2}\int_0^b \int_0^{2\pi} r\left(1 + 2iq_{00} z_R(r,\theta) - 2q_{00}^2 z_R^2(r,\theta)\right) dr d\theta$$

$$= 1 - \frac{8\pi}{b^2\lambda_{00}^2}\int_0^b \int_0^{2\pi} r z_R^2(r,\theta)\, dr d\theta$$

$$+ i\frac{4}{b^2\lambda_{00}}\int_0^b \int_0^{2\pi} r z_R(r,\theta)\, dr d\theta \qquad (2.3.8)$$

Thus we see that the attenuation of the reflected plane wave is only of the order $z_R^2(r,\theta)$ but that there is a phase change of order $z_R(r,\theta)$. A similar reflection coefficient may be derived for a wave incident upon an end face from the opposite direction, but here the phase change is of the opposite sign. We have therefore

$$R_R = 1 - \varepsilon_R + i\delta_R$$

$$R_T = 1 - \varepsilon_T - i\delta_T \qquad (2.3.9)$$

where

$$\delta_{R,T} = \frac{4}{b^2\lambda_{oo}} \int_0^b \int_0^{2\pi} r\, z_{R,T}(r,\theta)\, dr\, d\theta \qquad (2.3.10)$$

and

$$\varepsilon_{R,T} = \frac{8\pi}{b^2\lambda_{oo}^2} \int_0^b \int_0^{2\pi} r\, z_{R,T}^2(r,\theta)\, dr\, d\theta \qquad (2.3.11)$$

The effect of such complex reflection coefficients may be seen from equation 2.1.4. It is to add a term $(\delta_R - \delta_T)/l$ to the wavenumber, k, in the denominator which essentially determines where resonance is going to occur. Thus a fractional error in the measured velocity of sound results given by

$$\frac{\Delta c}{c} = -\frac{\Delta k}{k} = \frac{\delta_T - \delta_R}{kl} \qquad (2.3.12)$$

Equation 2.1.4 should be further modified by a factor $\exp(-i\delta_T/2)$ on the right hand side arising from the fact that the transducer, being geometrically imperfect, imparts a phase change to the wave it emits. But since all partial waves have this factor it may be omitted in a discussion of velocity errors.

Evaluation of the velocity error to be expected from a practical instrument is now possible given the form of the functions $z_R(r,\theta)$ and $z_T(r,\theta)$. It will be calculated for two important practical examples. However, the error will only arise, in principle, for a cavity of

fixed length (*1) as will be argued in section 4.2 (although end effects will be encountered in a variable path cavity if the end faces - in particular the moving one - change their alignment during a measurement). Whether or not this is true for a cavity operated above the first cut off frequency cannot be said on the basis of this simple theory.

2.3.2 Tilted End Faces.

It will now be assumed that the end faces are perfectly flat, but tilted off axis as in figure 2.8. If the maximum angle of tilt is χ where $\chi \ll 1$ in a direction $\theta=\theta_0$ we have

$$z_{R,T}(r,\theta) = \pm \chi_{R,T} \cos(\theta - \theta_{0_{R,T}}) \qquad (2.3.13)$$

so that

$$\delta_{R,T} = \frac{4b\chi_{a,T}}{3\lambda_{00}} \int_0^{2\pi} \cos(\theta - \theta_{0_{R,T}})\, d\theta \qquad (2.3.14)$$

$$= 0$$

and

---

(1) It would be more correct to say that it only arises in cavities whose measured geometrical length (as opposed to their effective acoustic length) is used in the calculation of the velocity of sound. Thus it need be of no concern where the distance separating resonances is measured.

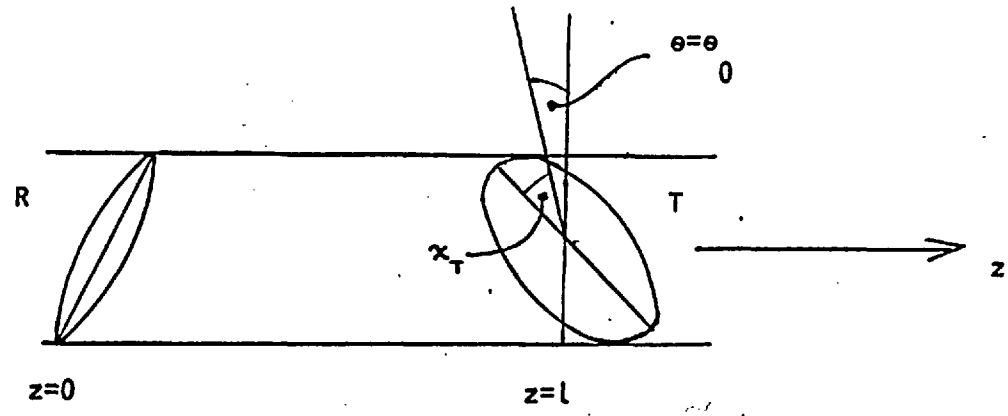

FIGURE 2.8

An Interferometer with Tilted Transducer and Reflector.

$$\varepsilon_{R,T} = \frac{8\pi\chi^2_{R,T}}{b^2\lambda_{oo}^2}\int_0^b\int_0^{2\pi} r^3\cos^2(\theta-\theta_{oR,T})\,dr\,d\theta$$

$$= 2\pi^2 b^2\chi^2_{R,T} \,/\, \lambda_{oo}^2 \qquad (2.3.15)$$

Thus, since $\delta_{R,T}$ is zero, the only effect of a tilted end face is to decrease Herzfeld's real reflection coefficient, γ, by an amount of order $b^2\chi^2_{R,T}/\lambda^2_{00}$. It is not even necessary to call for the finest engineering tolerances to ensure that this term is no greater than 10^{-5} or 10^{-6} and so entirely negligible compared to reflection losses from boundary layer mechanisms.

2.3.3 The Flatness of the End Faces.

End faces which are not flat, like imperfect transducers, are not easy to treat in a general way since it is difficult to find a model for them which typifies faults in a wide range of instruments. In order to obtain an approximate idea of what is to be expected δ and ε will be calculated for a parabolically concave or convex end face. We write

$$\chi_{R,T}(r,\theta) = \chi_{R,T}\, r^2/b^2 \qquad (2.3.16)$$

Again, χ is a parameter which is a measure of the geometrical imperfection present being the depth of the parabolic face. From equation 2.3.10

$$\delta_{R,T} = \frac{4\chi_{R,T}}{b^4\lambda_{oo}}\int_0^b\int_0^{2\pi} r^3\,dr\,d\theta = 2\pi\,\frac{\chi_{R,T}}{\lambda_{oo}} \qquad (2.3.17)$$

whilst from equation 2.3.11

$$\varepsilon_{R,T} = \frac{8\pi\,\chi^2_{R,T}}{b^6\,\lambda^2_{00}} \int_0^b \int_0^{2\pi} r^5\, dr d\theta = \frac{8\pi}{3} \cdot \frac{\chi^2_{R,T}}{\lambda^2_{00}}$$

(2,3,18)

As before $\varepsilon_{R,T}$ is easily made small enough to be of no consequence, but now $\delta_{R,T}$ is of the order $\chi_{R,T}/\lambda_{00}$. But from equation 2.3.12 it can be seen that if the fractional error in a velocity measurement is not to become comparable to the precision otherwise expected from the instrument, then the expression $\chi_{R,T}/k\,\lambda_{00}\,l_{00}$ must not exceed several parts in 10^4.

CHAPTER III

THE PROBLEM OF THE BOUNDARY LAYER

It has already been pointed out that the simple boundary conditions of Chapter.II are not entirely realistic. Hitherto we have required only the normal component of the particle velocity to vanish at the boundary whereas for a viscous fluid the tangential component should also vanish. Furthermore, the presence of a solid boundary may be expected to disturb the temperature field associated with the particle velocity field. In the vicinity of the interface acoustic propagation would tend to be isothermal rather than adiabatic due to the enormous thermal conductivity of a solid compared to a gas. Thus the velocity of sound would lie somewhat to the Newtonian side of the Laplacian value.

3.1 The Theory of the Boundary Layer.

Helmholtz was the first to attempt to treat this problem in 1863. By taking the effect of viscosity into account he was able to derive a quantitative estimate for the decrease in the velocity of sound propagated in an infinitely long tube. Five years later Kundt reported only a qualitative agreement with Helmholtz's predictions and suggested that the thermal conductivity of the walls be taken into account. This calculation was carried out by Kirchhoff in the same year leading to results which we prefer to quote in the following form:

$$\frac{\Delta c}{c} = \frac{A}{b}(2\omega)^{-\frac{1}{2}} \qquad (3.1.1)$$

expressing the fractional error in velocity, c, to be added to values measured in infinite tubes to obtain the values which would be measured in the unbounded medium. Here

$$A = \nu^{\frac{1}{2}} + (\sigma - 1)\left(\frac{K}{\rho c_p}\right)^{\frac{1}{2}} \qquad (3.1.2)$$

The acoustic absorption coefficient was found to be

$$\alpha = \frac{A}{b\,c}\left(\frac{\omega}{2}\right)^{\frac{1}{2}} \qquad (3.1.3)$$

Considerable discussion of these results has taken place. Weston[36] has clarified the exact conditions under which Kirchhoff's various approximations apply, and Shields, Lee and Wiley[37] have tested them against a more exact numerical solution of the problem. They find that the fractional error due to approximation in the correction is no greater than the fractional correction itself. Other work has also been done to extend the scope of the Kirchhoff-Helmholtz corrections. Molecular slip, flexible or porous walls and walls with low thermal conductivity could all, in principle, affect the form of the correction. These effects have been investigated theoretically by Henry[38] together with the effect of a temperature discontinuity at the boundary (an analysis later corrected by Weston[36]). Similar treatments to that of Kirchhoff have also been given to finite

amplitude propagation in tubes and to the propagation of pulses. But, most important for our purposes, the effect of end reflectors has been considered. In 1907 Thiesen derived a quantitative expression for the boundary layer effect on the velocity of sound in an interferometer rather than in an infinite cylinder[39]. The existence of a second small term in addition to the term found by Kirchhoff was proven:

$$\frac{\Delta c}{c} = \frac{A}{b}(2\omega)^{-\frac{1}{2}} - \frac{A'}{l}\left(\frac{\omega}{2}\right)^{-\frac{1}{2}}$$

$$= \left\{\frac{A}{2b} - \frac{A'}{l}\right\}\left(\frac{\omega}{2}\right)^{-\frac{1}{2}} \qquad (3.1.4)$$

where

$$A' = A - \nu^{\frac{1}{2}} \qquad (3.1.5)$$

At infinite cavity lengths this result agrees with Kirchhoff's as expected.

More recently Fritche[40] has given a somewhat wider and simpler treatment of the problem which is capable of giving the boundary layer corrections to the phase velocities and absorption coefficients of the higher modes as well as to those of the plane wave mode which is the only mode of propagation to which the results of Kirchhoff and Thiesen may be applied. Unfortunately, since his main preoccupation was with the accurate measurement of absorption coefficients, the treatment of velocity errors was developed to a lesser extent. Because of this and because all of these workers have written in German we shall outline a solution to the boundary layer problem for a variable path interferometer which will show that Fritche's approach yields the same answer as originally obtained by Thiesen when applied to plane waves. It will also be indicated how the corrections to the phase velocities

and absorption coefficients of the higher modes may be obtained should they be required.

3.1.1 Towards a Simple Statement of the Problem.

In considering a fluid where the effects of heat conduction and viscosity may no longer be ignored it becomes necessary to employ as many as five equations in the initial specification of the problem. This section will be devoted to reaching a briefer and more tractable statement. The five equations are:

$$\frac{\partial \rho}{\partial t} + \rho_0 \nabla . \underline{v} = 0 \qquad (3.1.6)$$

(the equation of continuity asserting the conservation of the fluid),

$$\rho_0 \frac{\partial \underline{v}}{\partial t} + \nabla P = \eta_1 \nabla^2 \underline{v} + \eta_2 \nabla \nabla . \underline{v} \qquad (3.1.7)$$

(the Navier-Stokes equation which is the equation of motion for a viscous fluid replacing the simpler equation of Euler for an ideal fluid),

$$P = \rho \frac{RT}{M} = \rho (c_p - c_v) T \qquad (3.1.8)$$

(the equation of state for an ideal gas which should be a satisfactory approximation to the virial equation of state for the purposes of examining a small correction to ideal propagation at any pressure likely to be of interest),

$$-P \nabla . \underline{v} = \rho c_v \frac{\partial T}{\partial t} + \nabla . \underline{W} \qquad (3.1.9)$$

(stating that energy is conserved in an elementary volume of fluid if frictional losses may be neglected) and, finally

$$\underline{W} = - K \nabla . T \qquad (3.1.10)$$

which is Fourier's Law of heat conduction. Compared to conduction losses, losses from a volume element of fluid by radiation may be shown to be entirely negligible for our purposes. Zero subscripts indicate here that the subscripted variable takes its mean value - that is its value in the absence of an acoustic disturbance. The vector $\underline{v}$ is the particle velocity and c_p and c_v are the specific heats per unit mass at constant pressure and volume respectively. η_1 is the layer viscosity whilst η_2 is a quantity given by $\eta_2 = \zeta + 1/3 \eta_1$ where ζ is the bulk viscosity. $\underline{W}$ is a vector giving the field of heat flow associated with the particle velocity field $\underline{v}$.

Kirchhoff, Thiesen and Fritche all proceed in essentially the same way to reduce these five equations to three partial differential equations in three variables. Unlike the particle velocity field for an ideal fluid, $\underline{v}$ may no longer be considered to be irrotational. We must therefore write

$$\underline{v} = \nabla \varphi + \nabla \wedge \underline{a} \qquad (3.1.11)$$

where φ and $\underline{a}$ are respectively scalar and vector fields. We also require that $\nabla . \underline{a}$ be zero in order that φ and $\underline{a}$ thus defined are uniquely specified. Taking the divergence of both sides of this

equation therefore gives:

$$\nabla^2 \varphi = \nabla . \underline{v} \qquad (3.1.12)$$

Thus, by substituting for $\underline{v}$ and $\nabla . \underline{v}$ from equation 3.1.11 and 3.1.12 into the Navier-Stokes equation, 3.1.7, we obtain:

$$\underline{V} \equiv \nabla \Phi + \nabla \wedge \underline{A} = 0 \qquad (3.1.13)$$

where

$$\Phi \equiv \frac{\partial \varphi}{\partial t} + \frac{P}{\rho_0} - (\nu_1 + \nu_2) \nabla^2 \varphi \qquad (3.1.14)$$

and

$$\underline{A} \equiv \frac{\partial \underline{a}}{\partial t} - \nu_1 \nabla^2 \underline{a} \qquad (3.1.15)$$

where ν_1 (previously ν) $= \eta_1 / \rho_0$ and $\nu_2 = \eta_2 / \rho_0$.

Since the divergence of $\underline{a}$ is zero we have:

$$\nabla . \underline{A} = 0 \qquad (3.1.16)$$

making an obvious analogy between equations 3.1.13 and 3.1.11. Thus the Navier-Stokes equation has been used to show that a new "particle velocity", $\underline{V}$, may be expressed in terms of a scalar potential, Φ, and a vector potential, $\underline{A}$ related to the true velocity potentials as above.

Taking the divergence of equation 3.1.13 yields:

$$\nabla^2 \mathfrak{P} = 0 \qquad (3.1.17)$$

which is the first of the new equations, $\mathfrak{P}$ being the first of the new variables.

The variables P, $\underline{W}$ and $\underline{v}$ may now be eliminated from the energy equation 3.1.9 using the equation of state, 3.1.8, Fourier's law, 3.1.10, and equation 3.1.12. If the acoustic motion is of sufficiently small amplitude this yields:

$$-\nu_3 \nabla^2 \Theta + \frac{\partial \Theta}{\partial t} + \nabla^2 \varphi = 0 \qquad (3.1.18)$$

where $\nu_3 = K/\rho_0 c_v$ is the thermal diffusivity and

$$\Theta = \frac{1}{\sigma - 1} \frac{T - T_0}{T_0} \qquad (3.1.19)$$

$(T-T_0)/T_0$ being the fractional change in temperature associated with a given point in the fluid (giving a similar interpretation to the scalar field Θ). Equation 3.1.18 is the second of the three new fundamental equations and Θ the second new variable.

The remaining new equation is obtained from equation 3.1.14 which on differentiating with respect to time becomes:

$$\frac{\partial \mathfrak{P}}{\partial t} = \frac{\partial^2 \varphi}{\partial t^2} - (\nu_1 + \nu_2) \frac{\partial}{\partial t} \nabla^2 \varphi + \frac{\partial}{\partial t}\left(\frac{P}{\rho_0}\right) \qquad (3.1.20)$$

In order to evaluate the last term we turn to the equation of state 3.1.8. For the small changes in P, ρ and T associated with an acoustic

disturbance it gives:

$$\frac{P - P_0}{P_0} = \frac{\rho - \rho_0}{\rho_0} + \frac{T - T_0}{T_0} = \frac{\rho - \rho_0}{\rho_0} + (\sigma - 1)\,\theta$$

(3.1.21)

Differentiating this with respect to time and substituting for $\partial\rho/\partial t$ from the equation of continuity we obtain:

$$\frac{\partial}{\partial t}\left(\frac{P}{\rho_0}\right) = -\frac{c^2}{\sigma}\nabla^2\varphi + c^2\frac{(\sigma-1)}{\sigma}\frac{\partial\theta}{\partial t} \qquad (3.1.22)$$

where $c=(\sigma P_0/\rho_0)^{1/2}$ is the velocity of sound in the absence of boundary layer effects. Thus from equation 3.1.20

$$\frac{\partial\Phi}{\partial t} = \frac{\partial^2\varphi}{\partial t^2} - (\nu_1+\nu_2)\frac{\partial}{\partial t}\nabla^2\varphi + \frac{c^2}{\sigma}\nabla^2\varphi + \frac{c^2}{\sigma}(\sigma-1)\frac{\partial\theta}{\partial t}$$

(3.1.23)

which is our third new equation and φ the remaining new variable. Assuming a harmonic time dependence of angular frequency, ω, for the fields Φ, θ and φ the equations become:

$$\nabla^2\Phi = 0 \qquad (3.1.24)$$

$$\nu_3\nabla^2\theta + i\omega\theta - \nabla^2\varphi = 0 \qquad (3.1.25)$$

$$\frac{c^2}{\sigma}(\sigma-1)i\omega\theta + \left\{\frac{c^2}{\sigma} - i\omega(\nu_1+\nu_2)\right\}\nabla^2\varphi + \omega^2\varphi - i\omega\Phi = 0$$

(3.1.26)

where the functions Φ, θ and φ no longer have time as an argument, but are functions solely of position.

The procedure now adopted by Kirchhoff was to eliminate Φ and φ from three equations similar to these leaving a single equation of fourth order in θ. Solution of this equation yielded a complex wavenumber which could be associated with the propagation of any of several acoustic variables since they would all propagate with a constant phase relationship with θ. Thus the required corrections to velocity and absorption coefficients were available from the real and imaginary parts of the wavenumber respectively. Fritche and Thiesen, on the other hand, start by expanding Φ, θ and φ in terms of the solutions of the wave equation:

$$\nabla^2 \psi_n + q_n^2 \psi_n = 0 \qquad (3.1.27)$$

and point out that they must all contain the same number of terms ψ_1, ψ_2, ψ_3, etc. in their expansions so that the wave fields of the functions are of the same general form. Their respective phase relationships at any given point may be accounted for in the coefficients of the expansions. Thus

$$\varphi = \sum_{n=0}^{N} \psi_n \qquad (3.1.28)$$

$$\theta = \sum_{n=0}^{N} a_n \psi_n \qquad (3.1.29)$$

$$\Phi = \sum_{n=0}^{N} b_n \psi_n \qquad (3.1.30)$$

where a_n and b_n will generally be complex. Substitution of these series into the three fundamental equations 3.1.24 to 3.1.26 yields

$$q_n^2 b_n = 0 \qquad (3.1.31)$$

$$\omega^2 - q_n^2 \left\{ \frac{c^2}{\sigma} - i\omega(\nu_1 + \nu_2) \right\} + \frac{c^2}{\sigma}(\sigma - 1) i\omega a_n - i\omega b_n = 0 \qquad (3.1.32)$$

and

$$-\nu_3 q_{nn}^2 a + i\omega a_n + q_n^2 = 0 \qquad (3.1.33)$$

Thus if $q_n \neq 0$ we have $b_n = 0$ from the first equation whilst from the last two

$$q_n^4 \left\{ \frac{1}{\sigma k^2} + \frac{1}{q_V^2} \right\} \frac{1}{q_T^2} - q_n^2 \left\{ \frac{1}{k^2} + \frac{1}{q_V^2} + \frac{1}{q_T^2} \right\} + 1 = 0 \qquad (3.1.34)$$

where

$$k^2 = \omega^2 / c^2 \qquad (3.1.35)$$

as before, and

$$q_T = \left\{ \frac{i\omega}{\nu_3} \right\}^{\frac{1}{2}} = \frac{1+i}{\sqrt{2}} \left\{ \frac{\omega \rho c_v}{K} \right\}^{\frac{1}{2}} \qquad (3.1.36)$$

and

$$q_V = \left\{ \frac{i\omega}{\nu_1 + \nu_2} \right\}^{\frac{1}{2}} = \frac{1+i}{\sqrt{2}} \left\{ \frac{\omega}{\nu_1 + \nu_2} \right\}^{\frac{1}{2}} \qquad (3.1.37)$$

From the last equation, 3.1.33,

$$a_n = \frac{1}{i\omega} \frac{q_n^2 q_T^2}{q_n^2 - q_T^2} \qquad (3.1.38)$$

and from the wave equation q_0 will be zero so that $a_0 = 0$ also. It then follows from equation 3.1.32 that $b_0 = -i\omega$. So finally

$$\varphi = \Psi_0 + \Psi_1 + \Psi_2 \qquad (3.1.39)$$

$$\Theta = a_1 \Psi_1 + a_2 \Psi_2 \qquad (3.1.40)$$

$$\Phi = -i\omega \Psi_0 \qquad (3.1.41)$$

The small number of terms arises from equation 3.1.34 which being quadratic in q_n^2 has only two independent solutions which we call q_1 and q_2. These are approximately

$$q_1^2 \doteq k^2 \left\{ 1 + \frac{i\omega}{c^2} \left[\nu_1 + \nu_2 + \left(\frac{\sigma - 1}{\sigma} \right) \nu_3 \right] \right\} \doteq k^2 \qquad (3.1.42)$$

and

$$q_2^2 \doteq \sigma q_T^2 \left\{ 1 - \frac{i\omega\sigma}{c^2} \left[\nu_1 + \nu_2 - \frac{\nu_3}{\sigma} \right] \right\} \doteq \sigma q_T^2 \qquad (3.1.43)$$

where q_1 and q_2 are to be regarded as the complex wavenumbers of the

Ψ_1 and Ψ_2 waves respectively. Evaluation of the imaginary part of q_1 will yield the classical absorption coefficient for a viscous gas with a small, but finite, thermal conductivity. This will be put aside until we are in a position to evaluate the propagation constant for an infinite tube, however. But we are now ready to retrieve the conventional acoustic variables $\underline{v}$ and p from the functions $\underline{\Phi}$, Θ and φ and to assess some of the qualitative aspects of the wave field when boundary layer effects are present.

3.1.2 The Existence of an Acoustic Boundary Layer and its Properties.

The particle velocity, $\underline{v}$, may be calculated from equation 3.1.1 once the vector potential, $\underline{a}$, is known. From equation 3.1.15 we have:

$$\nabla^2 \underline{a} + q_3^2 \underline{a} = -\frac{\underline{A}}{\nu_1} \qquad (3.1.44)$$

where

$$q_3 = \left\{\frac{i\omega}{\nu_1}\right\}^{\frac{1}{2}} = \frac{1+i}{\sqrt{2}} \left\{\frac{\omega}{\nu_1}\right\}^{\frac{1}{2}} \qquad (3.1.45)$$

The solution of this differential equation will be

$$\underline{a} = -\frac{\underline{A}}{i\omega} + \underline{\Psi}_3 \qquad (3.1.46)$$

so that

$$\underline{v} = \nabla\varphi + \nabla\wedge\underline{a}$$

$$= \nabla(\Psi_0 + \Psi_1 + \Psi_2) - \frac{1}{i\omega}\nabla\wedge\underline{A} + \nabla\wedge\underline{\Psi}_3$$

$$= \nabla(\Psi_1 + \Psi_2) + \nabla\wedge\underline{\Psi}_3 - \frac{1}{i\omega}(\nabla\Phi + \nabla\wedge\underline{A})$$

Thus

$$\underline{v} = \nabla(\Psi_1 + \Psi_2) + \nabla\wedge\underline{\Psi}_3 \qquad (3.1.47)$$

while

$$\Theta = a_1\Psi_1 + a_2\Psi_2 \qquad (3.1.48)$$

and

$$\nabla^2\Psi_n + q_n^2\Psi_n = 0 \qquad (3.1.49)$$

In the absence of thermal conduction and friction $\nu_1=\nu_2=\nu_3=0$ so that from equations 3.1.42 and 43 $q_1=k$ whilst the imaginary (dissipative) parts of q_2 and q_3 become infinite. Thus the Ψ_2 and $\underline{\Psi}_3$ waves do not propagate whilst the Ψ_1 wave propagates with the real wavenumber, k, of an unattenuated sound wave in an ideal fluid. The three basic equations 3.1.47 to 49 then become:

$$\underline{v} = \nabla \Psi_1 \qquad (3.1.50)$$

$$\Theta = a_1 \Psi_1 \qquad (3.1.51)$$

where from equation 3.1.33 $a_1 = i\omega/c^2$, and

$$\nabla^2 \Psi_1 + k^2 \Psi_1 = 0 \qquad (3.1.52)$$

It may now be seen that $\Psi_1 = \varphi$ is the familiar velocity potential of an adiabatic sound wave in an inviscid fluid.

When ν_1, ν_2 and ν_3 take on finite values, however, Ψ_2 and Ψ_3 are able to propagate, but even then only for very short distances since they are so highly attenuated. Using the values presented with table 2.1 to calculate q_2 and q_3 at a pressure of one atmosphere and a temperature of 4.2 K for a frequency of 10 kHz we have:

$$q_2 \doteq (1+i)\left\{\frac{\alpha\omega}{2\nu_3}\right\}^{\frac{1}{2}} \doteq (1+i) \times 1.1 \times 10^2 \text{ cm}^{-1}$$

and

$$q_3 \doteq (1+i)\left\{\frac{\omega}{2\nu_1}\right\} \doteq (1+i)\times 4.9\times 10^3 \ \mathrm{cm}^{-1}$$

the imaginary parts of which may be seen to constitute a massive absorption coefficient. The distances these waves travel before becoming severely attenuated are therefore of the order of 0.01 cm. This being the case they would not be expected to be present throughout the wave field in any significant strength, but would appear only at boundary surfaces if at all. The distance of 0.01 cm would then be a measure of the thickness of the "boundary layer" or that layer in which they may be said to propagate. The application of suitable boundary conditions for a gas-solid interface shows that they do in fact occur.

From the expressions used to calculate q_2 and q_3 it can be seen that the propagation of Ψ_2 and $\underline{\Psi}_3$ depends upon ν_3, the thermal diffusivity, and ν_1, the shear viscosity, respectively. We shall thus refer to them as a "temperature" wave (recalling Herzfeld's usage mentioned in section 2.1) and a "viscous" wave. This is not, of course, intended to suggest that Ψ_2 and $\underline{\Psi}_3$ represent wave-like temperature or viscosity fields - their physical interpretation is only available through the three equations 3.1.39 to 41.

It is also important to realise that whilst the waves Ψ_2 and $\underline{\Psi}_3$ contribute to the particle velocity, $\underline{v}$, and to the "excess temperature", Θ, they do not contribute to the acoustic pressure, p. Consequently the work integral per cycle

$$dW \propto \oint p v \, dt$$

for some elementary area will not vanish due to the phase shift in $\underline{v}$ relative to p brought about by the contributions of Ψ_2 and Ψ_3 to $\underline{v}$. Were it not for this p and $\underline{v}$ would remain in phase and boundary layer losses would not occur. Substituting for φ in equation 3.1.25 from equation 3.1.22 we find

$$p = \frac{\rho_0 c^2}{\sigma q_T^2} \left\{ \nabla^2 \theta + \sigma q_T^2 \theta \right\} \qquad (3.1.53)$$

Since θ itself depends only upon Ψ_1 and Ψ_2 it can be seen that Ψ_3 will not contribute to the acoustic pressure. Noting that $q_2^2 = \sigma q_T^2$ this becomes

$$p = \frac{\rho_0 c^2}{q_2^2} \left\{ a_1 \left(\nabla^2 \Psi_1 + q_2^2 \Psi_1 \right) + a_2 \left(\nabla^2 \Psi_2 + q_2^2 \Psi_2 \right) \right\}$$

$$(3.1.53)$$

Since the second term on the right hand side is zero, p will not depend upon Ψ_2 either which confirms our assertion that the acoustic pressure remains unchanged by boundary layer effects.

3.1.3 Boundary Layer Corrections Associated with the Radial Boundary Conditions.

If the wave equation for $\underline{\Psi}_3$ is expressed in cylindrical coordinates and it is assumed that $\underline{\Psi}_3$ has no azimuthal dependence, it becomes

$$\nabla^2 \Psi_{3r} + \left(q_3^2 - \frac{1}{r^2}\right)\Psi_{3r} = 0 \qquad (3.1.55)$$

$$\nabla^2 \Psi_{3\theta} + \left(q_3^2 - \frac{1}{r^2}\right)\Psi_{3\theta} = 0 \qquad (3.1.56)$$

and

$$\nabla^2 \Psi_{3z} + q_3^2 \Psi_{3z} = 0 \qquad (3.1.57)$$

where the subscripts r,θ and z refer to the directional components of $\underline{\Psi}_3$. Demanding symmetry about the z axis limits the generality of the treatment, but greatly simplifies the problem at this stage because it enables the vector field, $\underline{\Psi}_3$, to be replaced by a scalar field. We write

$$\Psi_{3r} = \Psi_{3z} = 0 \qquad (3.1.58)$$

and

$$\Psi_{3\theta} = -\frac{\partial^2 G}{\partial r \, \partial \theta} \qquad (3.1.59)$$

where G satisfies the wave equation

$$\nabla^2 G + q_3^2 G = 0 \qquad (3.1.60)$$

The scalar function G is then seen to have a propagation constant q_3, so that in conformity with our current notation we denote it by Ψ_3.

We are now in a position to express $\underline{v}$ in terms of these functions so that the appropriate boundary conditions may be applied to them. We have

$$\underline{v} = v_r \underline{r} + v_\theta \underline{s} + v_z \underline{t}$$

$$= \nabla(\Psi_1 + \Psi_2) + \nabla \wedge \underline{\Psi}_3 \qquad (3.1.61)$$

Thus

$$v_r = \frac{\partial}{\partial r}\left\{\Psi_1 + \Psi_2 + \frac{\partial^2 \Psi_3}{\partial z^2}\right\} \qquad (3.1.62)$$

$$v_\theta = 0 \qquad (3.1.63)$$

$$v_z = \frac{\partial}{\partial z}\left\{ \Psi_1 + \Psi_2 - \left(\frac{\partial^2 \Psi_3}{\partial r^2} + \frac{1}{r}\frac{\partial \Psi_3}{\partial r} \right) \right\} \qquad (3.1.64)$$

to which we add

$$\Theta = a_1 \Psi_1 + a_2 \Psi_2 \qquad (3.1.65)$$

to form the current set of working equations for the problem.

If the wave, Ψ_1, is now expanded in terms of Bessel functions of the first kind of order zero we have

$$\Psi_1 = \sum_n A_n J_0(X_n r/b) e^{iq_{1n}z} \qquad (3.1.66)$$

Thus Ψ_1 satisfies the wave equation as required (these terms being of the same form as the terms φ_{0n} of the previous chapter in the expansion of Φ). The value of X_n and hence of q_{1n} will be determined by the radial boundary conditions applied to the wave field. Previously it was required that

$$\frac{\partial}{\partial r} J_o\left(\frac{X_{on} r}{b}\right)\Bigg|_{r=b} = 0 \qquad (3.1.67)$$

Since the new radial boundary condition to be derived from equations 3.1.62 and 65 will be different, we expect X_n to differ slightly from X_{On}. Consequently q_{1n}, which is given by

$$q_{1n}^2 = q_1^2 - \left(\frac{X_n}{b}\right)^2 \qquad (3.1.68)$$

will change as well. In particular, the "plane wave" wavenumber, q_{10}, will be less than q_1 because X_0 will not be exactly zero like X_{00}.

For Ψ_2 and Ψ_3 we write

$$\Psi_2 = \sum_n B_n J_o(Y_n r/b) e^{iq_{1n}z} + \sum_n C_n J_o(X_n r/b) e^{iq_{2n}z} \qquad (3.1.69)$$

and

$$\Psi_3 = \sum_n D_n J_o(Z_n r/b) e^{iq_{1n}z} + \sum_n E_n J_o(X_n r/b) e^{iq_{3n}z} \qquad (3.1.70)$$

where

$$q_{2n}^2 = q_2^2 - \left(\frac{X_n}{b}\right)^2$$

$$q_{3n}^2 = q_3^2 - \left(\frac{X_n}{b}\right)^2$$

$$q_{1n}^2 = q_2^2 - (Y_n/b)^2$$

$$q_{1n}^2 = q_3^2 - (Z_n/b)^2 \qquad (3.1.71)$$

This method of expanding Ψ_2 and Ψ_3 enables them to share the same phase on the cylinder walls and on the end faces of the cavity as the Ψ_1 wave from which they arise whilst differing from Ψ_1 over the cross section of the cavity (where they are expected to be of negligible amplitude in any case).

The new radial boundary conditions derived from equations 3.1.62 to 65 which Ψ_1, Ψ_2 and Ψ_3 must satisfy are

$$v_r = 0 = A_n \frac{d}{dr} J_0\left(\frac{X_n r}{b}\right) + B_n \frac{d}{dr} J_0\left(\frac{Y_n r}{b}\right) - q_{1n}^2 D_n \frac{d}{dr} J_0\left(\frac{Z_n r}{b}\right) \qquad (3.1.72)$$

$(r=b)$

$$v_z = 0 = A_n J_0(X_n) + B_n J_0(Y_n) - \left(\frac{Z_n}{b}\right)^2 D_n J_0(Z_n) \qquad (3.1.73)$$

$$\Theta = 0 = a_1 A_n J_0(X_n) + a_2 B_n J_0(Y_n) \qquad (3.1.74)$$

Terms with propagation constants q_{2n} or q_{3n} have been neglected so that these boundary conditions apply to within a distance of the interferometer end faces approximately equal to the boundary layer thickness. Should $B_n = D_n = 0$ it can be seen that the first of these three equations reduces to the original boundary condition, 3.1.67, and that for an inviscid fluid and thermally non-conducting walls the latter two would not be appropriate.

The function $J_0(X_n r/b)$ may be expanded in terms of the original orthogonal functions $J_0(X_{0n} r/b)$ which will lead to a relation expressing $dJ_0(X_n r/b)/dr$ in terms of these functions and to a value of X_n. We write

$$J_o(X_n r/b) = \sum_k G_k J_o(X_{ok} r/b) \qquad (3.1.75)$$

so that

$$G_k = \frac{2}{b^2 J_o^2(X_{ok})} \int_o^b r\, J_o\left(\frac{X_{ok} r}{b}\right) J_o\left(\frac{X_n r}{b}\right) dr \qquad (3.1.76)$$

where the familiar orthogonality relations of Chapter II (equation 2.2.29) have been used. Evaluating the integral, G_k becomes

$$q_k = \frac{2b}{(X_n^2 - X_{on}^2) J_0(X_{ok})} \left. \frac{d}{dr} J_0\left(\frac{X_n r}{b}\right) \right|_{r=b} \qquad (3.1.77)$$

Since X_k will be closely equal to X_{0k} the only significant term in this series will be the kth so that

$$\left. \frac{d}{dr} J_0\left(\frac{X_n r}{b}\right) \right|_{r=b} = \frac{(X_n^2 - X_{on}^2)}{2b} J_0(X_{on}) \qquad (3.1.78)$$

which is the promised relation between $dJ_0(X_n r/b)/dr$ and the function $J_0(X_{On})$.

The assumption that $X_n \doteq X_{On}$ also allows Y_n and Z_n to be evaluated from equations 3.1.71:

$$(Y_n / b)^2 = q_{r2}^2 - q_{r,n}^2$$

$$\doteq q_{r2}^2 - q_{r1}^2 + \left(\frac{X_{on}}{b}\right)^2$$

$$\doteq q_{r2}^2 \gg 1 \qquad (3.1.79)$$

if $q_2^2 \gg q_1^2 - (X_{On}/b)^2$. This is plausible if it is assumed that only modes where n is small are required in the approximations for Ψ_1, Ψ_2 and Ψ_3. Similarly

$$(Z_n/b)^2 \doteq q_{r_3}^2 \gg 1 \qquad (3.1.80)$$

Thus we now have complete expressions for the radial dependence of ψ_1, ψ_2 and ψ_3. Since this information has been derived solely from consideration of a set of radial boundary conditions it should enable a wavenumber to be calculated which is appropriate for propagation in an infinite tube. This we may calculate from equation 3.1.68 once $(X_n/b)^2$ has been explicitely evaluated which we do from equation 3.1.78:

$$\left(\frac{X_n}{b}\right)^2 = \left(\frac{X_{on}}{b}\right)^2 - \frac{2}{b\,J_o(X_{on})}\frac{d}{dr}J_o\left(\frac{X_n r}{b}\right)\Bigg|_{r=b} \qquad (3.1.81)$$

The last term on the right hand side of this equation may be obtained from the radial boundary conditions and the relations

$$\frac{d}{dr}J_o\left(\frac{Y_n, Z_n r}{b}\right) = -iq_{r_{2,3}}J_o\left(\frac{Y_n, Z_n r}{b}\right) \qquad (3.1.82)$$

which are approximately true since the moduli of Y_n and X_n are very large. We find

$$\left(\frac{X_n}{b}\right)^2 = \left(\frac{X_{on}}{b}\right)^2 - i\frac{2}{q_3 b}\left\{q_{in}^2\left(1-\frac{a_1}{a_2}\right) - q_2 q_3 \frac{a_1}{a_2}\right\}$$

$$\doteq \left(\frac{X_{on}}{b}\right)^2\left\{1+\frac{i2}{q_3 b}\right\} - 2iq_1^2\left\{\frac{1}{q_3 b} + \frac{\sigma-1}{q_2 b}\right\}$$

(3.1.83)

This, together with equation 3.1.68, will enable the propagation constant for any 0nth mode to be calculated. For the moment we shall consider only the "plane wave" solution for which n=0 and $X_{0n}=0$ causing the first term to disappear leaving

$$\left(\frac{X_0}{b}\right)^2 = (1+i)\frac{q_1^2}{b}\left\{\nu_1^{\frac{1}{2}} + (\sigma-1)\left(\frac{K}{\rho c_p}\right)^{\frac{1}{2}}\right\}\left(\frac{\omega}{2}\right)^{-\frac{1}{2}}$$

(3.1.84)

where we have substituted for q_1, q_2 and q_3. From equation 3.1.68 the real part of q_{10} is

$$k_{10} \doteq k\left[1 + \frac{1}{b}\left\{\nu_1^{\frac{1}{2}} + (\sigma-1)\left(\frac{K}{\rho c_p}\right)^{\frac{1}{2}}\right\}(2\omega)^{-\frac{1}{2}}\right]$$

(3.1.85)

leading to a fractional error in measured velocity of

$$\frac{\Delta c}{c} \doteq -\frac{1}{b}\left\{\nu_1^{\frac{1}{2}} + (\sigma-1)\left(\frac{K}{\rho c_p}\right)^{\frac{1}{2}}\right\}(2\omega)^{-\frac{1}{2}} \qquad (3.1.86)$$

which is the Kirchhoff-Helmholtz correction of equation 3.1.1. The corresponding absorption coefficient, α, will be given by the imaginary part of q_{10} :

$$\alpha = \frac{1}{2c^3}\left\{\nu_1 + \nu_2 + (\sigma-1)\frac{K}{\rho c_p}\right\}\omega^2 + \frac{1}{bc}\left\{\nu_1^{\frac{1}{2}} + (\sigma-1)\left(\frac{K}{\rho c_p}\right)^{\frac{1}{2}}\right\}\left\{\frac{\omega}{2}\right\}^{\frac{1}{2}} \qquad (3.1.87)$$

which is clearly the sum of the classical absorption coefficient, α, attributable to losses from thermal conduction and friction within the body of the gas itself, and to the boundary layer absorption coefficient, α_{KH}, of Kirchhoff and Helmholtz due to the same mechanisms occurring at the walls of the tube.

Similar expressions may be obtained for higher modes by taking the first term on the right hand side of equation 3.1.83 into account. We find

$$q_{1n}^2 \doteq k^2\left[1 - \left(\frac{X_{on}}{q_1 b}\right)^2 + \frac{(1+i)}{(2/\omega)^{\frac{1}{2}}b}\left\{\nu_1^{\frac{1}{2}}\left(1-\left(\frac{X_{on}}{q_1 b}\right)^2\right) + (\sigma-1)\left(\frac{K}{\rho c_p}\right)^{\frac{1}{2}}\right\}\right] \qquad (3.1.88)$$

At low frequencies where boundary layer losses predominate over losses

occurring in the gas itself it is not possible to ignore terms which are powers of $(X_{on}/q_1 b)$ even for the lower values of n. Thus

$$k_{in} \doteq k\left\{1-\left(\frac{X_{on}}{q_1 b}\right)^2\right\}^{\frac{1}{2}}\left[1+\frac{1}{b}\left\{\nu_1^{\frac{1}{2}}+\frac{(\sigma-1)}{\left(1-\left(\frac{X_{on}}{q_1 b}\right)^2\right)}\left(\frac{K}{\rho C_p}\right)^{\frac{1}{2}}\right\}(2\omega)^{-\frac{1}{2}}\right] \tag{3.1.89}$$

and

$$\alpha_{in} \doteq \left\{1-\left(\frac{X_{on}}{q_1 b}\right)^2\right\}^{\frac{1}{2}}\frac{1}{bc}\left\{\nu_1^{\frac{1}{2}}+\frac{(\sigma-1)}{\left(1-\left(\frac{X_{on}}{q_1 b}\right)^2\right)}\left(\frac{K}{\rho C_p}\right)^{\frac{1}{2}}\right\}\left\{\frac{\omega}{2}\right\}^{\frac{1}{2}} \tag{3.1.90}$$

These last two expressions are, however, not very useful for high accuracy acoustic measurements since it is common practice to work either at very high frequencies where boundary layer effects may be ignored altogether, or at frequencies below the lowest cut-off frequency where such modes do not propagate. There is seldom any good reason for operating at intermediate frequencies where both systematic errors arising from boundary layer effects and from a complex wave field have to be accounted for.

3.1.4 The Boundary Layer Corrections for the End Faces of an Interferometer.

There is no need to recalculate the wave field in the cavity by summing posative and negative going disturbances with appropriate boundary conditions for the waves Ψ_1, Ψ_2 and Ψ_3. Instead the reflection coefficient, γ, of a single end face will be calculated and substituted into equation 2.1.4 in place of R_R and R_T. If complex (γ becoming $\gamma\exp(-i\delta)$) rather than real as supposed in Chapter II, then the denominator will become

$$1 - \gamma^2 e^{-2(\alpha + i[k+\delta/\ell]\ell)}$$

Thus the denominator of $R_G(l)$ and $X_G(l)$ in equations 2.1.10. and 11 will be altered in one respect only. The wavenumber k will become $k+\delta/l$ so that resonance will occur when

$$\ell = N\lambda/2 - \delta\lambda/2\pi \qquad (3.1.91)$$

leading to a fractional error in velocity of

$$\frac{\Delta c}{c} = -\frac{\delta\lambda}{2\pi\ell} \qquad (3.1.92)$$

It now only remains to calculate δ to arrive at an expression for the boundary layer correction appropriate for velocities measured in interferometers rather than in infinite tubes. This is obtained by adding the correction 3.1.92 to our original correction 3.1.86.

Supposing the three waves Ψ_1, Ψ_2 and Ψ_3 to be present at a boundary at z=0 we have

$$v_r = 0 : \quad A_n + C_n - q_{r3n}^2 E_n = -F_n \qquad (3.1.93)$$

$$v_z = 0 : \quad q_{1n} A_n + q_{2n} C_n + \left(\frac{X_n}{b}\right)^2 q_{r3n} E_n = q_{r1n} F_n \qquad (3.1.94)$$

and

$$\theta = 0 : \quad a_1 A_n + a_2 C_n = -a_1 F_n \qquad (3.1.95)$$

where F_n is the amplitude of the nth component of an incident Ψ_1 wave. Since Ψ_2 and Ψ_3 waves are so rapidly damped, it is assumed that no such waves are incident upon the boundary, and that only those arising from the immediate incidence of the Ψ_1 wave are present. The components of the Ψ_2 and Ψ_3 waves propagating inwards from the cylinder walls have also been ignored for the same reason. From the first equation we have

$$q_{r3n} E_n = \frac{1}{q_{r3n}} (A_n + F_n + C_n) \qquad (3.1.96)$$

which is of the first order of smallness in view of the magnitude of q_{3n}. Again considering only the "plane wave" case for which $X_{0n} = X_{00} = 0$ we also find from equation 3.1.83 that $(X_n/b)^2$ is of the first order of smallness for a similar reason. Thus the second equation here,

3.1.94, may to a good approximation be written

$$q_{1n} A_n + q_{2n} C_n = q_{1n} F_n \qquad (3.1.97)$$

Thus from the third equation, 3.1.95:

$$\begin{aligned} \gamma e^{-i\delta} &\doteq \gamma(1-i\delta) \\ &= A_0 / F_0 \\ &= \frac{a_2 q_{10} - a_1 q_{20}}{a_2 q_{10} + a_1 q_{20}} \end{aligned} \qquad (3.1.98)$$

giving

$$1-\gamma = \frac{(\sigma-1)}{c}\left(\frac{K}{e C_p}\right)^{\frac{1}{2}} (2\omega)^{\frac{1}{2}} \qquad (3.1.99)$$

and

$$\delta = -\frac{(\sigma-1)}{c}\left(\frac{K}{e C_p}\right)^{\frac{1}{2}} (2\omega)^{\frac{1}{2}} \qquad (3.1.100)$$

The former equation quoted in Chapter II (equation 2.1.14) was that originally derived by Herzfeld, and from the latter we obtain

$$\frac{\Delta c}{c} = \frac{-\delta}{kl} = \frac{(\sigma-1)}{l}\left(\frac{K}{\rho C_p}\right)^{\frac{1}{2}}\left(\frac{\omega}{2}\right)^{-\frac{1}{2}} \qquad (3.1.101)$$

which was the second term added to the Kirchhoff-Helmholtz correction by Thiesen (Cf equations 3.1.4 and 5).

No absorption coefficient correction arises from the end effects in the sense that it does from the radial boundary layer effect. The absorption coefficient, α, measured from the decay in the size of the resonances or the diameters of the impedance circles of Chapter II, will be correctly evaluated if one proceeds on the assumption that the resonances decay as implied by the function $R_G(l)$ (see equation 2.1.10) where γ takes Herzfeld's real value. The maximum value of this function is approximately proportional to $1/(\alpha l+\beta)$ where $\beta=1-\gamma$ and the minimum to $\alpha l+\beta/2$ which is negligible in comparison so that the former expression is a good approximation for an impedance circle diameter in arbitrary units. Thus the measurement of the diameters of two impedance circles will give α and β in arbitrary units. How these may be converted to absolute units is described in the following chapter where practical interferometer designs are discussed. If, on the other hand, it is assumed that $\beta=0$ (or that $\gamma=1$) when in fact β is of the order of αl, then an error would arise in the calculation of on the basis of measurements made on two impedance circles. But examination of three or more impedance circles should reveal that their diameters do not decrease as described by the incorrect function $1/\alpha l$, and the correct functional dependence would then become apparent.

3.2 Objections to the Boundary Layer Corrections.

Unfortunately, while the boundary layer corrections derived in the previous section appear to be theoretically sound and complete for the purposes of audio frequency or ultrasonic acoustic interferometry, it has been suggested in the past that they are, nevertheless, incorrect. Two types of criticism have arisen. Firstly the dependence of the effect upon the square root of the frequency is challenged, and secondly, given this dependence, the constant of proportionality is said to be incorrect. Since the experimental sources for both these views seem to be somewhat tenuous whilst the theory of the boundary layer, widely applied to other phenomena, seems reliable, it is surprising that they have gained the currency they have.

The only experimental information known to count against the order of the frequency arises from the work of Schneebeli and Seebeck [41, 42] which goes back to the years 1869 and 1870 respectively. Their instruments were somewhat crude judged by present day standards being mechanically excited resonant systems of indeterminate engineering finish. In order to investigate the boundary layer effect it is absolutely essential that microscopic protrusions and interstices on the cavity walls are small not only compared to the acoustic wavelength used, but also to the boundary layer thickness. These important features of the instruments used are simply not discussed - an omission which still seems to be acceptable today. No doubt the historical reason is that the early interferometers were fashioned from glass tubes containing fine powder whose distribution after the decay of the sound left a record of the acoustic field. Such devices frequently had side ports welded to the cavity for the admission and evacuation of gas and had end faces which were equally crude. It was assumed that if rough and ready instruments like these could be shown to operate much as predicted by a simple theory of the acoustic

interferometer such as we gave in section 2.1 then they were suitable for accurate studies of the boundary layer theory. Unfortunately there is no justification for such an assumption. The smaller the effect to be investigated the greater are the demands upon the geometry of the cavity. Notwithstanding this the results of Schneebeli and Seebeck are often taken to have demonstrated a frequency dependence for the velocity decrease of order 3/2.

The only theoretical support for the work of Schneebeli and Seebeck has been given by Schweikert [43] who derived the following formula for the measured velocity, c', in an interferometer

$$c' = c\left\{1 - \frac{\alpha c}{2N\pi\omega}\right\} \qquad (3.2.1)$$

from considering the superposition of an incident wave upon a reflector at z=l

$$\rho_i = S e^{-\alpha z} \sin(\omega t - kz) \qquad (3.2.2)$$

and a reflected wave

$$\rho_r = S r e^{-\alpha(2l-z)} \sin(\omega t - k[2l-z]) \qquad (3.2.3)$$

The resultant acoustic (i. e. excess) density was written as

$$\rho = \rho_i + \rho_r$$

$$= S\left\{ e^{-\alpha z}\sin(\omega t - kz) + r e^{-\alpha(2\ell - z)}\sin(\omega t - k[2\ell - z])\right\} \qquad (3.2.4)$$

from which he deduces that the acoustic intensity at some point z in the cavity is

$$S^2 =$$

$$S^2.\left\{A^2 + B^2 + C^2 + 2AB\cos 2kz + 2AC\sin 2kz\right\} \qquad (3.2.5)$$

where

$$A = e^{-\alpha z},$$

$$B = r\, e^{-\alpha(2\ell - z)}\cos 2k\ell$$

and

$$C = r\, e^{-\alpha(2\ell - z)}\sin 2k\ell$$

Differentiation shows that this has a maximum at

$$l \doteq \frac{N\lambda}{2} + \frac{\alpha}{2k^2} \qquad (3.2.6)$$

rather than at $l=N\lambda/2$. Since our equations 2.1.10 and 2.1.11 do not give this result, it must be the case that an error has arisen either in our own or in Schweikert's analysis. To show that it must be in Schweikert's consider the acoustic density at the reflector ($z=l$) when $r=1$. According to the physical presuppositions of Schweikert which are essentially those of section 2.1, the acoustic density should vanish at $z=l$ whereas we find from equation 3.2.4 that

$$\rho = 2s e^{-\alpha l} \sin(\omega t - kl) \qquad (3.2.7)$$

Only if the reflection coefficient, r, is negative will we obtain the correct answer. But in replacing the positive sign in equation 2.1.4 by a negative sign it ceases to be possible to derive Schweikert's correction 3.2.1 and we find instead that $l=N\lambda/2$ at resonance as in section 2.1. But even were Schweikert's equation 3.2.1 correct his proof that a frequency dependence of order 3/2 for the decrease in the velocity of sound occurs is not. Moreover, the proof requires one to take the dependence of the orthodox absorption coefficient, α_{KH}, on the square root of the frequency to be correct, yet not that of the orthodox velocity correction to which it is intimately related. The absorption coefficient is substituted into equation 3.2.1 to give a fractional velocity error of

$$\frac{\Delta c}{c} = \frac{-1}{2lb}\left\{\nu^{\frac{1}{2}} + (\sigma-1)\left(\frac{K}{ec_p}\right)^{\frac{1}{2}}\right\}\frac{1}{2^{\frac{1}{2}}\omega^{\frac{3}{2}}} \qquad (3.2.8)$$

This fractional correction to the velocity is smaller than that predicted by the boundary layer theory by a factor $1/2N_T$ and so might be difficult to detect even in the absence of the boundary layer effect conventionally predicted. But in using the predicted absorption coefficient, α_{KH}, it is surely admitted that the expected boundary layer reduction in velocity should also occur. Thus on Schweikert's theory it still remains to be explained why Schneebeli and Seebeck did not see a much larger dependence on the square root of the frequency in addition to the dependence on its 3/2th power.

By far the largest majority of workers investigating the boundary layer effect agree that it must depend upon the square root of the frequency but find various degrees of disagreement on the validity of the size of the coefficient of proportionality. It is often confirmed exactly but may be in error by as much as 40 per cent. It seems quite likely, however, that this may be attributed to the casual approach most workers have towards the engineering finish to the inner walls of their acoustic cavities and to a lesser extent to the poor knowledge of the transport properties of the gases used in the evaluation of the theoretical constant of proportionality. The problem of the constant of proportionality need not worry us, however, since it can easily be measured as will be shown in the next chapter.

CHAPTER IV

PRACTICAL DESIGN CONSIDERATIONS FOR AN ACOUSTIC THERMOMETER

If an acoustic thermometer is to achieve an accuracy comparable to that of the conventional constant volume gas thermometer it is essential that velocities should be measurable to one or two parts in ten thousand. This would represent an error in measured temperature of about 1mK at the normal boiling point of helium-4 and about 6mK at the hydrogen boiling point. Slightly less accuracy is required, however, to make a useful investigation of the errors thought to exist in the temperatures assigned to the normal boiling point of helium-4 on the scales T-58 and T-62 and to the hydrogen boiling point on IPTS-68. Several recent measurements have suggested that the value of 4.215K for the helium point is too low by approximately 10mK while the error in the hydrogen point may be measured in tens of mKs rather than mKs. Growing suspicion of the value assigned to the hydrogen point has led to the suggestion that the extension of IPTS-68 down to the triple point of hydrogen was premature - a point of view which should be seen in the light of the continued debate as to whether the IPTS should be maintained as a thermodynamic temperature scale or a stable and rarely altered means of comparison for individual temperature measurements. Either way the necessity for thermodynamic temperatures, whether

embodied in the definition of the IPTS or used as corrections to it, remains, and so every effort has been made to design an acoustic thermometer which will provide thermodynamic temperatures of the highest accuracy available from this method.

4.1 High Frequencies vs. Low Frequencies.

The first decision to be taken in the design of an acoustic interferometer is whether to operate at high or low frequencies. In operating at high frequencies all the problems of a complex wave field dealt with in Chapter II arise. The difficulty with this type of systematic error is that it cannot be corrected for in the absence of a knowledge of the way in which the transducer vibrates. Our guesses as to the form of the function $\xi_0(r,e)$ (equations 2.2.54 and 62) are plausible and so serve to show what order of velocity error may be expected. However, it will have been noticed that no azimuthal dependence of the amplitude of vibration of the transducer was specified. This was not because it made the problem mathematically intractable, but rather because the azimuthal dependence of one transducer might differ greatly from that of another depending upon such things as the eveness of clamping of a diaphragm or a quartz crystal and the homogeneity of their constituent materials. Many such parameters could be enumerated. Moreover, the radial dependences are only plausible guesses and as such could not be relied upon to correct measurements from a given instrument. It might be the case, for example, that a quartz crystal clamped as in figure 2.7(c) might vibrate only over a small region of its face at the centre. Were this the case the amplitudes of Table 2.5 for a/b=1/4 might be more appropriate than those for a/b=1. But, far worse, it might, unbeknown to its user, vibrate over a small region slightly off centre in which case no useful assessment of a velocity error would be made at all on the simple assumptions of Chapter II. All that may reliably be said is

that at a frequency of 1MHz in a cavity of diameter 2cm (the example of Table 2.5) a reasonable guess would suggest that errors would be negligible. Such a situation is obviously unsatisfactory from the point of view of obtaining the very highest accuracy.

An equally serious problem at high frequencies is that of deciding how the imperfections in the geometry of one's cavity will affect the measured velocity. The results of section 2.3 apply only below the first cut-off frequency, f_{10}. At higher frequencies geometrical errors could only be more serious; firstly because the wavelengths are not so large compared to the cavity imperfections and secondly because it would be expected that modes akin to the normal modes φ_{mn}, for the ideal cavity would propagate. A superposition of such modes would not correspond exactly to the previous superposition of normal modes since there would be perturbations entering our previous calculation due to the complex boundary conditions of the imperfect end faces of the cavity. A brief investigation suffices to show how unwieldy the problem becomes when an indefinite number of higher modes may propagate in the cavity.

Less important at higher frequencies, however, is the problem of the boundary layer. Reference to the values of Table 2.1 shows that at about 1MHz the absorption coefficient attributable to losses within the gas is not significantly larger than the boundary layer absorption coefficient. However, at 10MHz the former absorption mechanism is so severe as to make measurements of velocity virtually impossible. But, fortunately, boundary layer velocity errors have become fairly small by the time the frequency has approached 1MHz (which is presumably why Plumb and Cataland chose to work at this frequency). From equation 3.1.86 we find that the error to be expected in a temperature measurement at the normal boiling point of helium-4 is only about 0.1mK based on the values presented with Table 2.1. This may be

considered negligible but could be corrected for if desired.

Nevertheless, since the two main problems of operating at high frequencies seem insurmountable in principle it was felt that the advantage to be gained with regard to the boundary layer was not worthwhile and that a low frequency design of acoustic interferometer should be adopted. This would be further justified in that it would offer a more independent check on the ultrasonic work of Plumb and Cataland by encountering, and hopefully circumventing, an entirely different kind of main systematic error - the boundary layer error.

The generally accepted view that the boundary layer effect depends upon the square root of the frequency was defended in the last chapter, but there is no reason why it should not be tested experimentally for a given instrument. Having ensured that the acoustic absorption coefficient and the velocity of sound both vary as expected with frequency, it would then be possible to obtain the constant of proportionality, A, between each of them and the square root of the frequency from a measurement of the absorption coefficient. This could then be used to correct the measured velocity. Assuming the frequency to be sufficiently low so that the boundary layer absorption mechanism is the predominant one, we have

$$\alpha = \frac{A}{bc}\left\{\frac{\omega}{2}\right\}^{\frac{1}{2}} \qquad (4.1.1)$$

and

$$\frac{\Delta c}{c} = \frac{A}{2b}\left\{\frac{\omega}{2}\right\}^{-\frac{1}{2}} \qquad (4.1.2)$$

so that

$$\frac{\Delta c}{c} = \frac{\alpha c}{\omega} \qquad (4.1.3)$$

which expresses the fractional correction to be added to velocities measured in tubes. This is only approximately correct for a short interferometer because Thiesen's end correction has not been accounted for. Strictly

$$\frac{\Delta c}{c} = \left\{\frac{A}{2b} - \frac{A'}{l}\right\}\left\{\frac{\omega}{2}\right\}^{-\frac{1}{2}} \qquad (4.1.4)$$

$$= \frac{\Delta l}{l}$$

However, if we may anticipate the discussion of the next section on the relative merits of variable path and variable frequency interferometry, it will be apparent that in a variable path instrument where wavelengths are measured from the separations of the resonances, the total error in the separation of the first and Nth resonance will be

$$\Delta l_N - \Delta l_1 = \left\{\frac{A}{2b} l_N - A' - \frac{A}{2b} l_1 + A'\right\}\left\{\frac{\omega}{2}\right\}^{-\frac{1}{2}}$$

$$= \frac{A}{2b}(l_N - l_1)\left\{\frac{\omega}{2}\right\}^{-\frac{1}{2}} \qquad (4.1.5)$$

so that

$$\frac{\Delta c}{c} = \frac{\Delta l_N - \Delta l_1}{l_N - l_1} = \frac{A}{2b}\left\{\frac{\omega}{2}\right\}^{-\frac{1}{2}} = \frac{\alpha c}{\omega} \qquad (4.1.6)$$

as before. Thus only if a single resonance is detected in a cavity whose absolute length is measured in order to derive the velocity will it be necessary to allow for Thiesen's term. This applies, in principle, both to variable path and variable frequency instruments, De Laet's interferometer being an example of the latter. In practice, however, variable path interferometers are not used in this way. Further problems encountered in using variable frequency instruments will be dealt with in the following section.

In order to measure the radial boundary layer correction in a variable path interferometer, the absorption coefficient, α, must be measured for substitution into equation 4.1.3 (a rough uncorrected value being good enough for the velocity substitution).

The measurement of may be carried out in either of two ways. At resonance $X_G(l)=0$, and

$$R_q(l) = R_q(N\lambda/2) = \frac{1 + \gamma e^{-2\alpha l}}{1 - \gamma^2 e^{-2\alpha l}} \qquad (4.1.7)$$

or, putting $\gamma=\exp(-\beta)$ where $\beta<<1$:

$$R_G(N\lambda/2) \doteq \frac{1}{\alpha l + \beta} \qquad (4.1.8)$$

Since, for practical values of αl and β, R_G at antiresonance is very small compared to R_G at resonance, this gives the values of the diameters of the impedance circles to a high degree of accuracy. Thus by fitting a function of the form $1/(aN+b)=D_N$ to the experimentally measured diameters, D_N, where $a/b=\alpha N\lambda/2\beta$, the ratio α/β may be calculated. In order to evaluate α, a further relation with β is required. (*1) This may be obtained from the rate of change of the phase, φ, of the impedance of the gas column with l:

$$\tan\varphi = -\frac{X_G(l)}{R_G(l)} = \frac{-\gamma(\gamma+1)\sin 2kl}{1-\gamma^3 e^{-4\alpha l} - \gamma(\gamma-1)e^{-2\alpha l}\cos 2kl} \qquad (4.1.9)$$

On differentiating one finds at resonance:

---

(1) In ultrasonic interferometry where reflection coefficients are expected to be low and classical absorption coefficients high, and where quartz crystal transducers are commonly used, this second relationship is easily obtained by measuring the value of R_G at antiresonance. (See, for example, Refs. 26 and 27 or Howard C. Hardy, J. Acoust. Soc. Amer. 15,2 (1943)). Because in the present case the transducer impedance is not zero so that circles do not lie symmetrically about the real axis, a more complicated procedure has to be devised.

$$t \equiv \left.\frac{dl}{d\tan\varphi}\right|_{\varphi=0}^{\cdots} = \frac{-(1-e^{-2\beta(1+\chi)})(1+e^{-\beta(1+2\chi)})}{k(e^{-\beta}+e^{-2\beta})} \qquad (4.1.10)$$

where χ=Na/b. To a good approximation if $\beta \ll 1$ and χ is of order no greater than unity:

$$\beta = -\frac{kt}{1+\chi} \qquad (4.1.11)$$

which, taken with the expression for a/b, enables α to be calculated. t may be evaluated by plotting a graph of $\tan\varphi$ against Z from values obtained by measurements on the impedance circles. Then

$$t \equiv \left.\frac{dl}{d\tan\varphi}\right|_{\varphi=0} = \left.\frac{dZ}{d\tan\varphi}\right|_{\varphi=0} \cdot \left.\frac{dl}{dZ}\right|_{\varphi=0} \qquad (4.1.12)$$

the latter gradient being obtained from the original experimental curve of Z(l) once a value of Z at resonance has been obtained.

A graphically less arduous way of calculating α is to express dZ/d(tanφ) at resonance in terms of quantities already calculated for drawing the impedance circles. We see from Figure 2.2 that

$$Z = \left\{(R_T+R_q)^2 + (X_T-X_q)^2\right\}^{\frac{1}{2}} \qquad (4.1.13)$$

Substituting

$$R_G = r_N + r_N \cos\varphi \doteq 2r_N \qquad (4.1.14)$$

and

$$X_G = r_N \sin 2\varphi \doteq 2r_N \tan\varphi \qquad (4.1.15)$$

where r_N is the radius of the Nth impedance circle and where the approximations apply near resonance, we obtain

$$Z = \left\{ Z_T^2 + 4r_N(R_T - X_T \tan\varphi) + 4r_N^2 \right\}^{\frac{1}{2}} \qquad (4.1.16)$$

so that

$$\left.\frac{dZ}{d\tan\varphi}\right|_{\varphi=0} = \frac{2r_N X_T}{Z_{RES}} \qquad (4.1.17)$$

t may be found from equation 4.1.10 and the calculation proceeds as before.

The second way to calculate the absorption coefficient is from its relationship with the half widths of the resonances. The height of the function $R_G(l)$ at $l=N\lambda/2$ (or the diameter of the Nth impedance circle) is known to be $1/(\alpha l+\beta)$. By solving the equation

$$R_G(l) = \frac{1}{2(\alpha l + \beta)} \qquad (4.1.18)$$

we may therefore calculate Δ_N, the half width of the Nth resonance at half the height of the resonance. It is given by

$$\Delta_N = \frac{\alpha l + \beta}{k} \qquad (4.1.19)$$

which is compatible with the expression $\alpha l/k$ quoted in Chapter II where reflection losses were assumed to be negligible. Reference to figure 2.2 shows that the corresponding value of Z, Z_{HALF}, at the half height of $R_G(l)$ are given by the distances of the upper and lower extremities of the impedance circles from the origin. And the useful value of Z_{HALF} - that is the one encountered between Z_{MAX} and Z_{MIN} on the resonance - will be the shorter. A similar conclusion will also be reached for the case where X_T is negative and the circles lie below the real axis since they are still traversed in a clockwise direction. Thus we write quite generally

$$Z_{HALF} = \left\{ (R_T + r_N)^2 + (|X_T| - r_N)^2 \right\}^{\frac{1}{2}}$$

$$= \left\{ Z_T^2 + 2r_N^2 + 2r_N(R_T - |X_T|) \right\}^{\frac{1}{2}} \qquad (4.1.20)$$

It is now a simple matter to read off the corresponding value of l, l_{HALF}, from the experimental Z(l) curve and to take the difference from l_{RES} to give Δ_N. Then if at least two resonances are available

α and β may be calculated from equation 4.1.19. However, it is probably better practice to calculate the ratio α/β from the circle diameters as already described, and to use it to solve each of the equations 4.1.19. This is because the value of α/β is likely to be comparatively accurate since the circle diameters are quite easy to measure. Half widths, on the other hand, may be a little more difficult to measure precisely, and so it is wasteful of useful statistical evidence to effectively expend one value on the calculation of the ratio when the figure is already available from another source.

Whether it is preferable to calculate the absorption coefficient from the gradient of the Z(l) curve at resonance or from the half width is difficult to say in advance. Both techniques will be examined in the light of the data which becomes available and agreement between the two methods will also be checked to ensure that the resonance curve is of the form assumed theoretically.

Should large values of αl or β be encountered, the validity of our assumption of section 2.1 that all the impedance circles touch at $\underline{Z}_G(l)=0$ may be questioned. It may be shown from equations 2.1.10 and 11 that while $X_G(l)=0$ at antiresonance, $R_G(l)=\beta/2+2\alpha l\neq 0$. Whether or not this will cause some small error depends upon how the impedance of the transducer, Z_T, is measured. If some single value is used to construct the impedance circle diagram (calculated, say, from the height of the resonance curve at the first antiresonance) then successive circles will require to be displaced in the direction of the positive real axis by a distance equivalent to $\beta/2+2\alpha l$ so that a second approximation of Z_{RES} can be made. The conversion of the shift $\beta/2+2\alpha l$ to the arbitrary units used in the complex plane (cms, say) is best accomplished by equating the diameter of some impedance circle to $1/(\alpha l+\beta)$ which will give the conversion factor to a high degree of

accuracy. However for the cases under consideration it is unlikely that the shift will amount to more than 10^{-5} or 10^{-6} of the impedance circle diameter so that it is probably quite satisfactory to continue as outlined in section 2.1. A better way of dealing with the problem would be to calculate the value, Z_T, for each impedance circle from the average of the values obtained from the antiresonances either side of the corresponding resonance. This way the circles would be plotted with the correct displacement from the point $\underline{Z}_G(l)=0$ right from the beginning.

4.2 Variable Path vs. Variable Frequency Interferometry.

Having decided to work below the first cut-off frequency it is necessary to choose between fixed path interferometry entailing the measurement of resonant frequencies, and variable path interferometry at some fixed frequency entailing the measurement of resonant cavity lengths.

Fixed path interferometry, requiring no moving parts, has the advantage of simplicity - a doubly important consideration in a liquid helium cryostat. It might also seem, *prima facie*, that resonant frequency measurements are straightforward compared with measurements of resonant cavity lengths. However, both of these advantages diminish on close examination. Firstly, the one single critical measurement of the length of the cavity needed in fixed path interferometry requires the exact definition of the positions of the ends of the cavity. Quite apart from the problem of allowing for the overall thermal contraction of the cavity, a precise knowledge of the mean position of the vibrating transducer at low temperatures is required. Thus careful consideration needs to be given to the coupling of the transducer to the cavity. The possibility of exciting a cavity with two rigid end reflectors through a port in one of them whilst monitoring the acoustic pressure through a port in either is to be viewed with

circumspection because, although it solves the problem of the length of the cavity, it can, as in section 2.2.4, result in the wasteful excitation of evanescent modes at the expense of the plane wave mode. As the ports become sufficiently small to be negligible the difficulty of adequate excitation of the cavity and of monitoring the intensity of the sound with sufficient sensitivity increase accordingly.

Regarding the measurement of the true resonant frequency, it will be appreciated that it requires, in principle, a frequency independent method of measuring the acoustic pressure in the cavity as the exciting frequency sweeps through resonance. This calls for a transducer whose impedance and a microphone whose sensitivity are sufficiently constant with changing frequency. Furthermore, if their diaphragms are to form the end reflectors of the cavity, their reflection coefficients must be frequency independent as well. (unless the reflection losses are negligible compared to losses in the body of the gas or on the cylinder walls). Given the narrowness of the resonances, these requirements should be met quite easily, thus enabling single uncorrected measurements of velocity to be made. However, as has been shown, velocity measurements made at several orders of resonance enable acoustic absorption coefficients, and so the boundary layer corrections to the velocity, to be measured rather than calculated from theoretical considerations whose applicability has occasionally been in doubt. This requires velocity measurements to be made at well separated frequencies where changes in the transducer and receiver characteristics are bound to occur. Even by using a transducer and microphone at frequencies well separated from their main natural resonant frequencies - e. g. far into the mass controlled region - one can still expect to see, with practical devices, lesser natural resonances superimposed upon a slow drift with frequency of impedance or sensitivity. Similar behaviour might also be expected for

their respective reflection coefficients. Thus for each resonance it would only be possible to calculate the sum $\alpha_N N\lambda/2+\beta_N$, rather than the absolute values of α_N and β_N. Consequently it would not be possible to make a measured boundary layer correction. This problem has been avoided by Smith and Harlow [44] in an experiment at room temperature where a long cavity was used so that $\alpha l \gg \beta$ thus enabling end face losses to be ignored. However, accommodation of such an instrument in a cryostat would cause considerable practical difficulties, and it also seems to be bad practice to dispose of one loss problem by making other losses large in comparison since it results in an overall reduction in the sensitivity of the instrument.

The additional inconvenience of having to recalculate the transducer impedance at each successive order of resonance has already been pointed out in section 2.1, but is no more serious than having to do it in the case of a variable path interferometer if the corrections for large absorption and reflection coefficients are made as suggested at the end of the previous section.

Both problems of absolute length measurement and of frequency stability are removed by using a variable path interferometer. Distances are measured relative to the first position of resonance which can be determined unequivocally since all acoustic impedances, sensitivities and reflection coefficients are guaranteed to be constant at constant frequency. Moreover, there is also the advantage of evading the the boundary layer end effect, which, it will be recalled, causes each peak to be shifted by the same amount so that the separations remain unchanged although the absolute resonant lengths of the cavity require a small correction inversley proportional to these lengths. The same applies to end effects attributable to imperfections in cavity geometry which were seen to arise in the same way - namely by adding a small 1/l term to the

wavenumber. For these reasons the variable path technique was chosen.

4.3 The Excitation of the Cavity and the Detection of Resonance.

Grimsrud and Werntz in their variable path interferometer made use of a separate microphone to monitor the acoustic pressure in addition to the transducer used to excite the cavity. De Laet used a similar technique in her variable frequency acoustic thermometer. Such a combination is very simple to use since the resonance curve obtained from the microphone will be of the form $R_G(l)$ so that the positions of resonance are immediately available from the positions of the maxima. Plumb and Cataland used only an x-cut quartz crystal transducer which also served to detect the resonances through the changes in its measured impedance brought about by the gas loading. It was explained in section 2.1 that because such a transducer has a very small and real impedance the resonance curve is also of the form of the function $R_G(l)$. We feel that the technique of using only a single transducer is to be preferred at low temperatures because of its greater constructional simplicity and reliability although at low frequencies we cannot avail ourselves of the use of a quartz crystal. Instead we have chosen to use a moving coil driven diaphragm which, having a complex impedance of the type indicated in figures 2.2 and 2.3, necessitates a much more detailed examination of the resonance curve which is no longer of the form given by $R_G(l)$.

The mechanical impedance of such a transducer is usually measured in terms of its electrical impedance. However, the measured electrical impedance has a purely electrical component which masks to some extent that part of the impedance attributable to the gas loading of the transducer. It has already been pointed out in section 2.2.3 that the mechanical impedance may be measured in arbitrary units directly from the reciprocal of the velocity amplitude provided that the driving force is constant. With our moving coil driven diaphragm this would

best be achieved by attaching a small piezoelectric accelerometer to the rear face of the diaphragm at its centre. At constant frequency the voltage across the faces of the accelerometer would be proportional to its velocity as required. The necessary constant driving force is obtained simply by driving the transducer at constant current. Since the accelerometer, being a natural piezoelectric crystal or a piece of synthetic piezoelectric ceramic, will have an extremely high impedance and will be in close proximity to the driving coil, it is necessary to know what the effect of interference in the accelerometer circuit from the drive circuit will be. Interference is likely to be due to three causes and, of course, of the same frequency as the driving current. These are (a) interference due to the motion of the accelerometer and its electrical leads in the stray magnetic fields from the permanent magnet providing the radial field for the moving coil, (b) induced interference from the driving current and (c) interference from the driving voltage due to resistive or capacitative coupling or a mixture of both.

Ideally we have for the accelerometer voltage:

$$V = V_o \sin(\omega t - \alpha') = \frac{b}{Z} \sin(\omega t - \alpha') \qquad (4.3.1)$$

where

$$\tan \alpha' = \frac{X}{R} = \frac{X_T - X_G(\ell)}{R_T - R_G(\ell)} \qquad (4.3.2)$$

and where b is some constant which determines the arbitrary units of the measured mechanical impedance, Z, of the loaded transducer.

Considering the first type of interference due to magnetic

induction we have instead of equation 4.3.1:

$$V = a\dot{\xi} + \frac{b}{Z}\sin(\omega t - \alpha')$$

$$= \frac{F}{Z}\cos(\omega t - \alpha') + \frac{b}{Z}\sin(\omega t - \alpha') \qquad (4.3.3)$$

where F is the amplitude of the constant driving force, a is a constant determining the amplitude of the interference and where we have supposed that

$$\xi = -\xi_o \sin(\omega t - \alpha')$$

$$\dot{\xi} = -\omega\xi_o \cos(\omega t - \alpha')$$

and

$$V \propto \ddot{\xi} = \omega^2 \xi_o \sin(\omega t - \alpha') \qquad (4.3.4)$$

Equation 4.3.3 may be written

$$V = V_o' \sin(\omega t - \beta) \qquad (4.3.5)$$

where

$$\tan\beta = \frac{-b}{aF} \qquad (4.3.6)$$

and

$$V_o' = \frac{1}{Z}\left\{a^2F^2 + b^2\right\}^{\frac{1}{2}} \qquad (4.3.7)$$

Thus even if this type of interference is very large, it is of no consequence since the reciprocal of the driving voltage still gives the mechanical impedance in arbitrary units. In fact an inductive accelerometer would serve our purposes just as well as the piezoelectric accelerometer except that it might be slightly more complex in construction.

The second type of interference due to inductive pick up of the driving current is more serious. We write

$$V = -a\sin(\omega t-\varphi) + \frac{b}{Z}\sin(\omega t-\alpha') \qquad (4.3.8)$$

where the first term on the right hand side represents the induced voltage. Advancing our time scale by φ/ω we have instead

$$V = a\sin\omega t + \frac{b}{Z}\sin(\omega t-\alpha) \qquad (4.3.9)$$

if $\alpha=\varphi-\alpha'$. Or

$$V = V_o'\sin(\omega t-\beta) \qquad (4.3.10)$$

where

$$\tan\beta = \frac{-\sin\alpha}{\cos\alpha + aZ/b} \qquad (4.3.11)$$

if a<<b/Z as it should be, and

$$V_o' = \frac{b}{Z}\left\{1 - \frac{aZ}{b}\cos\alpha\right\} \qquad (4.3.12)$$

or

$$Z' = Z\left\{1 + \frac{aZ}{b}\cos\alpha\right\} \qquad (4.3.13)$$

A similar expression could be derived for the third type of interference arising out of resistive or capacitative coupling.

We now need to know what values of aZ/b are tolerable so that a check can be made that such interference as is found to occur will be negligible. In the presence of interference our experimental resonance curve, Z(l), will take the value

$$Z'_{RES} = Z_{RES}\left\{1 + \frac{aZ_{RES}}{b}\cos\alpha\right\} \qquad (4.3.14)$$

at $l=N\lambda/2$. Errors in the measured position of resonance will arise if this differs from the value of Z_{RES}, Z''_{RES}, calculated from the constructed impedance circle diagram. We have

$$Z''_{RES} = \left\{ (R'_T + D'_N)^2 + X'^2_T \right\}^{\frac{1}{2}}$$

$$\doteq \left\{ Z'^2_T + D'^2_N + 2R'_T D'_N \right\}^{\frac{1}{2}}$$

$$\doteq Z_{RES} \left\{ 1 + \frac{a}{b Z^2_{RES}} \left[Z^3_T \cos\alpha_T + D^3_N \cos\alpha + D_N Z^2_T + R_T D^2_N \cos\alpha \right] \right\} \qquad (4.3.15)$$

which is, unfortunately, not the same as equation 4.3.14. D'_N is defined in the same way as Z' since it is the difference of the maximum and minimum values of Z. Inspection of figure 2.2 will reveal that $\cos\alpha$ takes the same values for these two values of Z. The error in the value of Z_{RES} for the purposes of calculating the error in the position of resonance will be given by the difference of the two correction terms of Z'_{RES} and Z''_{RES}, and may be calculated once rough values of Z_T, D_N, R_T, $\cos\alpha$ and $\cos\alpha_T$ have been obtained. Typically we might take $Z_T \doteq D_N \doteq 2Z_{RES}/3$ and $\cos\alpha \doteq \cos\alpha_T \doteq 1$ so that

$$Z''_{RES} = Z_{RES} \left\{ 1 + \frac{32}{27} \frac{a Z_{RES}}{b} \right\} \qquad (4.3.16)$$

giving an effective error in Z_{RES} of

$$\Delta Z_{RES} = \frac{5}{27} \frac{a Z_{RES}}{b} \qquad (4.3.17)$$

obtained by subtracting Z'_{RES}. The resulting error in l_{RES}, l_{RES}, will be given by

$$\Delta l_{RES} = \Delta Z_{RES} \frac{dl}{dZ}_{RES}$$

$$\doteq \frac{5}{27} \frac{a Z_{RES}}{b} \frac{\Delta_N}{\Upsilon_N} \qquad (4.3.18)$$

where $\Delta_N \doteq dl/k$ is the half width of the Nth resonance. Thus

$$\frac{\Delta l}{l} \doteq \frac{5}{27} \frac{a Z_{RES}}{b \Upsilon_N} \frac{d}{R} \qquad (4.3.19)$$

Typically aZ/b=0.01 while d/k=0.001. Thus the error is likely to be negligible especially since it will be reproduced to some extent from one resonance to the next so that the separations of the resonances are affected to a lesser degree. Simple checks on the voltage amplitudes a and b/Z should ensure that this is, in fact, the case.

Apart from the errors which arise from misalignment and lack of flatness in the diaphragm which have already been treated in section 2.3, there still remains the problem of coupling the transducer to the cavity which, if not approached carefully, might lead to a new kind of geometrical error. The larger the diameter of the diaphragm compared to that of the cavity, the more efficient and sensitive it will be in exciting and responding to plane waves, and the easier to align accurately. It will also have a lower spring rating which should help to keep its impedance, Z_T, low compared to the impedance of the gas loading which is the real goal of the measurements. However, as may be seen from figure 2.7(a) a diaphragm such as this has to be mounted a small distance from the mouth of the cavity to allow it to vibrate freely unlike the less effective, but at present more predictable, diaphragm of figure 2.7(b). Prima facie this gap might well present a

cavity imperfection which could lead to velocity errors. However, an analysis of the type undertaken in section 2.1 would suggest that the complete system might be considered as two interferometers with two sets of standing waves loading the diaphragm. The first set of standing waves would occur between the exposed part of the diaphragm and the movable reflector as before, and the second set between the masked part of the diaphragm and the end of the cavity which masks it. Since the length of this second interferometer is constant, the loading of the second set of standing waves would merely contribute a constant term to the impedance of the transducer, $\underline{Z}_T$. Thus their effect would automatically be taken into account by the existing procedures for analysing the resonance curve. A very small effect might arise due to the fact that the boundary layer correction to the original plane waves would be different for a short distance from the diaphragm where the cavity has a wider diameter. This effect would not be noticable since the difference in the small correction would only apply at most over a fraction $2g/\lambda$ of total distance travelled by the waves where g is the width of the gap. We might expect g to be of the order of 0.03cm and the wavelength about 3cm. However, it should be possible to investigate the effect experimentally by superimposing a direct current on the alternating current used to drive the transducer. This would shift its mean position and enable any significant effect which depended upon the width of the gap to be observed.

4.4 Some Remaining Systematic Errors of Acoustic Origin.

Hitherto, the discussion of systematic errors has centered entirely on the problems associated with the wave field at higher frequencies and the boundary layer at lower frequencies. It will now be demonstrated that other likely sources of systematic error will be of no consequence.

4.4.1 The Effect of Finite Sound Amplitudes.

Elements of an acoustic wave propagate with a velocity proportional to their amplitude. Thus the high pressure part of the wave is expected to draw level with the trough of the wave after a certain distance leading to the formation of a shock wave. It is essential that amplitudes used in acoustic interferometery are sufficiently low to prevent this effect becoming significant before the sound wave has decayed to a negligible amplitude.

We have for the velocity of such a wave

$$c' = c + \frac{\sigma + 1}{2} \omega \xi_0 \qquad (4.4.1)$$

where $\omega \xi_0$ is the particle velocity amplitude at some point on the wave[45]. Thus the relative velocity of a peak with respect to the trough in front will be

$$(\sigma+1)\omega\xi_0 = 8\omega\xi_0/3 \qquad (4.4.2)$$

for monatomic helium-4. In order to calculate a value of ξ_0, let us assume that the acoustic power, $\dot{W}$, radiated into the cavity is as large as 10mW. Thus

$$\dot{W} = \rho c \pi b^2 \omega^2 \xi_0^2 = 0.01 \text{ Watts} \quad (4.4.3)$$

giving $\xi_0 = 2 \times 10^{-7}$ cm at the normal boiling point of helium-4 at a frequency of 3.3kHz. Thus from equation 4.4.2 the velocity of approach of peak and trough is approximately 3.1×10^{-3} cm/s which implies that the shock wave would have formed after about 600 seconds - the time taken to travel one half wavelength at this speed. By this time the wave itself has traveled 3.6×10^{6} cm and acquired an attenuation factor $\exp(-dz)$ with an exponent of 10^{3} or 10^{4}. Thus we may conclude that at realistic amplitudes the velocity of sound is for all practical purposes equal to the velocity of sound at vanishingly small amplitudes.

4.4.2 The Effect of Frequency Dispersion.

When the frequency of the sound is sufficiently high the period of oscillation becomes comparable to the mean collision rate of the helium molecules so that translational relaxation occurs. Under these conditions the slower molecules will be incapable of transmitting the disturbance since the acoustic driving force on some volume element of gas will have changed its direction before the necessary molecular collisions can take place. Thus only the faster molecules participate in sound transmission and acoustically the gas appears to be warmer than it would at lower frequencies so that the velocity of sound is too great. The mean collision frequency, f_c, of the molecules will be given by

$$f_c = 8 \sigma n \left\{ \frac{kT}{\pi m} \right\}^{\frac{1}{2}} \quad (4.4.4)$$

where n is the number of molecules per unit volume, m is their mass

and k is the Boltzman constant. The total scattering cross section, σ, may simply be calculated from the approximate cross sectional area of the helium atom for our present purposes. At a temperature of 4.2K and a pressure of 1 atmosphere we find $f_c = 10^{11}$ per second which is higher than the highest acoustic frequencies we are likely to use by some seven orders of magnitude. Thus we may consider that translational relaxation is entirely negligible. Other mechanisms of molecular relaxation are not, of course, available to a monatomic gas.

4.4.3 Approximations in the Radial Boundary Condition.

We have assumed in Chapter II in requiring that the radial particle velocity vanishes at the cylindrical walls of the cavity that there is a perfect acoustic mismatch between gas and walls. In practice, however, the walls will not be entirely rigid and some sound will propagate into them. But, since the acoustic mismatch is as large as it is, it has usually been assumed that this effect is negligible - especially in comparison to the boundary layer effect. Such a point of view probably arises because an incorrect analogy is drawn between this radial boundary condition and the end face boundary condition where the reflection loss will be proportional to the ratio of the specific acoustic impedances of gas and end face, $\rho_G c_G / \rho_W c_W$. In a copper cavity filled with helium-4 gas at a pressure of 1 atmosphere and a temperature of 4.2K this will be of the order of 10^{-6}. This ratio is derived by demanding that both the normal particle velocity and acoustic pressure be continuous at the end face. In order to obtain the particle velocity, the velocity potential has to be differentiated with respect to z so that the wavenumber appears as a factor in the expressions for the particle velocities either side of the boundary - hence the existence of the ratio of the velocities in the expression for the attenuation on reflection. In the case of the radial boundary condition, on the other hand, differentiation of the

velocity potential is with respect to r, and so does not lead to this factor. Thus only the ratio of the densities of the two media enters into the expression for the loss. Del Grosso [46] has done this calculation and obtained a result from which we may derive the following characteristic equation appropriate to our system:

$$\frac{J_o(X)}{X\,J_o(X)} \doteq -\frac{\rho_w}{\rho_q}\,\frac{K_o(b/k_q)}{(b/k_q)\,K_1(b/k_q)} \qquad (4.4.5)$$

where K_0 and K_1 are modified Bessel functions of the second kind and where X will equal X_{0n} if the ratio of the densities becomes infinite. Notice that c_w does not enter this equation (*1). Turning to the plane wave case, we assume that $X \doteq X_{00} = 0$ so that we may write

$$\frac{2}{X_o^2} \doteq \frac{\rho_w}{\rho_q}\,\frac{K_o(b/k_q)}{(b/k_q)\,K_1(b/k_q)} \qquad (4.4.6)$$

The ratio containing the Bessel functions is of order unity for situations of immediate interest, so that, very roughly, we may write

---

(1) Except, that is, as a second order term which we have omitted in this case. Del Grosso retained it since his interest was in liquid filled cavities where velocities in the two media are comparable.

$$\frac{X_o^2}{2} \doteq \frac{\rho_g}{\rho_w} \doteq 10^{-3} \qquad (4.4.7)$$

leading to a fractional error in measured velocity of $(X_0/bk_G)^2/2 \doteq 10^{-3}$. This is small, though by no means negligible, but since we are plotting velocity isotherms and extrapolating to zero pressure, the ratio of the two densities in the characteristic equation will, in fact, tend to infinity and our final answer for the velocity of sound will not be affected. However, the higher points on the velocity isotherm will be depressed to some extent which will change the measured second acoustic virial coefficient by a small amount.

4.4.4 Parametric Oscillation.

Hitherto we have treated the length of the cavity, l, as a variable with no time dependence. In fact it oscillates with the transducer:

$$l = l_o + \xi_o e^{i\omega t} \qquad (4.4.8)$$

Breazeale and Adler [47] have investigated the effect of such a variation and conclude that fractional harmonics of the fundamental resonant frequencies will occur in the cavity if the amplitude of vibration of the transducer, ξ_0, exceeds a threshhold value, $\alpha_0 l\, c/\omega$. We may assume that this quantity will be of the order 10^{-3} cm whereas we have already calculated a rough value for ξ_0 of 10^{-7} cm. Thus we assume that we may continue to regard the length of the cavity as being constant without incurring any error whatsoever.

CHAPTER V

THE PRACTICAL INSTRUMENT AND TESTS ON THE SYSTEM.

A practical instrument was constructed in accordance with the principles outlined in the previous chapter. It was designed to be operated at some fixed frequency below the first cut off frequency and could be brought into resonance by moving an acoustic reflector. The main innovations were in the use of an optical (laser) interferometer to measure the separations of the positions of resonance and in the use of an accelerometer to measure mechanical impedances directly.

Careful tests have been carried out on the system to ensure that its behaviour conforms with all the relevant theoretical assumptions of the previous chapters.

5.1 The Acoustic Interferometer.

The acoustic interferometer is shown in Figure 5.1 suspended in its vacuum can, V, and surrounded by a radiation shield, R. At the bottom of the instrument the transducer assembly may be seen hanging on the lower end of the acoustic cavity, G, whose length may be increased by withdrawing the piston, H. The lower face of this piston is the acoustic reflector whilst the upper end carries a cube corner reflector, J, which is the moving mirror of the optical interferometer. The fiducial mirror of the optical interferometer, a semi-reflecting beam splitter, L, is situated in the horizontal plate above the piston. By these means the length of the acoustic cavity -

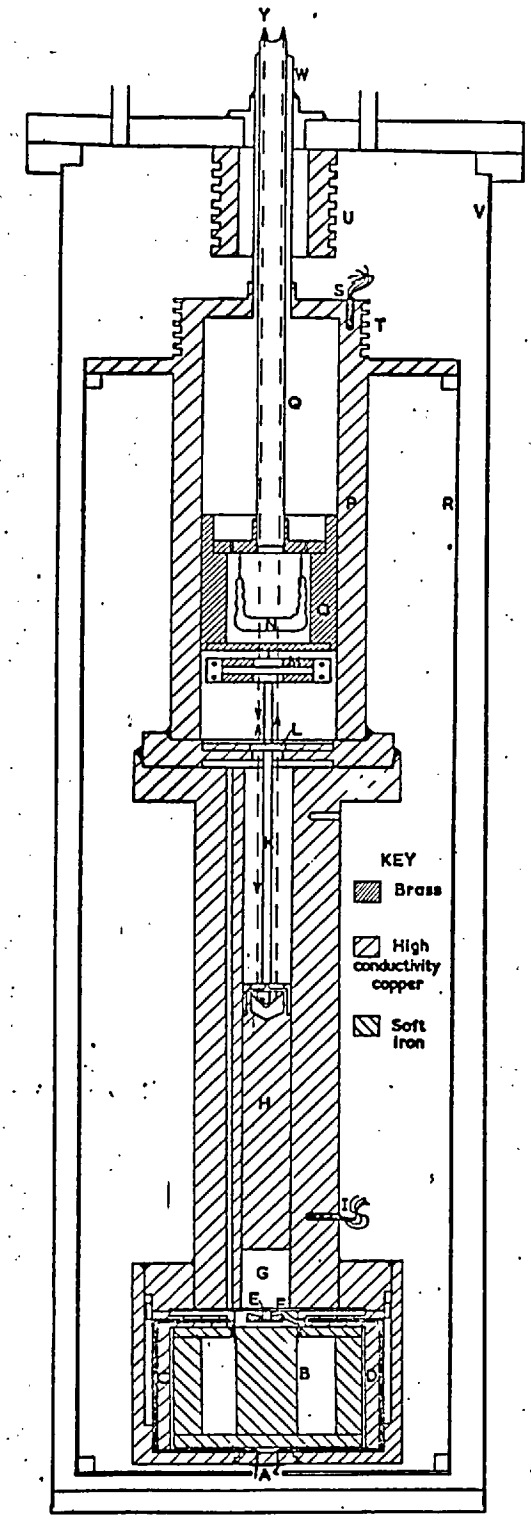

Figure 5.1

The Acoustic Interferometer.

A - Stycast Seals, B - Permanent Magnet Assembly, C & D - Electrical Lead Screens, E - PZT Accelerometer, F - Transducer Diaphragm, G - Acoustic Cavity, H - Piston Reflector, I - Germanium Resistance Thermometers, J - Cube-Corner Reflector, K - Pushrods, L - Beam Splitter, M - Gimbals, N - Optical Window, O - Bearing, P - Upper Chamber, Q - Moving Tube, R - Radiation Shield, S - Temperature Controlling Sensor, T - Thermal Anchoring Grooves (with heater), U - 4.2K Thermal Anchoring Grooves, V - Vacuum Can, W - Central Supporting Tube, Y - Laser Beams.

or rather changes in length - may be measured without any of the problems of indeterminate thermal contractions encountered in the conventional pushrod technique where reflector displacements are measured outside the cryostat with a micrometer bearing on the end of the pushrod. Both Plumb and Cataland and Grimsrud and Werntz suffered from this problem.

Above the beam splitter a second coaxial chamber, P, can be seen guiding a sliding brass bearing, O. This bearing serves two functions. Firstly it carries gimbals, H, through which the vertical actuation is transmitted to the piston without transmitting any lateral force. This was intended to help maintain the alignment of the acoustic interferometer. Secondly it houses a cryogenic vacuum tight optical window, N, sealing the end of a moving tube down which the light travels to the optical interferometer and up which the two beams - one from the moving mirror, one from the fiducial - return. This light tube also serves to actuate the brass bearing and so the piston via the gimbals and two thin pushrods, K, passing either side of the beam splitter. The thermometric gas for the interferometer descends through the annulus between the moving tube and a wider supporting tube, W, and thence through various channels drilled for that purpose into the cavity and the spaces behind the transducer diaphragm.

In accordance with good cryogenic practice the instrument was made almost entirely with oxygen free high conductivity copper to diminish the risk of thermal gradients appearing in the walls of the cavity. Most of the parts were assembled using Wood's metal - a low melting point solder.

5.1.1 The Cavity, its Dimensions and Alignment.

The first cut off wavelength will be given by

$$\lambda_{10} = 2\pi b / 1.84 = 3.42 b \qquad (5.1.1)$$

Thus, having decided to work below the first cut off frequency, we are obliged to use wavelengths greater than 3.42 cavity radii. It was decided, somewhat arbitrarily, that a little over five half wavelengths should be a sufficient length for the cavity giving three more than the absolute minimum of two required to calculate α and β. Should any unexpected systematic deviation of measured velocity with acoustic path occur it would be likely to be greatest in the early orders of resonance where $l \doteq \lambda$. By the fifth order it might be expected to show a change and thus betray its presence. To keep the cavity as short as possible it was desirable to use a bore of small radius. On the other hand, boundary layer errors would then increase and the loading of the gas column on the transducer would decrease so leading to a drop in sensitivity. The value of b=1cm was finally chosen which just enabled the smallest cube corner reflector which could be obtained to be mounted on the rear face of the moving acoustic reflector. This formed the aforementioned moving reflector, J, of the optical interferometer. A usable cavity length of 9.4cm was therefore made available which allowed five half waves to be accomodated when operating at a cut off frequency of $0.9 f_{10}$. A plot of f_{10} for this cavity is shown as a function of temperature in Figure 5.2.

It was in order to ensure good alignment of the moving acoustic reflector in any position that it was made in the form of a piston 10cm long (not including the cube corner housing or retaining cap). Being of copper it was chrome plated on its curved surface to diminish

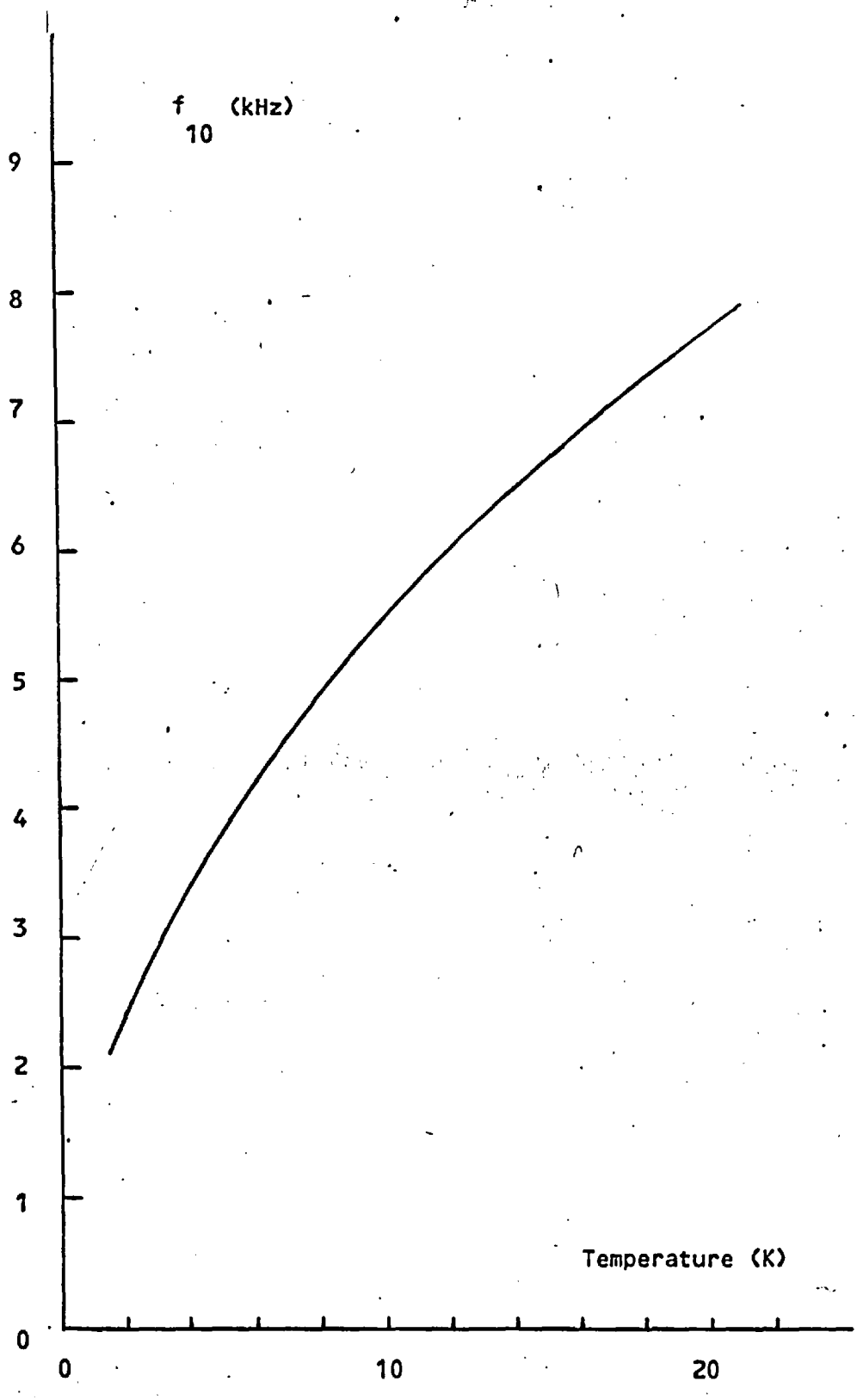

Figure 5.2

The First Cut Off Frequency as a Function of Temperature.

wear and to prevent it sticking to the unplated copper walls of the bore. This measure was thought to be necessary at the fine tolerances to which the bore and cylinder were lapped. Clearance was estimated to be a few ten thousandths of a centimetre. The face of the piston was aluminised to give it an optically reflecting surface and an autocollimator was used to measure the squareness of the piston face at various positions in the bore. By rotating the piston through 180^{o} on its axis and measuring the angular displacement of the reflected beam in two mutually orthogonal planes, an estimate of its alignment could be made. This method did not require the direction of the axis of the cavity to be determined independently. It was found that the piston face was out of true by less than an angle of 15 microradians (+ or - 10 per cent) in the worst case and about half this in the best. At the walls of the bore this is equivalent to an axial displacement of 15×10^{-6} cm or less than 5×10^{-6} of the cut off wavelength leading to a reflection loss of approximately 2×10^{-11} (calculated from equation 2.3.15) which is entirely negligible. Due to the method of lapping the end faces, it would be expected that the depth of any convexity or concavity would be far less than the "depth", $b\chi$ of any tilt, χ. But since this interferometer is operated in such a way as to measure the separation of resonances rather than absolute resonant lengths in accordance with the recommendations of section 4.2, no errors in measured velocity will arise from these causes, it being a question merely of keeping reflection losses to a minimum.

A longitudinal groove (not shown in figure 5.1) had been cut in the side of the piston to take a sprung Teflon pad should it be needed. This was designed to hold the piston hard against the opposite wall of the bore as it moved. But in the light of these alignment figures it was discarded since it was felt that it might add to the difficulties

of ensuring that the interferometer bore remained scrupulously clean after assembly. It has already been pointed out that, in any case, lateral forces cannot be transmitted to the piston because of the gimbals (themselves travelling on the bearing in the upper coaxial chamber).

The diaphragm of the moving coil transducer was held at its perimeter between two flat copper surfaces. The upper copper surface was machined on the flange at the lower end of the bore which was turned on a close fitting mandrel. This seemed the best way of ensuring that the diaphragm was square to the axis. Similar tests to those carried out on the piston were performed on this surface. A circular optical plate of the same diameter as the diaphragm was made and laid on the inverted cavity so that its lower face occupied the same position as would the radiating surface of the diaphragm. This face was aluminised except for a circular window of two centimetres diameter which looked into the mouth of the cavity. The autocollimator was thus able to focus on two reflected graticules simultaneously - one from the piston face as before, and one, in effect, from the radiating face of the diaphragm. This enabled the angular misalignment of transmitter and reflector to be measured directly. It was found never to exceed 28 microradians (+ or - ten per cent) representing an axial displacement of 28×10^{-6} cm at the walls of the cavity or approximately 8×10^{-6} of the cut off wavelength. Again such a figure represents an entirely negligible reflection loss.

5.1.2 The Transducer and the Accelerometer.

After checking the alignment of the transducer with the cavity there still remain two other geometrical problems - the flatness of the diaphragm and its coupling to the cavity.

Every care was taken to ensure that the diaphragm was flat. It was punched from Duralumin sheet 0.25mm in thickness, laid between two lapped steel blocks and subjected to a load of some fifty tons in an hydraulic press. It was then annealed for several hours at a temperature of 450 ^{o}C between the same lapped blocks under a load of approximately 20kg. Subsequent measurements with an engineer's micrometer capable of discerning differences of less than 10^{-3} cm failed to show any variations in thickness.

Experiments with diaphragms of several thicknesses loaded with a range of weights had shown that a lower spring rating made for greater sensitivity. Changes of mass, on the other hand, were not nearly so important. Accordingly, the diaphragm finally chosen for use had eight holes of 1cm diameter punched on a circle surrounding the central region which radiated into the cavity. Apart from lowering the spring rating they also diminished the gas loading on the diaphragm due to the pockets of gas in the transducer housing - in particular the gas between the outer region of the diaphragm and the flange at the base of the bore, which, it will be recalled from section 4.3, adds a constant term to the impedance of the transducer, and so lowers its sensitivity.

It was not possible to check the flatness of the diaphragm *in situ*, but it was felt that it could not possibly be distorted after this preparation. The flat clamping copper surfaces and the comparatively greater contraction of the diaphragm on cooling would also help to remove distortion had it occurred.

The unclamped diameter of the diaphragm was four times that of the

cavity. Had it been clamped at the edge of the cavity (see figure 2.7(b)) it would have suffered from the drawbacks outlined in section 4.3. Furthermore, there would have been insufficient space on the rear face to accommodate the driving coil and accelerometer which both require to be situated well in from the edge of the diaphragm to function to the best advantage.

The driving coil was wound on a perforated paper former, the purpose of the perforations being to prevent standing waves occurring in the gap between the rear face of the diaphragm and the pole piece of the permanent magnet. It was earthed at a centre tap and driven by a floating drive voltage. It was hoped that the resulting symmetry in the drive circuit would inhibit interference between the driving current and the accelerometer circuit. Every care was taken to ensure that the coil was aligned centrally in the gap of the permanent magnet assembly. Using a cryogenic varnish, it was stuck to the diaphragm in a specially constructed jig which held it central and kept it perfectly circular. The diaphragm itself was exactly located by a brass ring encircling the two copper clamping faces. Another jig was made which tightly fitted the gap in the permanent magnet assembly. The securing screws of the assembly were loosened, the jig inserted and the screws retightened. The assembly as a whole was centralised by being accurately placed in the copper housing which had the lower clamping ring machined on its upper face.

The accelerometer was a small lead zirconate titanate (PZT) synthetic piezoelectric element in the form of a cylinder. Supplied by the Brush Clevite Company, it had been poled axially to form the piezoelectric designated as "type 5A" and was plated on its end faces. It was loaded with a 4g disc of brass which also functioned as an electrical screen. The accelerometer assembly was glued together with cryogenic varnish and attached to the diaphragm in the same way.

Leads to both accelerometer and coil were tightly twisted and led away through screens of hypodermic tubing to pass through separate Stycast seals in the base of the transducer housing. They were then immediately rescreened and taken out of the cryostat through separate tubes and vacuum seals.

5.1.3 The Optical Interferometer.

The design of the optical interferometer is shown in Figure 5.3 and the situation of the low temperature components - already discussed - in Figure 5.1. The beam splitter providing the optical fiducial is located at some distance from the transducer diaphragm whose position it represents. But since the whole instrument is maintained at the same constant temperature, this is of no consequence. The same applies to the cube corner reflector moving at constant separation from the acoustically reflecting face of the piston. In this configuration there is approximately zero optical path for maximum acoustic path. Should the optical path increase to half the length of the cavity of the laser which is used, the output of the interferometer would be expected to fall owing to interference between the closely spaced wavelengths in the spectrum of the laser light. This calls for the use of a laser with a cavity at least twice as long as the maximum acoustic cavity length. Alternatively, a more sophisticated laser with only a single line could be employed, or a more elaborate interferometer which could function either side of zero optical path. In this case a 1mW helium-neon laser supplied by Spectra-Physics Ltd. was used with a cavity about 27cm long. An external magnet was supplied to polarise the beam.

Having used a cube corner for the full reflector, the only alignment required within the cryostat was that of the beam splitter. This was achieved simply by ensuring that the mating faces of the beam splitter plate and the upper cavity against which it was held were

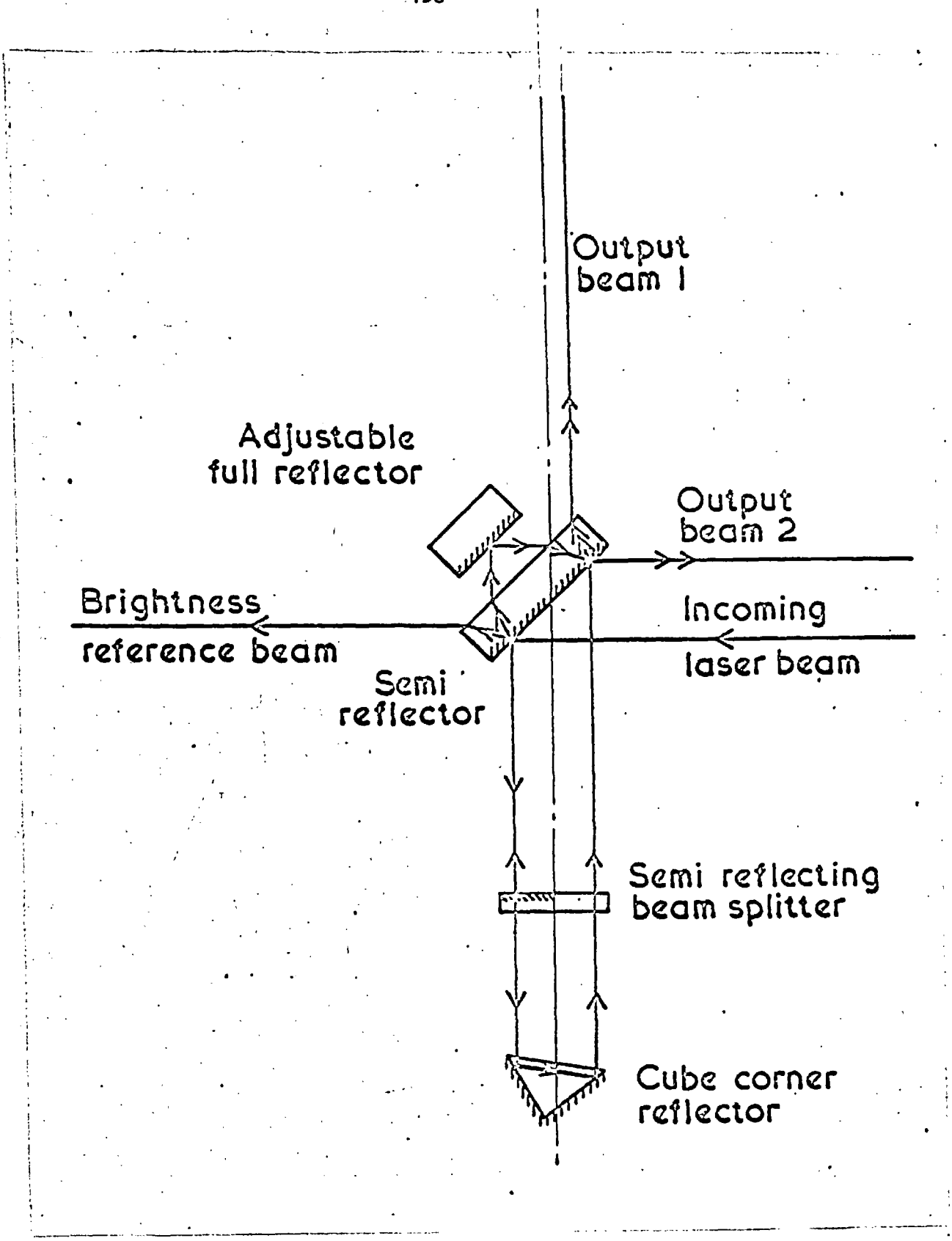

Figure 5.3

The Optical Interferometer.

true. It was with this in mind that Wood's metal solder was employed for assembly and sealing rather than the neater and cleaner crushed indium technique. With the latter changes of alignment unavoidably occur as the indium wire is crushed between the mating surfaces.

The laser was mounted on an adjustable bench hinged about the point where its beam impinged upon the semi-reflector which diverted half the light down into the cryostat. A single screw was used to tilt the bench until two beams of light re-emerged. The laser could then be positioned exactly so that the emergent beams were parallel and also coplanar with the laser beam. By adjusting the small room temperature reflector the two beams could be superimposed and aligned in the same direction. They would then interfere. Once aligned only occasional small adjustments were made. The stability of the optical interferometer was ensured by hanging the cryostat from a thick stainless steel optical table, itself supported on a heavy iron frame. All vacuum pumps were mechanically isolated from the frame with the aid of dampers and anti-vibration mountings both on the pumps and in the vacuum lines.

The light entered and left the cryostat through the moving tube which also served to raise and lower the piston. The beams were about 2 or 3 mm in diameter and the tube was 11.7mm internal diameter which enabled them to be kept well separated from each other and from the walls of the tube. At its room temperature end it was sealed with an optical window, and at its lower end was the cryogenic vacuum tight optical window welded onto a graded glass seal on a thin Covar tube. It was felt to be necessary to evacuate the moving tube in case gas convection or oscillation occurred over the large thermal gradient and made the optical interferometer unstable. Some consideration was also given to sealing the two cold components of the interferometer in a vacuum for the same reason. However, with the present type of

interferometer, this would have required a complex system of thin bellows to link the stationary beam splitter plate with the moving tube and piston. Such a system would almost certainly have been unreliable and so the idea was rejected. In fact such optical instability did occur as will be explained, and reduced the maximum pressure at which it was possible to operate the thermometer. A more satisfactory method would have been to provide two separate evacuated tubes into the instrument. One, being stationary, would descend to the fiducial, and the other, much as in the present instrument, would move with the reflector on the piston. However, no interruption of its vacuum to accomodate a stationary beam splitter would be necessary.

The window, in any case, was the cause of considerable difficulty. Attempts were made to glue optical flats into thin swaged copper tubes. Several of these functioned for a period of time, and then failed, even though all of them had been shock tested by plunging into liquid nitrogen many times whilst being monitored for leaks with a mass spectrometer. It seems that the usual resins available in a cryogenic laboratory are prone to crystallisation after prolonged thermal cycling. The problem with welding optical windows onto graded glass seals, on the other hand, is that they become optically unsatisfactory. However, after making several - all of a diameter larger than that required for optical purposes - one was obtained with a sufficiently good central region for optical interferometry. This has now been in use for some time.

The two sets of fringes obtained from the optical interferometer were in approximate quadrature since the fiducial beam in output 1 (see Figure 5.3) has had four reflections compared to the three in output 2. Both outputs were monitored by solar cells as was the intensity of the laser. After attenuation to the mean level of the fringe signals, the latter signal was subtracted from them to

compensate for any variation in laser intensity. The resultant signals were then amplified through d.c. amplifiers and subsequently used to trigger a bi-directional counter giving two counts for every fringe. The wavelength of the light was 6.3299×10^{-5} cm in vacuo, thus giving a precision of approximately 1.58×10^{-5} cm in a length measurement. A small correction was made to the wavelength to account for the refractive index of the thermometric helium which filled the optical interferometer. The density of the gas was calculated from a preliminary (and always sufficiently accurate) value of its temperature. Using the law of Gladstone and Dale:

$$\mu - 1 \propto \rho \qquad (5.1.2)$$

it was possible to correct the refractive index, μ, at STP for the prevailing conditions. The correction was of the order P/T parts in 10^{7} at a pressure of P N/m^{2} and a temperature of TK.

5.2 Control and Measurement of Temperature and Pressure.

5.2.1 The Cryostat.

The cryostat was supplied by the British Oxygen Company and was of conventional modern design. The whole assembly hung from the optical bench and could be taken apart layer by layer as shown in Figures 5.4 to 5.8. The outer layer was a standard British Oxygen Company stainless steel dewar modified so that the internal vacuum - usually common to the air/liquid nitrogen wall and the liquid nitrogen/liquid helium wall - could be split into two to facilitate precooling. This dewar could be disconnected from its vacuum lines and lowered on extensible springs from the optical bench against which it sealed to reveal the vacuum can in which the acoustic interferometer and radiation shield were suspended. Two vacuum lines also carrying the

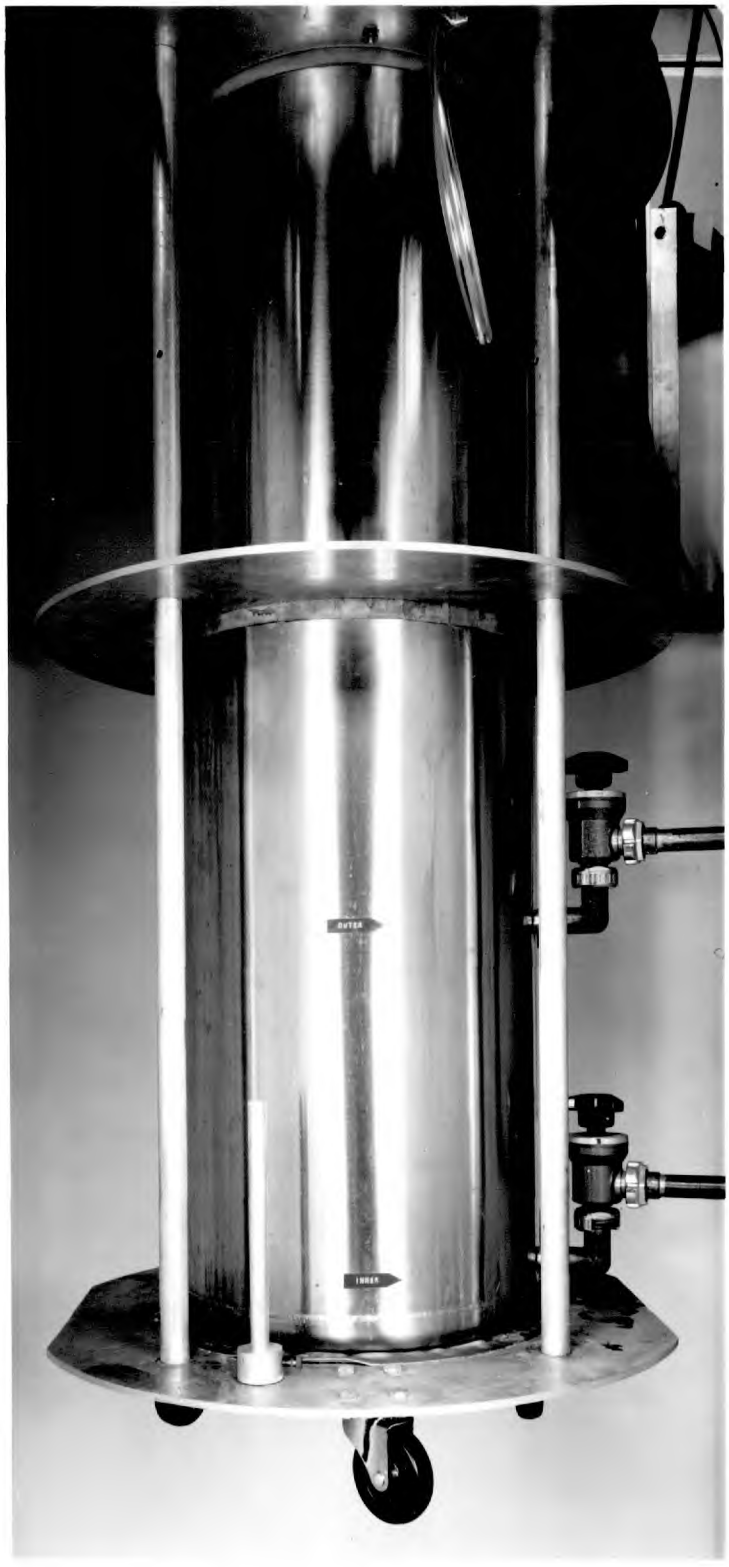

Figure 5.4

The Dewar Hanging from the Optical Table.

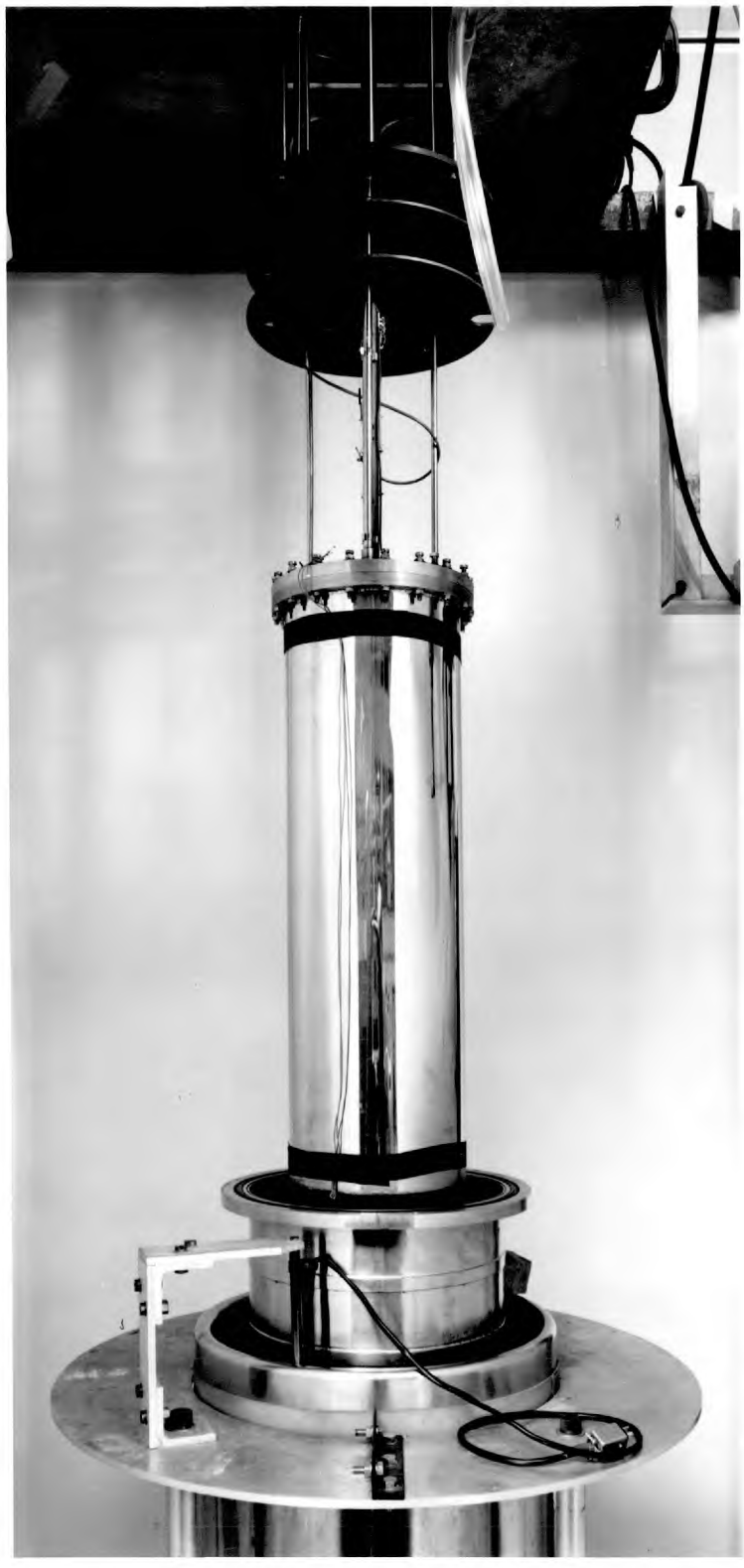

Figure 5.5

The Interferometer Vacuum Can.

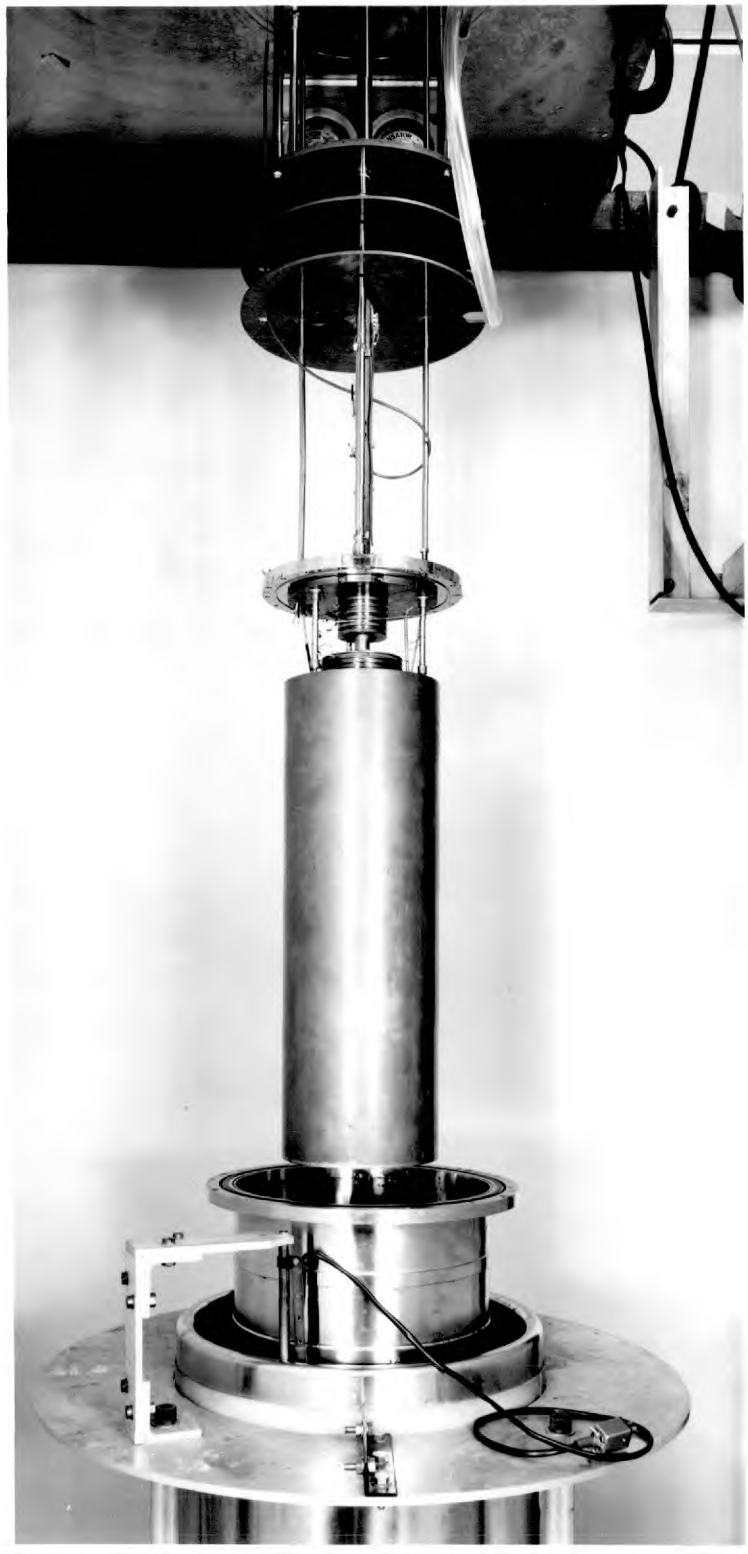

Figure 5.6

The Radiation Shield.

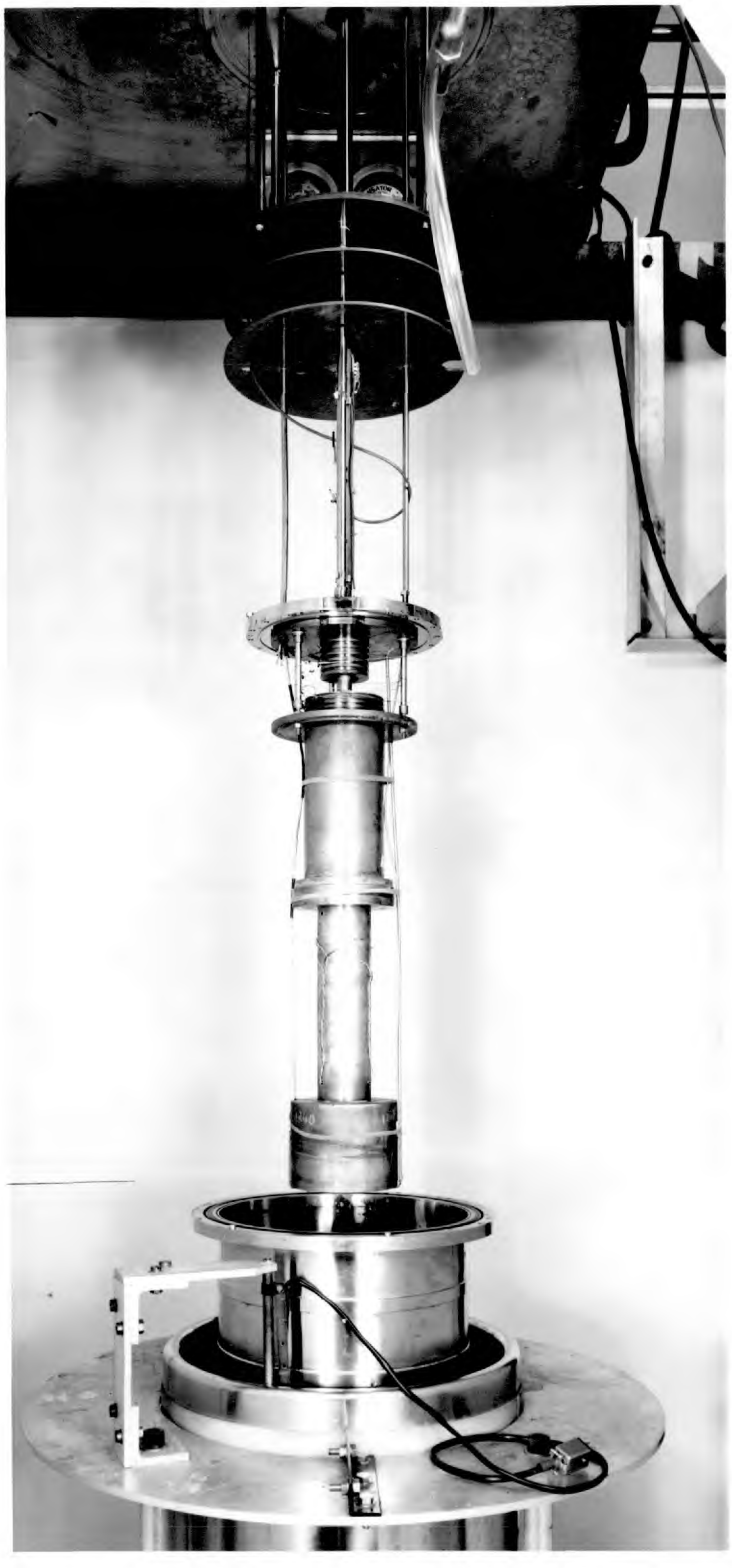

Figure 5.7

The Interferometer.

various electrical leads descended to the can from the optical bench above as did the large central tube within which the evacuated light tube moved. Three copper radiation baffles cooled by the gas boiling off from the liquid helium bath prevented room temperature radiation from the optical bench falling upon the can. This method of insulating the bath from above is preferable to the older and much more complicated technique of inserting another vacuum above the bath as well as around it.

To operate the system it first had to be precooled. A few hundred N/m^2 pressure of air was let into the nitrogen/helium vacuum wall as thermal exchange gas, and the helium bath was filled with helium gas at atmospheric pressure. Helium exchange gas was also let into the interferometer vacuum can at low pressure. The liquid nitrogen bath was then filled and the interferometer gradually cooled to approximately 80K over a period of about 36 hours. Liquid helium could then be transferred into the helium bath until it covered the vacuum can to a depth of up to 30cm - sufficient for almost 48 hours operation under the most favourable conditions. If care was taken to ensure that the liquid level did not fall below the bottom of the interferometer vacuum can, it was a matter of minutes to top up the bath in the mornings so that a velocity measurement could be taken in the afternoon and evening. After transferring the liquid helium, the helium exchange gas was evacuated from around the interferometer and the temperature and pressure controlling systems for the interferometer and its charge of thermometric gas could be switched on. The exchange gas in the nitrogen/helium wall, being air, solidified immediately the liquid helium transfer was initiated so that there was no need to evacuate this space.

The simple design of this cryostat ensured complete reliability except on two occasions when the only demountable vacuum seal in the

system leaked at low temperatures. This was a crushed indium wire seal on the flange of the interferometer vacuum can which probably leaked because it was not tightened sufficiently. However, the whole system may now be considered to be entirely reliable.

5.2.2 Temperature Measurement and Control.

Three four-lead germanium resistance thermometers were inserted into the walls of the interferometer so that they would be in thermal contact with the thermometric gas (see Figure 5.1). All had been calibrated at the normal boiling point of helium to within less than 1mK and carried the NBS acoustic scale, NBS-65, of Plumb and Cataland. The latter calibration was obtained through a comparison with a thermometer sent to the NPL from the NBS and originally calibrated against a resistance thermometer taken directly from their high frequency acoustic thermometer. Our comparison depended upon transfer via a computed fit and is therefore only accurate to + or - 2mK. Plumb and Cataland, it will be recalled, found that their temperature was 10mK above that defined on the T-58 and T-62 vapour pressure scales at the normal boiling point of helium. This was subsequently confirmed by Rodgers et al.[48] to within 3mK and by Cetas and Swenson[13]. Cetas and Swenson using a magnetic thermometer calibrated against the old platinum resistance thermometer scale, NBS-55 (see Figure 1.1), between 20 and 30K find the vapour pressure scale value too low by 6.7mK with a similar precision so that this result, too, would seem to confirm a figure in the order of 10mK. We have found our NBS-65 calibration to be 8mK (+ or -2mK) high relative to T-58 and T-62 at this point which is compatible with the other measurements.

In an experimental measurement of velocity the interferometer was brought to a temperature within several mK of the required temperature (always a fixed point for the work done to date). The values of velocity thus obtained were subsequently corrected to their exact

boiling point values using the gradient of the resistance-temperature curve for the germanium resistance thermometer. Thermometer resistances at temperatures other than the normal boiling point of helium were only known roughly for these thermometers, but when the need arose one was replaced by another calibrated thermometer, or, on one occasion, corrections to the velocities were made in retrospect when a calibrated thermometer subsequently became available. Errors introduced by uncertainties in the reproduction of the true fixed point temperature will be dealt with when the results themselves are discussed.

The temperature of the interferometer was controlled by a fourth germanium resistor - a two lead element this time - which formed an arm of an equal ratio a.c. Wheatstone bridge. The in-phase component of the out-of-balance signal from the bridge was selected by a phase sensitive detector whose output was used to control the current in a heater on the interferometer. Since the heater necessarily maintained the interferometer at a higher temperature than the ambient coolant bath, the latter had to be pumped slightly below its normal boiling point when measuring velocities at 4.2K. The controlling temperature was set by adjusting the resistance of another bridge arm and the quadrature component of the bridge output was nulled manually by a parallel variable capacitance. The lead to the controlling germanium sensor was of 1mm thick Karma wire as was a compensating lead in the other side of the bridge. Both electrical returns were via the cryostat itself thus enabling one side of the sensor to be soldered to the interferometer for good thermal contact.

With this controller temperatures could usually be held constant to better than + or -0.5mK for the duration of a measurement at 4.2K. At 20K they seldom varied by more than + or -2mK. However, these small drifts in temperature are easily corrected for. The velocity is

calculated from the positions of the first and last resonances which are recorded at the initial and final temperatures respectively. If there is a drift of ΔT, it may easily be shown that an error in measured velocity occurs of

$$\Delta c = \frac{c}{2} \frac{N}{N-1} \frac{\Delta T}{T} \qquad (5.2.1)$$

where N is the order of the last peak (usually five for our instrument). Accordingly the error in measured temperature will be

$$2T \frac{\Delta c}{c} = \frac{N}{N-1} \Delta T \qquad (5.2.2)$$

Thus if a rough value of ΔT is obtained from the monitored resistance thermometers this is easily corrected for.

5.2.3 Pressure Measurement and Control.

It was necessary that the pressure of the thermometric gas was held sufficiently constant for the duration of a velocity measurement. However, it became unstable above a certain value which was quite well defined for any given temperature. It appeared that gas convection took place within the annular region between the stainless steel supporting tube and the tube moving within it. (*1) The situation was

---

(1) A similar problem was encountered by Plumb and Cataland (see Reference 24). It would seem to be bad practice to use this

greatly improved by winding nylon cord around the inner tube so that the direct path of the gas was almost entirely obstructed whilst allowing it impeded access to the interferometer via a helical path. Nevertheless, it was not possible to operate the instrument much above 0.3 of an atmosphere at the boiling point of helium or about 1 atmosphere at the hydrogen boiling point. The onset of this pressure instability was accompanied by a marked deterioration in the stability of the temperature of the interferometer and, at the same time, an increase in the power required to maintain it at the chosen isotherm temperature. The stability of the optical interferometer was also adversely affected as has already been mentioned.

However, this problem has not greatly diminished the effectiveness of the instrument since it remains sensitive down to much lower pressures than these. In any case it is the lowest points on an isotherm that are the most valuable since they narrow the range of extrapolation to zero pressure. Their comparatively large boundary layer corrections are not necessarily any more problematical than smaller corrections at a greater distance from the intercept.

The pressure was controlled by a Texas Instruments pressure controller. This functioned by bleeding helium in or out of the system through servo controlled needle valves. The necessary controlling

---

annulus to take the thermometric gas down to the interferometer - probably because it will be denser in the region passing through the helium bath than in the warmer interferometer below. It is suggested that in any future instrument a tube is provided which descends past the interferometer and rises to it from beneath or else that the descending tube should be vacuum insulated from its room temperature end right down to the interferometer.

signal was supplied from a quartz spiral Bourdon tube gauge from the same manufacturer. In the absence of the aforementioned instability, pressures could nearly always be held constant to within + or $-5 N/m^2$ for the duration of a measurement - about three hours.

The pressure of the thermometric gas was measured and frequently checked using a recently calibrated Kew pattern mercury barometer, the usual corrections to standard temperature and gravity being made. Pressure measurements are estimated to be accurate to + or $-5 N/m^2$ which represents only a very small part of the total error in a final value of isotherm temperature.

5.3 The Modus Operandi and Tests on the System.

5.3.1 The Measurement of Velocity.

The velocity measurement itself consisted of taking values of the amplitude of vibration of the transducer as a function of acoustic path so that a resonance curve of the form shown in Figure 2.3 could be constructed. The amplitude was obtained in arbitrary units by measuring the the r.m.s. voltage from the PZT accelerometer. It was amplified by a high impedance low noise differential amplifier, passed through a tuned filter (both from AIM Ltd.) and then fed to a Dynamco a.c. to d.c. converter. This device enabled the r.m.s. voltage to be determined directly in terms of its heating effect on a vacuum thermojunction by providing a d.c. output voltage which was continuously adjusted to have the same heating effect. This was then measured by a digital voltmeter from the same manufacturer reading from 0 to 1.9999. A full analysis of the performance of this measuring system will be given in the next section.

Each time a value of the accelerometer voltage was recorded so was the value of the acoustic path. The acoustic reflector was initially brought down to the transducer and the optical counter zeroed. It was then raised and held at about four hundred positions on the resonance

curve whilst readings were taken. Both numbers were punched onto paper tape, one immediately after the other. Between the movement of the piston and the recording of the points sufficient time was allowed to elapse to enable pressure and temperature equilibrium to be achieved. But since the movement on the resonances was generally only some ten or twenty wavelengths of light, this took only a few seconds. The density of points between resonances was low since the curve varied only gradually, but the resonances themselves were covered much more fully. Prior to a run a rough plot of the resonance curve was obtained on a graphical x-y plotter. This was retraced during the run proper, and enabled one to see where the greatest point densities were required. Generally, the procedure was the same for all points on all velocity isotherms except in one respect. In the earlier readings the values of the maxima and minima of the resonance curve were found simply by searching for the extreme values on the digital voltmeter by moving the piston up and down. Later, points were taken over the maxima and minima and fitted with a low order polynomial fit whose peak gave the values adopted for the maxima and minima in the calculation on the impedance circles. The method finally adopted was to take points with a very close spacing over the peaks and merely to select the greatest and the least. There seems to be no difference in the quality of the answers obtained in the three different ways which is why the last method, being the simplest, was adopted. An example of a resonance taken at 20K is shown in Figure 5.9.

The driving current was obtained directly from the floating output of a frequency standard. This was of the frequency synthesising type supplied by the company of Schlumberger and claims an accuracy better than one part in 10^7. It was used with an output impedance set to 600 ohms driving the transducer symmetrically through two 330 ohm resistances - a method which ensured that the driving current was

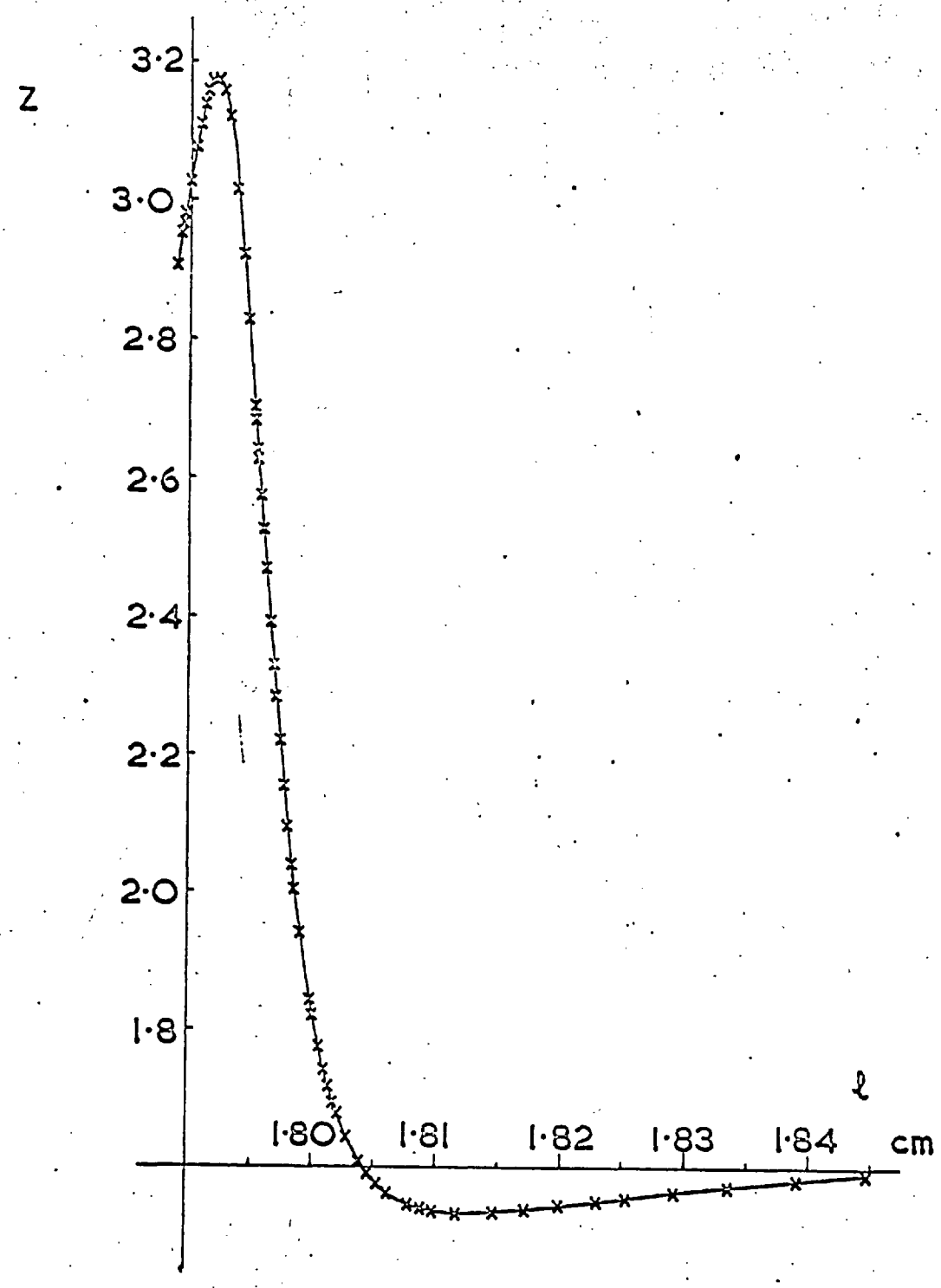

Figure 5.9

The First Resonance Taken at the Boiling Point of Hydrogen at a Pressure of 50030 N/m^2.

constant to at least one part in 10^4. The desired operating frequency was dialled digit by digit, each digit locking onto the internal frequency standard. This value of frequency was used in the calculation of the velocity.

The experimental curves were plotted on the NPL's computer controlled graph plotter and an occasional point was removed if it was found that that it lay well off an otherwise smooth curve. The data was then processed by computer rather than by manually drawing impedance circles as described in sections 2.1 and 4.1. However, the programme was an exact reformulation of the graphical procedure in terms of coordinate geometry and so, in principle, introduced nothing new. The data was split up into segments of resonances and anti-resonances (i.e. the slowly changing parts of the curve between the resonance peaks) and fitted with orthogonal polynomial fits. Values of Z_T were then calculated for each impedance circle from the anti-resonances either side of each resonance together with values of Z_{MAX} and Z_{MIN} followed by a first approximation of Z_{RES}. This enabled the six points closest to resonance on each peak to be selected and refitted with a low order orthogonal polynomial so that l_{RES} and dl/dZ could be accurately calculated. From the latter value an absorption coefficient could be calculated for each resonance. Absorption coefficients were also calculated from the half widths of the resonances and, as will be shown in Section 5.3.3, generally appeared to be more self consistent. The average of these was used to calculate the boundary layer correction to the velocity as explained in section 4.1.

5.3.2 Tests on the Accelerometer.

The first test to be performed on the accelerometer was to check that it did , indeed, yield impedance circles as expected. The signal from the accelerometer was amplified and split into in-phase and quadrature components with respect to the driving current (or the driving force). This was achieved by using a phase sensitive detector from AIM Ltd. The d. c. outputs were fed to the terminals of an x-y graph plotter so that mechanical impedance - or rather admittance - circles could be drawn directly.

$$\underline{V}(\ell) \propto \frac{1}{\underline{Z}_T + \underline{Z}_q(\ell)} \qquad (5.3.1)$$

The origin of the admittance plane was found by disconnecting the accelerometer input and marking the paper where the pen came to rest. This point represented a situation where no vibration was possible even with a finite driving force i. e. infinite impedance or zero admittance.

A similar test was carried out using the voltage across the driving coil instead of the accelerometer voltage so that another set of circles could be obtained - electrical impedance circles this time.

$$\underline{V}(\ell) \propto \underline{Z}_{COIL} + \frac{1}{\underline{Z}_T + \underline{Z}_q(\ell)} \qquad (5.3.2)$$

Two potential leads going down into the cryostat to the driving coil

had been provided for this purpose in case the accelerometer technique had proved unsatisfactory in practice. This enabled us to ensure that our direct mechanical "impedance" measurements were qualitatively similar to the electrical impedance measurements which constitute the raw data in the conventional and well established method of operating such an interferometer. The two sets of circles are shown in figure 5.10 and indicate clearly that, whatever the strict interpretation of the circles may be, they may still be regarded as impedance circles for our purposes since the true point of resonance will be obtained by exactly the same procedures that have already been described with regard to mechanical impedance circles proper. The only point for careful consideration arises with the calculation of absorption coefficients where the wrong sign will be obtained unless the slope of "Z" is correctly expressed at resonance. Accordingly we shall feel free to talk of the various distances on the diagrams as representing the same quantities as they did in figure 2.2 - in particular, the distance of the circles from the origin will be taken to be a measure of Z_T although, from equations 5.3.1 and 2 it will be apparent that it is not.

The short distance of the accelerometer circles from the origin compared to their diameters shows that the newer method is the more sensitive one. The greater ratio of Z_T to $Z_G(l)$ in the case of the electrical measurements is the result of the purely electrical impedance of the device being included in its total measured impedance. This effect was predicted in section 4.3 and leads to a loss of sensitivity in the detection of the position of resonance and hence in the measurement of velocity. Since the purely electrical component of the transducer impedance remains the same at increasingly lower pressures, the instrument tends to become less sensitive at the lower end of the isotherms where the effect is least welcome. However,

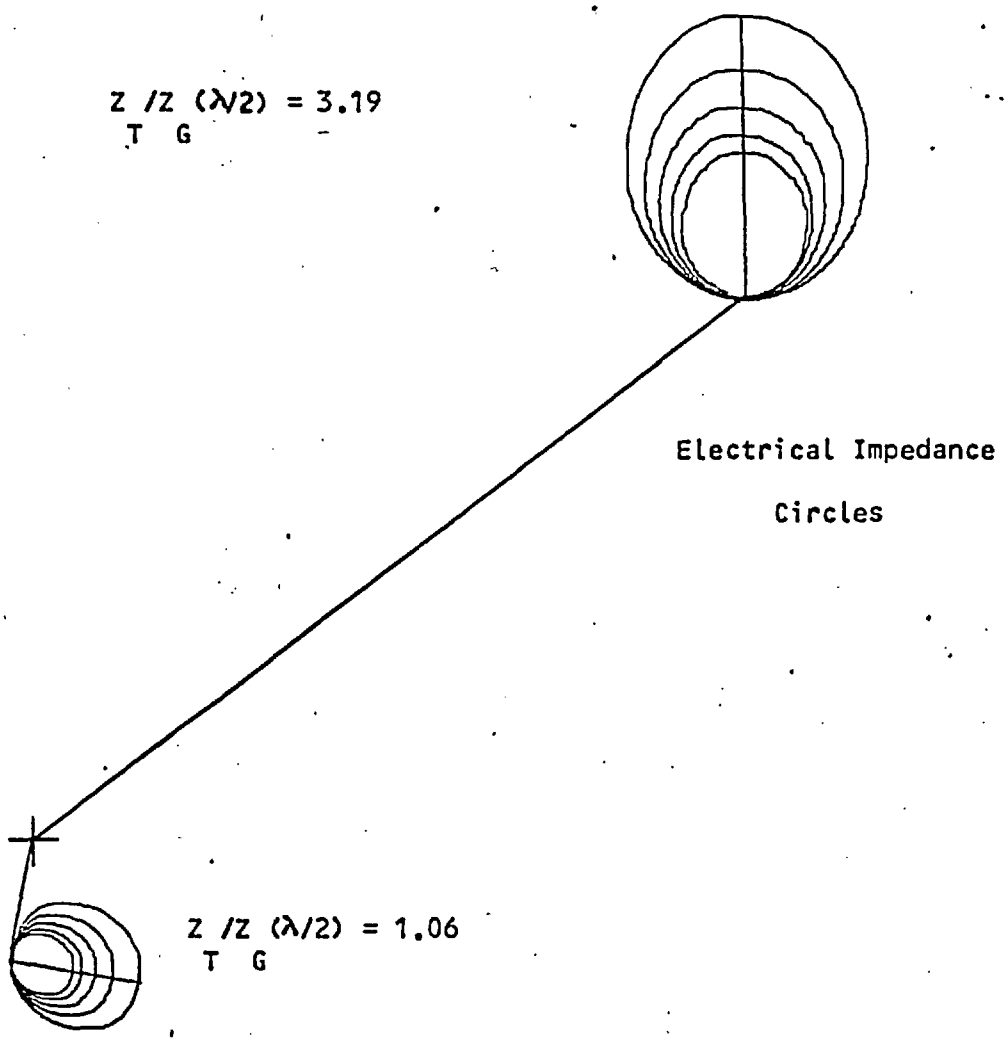

Figure 5.10

A Comparison of the Accelerometer Technique for Detecting Resonance with the Conventional Technique.

the purely mechanical contribution to Z_T in either type of impedance diagram may be expected to fall to some extent due to the fact that the internal gas loading of the transducer (that due to the pockets of gas behind the diaphragm for example) falls at lower pressures in the same way that $Z_G(l)$ does. Thus the impedances tend to remain of comparable size even at low pressures in the accelerometer method.

The poor quality of the circles (i. e. their ovality) was traced to a phase error in the circuitry responsible for resolving the input voltage into in-phase and quadrature components. It can be seen that it is similar for both types of measurement. The quality achieved in this sort of application using the type of phase sensitive detector commercially available is not likely to be significantly better than this. Lengthy investigations with an accurate impedance bridge would be required for exact plotting of the circles. However, this was considered to be an adequate demonstration that the accelerometer signal was behaving in a qualitatively similar way to the electrically measured impedance, only with greater sensitivity as expected.

Simple tests were also carried out at room temperature on the accelerometer leads to ensure that there was no serious interference from the driving current in accordance with the criteria of Section 4.3. Dummy leads in physical, but not electrical, contact with the accelerometer were substituted for the normal leads and the accelerometer was short circuited and earthed. The interference voltages were then read on an oscilloscope and compared to the normal accelerometer signal obtained under similar conditions. The results are shown in Table 5.1 where it can be seen that the interference voltages are hardly ever in excess of 10^{-3} of the signal from the interferometer and always less than one per cent. Since the smaller voltages could not be read very easily, an upper limit to the signal to noise ratio had to be calculated from the smallest visible

TABLE 5.1

Interference in the Accelerometer Leads from the Driving Coil.

Frequency (kHz)	Accelerometer Signal (Vp-p)	Noise in Leads (Vp-p)	Signal to Noise Ratio
2.0	0.28	7×10^{-5}	4×10^{3}
4.0	0.05	$<<5\times10^{-5}$	$>>1\times10^{3}$
6.0	0.04	$<<5\times10^{-5}$	$>>8\times10^{2}$
8.0	0.07	$<<5\times10^{-5}$	$>>1\times10^{3}$
10.0	0.02	$<<5\times10^{-5}$	$>>4\times10^{2}$

N. B. 5×10^{-5} was the smallest readable voltage although smaller voltages could be seen.

interference voltage so that the figure, as written, will almost certainly be pessimistic. But, in any case, they represent an entirely negligible error when substituted into equation 4.3.19.

The linearity of the PZT accelerometer and its associated circuitry was tested by plotting the amplified output signal against the current passing through the transducer coil. Block diagrams of the accelerometer circuit and the drive circuit, both described in the previous section, are shown in Figure 5.11. In the latter circuit a transformer has been added across one of the 330 ohm series resistances in order to isolate it from the voltmeter which would otherwise earth one end of it. The voltmeter used was in fact the a.c. to d.c. converter and associated digital voltmeter which also served to measure the amplitude of the accelerometer signal.

Like the circle tests, these were carried out at the normal boiling point of helium-4 at a pressure of 16690N/m^2 in the acoustic cavity and a driving frequency of 3.3kHz. Measured values of the driving current in terms of the voltage dropped across the series resistor and output signal are shown in Table 5.2, and their ratio plotted as a function of the former in Figure 5.12. It can be seen that above an output reading on the digital voltmeter of 0.1500 the system is linear to better than one per cent. In practice voltages read are always greater than than 0.1500 under these conditions, so it is felt that this figure represents the linearity achieved in an actual temperature measurement. The linearity of the driving current measurements should be considerably better (about 0.07 per cent, which is the linearity for the converter specified by the manufacturer).

However, even if non-linearities were far worse than this, it should still not affect measured temperatures. This is because on extrapolation of measured velocity to zero pressure the range of the voltages measured becomes increasingly small compared to the voltage

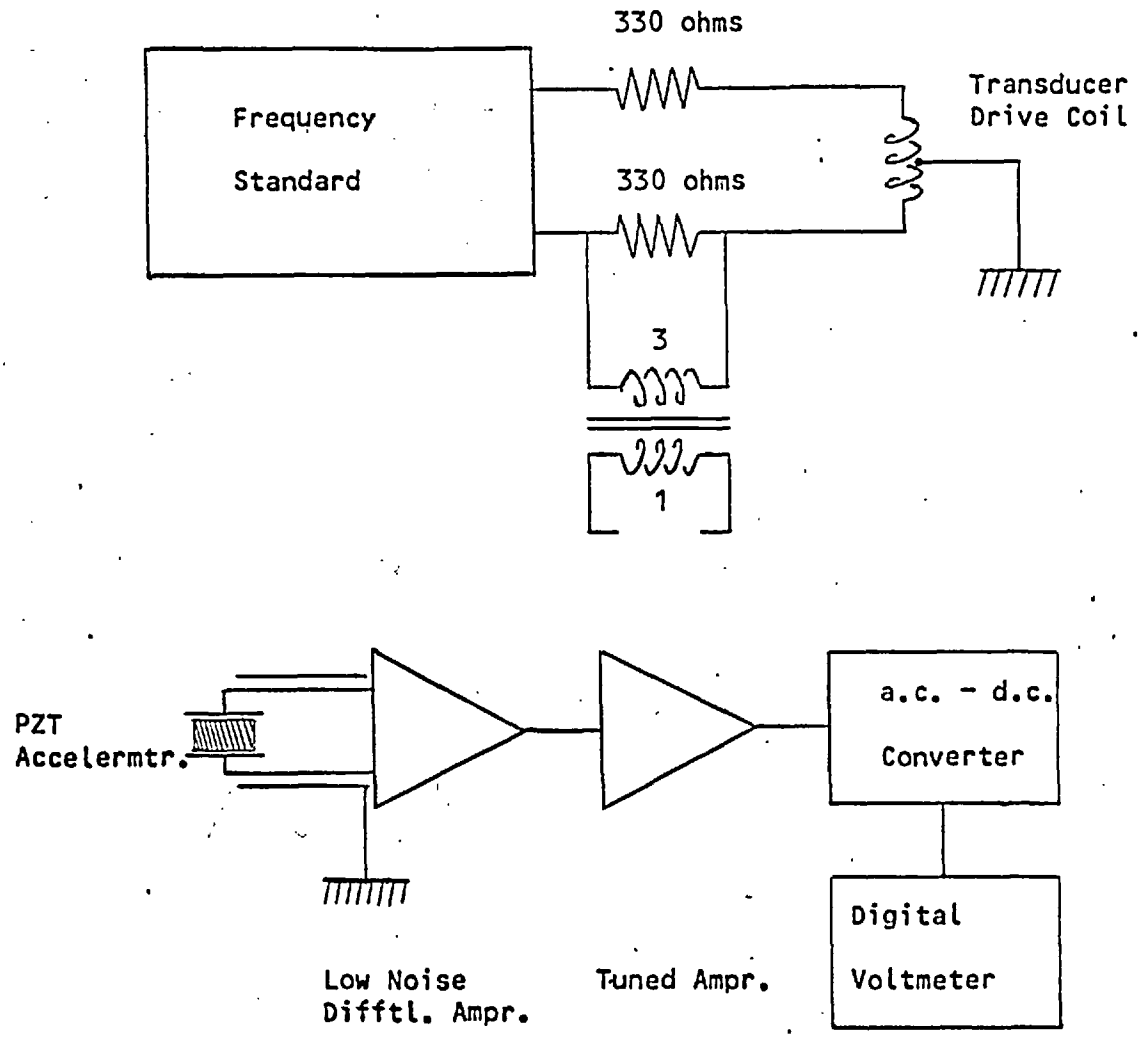

Figure 5.11

Circuits for Accelerometer Linearity Tests.

TABLE 5.2

The Linearity of the Accelerometer.

Current	Accelerometer Signal	Ratio
0.0522	0.1853	3.549
0.0754	0.2740	3.632
0.0929	0.3412	3.672
0.1265	0.4702	3.716
0.1510	0.5635	3.732
0.1760	0.6575	3.736
0.2003	0.7485	3.737
0.2258	0.8472	3.752
0.2497	0.9350	3.744
0.2754	1.0378	3.768
0.3184	1.1972	3.760
0.3186	1.1972	3.758

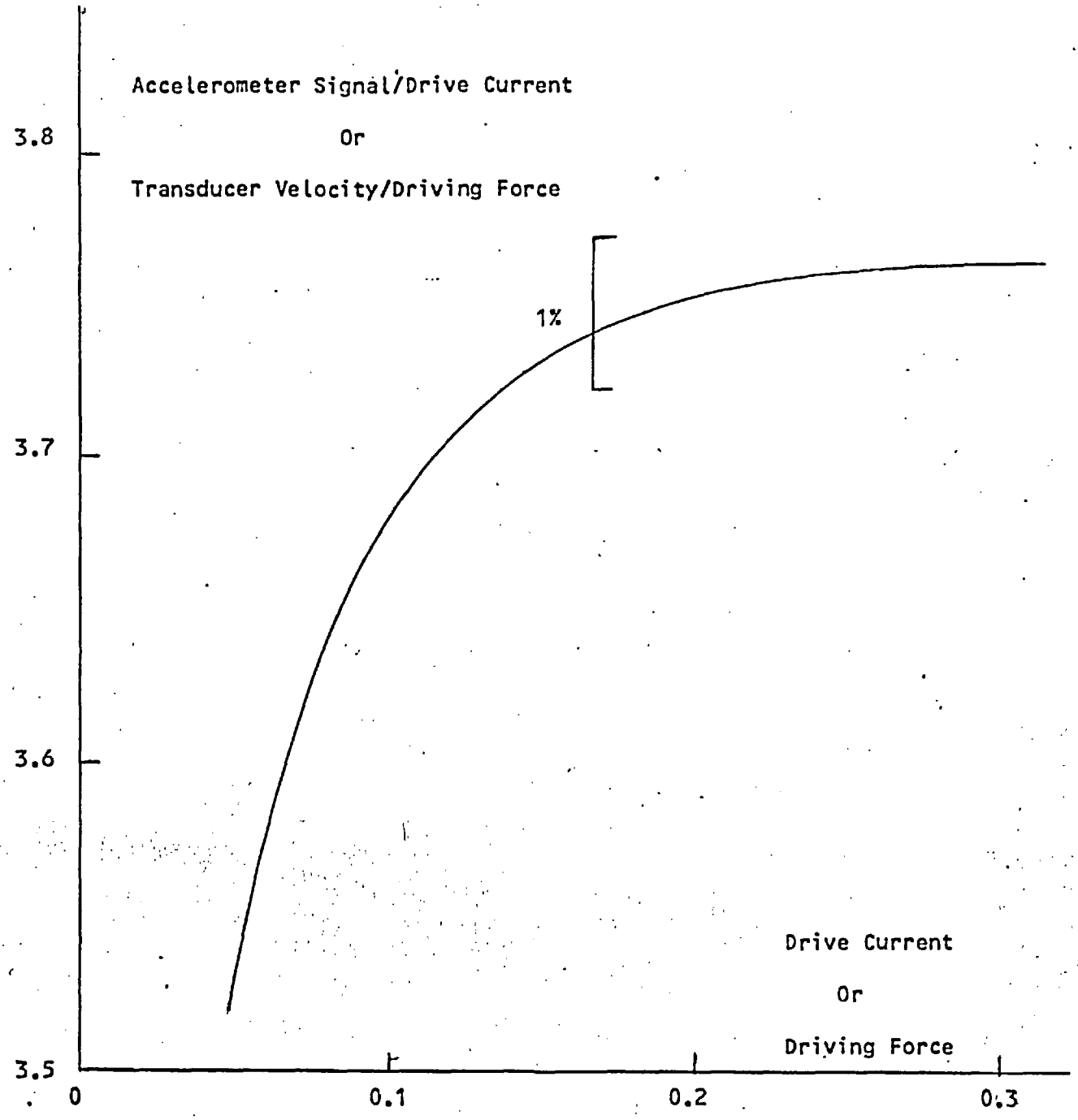

Figure 5.12

The Linearity of the Accelerometer.

characteristic of the impedance, Z_T. Consequently non-linearities in the system are removed by extrapolation just like gas imperfections.

5.3.3 Tests on the Boundary Layer Corrections.

In view of the aforementioned suspicion of the orthodox frequency dependence of the boundary layer effect of order 1/2, it was decided, as suggested in Chapter III, that it should be tested experimentally. Accordingly several velocity and absorption coefficient measurements were taken at the same temperature and pressure, but at varying frequencies. The results are shown in Table 5.3. At the lower frequencies, the reactance of the transducer appeared to become somewhat small leading to resonances of a fair degree of symmetry reminiscent of those characteristic of a quartz crystal transducer. Thus the true point of resonance lay close to the peak so that its exact location was difficult since the height of the resonance curve becomes rather insensitive to changes in cavity length under these conditions. The situation is further complicated because small amounts of noise or a small scatter on the points becomes more serious when the curve becomes flatter. Absorption coefficients were calculated both from the slopes of the resonance curves at resonance and from the half widths of the resonances. It can be seen that the latter values are more self consistent and so it has been decided to use these for the calculation of the boundary layer corrections. Their superiority is most in evidence at the low frequencies where the symmetry of the resonances makes the measurement of the slope at resonance harder, if anything, than the location of the resonance itself. This is because the slope near the maxima varies considerably with position and also because, even when the exact position of resonance is correctly defined, noise can seriously change the slope of a fit put through a mere six points (see Section 5.3.1). At higher frequencies when the slope of the curve is very steep at resonance, it can be seen that the

TABLE 5.3

Tests on the Frequency Dependence of the Boundary Layer Effect.

f (kHz)	Date	$\alpha \times 10^3$ (from slope) (/cm)	$\alpha \times 10^3$ (from h/wdth) (/cm)	c (meas'd) at b. p. (cm/s)	c corr'd for b. layer (cm/s)
1.5	27/04/71	1.125	1.153	(velocity not	
		1.176	1.158	successfully taken)	
	29/10/71	1.110	1.058	(11957.6)	
		1.262	1.151	11954.5	
	04/11/71	1.545	1.259	(11957.1)	
	(I)	0.894	1.099	11953.5	
	04/11/71	1.318	1.158	(11960.4)	
	(II)	0.942	1.155	11956.4	
Mean:		1.171	1.149	11954.8	
Std. Error:		0.064	0.019	0.7	
					11972.2
1.75	25/06/71	1.135	1.296	(11952.4)	
	(I)	5.095	1.550	11950.7	
	08/07/71	1.668	1.233	(11956.4)	
		1.117	1.119	11951.5	
	20/07/71	1.202	1.086	(11956.5)	
		2.888	1.167	11950.7	
Mean:		2.184	1.288	11951.0	
Std. Error:		0.587	0.060	0.4	
					11967.7
2.05	15/06/71	1.306	1.270	(119604)	
		1.287	1.276		
		1.257	1.267	11957.6	
Mean:		1.283	1.271		
Std. Error:		0.012	0.001		
					11971.7

continued.....

2.25	25/06/71 (II)	1.320	1.376	(11960.4)	
		1.358	1.397		
		1.376	1.346	11958.0	
Mean:		1.351	1.373		
Std. Error:		0.013	0.012		
					11971.9
2.50	24/06/71	1.398	1.412	(11959.9)	
		1.464	1.382		
		1.454	1.414	11956.8	
Mean:		1.438	1.403		
Std. Error:		0.017	0.009		
					11969.6
3.0	07/07/71	1.661	1.677	(11961.9)	
		2.995	1.739		
		1.742	1.624		
		1.625	1.801	11958.3	
Mean:		2.006	1.710		
Std. Error:		0.286	0.033		
					11971.0
3.3	10/01/71	1.739	1.742	(11952.3)	
		1.669	1.645		
		1.676	1.780		
		1.770	2.636*	11959.1	
Mean:		1.714	1.951 (use 1.723)		
Std. Error:		0.021	0.200		
					11971.0

* These values are rejected as being spurious since they are more than three standard deviations from the mean

two absorption coefficients agree very well when the occasional spurious point has been removed. Spurious points have been marked in Table 5.2 and the justification for each rejection is that the value rejected compares badly with the remaining values taken at the same frequency. Because of the prevalence of such points at the two lowest frequencies (1.5 and 1.75kHz) and because of the large scatter in the raw velocity measurements they have been repeated several times. The mean of the better answers has been taken and treated as a single point. In our judgement the weight deserved by these two averaged points is more nearly comparable to that merited by the higher frequency points, and so all points will be treated equally without, we feel, unduly overrating the importance of any one measurement relative to another. Had all the low frequency measurements been employed as individual points in the curve fitting investigations about to be described, then a seriously misleading influence would have been exerted on the functions being fitted to the points.

It was assumed that

$$\alpha = \frac{A\,\pi^{\frac{1}{2}}}{b\,c}\,f^{p} \qquad (5.3.3)$$

and $\log_{10}\alpha$ was fitted with a straight line as a function of $\log_{10} f$ so that

$$\log_{10}\alpha = \log_{10}\left\{\frac{A\,\pi^{\frac{1}{2}}}{b\,c}\right\} + p\log_{10} f \qquad (5.3.4)$$

thus enabling p to be obtained from the slope of the fit. It was found

that

$$p = 0.519 \text{ + or - } 0.066(\text{std. error})$$

where the standard error has been quoted. We feel that, unless one is prepared to consider values for p which are not simple fractions, this shows that the orthodox frequency dependence for the boundary layer absorption coefficient is correct, and certainly that an order of 3/2 is not applicable to our instrument. The latter conclusion is further reinforced by a plot of the absorption coefficient against the square root of the frequency. Here we find that a polynomial fit to the points of order three has a somewhat larger standard deviation than a linear fit. A value of

$$A = 0.211 \text{ + or - } 0.027(\text{std. error})$$

was calculated from the slope of the linear fit which compares very well with the theoretical value of 0.198 calculated from such rough values of the transport properties of helium gas that were available for this temperature and pressure. If, in addition to the seven experimental points of α and $f^{1/2}$, we include the origin we obtain a better value still:

$$A = 0.201 \text{ + or - } 0.009(\text{std. error})$$

The latter step is quite legitimate since, whatever the frequency dependence of the boundary layer effect, we may assume that absorption losses will disappear at zero frequency where the particle velocity at any point in the gas, and so the rate of working, will be zero too. In any case, it was found with the first fit that the line passed by the origin well within a distance given by the standard error of the intercept. The results of these fits are shown in Tables 5.4 and 5.

In order to assess the dependence of measured velocity upon frequency, the velocities were fitted against the reciprocal of the square root of the frequency with linear, quadratic and cubic

TABLE 5.4

Linear Fit of the Logarithm of the Measured Absorption Coefficients as a Function of the Logarithm of the Frequencies.

Log f 10 Data	Log 10 Data	Log 10 Calc'd	Residuals
3.17609	-2.93968	-2.94528	-0.00560
3.24304	-2.89008	-2.91055	-0.02047
3.31175	-2.89585	-2.87490	+0.02095
3.35218	-2.86233	-2.85393	+0.00840
3.39794	-2.85294	-2.83019	+0.02275
3.47712	-2.76700	-2.78911	-0.02211
3.51851	-2.76371	-2.76764	-0.00392

Result:

Constant Term = -4.59301 + or - 0.22280(std. error)
Linear Coefft. = +0.51879 + or - 0.06640(std. error)

Standard Deviation of Points = 0.0199

TABLE 5.5

Polynomial Fits of the Measured Absorption Coefficients as a Function of the Square Root of the Frequency.

Linear Fit:

$\sqrt{f}$ Data ($\sqrt{Hz}$)	$\alpha \times 10^3$ Data (/cm)	$\alpha \times 10^3$ Calc'd from 7 pts. (/cm)	Resdls. $\times 10^5$ (/cm)	$\times 10^3$ Calc'd from 8 pts. (/cm)	Resdls. $\times 10^5$ (/cm)
0	0			-0.01003	-0.01003
38.7928	1.14900	1.12630	-2.26983	1.14407	-0.49292
41.8330	1.28800	1.22428	-6.37160	1.23654	-5.14584
45.2769	1.27100	1.33303	+6.20257	1.33917	+6.81665
47.4342	1.37300	1.40114	+2.81404	1.40345	+3.04498
50.0000	1.40300	1.48216	+7.91565	1.47991	+7.69087
54.7723	1.71000	1.63284	-7.71599	1.62212	-8.78836
57.4456	1.72300	1.71725	-0.57484	1.70178	-2.12203

Result for seven point fit:

Constant Term = $-(0.96590 \pm 1.92451(\text{std. error})) \times 10^{-4}$

Linear Coefft. = $+(3.15749 \pm 0.39821(\text{std. error})) \times 10^{-5}$

Standard Deviation of Points = 6.55×10^{-5}

The Standard Deviations for the quadratic and cubic fits are 6.03×10^{-5} and 6.95×10^{-5} respectively.

Result for eight point fit:

Constant Term = $-(1.00334 \pm 5.78865(\text{std. error})) \times 10^{-5}$

Linear Coefft. = $+(2.97988 \pm 0.12804(\text{std. error})) \times 10^{-5}$

Standard Deviation of Points = 6.11×10^{-5}

The Standard Deviations for the quadratic and cubic fits are 6.44×10^{-5} and 6.06×10^{-5} respectively.

polynomials. It was found once more that the standard deviation of the fit deteriorated a little on raising its order to two or three. Again, the lack of improvement in the fit with the cubic polynomial suggested that no dependence on the 3/2th power of the frequency was present in the measured velocities. A value for A of 0.208 + or - 0.082(std. error) which is in very good agreement with the values calculated from the absorption coefficients was obtained from the linear fit using equation 4.1.2, and the value of the intercept, interpreted as the value of the velocity at infinite frequency (when the boundary layer error in the velocity is zero), was

$$c_\infty = 11971.4 \text{ + or - } 5.9(\text{std. error}) \text{ cm/s}$$

Reference to Figure 5.13 shows that all the corrected velocities lie within one standard error bar of this value as would be expected. This value was subtracted from the measured values of velocity. and the following form for the frequency dependence was assumed:

$$c_\infty - c = \frac{A c}{2 b \pi^{\frac{1}{2}}} f^p \qquad (5.3.5)$$

A straight line fit of $\log_{10}(c-c_\infty)$ against $\log_{10} f$ was then carried out as before:

$$\log_{10}(c_\infty - c) = \log_{10}\left\{\frac{A c}{2 b \pi^{\frac{1}{2}}}\right\} + p \log_{10} f \qquad (5.3.6)$$

so that the order of the frequency dependence could be obtained. It was found that

$$p = -0.483 \text{ + or - } 0.172(\text{std. error})$$

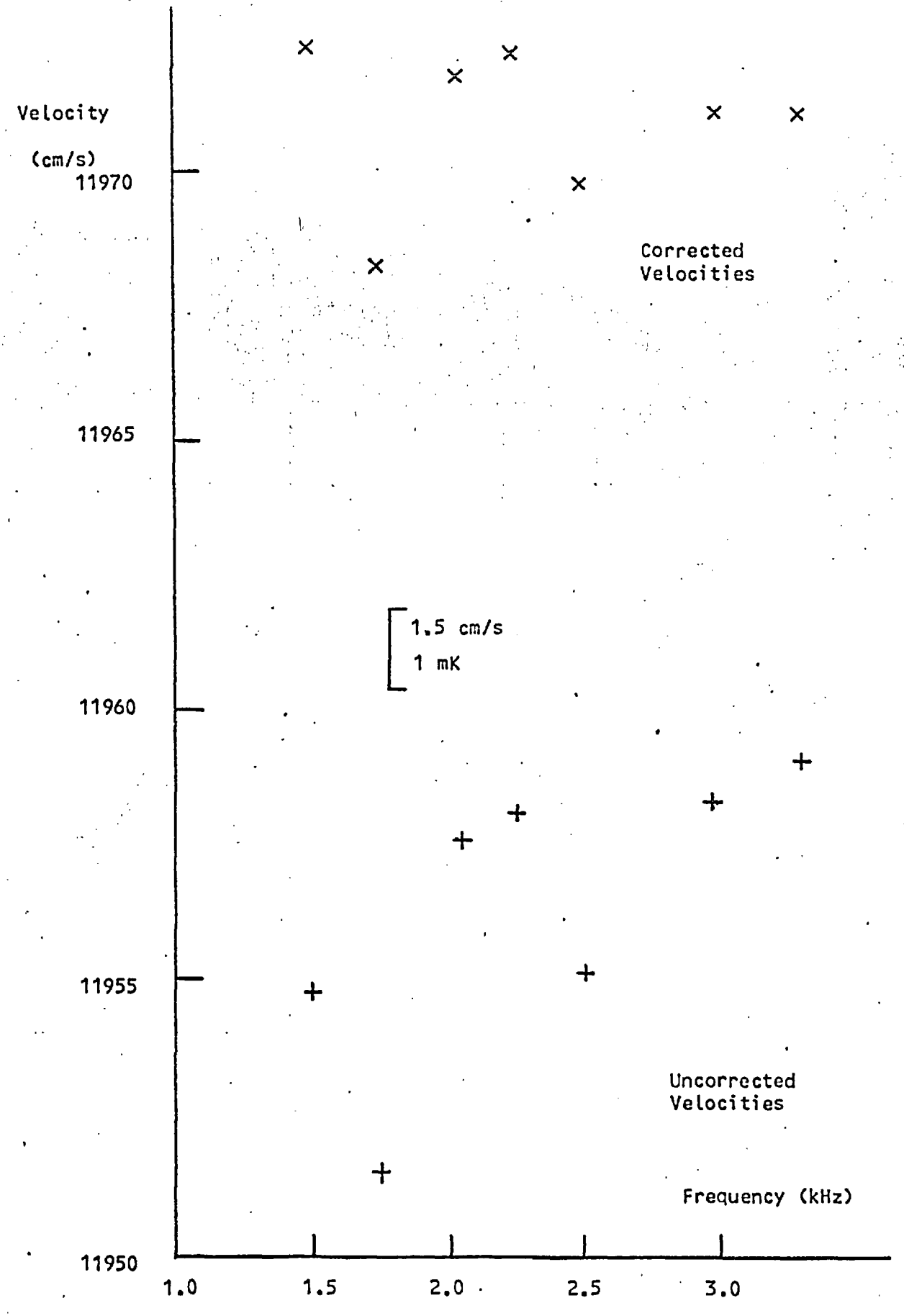

Figure 5.13

The Boundary Layer Correction as a Function of Frequency.

which again is a satisfactory answer from the point of view of the orthodox theory showing that our initial assumption that the frequency dependence was of order one half was self consistent. However, this answer suffers from the rather inaccurate value obtained for c_∞, and so it was decided to investigate a fit of the corrected velocities against the reciprocal of the square root of the frequency to ensure that they were constant to within the statistical error of the fit. Corrections were made to the measured velocities from equation 4.1.3

$$\Delta c = \frac{\alpha c}{\omega}^{2} \qquad (5.3.7)$$

and we obtained

$$c = 11971.6 \text{ + or - } 5.0(\text{std. error})$$
$$- (39.977 \text{ + or - } 235.865(\text{std. error}))/f^{1/2}$$

This function was chosen to represent any frequency dependence that might remain in the purportedly corrected velocities because it was assumed that such errors would in any case vanish at higher frequencies where the boundary layer effect becomes negligible. It can be seen that the magnitude of the remaining frequency dependence is far less than one standard error and so may well be of purely statistical origin. Furthermore, at the highest frequency (3.3kHz) where temperature measurements are made it amounts to only 58 parts per million in the velocity equivalent to approximately 0.5mK which is virtually negligible, and far less than the uncertainty in the frequency independent term (+ or - 2.3mK). The details of the last three fits are given in Tables 5.6 to 8.

TABLE 5.6

Polynomial Fits of the Measured Velocity as a Function of the Reciprocal of the Square Root of the Frequency.

Linear Fit:

$100/\sqrt{f}$ Data ($/\sqrt{Hz}$)	c Data (cm/s)	c Calc'd (cm/s)	Residuals (cm/s)
2.58199	11954.8	11953.3	-1.5
2.39046	11951.0	11954.7	+3.6
2.20863	11957.6	11955.9	-1.7
2.10819	11958.0	11956.6	-1.4
2.00000	11956.8	11957.4	+0.6
1.82574	11958.4	11958.6	+0.2
1.74078	11959.1	11959.2	+0.1

Result of Linear Fit:

Constant Term = 11971.4 + or - 5.9(std. error)
Linear Coefft. = -699.866 + or - 276.634(std. error)

Standard Deviation of Points = 2.03

The standard deviations for the quadratic and cubic fits are both 2.27.

TABLE 5.7

Polynomial Fits of the Logarithm of the Estimated Boundary Layer Velocity Error as a Function of the Logarithm of the Frequency.

Linear Fit:

$\log_{10}$ f Data	$\log_{10}$ c Data	$\log_{10}$ c Calc'd	Residuals
3.17609	1.22011	1.25218	+0.032
3.24304	1.30963	1.21987	-0.090
3.31175	1.13988	1.18671	+0.047
3.35218	1.12710	1.16720	+0.040
3.39794	1.16435	1.14512	-0.019
3.47712	1.11394	1.10690	-0.007
3.51851	1.08991	1.08693	-0.003

Result of Linear Fit:

Constant Term = 2.78499 + or - 0.57752(std. error)
Linear Coefft. = -0.48261 + or - 0.17210(std. error)

Standard Deviation of Points = 0.0516

The standard deviations for the quadratic and cubic fits are 0.0576 and 0.0627 respectively.

TABLE 5.8

A Linear Fit of the Corrected Velocity as a Function of the Reciprocal of the Square Root of the Frequency.

100/√f Data (/√Hz)	c Data (cm/s)	c Calc'd (cm/s)	Residuals (cm/s)
2.58199	11972.2	11970.6	-1.6
2.39046	11967.7	11970.7	+3.0
2.20863	11971.7	11970.8	-0.9
2.10819	11971.9	11970.8	-1.1
2.00000	11969.7	11970.8	+1.1
1.82574	11971.3	11970.9	-0.4
1.74078	11971.0	11970.9	-0.1

Result of Linear Fit:

Constant Term = 11971.6 + or - 5.0(std. error)
Linear Coefft. = -39.9768 + or - 235.865(std. error)

Standard Deviation of Points = 1.73

5.3.4 Tests on the Measured Diameters of the Impedance Circles.

Fundamental to the whole treatment of the raw data is the assumption of Section 4.1 that the circle diameters are of the form given by

$$D_N = \frac{1}{aN + b} \qquad (5.3.8)$$

If this is not true then it will certainly be impossible to measure the boundary layer corrections in the way we had hoped and, depending upon the reason for the discrepancy, it may not be possible to calculate the exact position of resonance as outlined in Section 2.1.

In order to demonstrate that our assumption was, in fact, correct, the first eight isotherm points taken at the normal boiling point of helium (see next chapter) were investigated. The reciprocals of the diameters of the circles (obtained by subtracting Z_{MIN} from Z_{MAX}) were plotted against the order of resonance, N, to ensure that straight lines were obtained. The diameters are given in Table 5.9 together with the pressure at which they were taken, and their reciprocals are plotted in Figure 5.14. As may be seen they confirm the predicted linear relationship very closely with the exception of the last point at the lowest pressure which is due to an error in the reading of Z_{MIN}. We have rejected this point and calculated the velocity from the first four resonances alone. The quality of the agreement suggests that in future we might use such plots to correct each impedance circle diameter - especially the first and last - in order to smooth out the scatter in the measured diameters. The slopes and intercepts are used to calculate the values of a and b and the ratio α/β as described.

TABLE 5.9

Measured Impedance Circle Diameters as a Function of the Order of Resonance.

Pressure N/m^2	Date	N	D_N
8470	10/01/71	1	0.9320
		2	0.6956
		3	0.5424
		4	0.4586
10700	17/01/71	1	1.1894
		2	0.8904
		3	0.6976
		4	0.5896
		5	0.5116
12510	13/01/71	1	1.5580
		2	1.1310
		3	0.8918
		4	0.7404
		5	0.6492
15940	11/01/71	1	1.9554
		2	1.4486
		3	1.1292
		4	0.9318
		5	0.8206
19700	15/01/71	1	2.6830
		2	1.9284
		3	1.4800
		4	1.2060
		5	1.0478
23260	09/01/71	1	3.9232
		2	2.8080
		3	2.1478
		4	1.7206
		5	1.4688
26660	08/01/71	1	5.9616
		2	4.1362
		3	3.2154
		4	2.5330
		5	2.0662

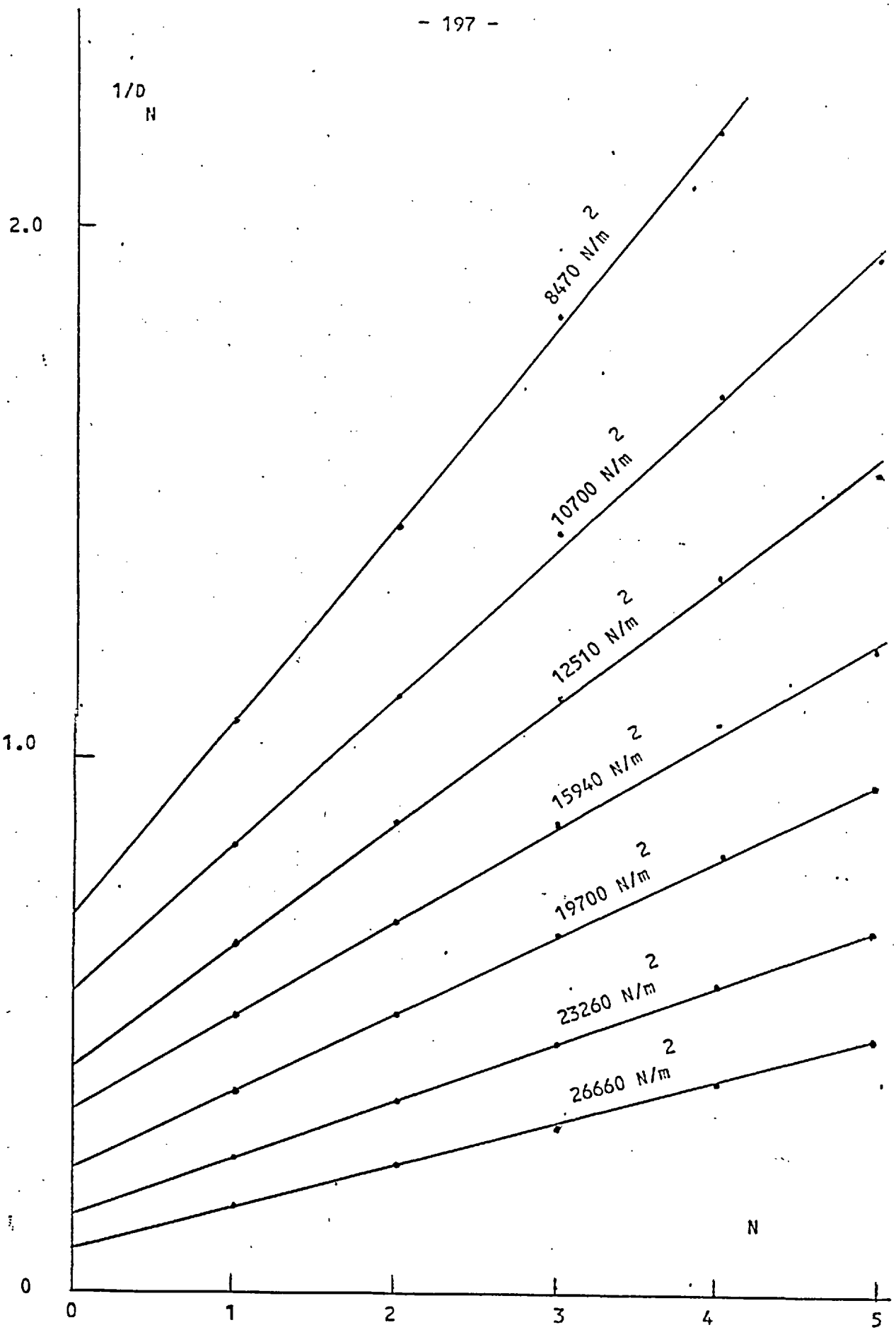

Figure 5.14

The Relation of the Impedance Circle Diameters, D_N, to the Order of Resonance, N.

5.3.5 Testing the Coupling of the Transducer to the Cavity.

At the end of Section 4.1 it was suggested that the mean position of the diaphragm might be shifted in order to investigate any unexpected effect there might be due to the gap (0.25mm) separating it from the mouth of the cavity. The shift was to be achieved by passing a direct current through the driving coil superimposed upon the usual alternating driving current.

Simple investigations with a diaphragm at room temperature using a dial gauge micrometer and some small weights had shown that it had a spring rating of approximately one ten thousandth of an inch per gram weight loading. However, the applicability of this figure to the cold diaphragm mounted in situ is of some doubt. It was estimated that if it did apply, the gap could be closed with a current of some 250mA through the coil which, it was felt, could lead to serious problems of temperature control if the coil resistance began to increase due its warming up. But, in any case, the restoring force of the diaphragm was far from linear over this distance and so no serious attempt was made to use a current of this magnitude since it would still not close the gap. The best that could be achieved without causing serious instability was a current of 30mA which was reversed to give an estimated total shift of (very roughly indeed) 0.06mm equivalent to 1/4 of the gap.

Measurements made with this current flowing through the coil yielded the following answers for velocities when corrected to the n.b.p. of helium-4

$$c = 11959.8 \text{ cm/s}$$

and

$$c = 11958.4 \text{ cm/s}$$

which shows that in a rather ill defined test no effect was observable which exceeded the normal scatter expected in two such measurements

(Cf the scatter amongst the velocity measurements of Section 5.3.4). The circuit employed for superimposing the direct current upon the alternating drive current is shown in Figure 5.15.

It is conceded that the limitations of this test are such as to guarantee no more than the absence of an error of the most unlikely magnitude. Had it been possible, an attempt would have been made to operate the diaphragm so that it almost touched the mouth of the cavity at the limit of its traverse since it is only in such a situation (where the gap is reduced to a distance comparable to the amplitude of vibration and to the boundary layer thickness) that any effect might' have been expected to show. However, we are content to assume that the gap is of no consequence for the reasons given in Section 4.3 and also because, if there were any effect, it would be expected to manifest itself as as a real or complex reflection coefficient which, irrespective of size, is cancelled out by using a variable path cavity.

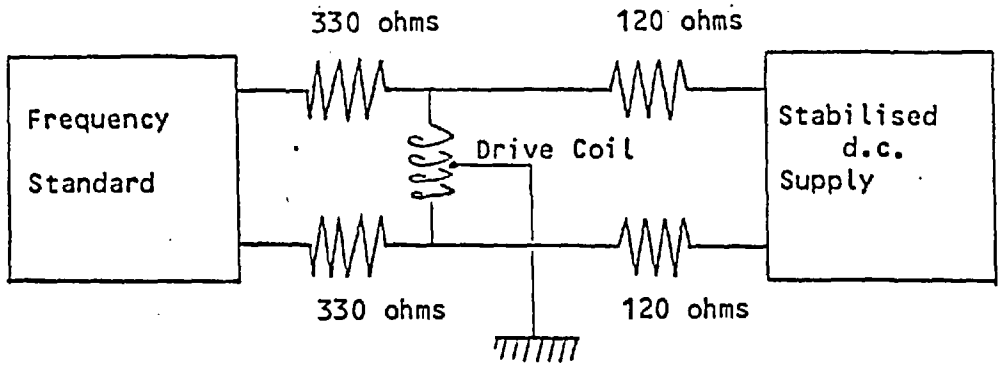

Figure 5.15

Circuit for Shifting Mean Position of Diaphragm.

CHAPTER VI

EXPERIMENTAL RESULTS

Three acoustic isotherms have been plotted at the normal boiling point of helium-4 and at the triple point and the normal boiling point of equilibrium hydrogen. The thermodynamic temperatures of these points have been evaluated from isotherm intercepts as described in Section 1.2 and rough values of the second virial coefficients have been obtained from the gradients of the isotherms. On making certain simplifying assumptions as to the form of the temperature dependence of the virial coefficients it is possible to calculate the approximate pressure dependence of the principal specific heats of helium-4 at these temperatures.

6.1 The Normal Boiling Point of Helium-4.

Thirteen measurements of the velocity of sound with changing pressure have been made at the normal boiling point of helium-4 at a frequency a little below the first cut off frequency of the cavity. Absorption coefficients have also been measured so that the boundary layer corrections can be calculated. The results of these measurements are shown in Table 6.1 together with the various corrections that have been made.

TABLE 6.1

Isotherm Data at the Normal Boiling Point of Helium-4.

Pressure (N/m^2)	Date	$\alpha \times 10^3$ (/cm)	c (Meas'd) at b.p. (cm/s)	c Corr'd for b. layer (cm/s)
8470	10/01/71	1.723	(11952.3) 11959.1	11971.0
10700	17/01/71	1.412	(11919.1) 11926.9	11936.6
12510	13/01/71	1.352	(11894.8) 11901.7	11911.0
14100	23/06/71	1.287	(11882.3) 11880.9	11889.7
14500	08/06/71	1.310	(11882.7) 11877.9	11886.8
15940	11/01/71	1.201	(11845.1) 11852.5	11860.6
18010	14/06/71	1.221	(11829.1) 11826.0	11834.2
19700	15/01/71	1.129	(11788.0) 11795.1	11802.7
21600	16/06/71	1.073	(11770.4) 11768.8'	11775.9
23260	09/01/71	1.056	(11732.6) 11740.1	11747.1
25010	17/06/71	1.013	(11719.4) 11717.1	11723.8
26660	08/01/71	1.004	(11679.9) 11687.5	11694.1
29890	19/01/71	0.865	(11628.0) 11635.9	11641.5

N.B. All measurements were made at a frequency of 3.3kHz exactly, and absorption coefficients have been calculated from the half widths of the resonances.

6.1.1 Reproduction of the Isotherm Temperature

We have already mentioned in Section 5.2.2 that the interferometer carried three germanium resistance thermometers all calibrated at the normal boiling point of helium-4. Their calibration was effected by mounting them in close fitting wells in the outer wall of a small copper vapour pressure bulb, good thermal contact being ensured by smearing them with conducting grease beforehand. A thin-walled stainless steel tube left the bulb and was connected to a mercury barometer so that the vapour pressure of the liquid helium which was condensed into the bulb could be measured. This vapour pressure tube was vacuum jacketed up to its room temperature end so that cold spots could not occur on its walls - especially at the surface of the liquid helium bath in which it was immersed. Fourteen readings of resistance were taken at pressures in the neighbourhood of one atmosphere. These resistances were then fitted with a quadratic polynomial so that the exact normal boiling point resistance (i.e. the resistance at a vapour pressure of 101325 N/m^2) could be calculated. Using the gradient of this resistance-pressure curve and the gradient of the pressure-temperature curve as given by the secondary scale T-58, a rough value of the resistance-temperature gradient could be calculated for each thermometer. This value was sufficiently accurate for us to be able to calculate how far from the true boiling point a velocity measurement might be made, and thus enabled the appropriate correction to be added to or subtracted from the measured velocity to bring it to its exact boiling point value.

Following our remarks in Section 1.1 on the necessary independence of a "primary" temperature measurement, it might be objected that the use of the scale T-58 was not available to us - even for the purposes of making a small correction - if we wished to maintain our claim to be doing primary thermometry. However, the gradient of vapour pressure

with temperature in T-58 is obtained directly from the Clausius-Clapeyron equation:

$$\frac{dP}{dT} = \frac{L}{T\Delta V} \qquad (6.1.1)$$

where L is the latent heat of evaporation of the liquid and ΔV the corresponding increase in volume. Our rough uncorrected acoustic temperature is sufficiently accurate for a value of T whilst L and ΔV may be measured without assigning a thermodynamic temperature to the boiling point. Thus this procedure requires only that the rough initial acoustic value and the value assigned on T-58 are sufficiently close to give dP/dT to the necessary degree of approximation. This was always the case, the actual difference being much smaller than the greatest tolerable difference. Thus the use of the scale T-58 is justified by our acoustic thermometry rather than presupposed by it.

One thermometer was always used to make the correction to the normal boiling point and the remaining two were used to check that no change had occurred in its calibration (on the assumption that an identical change in two thermometers would not occur). Resistance measurements on all three were taken at the start and the finish of each scan of the resonance curve. These values coincided closely with the temperature of the thermometric gas as the first and last resonances were traversed - temperatures which might be slightly different. To correct for this a small velocity correction was made from equation 5.2.1 to bring the measured velocity to the value which would have been obtained had the instrument remained at the temperature at which the first resonance was traversed. It was this value of velocity which was subsequently corrected to the normal boiling point value.

These corrections do not require that any temperature drift remains uniform since the velocity of sound is calculated solely from the positions of the first and last resonances. The positions of the intermediate points of resonance are calculated in order to evaluate the absorption coefficients which are affected only to a negligible extent by small changes in temperature.

All resistances were measured with a Diesselhorst d.c. potentiometer which, on recent calibration, has been shown to be more than accurate enough for our purposes. If the worst possible combination of decade errors is supposed to have occurred at this temperature, then it would only amount to a temperature error of 0.2mK at the most. (*1) This is exceedingly unlikely, however, and so we shall count it as three standard errors. The three four-lead resistance thermometers were connected in series together with two calibrated four-lead standard resistors of 100 and 1000 ohms nominal resistance. Thus the same current could be passed through all of them and the resistances of the germanium thermometers could therefore be calculated from the ratios of the voltages measured across their potential leads to the voltages measured across the potential leads of the standard resistors. The current was drawn from a current source of the optically stabilised type and was reversed so that the effect of small thermal voltages could be accounted for by taking the mean of

---

(1) This figure of 0.2mK for the potentiometer errors is likely to be overly pessimistic, in fact, since its most significant decades were set to the same values both for calibration and during the acoustic measurements. The remaining decades varied for each of the fourteen calibration points and for each of the thirteen isotherm points so that the errors would be expected to average out to a large extent.

the measured voltages obtained before and after reversing the current. This was standard practice for resistance measurements at all isotherm temperatures.

The estimate of the maximum possible error in the reproduction of the normal boiling point is + or - 1.1mK (counted as three standard errors again). This figure is obtained from the previous figure of 0.2mK for potentiometer errors to which we add firstly 0.4mK which is thought to be the maximum conceivable error which could arise from the head of helium vapour in the cold part of the vapour pressure tube in the calibrating instrument. This head of vapour would lead to too low a barometer reading at the true boiling point and so the estimated boiling point resistance would correspond to a slightly higher temperature where the measured vapour pressure would have risen to one atmosphere. On comparing the three resistance thermometers long after work was completed at this temperature, it was found that they all agreed to within 0.7mK, and that two of them agreed to within 0.2mK, the "working" thermometer being one of them. Since the working thermometer agreed so closely with one of the others it is a plausible assumption that this pair represent very closely the true boiling point calibration whilst the third thermometer is slightly in error. It has therefore been decided to use the working thermometer calibration and to assign it a maximum error of 1mK which we count as three standard errors once more. This generously embraces all three values and accords well with the general experience that in the absence of a drastic change of calibration, these thermometers are stable to within this figure. Thus combining this error with the previous errors of 0.2mK and 0.4mK by taking the root of their summed squares, we obtain an overall three standard error bar of 1.1mK or a standard error of 0.4mK. The greatest care was taken to ensure that the germanium thermometers were in good thermal contact with the

copper into which they were inserted both in the vapour pressure bulb during calibration and in the interferometer. In the former they were in direct contact with the liquid of the bath as was the vapour pressure bulb and so no temperature difference would be expected. In the interferometer, on the other hand, there was a danger of thermal conduction via the electrical leads into or out of the germanium "chip" within its sheath. To avoid this the leads were carefully varnished down to the copper body of the interferometer before reaching the resistance thermometers to "thermally anchor" them to the operating temperature of the interferometer (see Figure 5.1). A considerable length of wire, approximately one metre, was then suspended in the vacuum and anchored again at the temperature of the coolant bath by being wound on a copper bobbin in thermal contact with the bath. It was felt that these precautions precluded the possibility of the thermometers being at any temperature other than that of the interferometer.

6.1.2 The Boundary Layer Corrections at the NBP of Helium-4.

The measured values of the absorption coefficients are given in Table 6.1 and plotted as a function of pressure in Figure 6.1 where the theoretical curve (derived from the Kirchhoff-Helmholtz expression) is also shown. Additional points have been calculated from the absorption coefficients taken at lower frequencies for the purpose of confirming the theory of the boundary layer (see Section 5.3.3). These were converted to the appropriate value for a frequency of 3.3kHz by multiplying by the square root of the ratio of the frequencies e.g. by $(3300/2050)^{1/2}$ for the absorption coefficient measured at 2.050kHz. It can be seen that they are compatible with the values taken at 3.3kHz and, furthermore, that all values seem to confirm those predicted theoretically.

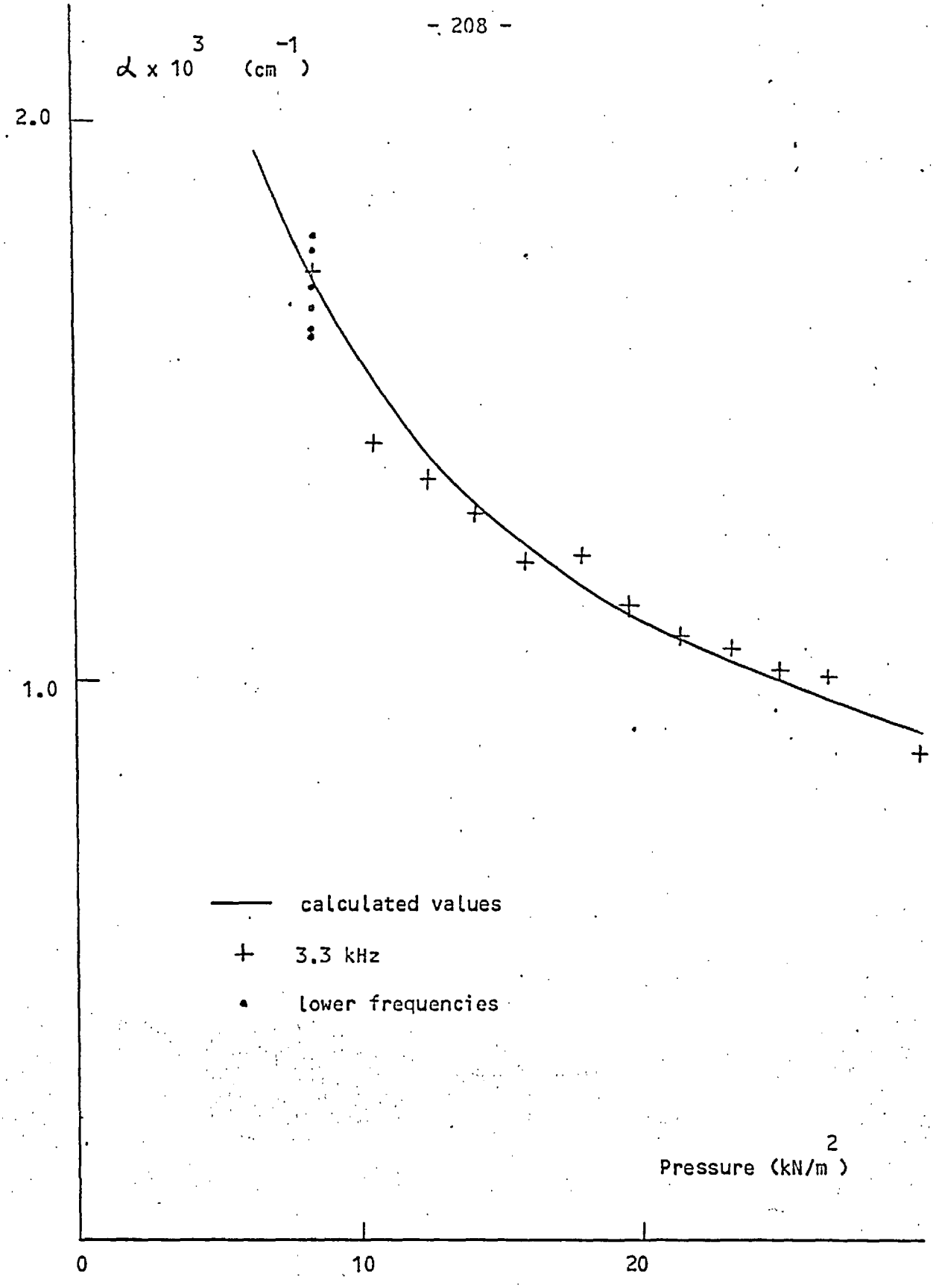

Figure 6.1

Measured Absorption Coefficients at the NBP of Helium-4.

6.1.3 The Isotherm at the NBP of Helium-4.

The squares of the measured velocities, both before and after correction for the boundary layer, are plotted in Figure 6.2 as a function of pressure. It can be seen that a significant curvature towards lower values becomes apparent at pressures above about $18kN/m^2$. Thus fitting a straight line to this data would be expected to yield an excessive value for the intercept leading to an overestimate for the normal boiling point of helium. If a quadratic is fitted to the points, on the other hand, then, provided that the curvature is attributable solely to the existence of a quadratic term as in the acoustic virial expansion, the correct intercept should be obtained. However, if the curvature is of a slightly different form attributable to small effects which are not dependent on the square of the pressure, or if the curvature arises from an unfortunate and statistically improbable, but nevertheless possible, distribution of points, then an incorrect answer will be obtained. In order to avoid these possibilities, it is advisable to fit a straight line to the lower portion of the isotherm if it can be shown to be linear, and to abandon the higher points. In fact straight lines have been fitted to progressively fewer and fewer points starting with all thirteen and finishing with the three at the lowest pressures. The resulting intercepts with their standard error bars are shown in Figure 6.3 together with comparable results using quadratic fits. As expected the value of the intercept for the linear fits decreases as the range of pressure is lowered, appears to become roughly constant for between four and seven experimental points and then rises erratically due, presumably, to the short range of the data compared to the range of the extrapolation and to the small number of points. Because of this we have decided to adopt the answer for the normal boiling point obtained from the linear fit to the first seven data points giving:

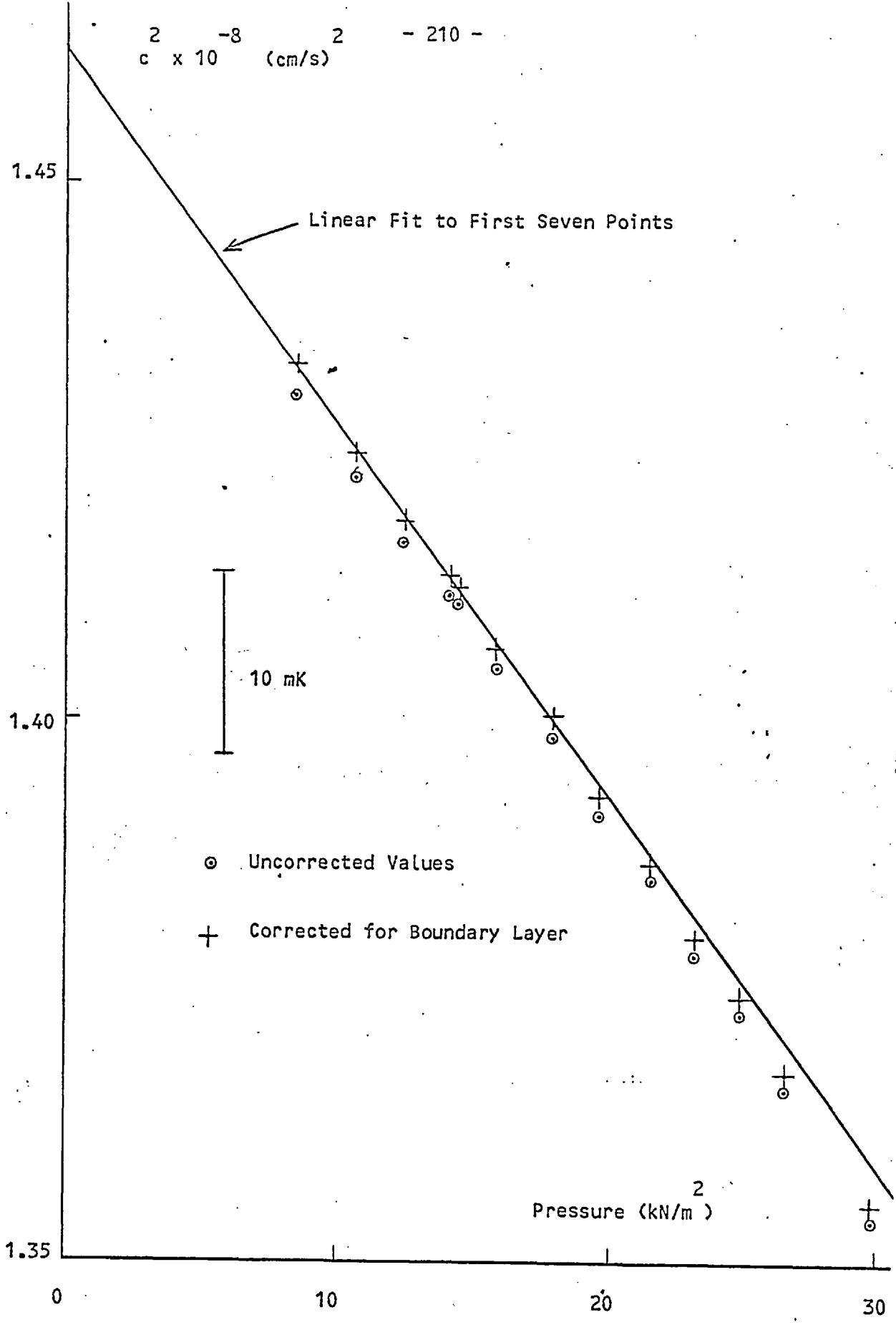

Figure 6.2

The Isotherm at the NBP of Helium-4.

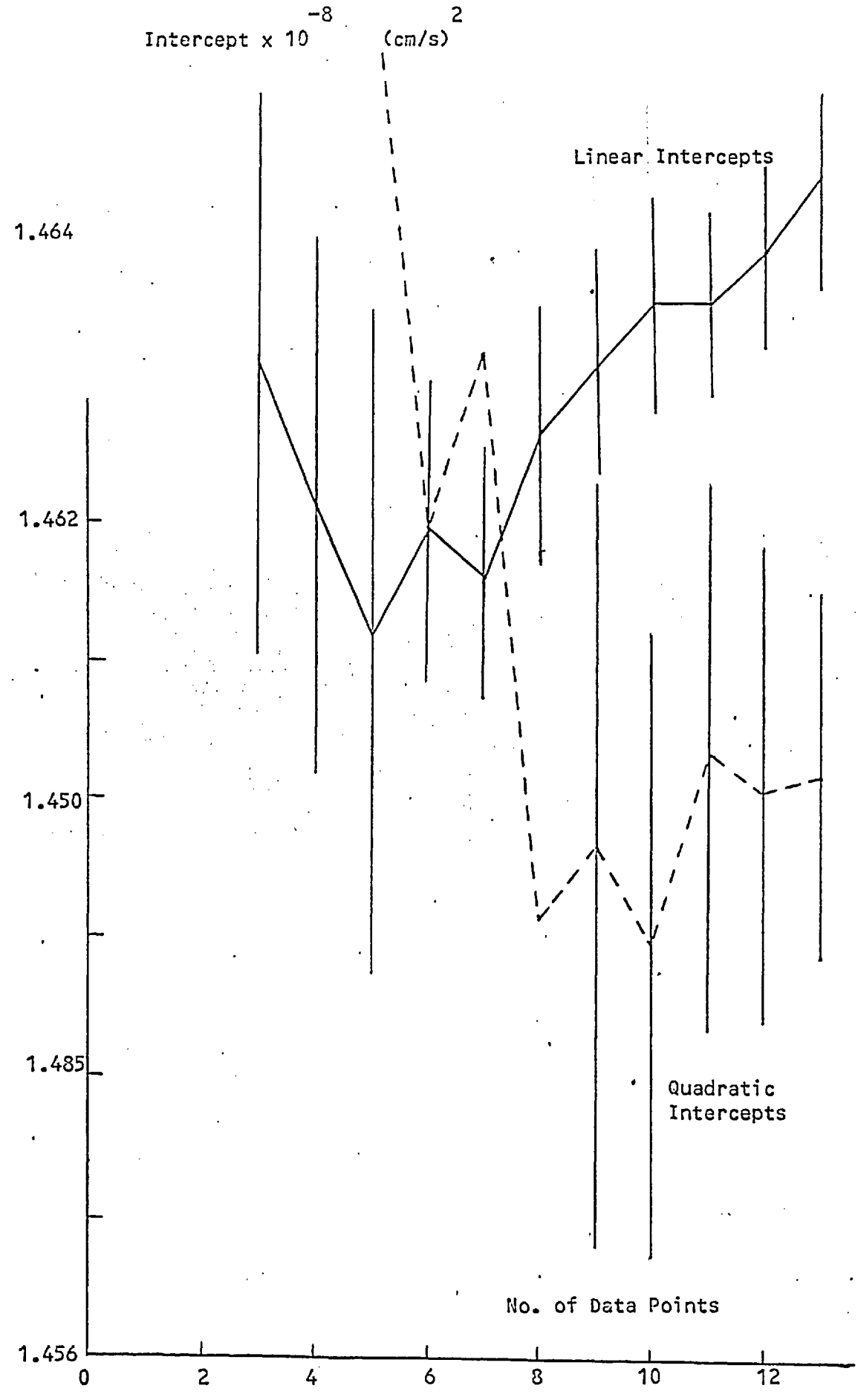

Figure 6.3

Values of Intercepts Calculated from Linear and Quadratic Fits to the Isotherm Points at the NBP of Helium-4.

T(intercept) = 4.2218K + or - 2.5mK(std. error)

Full details of this fit are given in Table 6.2 where it can be seen that the linear fit has a smaller standard deviation than a quadratic fit to the same points (the latter giving a consistent answer, however, as would be expected). The value obtained from a quadratic fit to all the data would be:

T(intercept) = 4.2177 + or - 3.8mK(std. error)

which differs by 4.1mK from the answer we have adopted. In fact this difference is almost accommodated by a single standard error bar in the latter answer and so may be considered to be compatible. Nevertheless we still prefer the answer based on the low pressure data both for the reasons given above and also because the standard deviation of the linear seven point fit is slightly lower than the standard deviation of the quadratic fit to all the data. This shows that the data at low pressures is better represented, if only marginally, by a straight line than is all the data by the quadratic, details of which are given in Table 6.3.

Our final answer for the normal boiling point of helium-4 will be given when we have accounted for the only remaining (known) systematic errors - those contributing to the standard error of 0.4mK in the reproduction of the correct isotherm temperature and that due to the standard error of 45 ppm in the gas constant (equivalent to 0.2mK). Taking the square root of the sum of the squares of these and the statistical standard error in the intercept, we obtain:

NBP of helium-4 = 4.2218 + or - 2.5mK(std. error)

the systematic errors making a negligible contribution to the total error due to the comparatively large random error.

TABLE 6.2

Polynomial Fits to the Low Pressure Data at the Normal Boiling Point of Helium-4.

Linear Fit:

Pressure (Data) (N/m^2)	$c^2 \times 10^{-8}$ (Data) ($cm/s)^2$	$c^2 \times 10^{-8}$ (Calc'd) ($cm/s)^2$	Residuals $\times 10^{-4}$ ($cm/s)^2$
8470	1.43305	1.43276	-2.9
10700	1.42482	1.42518	+3.5
12510	1.41872	1.41901	+3.0
14100	1.41365	1.41361	-0.4
14500	1.41296	1.41224	-7.2
15940	1.40674	1.40735	+6.1
18010	1.40048	1.40028	-2.1

Result of Linear Fit:

Constant Term = (1.46161 + or - 0.00088(std. error)) $\times 10^8$

Linear Coefft. = -340.5 + or - 6.3(std.error)

Standard Deviation of points = 4.99×10^4

The standard deviations for the quadratic and cubic fits are 5.45×10^4 and 6.12×10^4 respectively, and the corresponding intercepts are (1.46319 + or - 0.00385(std. error)) $\times 10^8$ and 1.47264×10^8.

TABLE 6.3

Polynomial Fits to All the Data at the Normal Boiling Point of Helium-4.

Quadratic Fit:

Pressure (Data) (N/m^2)	$c^2 \times 10^{-8}$ (Data) $(cm/s)^2$	$c^2 \times 10^{-8}$ (Calc'd) $(cm/s)^2$	Residuals $\times 10^{-4}$ $(cm/s)^2$
8470	1.43305	1.43280	-2.5
10700	1.42482	1.42529	+4.6
12510	1.41872	1.41909	+3.7
14100	1.41365	1.41358	-0.7
14500	1.41296	1.41217	-7.9
15940	1.40674	1.40712	+3.9
18010	1.40048	1.39972	-7.7
19700	1.39304	1.39362	+5.8
21600	1.38672	1.38666	-0.6
23260	1.37994	1.38052	+5.7
25010	1.37449	1.37393	-5.5
26660	1.36752	1.36767	+1.5
29890	1.35525	1.35521	-0.3

Result of Quadratic Fit:

$$\text{Constant Term} = (1.46019 \pm 0.00133(\text{std. error})) \times 10^{8}$$

$$\text{Linear Coefft.} = -312.0 \pm 14.9(\text{std. error})$$

$$\text{Quadratic Coefft.} = -(1.3 \pm 0.4(\text{std. error})) \times 10^{-3}$$

$$\text{Standard Deviation of Points} = 5.27 \times 10^{4}$$

The standard deviations for the linear and cubic fits are 7.35×10^{4} and 5.55×10^{4} respectively, and the corresponding intercepts are $(1.46442 \pm 0.00063(\text{std. error})) \times 10^{8}$ and 1.45976×10^{8}.

6.2 The Triple Point of Hydrogen.

Nine measurements of the velocity of sound and acoustic absorption coefficients have been taken at the triple point of hydrogen in exactly the same way as before. The data is shown in Table 6.4.

6.2.1 Reproduction of the Isotherm Temperature.

A platinum resistance thermometer was available at the NPL whose resistance had been measured at the triple point of hydrogen in one of our fixed point apparatuses. A germanium thermometer was calibrated against this and exchanged for one of the three already in the interferometer. Comparisons with the remaining two were immediately made so that any subsequent changes in any of the thermometers could be detected. It was estimated that the overall uncertainty in the reproduced temperature attributable to these calibrations was + or - 0.6mK which, again, we count as three standard errors. Unfortunately, however, when checking this calibrated resistance thermometer after the measurements were completed it was found to have changed by a small amount (about 3mK) since the calibration. This change must have occurred before comparison with the other two thermometers since all three remained in agreement throughout the time they were in use, and since a corresponding discrepancy was subsequently noticed in measurements of their helium boiling point resistances made before its removal from the cryostat. Consequently, it was decided to recalibrate all our resistance thermometers against a standard platinum resistance thermometer in a comparison cryostat. This showed that a small correction amounting to 3.3mK needed to be subtracted from our final answer. Given this correction our estimated uncertainty in the thermometer calibrations remains at 0.6mK. Combining this figure with an uncertainty of 0.75mK due to the maximum possible potentiometer error, we obtain a figure of 1.0mK for the overall error in the reproduced isotherm temperature or an estimated standard error of

TABLE 6.4

Isotherm Data at the Triple Point of Hydrogen.

Pressure (N/m^2)	Date	$\alpha \times 10^3$ (/cm)	c (Meas'd) at b.p. (cm/s)	c Corr'd for b. layer (cm/s)
10050	25/05/71	3.214	(21821.8) 21824.4	21865.0
10120	20/05/71	3.252	(21820.8) 21823.0	21864.1
20080	21/05/71 (I)	2.301	(21831.2) 21833.9	21863.0
30060	21/05/71 (II)	1.849	(21836.4) 21839.1	21862.5
39980	22/05/71	1.635	(21840.0) 21842.4	21863.1
50170	19/05/71	1.430	(21845.0) 21847.3	21865.4
59970	22/06/71	1.364	(21846.5) 21849.2	21866.5
64770	01/07/71	1.224	(21844.6) 21848.9	21864.4
69990	21/06/71	1.162	(21850.4) 21852.1	21866.8

N.B. All measurements have been made at a frequency of 6.0kHz exactly, and absorption coefficients have been calculated from the half widths of the resonances.

0.3mK. As before corrections for small drifts and conversions to the exact boiling point were made to the measured velocity.

The gradient for the resistance - temperature relation for this thermometer which was required for these corrections was obtained from a rough prior calibration in agreement with IPTS-68 and T-58. The justification for its use on this occasion is that, in retrospect, the calibration was confirmed to a sufficient degree of accuracy by acoustic measurements at 4.2K, 13.81K and 20.28K. Had this not been the case the calibration would have had to be corrected to achieve agreement with the uncorrected acoustic measurements. It would have then yielded a sufficiently accurate value for the gradient to make the corrections. Thus the temperatures finally arrived at are independent of any errors in the initial calibration and so our thermometry may still claim to be truly primary.

6.2.2 The Boundary Layer Corrections at the Triple Point of Hydrogen.

The measured absorption coefficients are plotted in Figure 6.4 as a function of pressure together with values calculated theoretically. Again it can be seen that there is good agreement between them.

6.2.3 The Isotherm at the Triple Point of Hydrogen.

The isotherm at the triple point of hydrogen is plotted in Figure 6.5. This time the curvature present in the previous isotherm at higher pressures is no longer visible. However, the standard deviation of a quadratic fit is marginally lower than that of the linear fit as may be seen from Table 6.5. But the points are more randomly distributed about the line in the linear fit and so we shall adopt the answer given by the linear intercept. As for the low pressure data at 4.2K we find, as we should, that the linear and quadratic intercepts are statistically compatible.

The data at this temperature is of a better quality than that obtained at the helium boiling point having a standard error on the

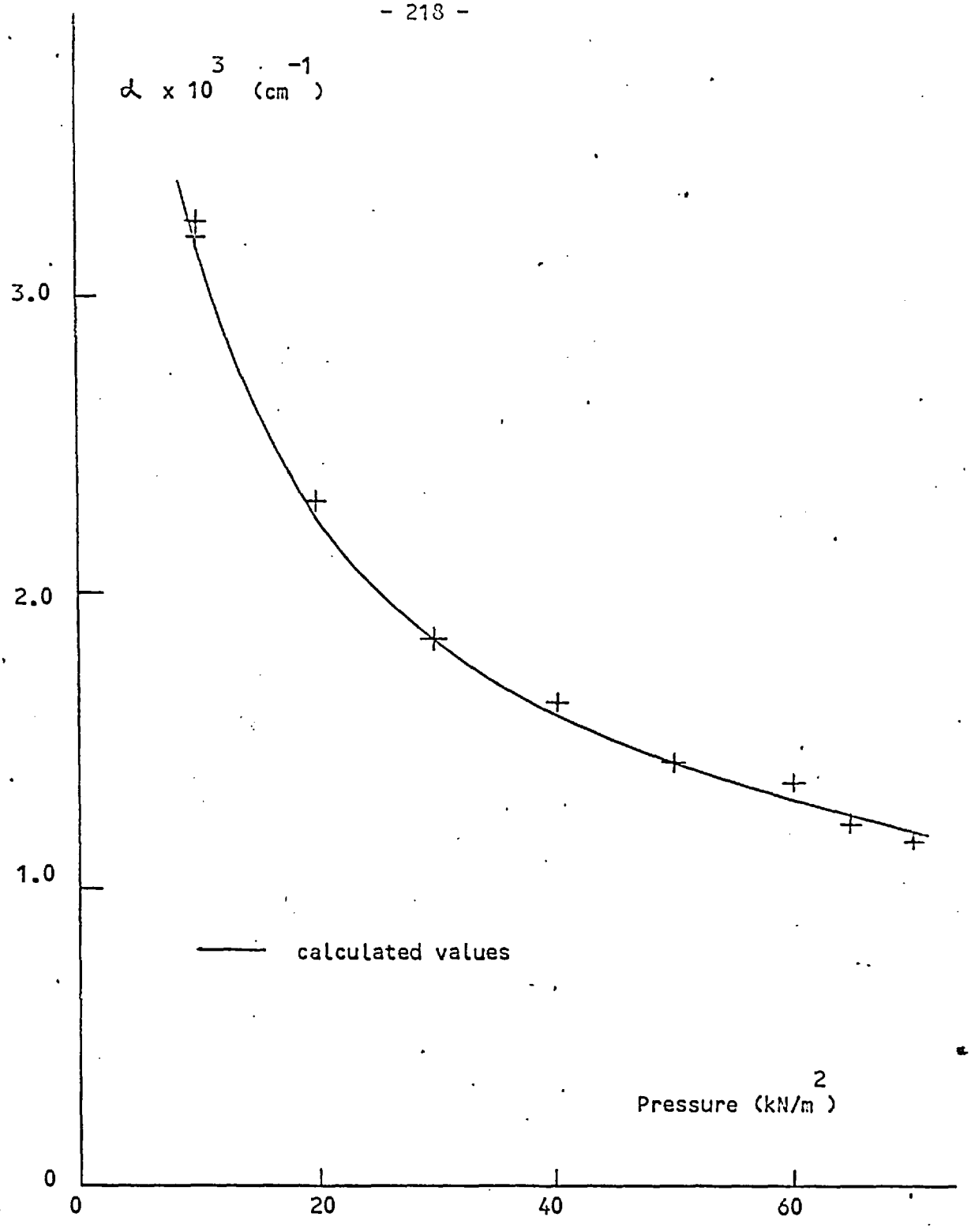

Figure 6.4

Measured Absorption Coefficients at the Triple Point of Hydrogen.

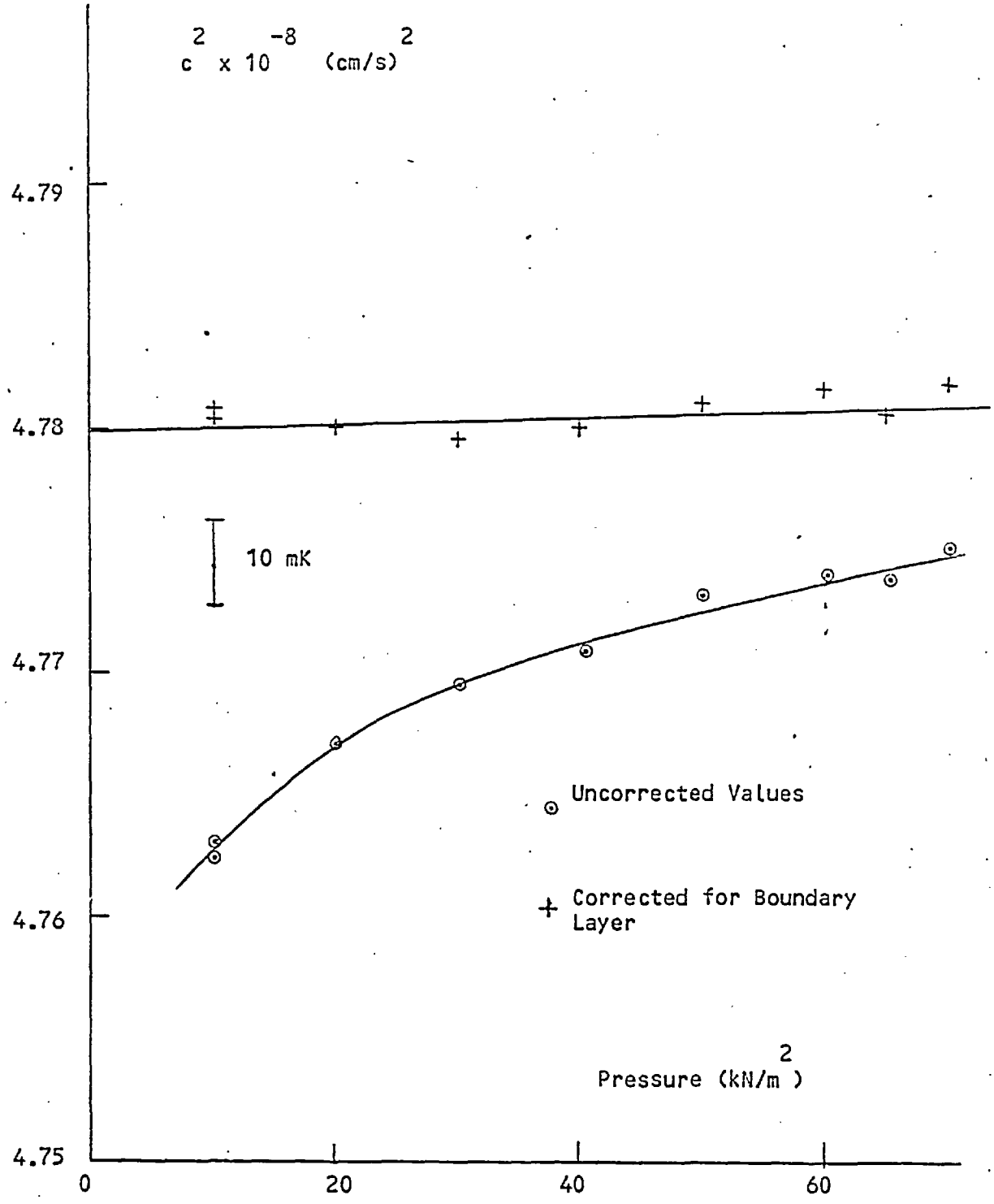

Figure 6.5

The Isotherm at the Triple Point of Hydrogen.

TABLE 6.5

Polynomial Fits to the Data at the Triple Point of Hydrogen.

Linear Fit:

Pressure (Data) (N/m^2)	$c^2 \times 10^{-8}$ (Data) ($cm/s)^2$	$c^2 \times 10^{-8}$ (Calc'd) ($cm/s)^2$	Residuals $\times 10^{-4}$ ($cm/s)^2$
10050	4.78078	4.78009	-6.9
10120	4.78039	4.78009	-3.0
20080	4.77991	4.78026	+3.5
30060	4.77969	4.78042	+7.3
39980	4.77995	4.78059	+6.4
50170	4.78096	4.78076	-2.0
59970	4.78144	4.78092	-5.2
64770	4.78052	4.78100	+4.8
69990	4.78157	4.78108	-4.9

Result of Linear Fit:

$$\text{Constant Term} = (4.77993 \pm 0.00040(\text{std. error})) \times 10^{8}$$

$$\text{Linear Coefft.} = 1.65 \pm 0.89(\text{std. error})$$

$$\text{Standard Deviation} = 5.86 \times 10^{4}$$

The standard deviations for the quadratic and cubic fits are 4.77×10^{4} and 4.28×10^{4} respectively, and the corresponding intercepts $(4.78096 \pm 0.00058(\text{std. error})) \times 10^{8}$ and 4.78233×10^{8}. The linear intercept has been chosen since the standard deviations are comparable and the signs of the residuals are slightly more randomly distributed.

intercept which is smaller even in absolute terms, and much less relative to the value of the intercept. This may seem surprising in view of the fact that there are approximately the same number of points and similar standard deviations for the two isotherms (the 4.2K standard deviation being the lower). The reason for this is almost certainly that whilst the maximum densities are comparable, the pressure range of the present isotherm is about six times the distance to be extrapolated whilst the comparable figure on the 4.2K isotherm is about one. The temperature corresponding to the linear intercept is given by:

T(intercept) = 13.8066K + or - 1.2mK(std. error)

To obtain our final answer we subtract the retrospective temperature correction of 3.3mK and combine the systematic errors with the random errors as before by taking the root of the summed squares of the standard errors from every source (the standard error due to the gas constant being 0.6mK at this temperature). Thus we have:

Triple Point of Hydrogen = 13.8033 + or - 1.7mK(std. error)

The comparable answer for the quadratic fit would 13.8063K with a total standard error of 1.9mK.

6.3 The Normal Boiling Point of Equilibrium Hydrogen.

Ten measurements of velocities and absorption coefficients have been made at this temperature. They are tabulated as before in Table 6.6.

TABLE 6.6

Isotherm Data at the Normal Boiling Point of Equilibrium Hydrogen.

Pressure (N/m^2)	Date	$\alpha \times 10^3$ (/cm)	c (Meas'd) at b.p. (cm/s)	c Corr'd for b. layer (cm/s)
10170	18/05/71	4.072	(26478.0) 26429.4	26492.1
20240	01/03/71	3.059	(26477.4) 26467.9	26515.0
30020	02/03/71	2.541	(26469.9) 26482.2	26521.2
40330	24/02/71	2.019	(26497.2) 26494.2	26525.3
49740	09/03/71	1.633	(26496.9) 26509.1	26534.3
50040	03/03/71	1.874	(26485.7) 26510.2	26539.1
60030	10/03/71	1.470	(26518.6) 26521.2	26543.9
69920	11/03/71	1.570	(26520.9) 26534.0	26558.3
80090	25/02/71	1.287	(26524.0) 26543.7	26563.6
97790	28/02/71	1.330	(26563.2) 26569.5	26590.1

N.B. All measurements have been made at a frequency of 7.25kHz exactly, and all absorption coefficients except that at a pressure of 60030 N/m^2 have been calculated from the half widths of the resonances. An excessively low value (0.000902/cm) was obtained for that at 60030N/m^2 for reasons which remain uncertain, and so it was evaluated from the gradient at resonance which agrees better with the theoretical value and with the other data (see Figure 6.6).

6.3.1 Reproduction of the Isotherm Temperature.

At the time these measurements were made no resistance thermometer calibration was available to enable us to reproduce the exact isotherm temperature. Instead, it was necessary to rely on a rough calibration on one of our existing three germanium thermometers. Subsequently, when an exact calibration became available, we were able to transfer it onto this thermometer and to make the necessary corrections to the measured velocities to allow for drift and to bring them to their true boiling point values. However, the same germanium thermometer was used for this purpose as was used at the triple point of hydrogen, and so an additional correction of 1.7mK has to be subtracted from our final answer as before.

The total uncertainty in the final reproduction in the isotherm temperature is + or - 4mK which, as usual, is counted as three standard errors.

6.3.2 The Boundary Layer Corrections at the NBP of Equilibrium Hydrogen.

The measured absorption coefficients are plotted against isotherm pressure in Figure 6.6 together with a plot of values calculated from the Kirchhoff-Helmholtz formula. Unfortunately they seem to have a larger scatter about the theoretical curve than in the previous cases which is particularly regrettable at this temperature because of the correspondingly higher corrections. These amount to about 100mK at the lowest pressures. However, large residuals close to the intercept are not necessarily any more problematic than smaller residuals some distance away. This would seem to be the case in the present isotherm where the standard error in the intercept is much smaller than these residuals as will be seen in the following section.

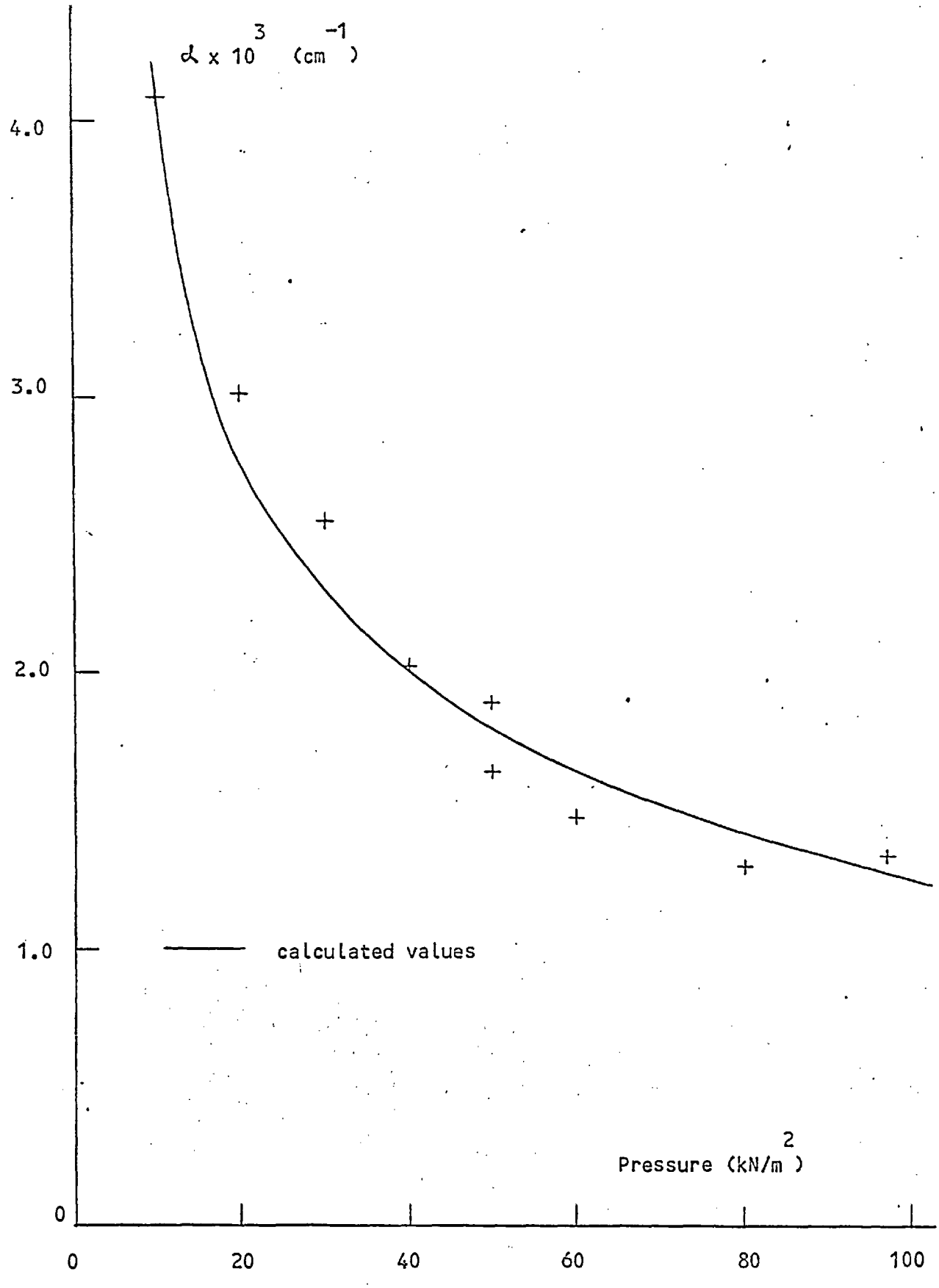

Figure 6.6

Measured Absorption Coefficients at the NBP of Equilibrium Hydrogen.

6.3.3 The Isotherm at the Normal Boiling Point of Equilibrium Hydrogen.

Values of the square of the acoustic velocity both before and after correction for the boundary layer are shown in Figure 6.7 plotted against pressure. Given the large scatters the isotherm would appear to be linear, but with the small number of points available it is possible that a considerable unresolved curvature exists. Were this the case, there could be a large error in the intercept. However, the isotherm appears to be linear in its central and upper regions which, given the form of the acoustic virial expansion, would suggest that it would remain linear down to the intercept. The evidence obtained from fitting the isotherm certainly does not suggest otherwise, the linear fit having a smaller standard deviation than the quadratic.

The details of the fits are given in Table 6.7. Adopting the value obtained from the linear intercept, we have:

T(intercept) = 20.2643K + or - 4.9mK(std. error)

Taking from this the retrospective temperature correction of 1.7mK and allowing for a standard error of 1.4mK in the reproduction of the isotherm temperature and 1.0mK due to the uncertainty in the gas constant, it becomes:

NBP of Equilibrium Hydrogen = 20.263K + or - 5mK(std. error)

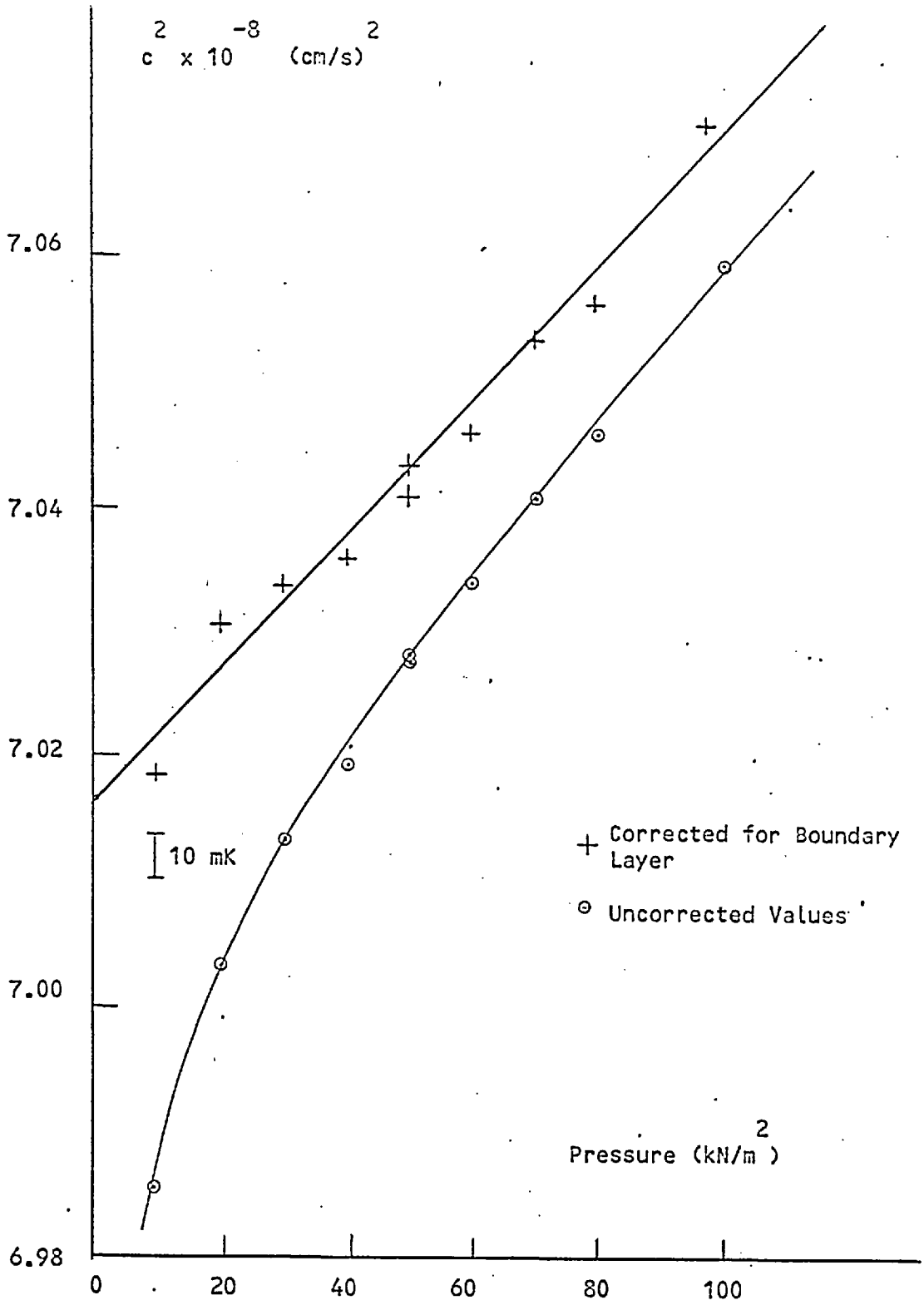

Figure 6.7

The Isotherm at the NBP of Equilibrium Hydrogen.

TABLE 6.7

Polynomial Fits to the Data at the Normal Boiling Point of Equilibrium Hydrogen.

Linear Fit:

Pressure (Data) (N/m^2)	$c^2 \times 10^{-8}$ (Data) ($cm/s)^2$	$c^2 \times 10^{-8}$ (Calc'd) ($cm/s)^2$	Residuals $\times 10^{-5}$ ($cm/s)^2$
10170	7.01831	7.02107	+2.8
20240	7.03045	7.02646	-4.0
30020	7.03374	7.03168	-2.1
40330	7.03592	7.03720	+1.3
49740	7.04069	7.04223	+1.5
50040	7.04324	7.04239	-0.9
60030	7.04579	7.04773	+1.9
69920	7.05343	7.05302	-0.4
80090	7.05625	7.05846	+2.2
97790	7.07033	7.06792	-2.4

Result of Linear Fit:

Constant Term = (7.01563 + or - 0.00170(std. error)) $\times 10^8$

Linear Coefft. = 53.5 + or - 3.0(std. error)

Standard Deviation of Points = 2.43×10^5

The standard deviations for the quadratic and cubic fits are 2.53×10^5 and 2.10×10^5 respectively and the corresponding intercepts are (7.01707 + or - 0.00301(std. error))$\times 10^8$ and 7.01019×10^8

6.4 The Second Virial Coefficient.

Another piece of evidence that suggests straight lines should be fitted to our isotherm data is afforded by the slopes of these lines. It will be recalled from section 1.3 that if the second virial coefficient, $B(T)$, of a pressure-volume expansion is of the form $a+b/T$ as past measurements would often suggest, then the second acoustic virial coefficient, $A_1(T)$, is also. Consequently, if our values of $A_1(T)$ lie on a straight line when plotted against reciprocal temperature, then there is further reason to be confident that the linear slopes, and therefore the linear fits, were the correct ones. Such a plot is shown in Figure 6.8 where it can be seen that our three points lie very close to a straight line. In each case the residual is less than two standard errors in the gradient obtained from the fit. Calculating values of a and b from equation 1.3.10 we obtain:

$$a = 18.63 \text{ + or - } 0.30(\text{std. error})$$

$$b = 419.0 \text{ + or - } 3.5(\text{std. error})$$

These values lie close to those obtained by other workers some of which are listed in Table 6.9.

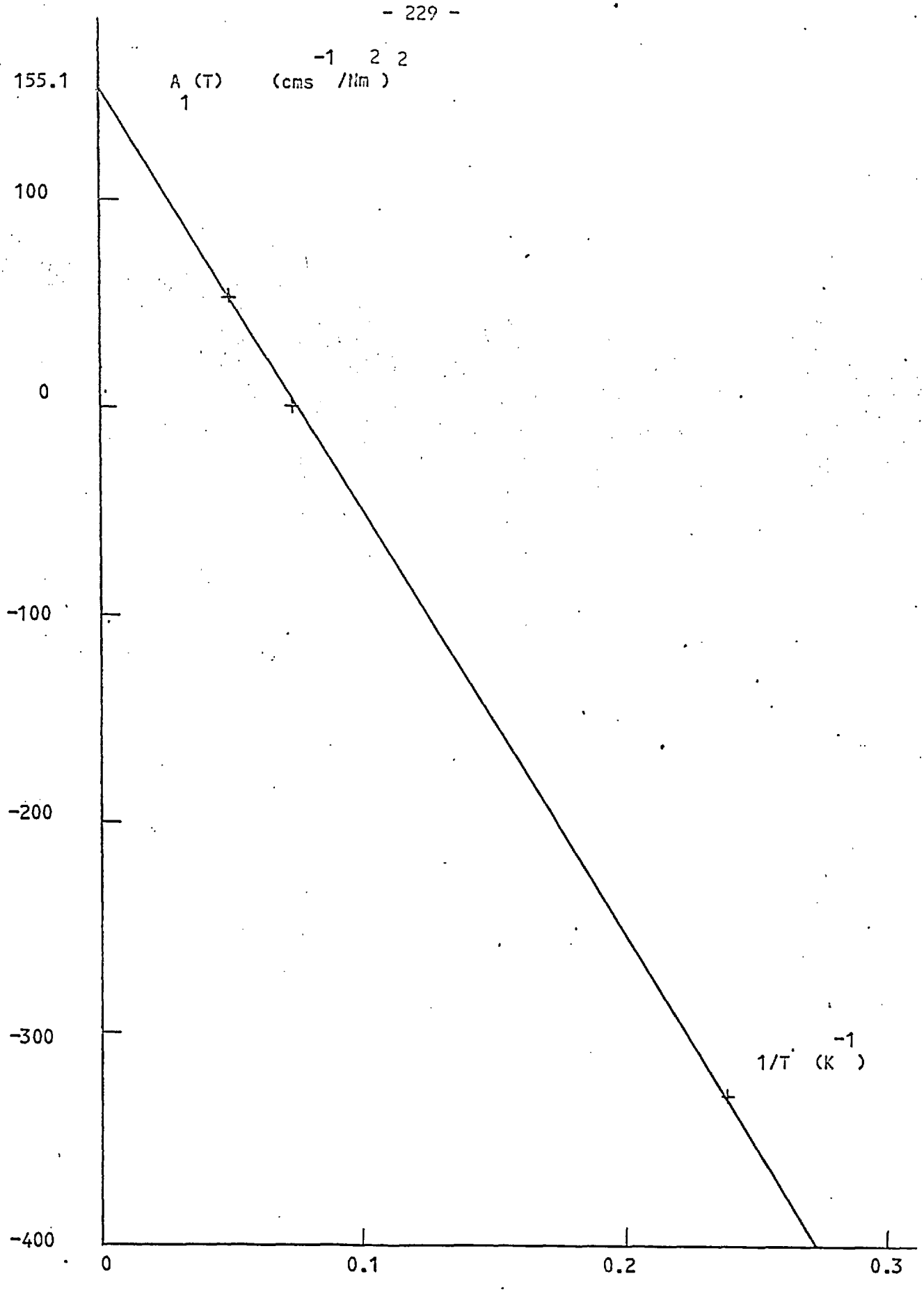

Figure 6.8

Measured Values of the Second Acoustic Virial Coefficient.

TABLE 6.8

A Linear Fit of $A_1(T)$ against 1/T.

10/T (Data)	$A_1(T)$ (Data)	$A_1(T)$ (Calc'd)	Residuals
0.49349	+53.4730	+51.8372	-1.64
0.72429	+1.65355	+3.51893	+1.87
2.36870	-340.494	-340.724	-0.23

Result:

Constant Term = 155.1 + or - 2.5(std. error)
Linear Coefft. = -2093.5 + or - 17.2(std. error)

Standard Deviation of Points = 2.49

N.B. T is expressed in K and $A_1(T)$ in $cm\ s^{-2}\ /N_m^{-2}$. To obtain a and b in $cm^3/mole$, multiply the constant term and the linear coefficient by 0.1 and substitute them into equations 1.3.10 for d and e respectively.

6.5 The Principal Specific Heats of Helium-4 and their Ratio.

Provided that care is taken not to extend our results beyond the pressure ranges within which our isotherms are linear, we may approximate in equations 1.4.2 and 1.4.4, obtaining:

$$\sigma \equiv \frac{C_p}{C_v} = \frac{Mc^2}{RT}\left\{1 - 2B(T)\frac{n}{V}\right\}$$

$$\doteq \frac{Mc^2}{RT}\left\{1 - 2B(T)\frac{P}{RT}\right\} \qquad (6.5.1)$$

and

$$C_p - C_v = R\left\{1 + \frac{2}{R}\frac{dB(T)}{dT}P\right\} \qquad (6.5.2)$$

Putting $B(T)=a+b/T$ we have

$$\sigma = \frac{Mc^2}{RT}\left\{1 - \frac{2}{RT}(a+b/T)P\right\} = \sigma_o\left\{1 - \frac{2}{RT}(a+b/T)P\right\}$$

$$(6.5.3)$$

and

$$C_p - C_v = R\left\{1 - \frac{2b}{RT^2}P\right\} \qquad (6.5.4)$$

giving

$$C_v = \frac{C_p - C_v}{\sigma - 1} = \frac{3R}{2}\left\{1 - \frac{2b}{RT^2}P\right\}\left\{1 + \frac{2}{RT}(a + b/T)P\right\}$$

$$= \frac{3R}{2}\left\{1 + \frac{2aP}{RT}\right\}$$

$$= C_{v_o}\left\{1 + \frac{2aP}{RT}\right\} \qquad (6.5.5.)$$

where the zero subscript refers to the ideal gas value of the subscripted variable. C_v, $(C_p - C_v)$ and σ have been calculated using the values of a and b given in the last section. Their values have been plotted in Figures 6.9 to 6.11. Clearly such values much be treated with care since they are based on values of a and b which are derived by fitting a straight line to only three points, two of which are rather close to each other.

6.6 Conclusions

There is nothing to be said in conclusion which has not already been said, but it may be useful to draw together our main results. For the three measured temperatures we found:

NBP of Helium-4 = 4.2218K + or - 2.5mK(std. error)

Triple Point of Hydrogen = 13.8033K + or - 1.7mK(std. error)

NBP of Equilibrium Hydrogen = 20.263K + or - 5mK(std. error)

and for the second virial coefficient of helium-4 the following temperature dependence was calculated:

$$B(T) = 18.63 - 419/T$$

From the considerations of Chapters II to IV and from the

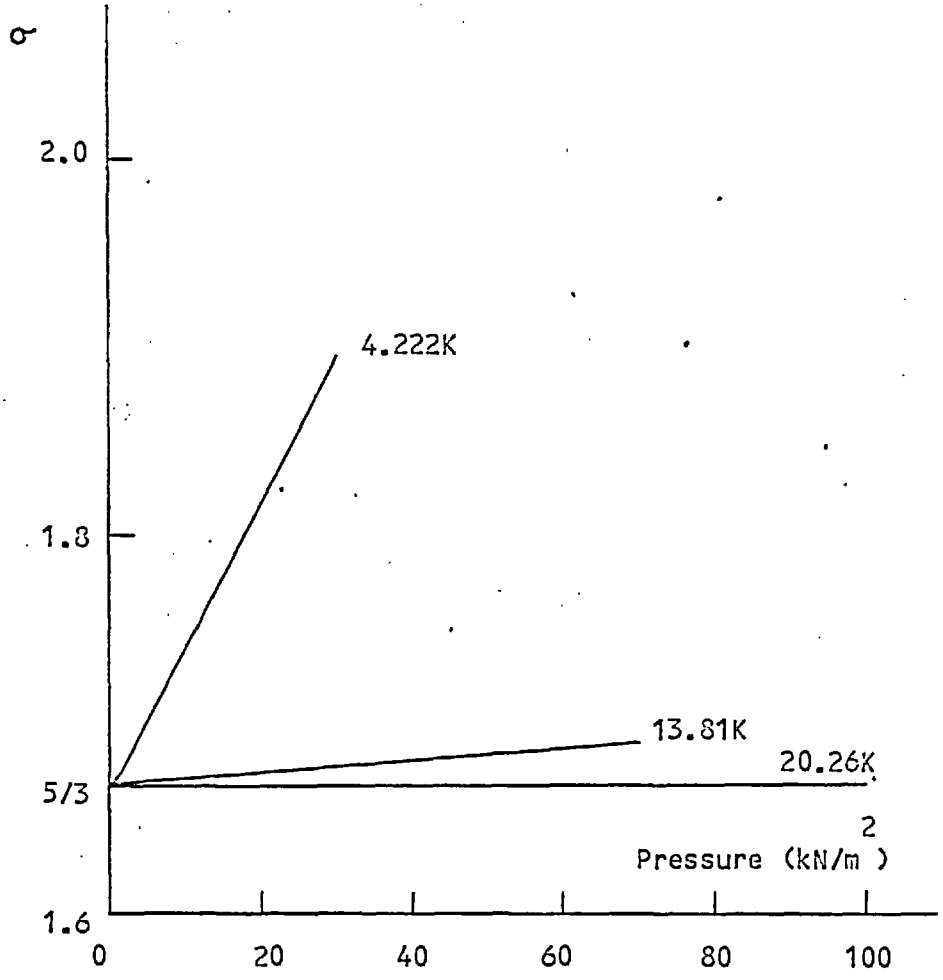

Figure 6.9

Measured Values of the Ratio of the Principal Specific Heats.

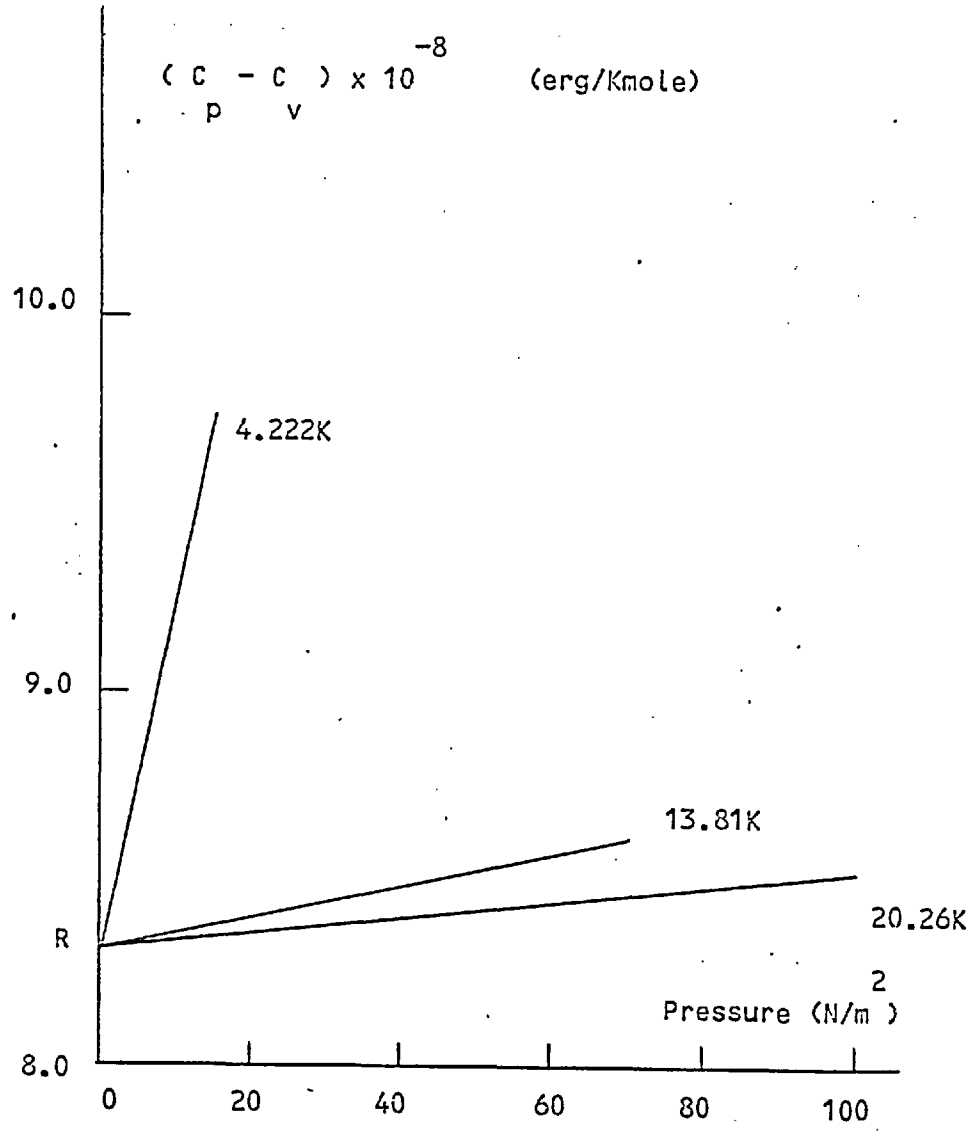

Figure 6.10

Measured Values of the Difference of the Principal Specific Heats.

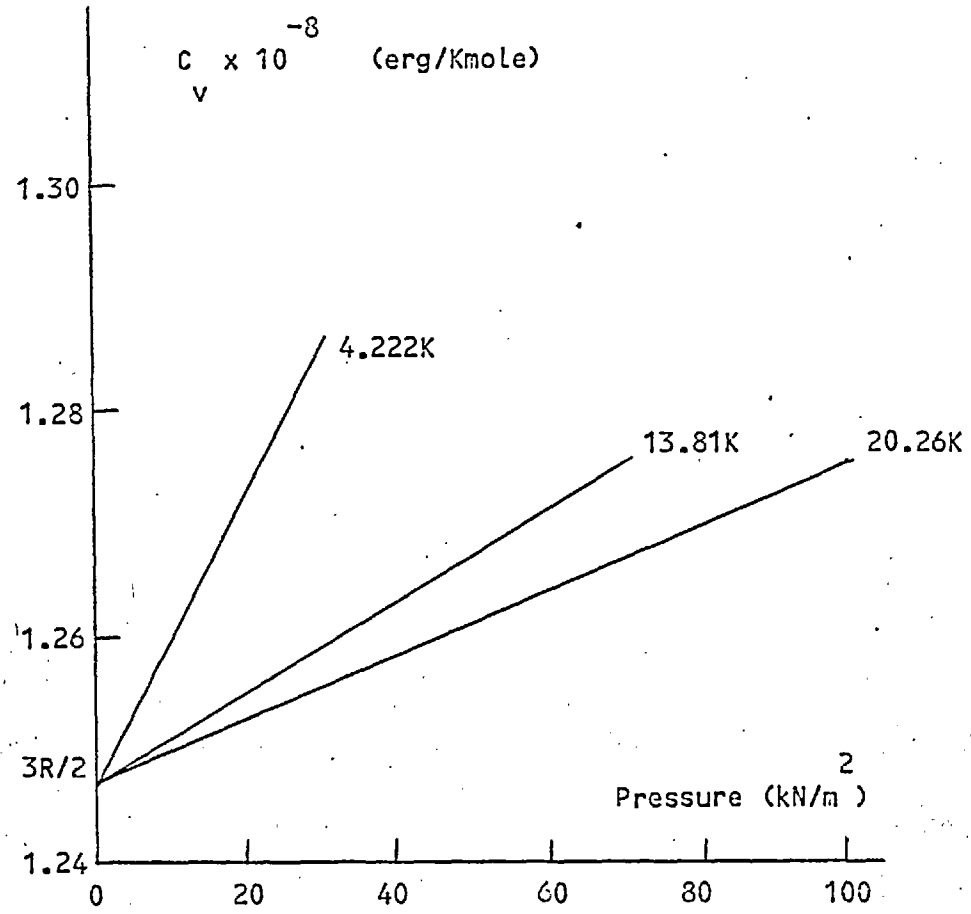

Figure 6.11

Measured Values of the Principal Specific Heat at Constant Volume.

investigations of Chapter V into the boundary layer effect, it would seem that, in the absence of hidden systematic errors, these temperatures are true thermodynamic temperatures. This belief is further supported by the agreement which exists between these results and those of the most recent primary gas thermometry and the ultrasonic thermometry of Plumb and Cataland both of which depend on the circumvention of entirely different types of systematic error. The values obtained by these other two methods are given in Table 6.9.

The only possible systematic error which we feel might be present in our work arises from the possibility that the wrong type of curves have been fitted to our isotherm data. The only way in which this can be checked is by accumulating further experimental data - in particular at the lowest pressures on the isotherms at 4.2K and 20.3K. It can easily be seen that in the latter case, for example, removal of the lowest point would suggest quite strongly that the appropriate function to fit to the points is a quadratic whose intercept would be higher than the currently adopted linear intercept by some tens of mKs.. For this reason we feel that the results reported here should be regarded as being preliminary. However, it does seem that these investigations have shown that, as a primary technique, low frequency acoustic thermometry is capable of providing information every bit as useful as that obtainable from ultrasonic thermometry, and somewhat better than has been obtained in the past at low frequencies.

TABLE 6.9

Comparable Results from Other Techniques.

Existing values of the three isotherm temperatures:

Present Work (K)	Ultrasonic Thermometry (K)*		Gas Thermometry (K)**
20.263 +- 0.005	20.265	[22]	20.2746 +- 0.0004
	20.285	[48,49]	
13.8033 +- 0.0017			
4.2218 +- 0.0025	4.225	[24]	4.2240 +- 0.0003

* Errors have not been assessed by Plumb and Cataland for their ultrasonic thermometry so that it is impossible to check for consistency when their results lie outside our three standard error bar.
** These are some preliminary results of K. H. Berry obtained at the NPL. We believe them to be the best values available from primary gas thermometry.

Existing values of a and b:

a	b	Source	Method
18.6 +- 0.3	-419.0 +- 3.5	Present work	l.f. acstc.
17	-385	[51]	prmy. gas
20	-408	[52]	prmy. gas
22 +- 4	-433 +- 22	[25]	l.f. acstc.
19.8 +- 6.3	-441 +- 3	[24]	ultrasonic

a and b for the last four cases were calculated by Rogers et al. [50]

APPENDIX 1.1

Proof of Equation 1.3.3 Relating B(T) and B'(T).

The density and pressure expansions for the product PV are

$$PV = nRT\left\{1 + B(T)\frac{n}{V} + C(T)\left(\frac{n}{V}\right)^2 + \cdots\right\} \quad (1.3.1)$$

and

$$PV = nRT\left\{1 + B'(T)P + C'(T)P^2 + \cdots\right\} \quad (1.3.2)$$

respectively. From equation 1.3.1

$$P = RT\left\{\frac{n}{V} + B(T)\left(\frac{n}{V}\right)^2 + C(T)\left(\frac{n}{V}\right)^3 + \cdots\right\} \quad (A.1)$$

so that from equation 1.3.2

$$PV = nRT\left\{1 + B'RT\left[\frac{n}{V} + B\left(\frac{n}{V}\right)^2 + C\left(\frac{n}{V}\right)^3 + \cdots\right] + C'R^2T^2\left[\frac{n}{V} + B\left(\frac{n}{V}\right)^2 + C\left(\frac{n}{V}\right)^3 + \cdots\right] + \cdots\right\} \qquad (A.2)$$

At sufficiently low pressures equations 1.3.1 and A.2 become approximately

$$PV = nRT\left\{1 + B(T)\frac{n}{V}\right\} \qquad (A.3)$$

and

$$PV = nRT\left\{1 + B'(T)RT\frac{n}{V}\right\} \qquad (A.4)$$

where second order and smaller terms in P and n/V have been ignored. Thus

$$B(T) = B'(T)RT \qquad (1.3.3)$$

APPENDIX 1.2

Proof of Equation 1.3.4 Relating C(T) and C'(T).

Knowing the relation between B(T) and B'(T), it is possible to calculate the relation between C(T) and C'(T). Substituting for B' in equation A.2 from equation 1.3.3 we obtain

$$PV = nRT\left\{1 + B(T)\frac{n}{V} + \left(B^2(T) + C'(T)R^2T^2\right)\left(\frac{n}{V}\right)^2 + \cdots\right\} \qquad (A.5)$$

Thus by comparison with equation 1.3.1

$$C'(T) = \left\{C(T) - B^2(T)\right\} \Big/ R^2T^2 \qquad (1.3.4)$$

APPENDIX 1.3

Proof of Equation 1.3.5 Relating $A_1(T)$ and $B(T)$.

We have

$$c^2 = \left(\frac{\partial P}{\partial \rho}\right)_S = A_0(T) + A_1(T)P + A_2(T)P^2 + \cdots \quad (A.6)$$

and

$$\left(\frac{\partial P}{\partial \rho}\right)_S = -\frac{(V/n)^2}{M}\left(\frac{\partial P}{\partial V}\right)_S$$

$$= -\frac{(V/n)^2}{M}\frac{C_P}{C_V}\left(\frac{\partial P}{\partial V}\right)_T \quad (A.7)$$

the second equality arising because

$$\left(\frac{\partial P}{\partial V}\right)_S = \frac{C_P}{C_V}\left(\frac{\partial P}{\partial V}\right)_T \quad (A.8)$$

It may also be shown that

$$\sigma \equiv \frac{C_P}{C_V} = 1 - \frac{T}{C_V}\left(\frac{\partial P}{\partial T}\right)_V^2 \Big/ \left(\frac{\partial P}{\partial V}\right)_T \qquad (A.9)$$

so that

$$c^2 = \frac{T}{M}\frac{(V\ n)^2}{C_V}\left(\frac{\partial P}{\partial T}\right)_V^2 - \frac{(V\ n)^2}{M}\left(\frac{\partial P}{\partial V}\right)_T \qquad (A.10)$$

which may be evaluated from the equation of state if it is remembered that

$$C_V = \frac{3R}{2} + T\int_\infty^V \left(\frac{\partial^2 P}{\partial T^2}\right)_V dV \qquad (A.11)$$

Thus from equations 1.3.3, A.10 and A.11

$$c^2 = \frac{\sigma_0 RT}{M}\left\{1 + \left[2B + \frac{4}{3}T\frac{dB}{dT} + \frac{4}{15}T^2\frac{d^2B}{dT^2}\right]\frac{n}{V}\right.$$

$$+ \left[\frac{13}{5}C + \frac{16}{5}C\frac{dC}{dT} + \frac{2}{15}T^2\frac{d^2C}{dT^2} + \frac{2}{5}B^2\right.$$

$$+ \frac{98}{45}T^2\left(\frac{dB}{dT}\right)^2 + \frac{8}{45}T^4\left(\frac{d^2B}{dT^2}\right)^2 + \frac{28}{15}TB\frac{dB}{dT}$$

$$\left.\left. + \frac{8}{15}T^2B\left(\frac{d^2B}{dT^2}\right) + \frac{56}{45}T^3\left(\frac{dB}{dT}\right)\left(\frac{d^2B}{dT^2}\right)\right]\left(\frac{n}{V}\right)^2\right.$$

$$\left. + \cdots \right\} \qquad (A.12)$$

where terms of the same order in n/V have been collected together and where σ_0 is the ratio of the principal specific heats of an ideal gas. By comparing this with the acoustic density expansion:

$$c^2 = A_0'(T) + A_1'(T)\frac{n}{V} + A_2'(T)\left(\frac{n}{V}\right)^2 + \cdots \qquad (1.3.8)$$

we obtain the following expression for the coefficient, $A_1'(T)$:

$$A_1'(T) = 2B(T) + \frac{4}{3}T\frac{dB(T)}{dT} + \frac{4}{15}\frac{d^2B(T)}{dT^2} \qquad (A.13)$$

The corresponding expression for the second acoustic virial coefficient in the pressure expansion is easily obtained from this by expressing $A_1(T)$ in terms of $A_1'(T)$. This is done as it was in

appendices 1.1 and 2 for the virial coefficients of gas thermometry i.e. by substituting for the pressure terms in the pressure viral expansion to obtain an expansion in terms of n/V which may be compared to the original density expansion. We thus obtain

$$A_1'(T) = A_1(T)RT$$

and

$$A_2'(T) = A_1(T)B(T)RT + A_2(T)R^2T^2 \qquad (A.14)$$

so that we find

$$A_1(T) = \frac{\sigma}{M}\left\{2B(T) + \frac{4}{3}\frac{dB(T)}{dT} + \frac{4}{15}\frac{d2B(T)}{dT^2}\right\}$$

(1.3.5)

APPENDIX 1.4

Proof of Equation 1.3.6 Relating $A_2(T)$ to B(T) and C(T).

The required relationship follows directly from equations A.12 and A.14. to give equation 1.3.6.

APPENDIX 2.1

Proof that the Zeros, X_{mn}, of Equation 2.2.18 are Real.

It has often been shown that

$$\int_0^1 r\, J_m(\alpha r)\, J_m(\beta r)\, dr = \frac{1}{\alpha^2-\beta^2}\left\{\beta J_m(\alpha) J_m'(\beta) - \alpha J_m'(\alpha) J_m(\beta)\right\} \qquad (A.15)$$

where $\alpha^2 \neq \beta^2$. If β is the complex conjugate of α we may write instead:

$$\int_0^r r\, J_m(\alpha r)\, J_m(\bar{\alpha} r)\, dr =$$

$$\frac{r}{\alpha^2-\bar{\alpha}^2}\left\{J_m(\alpha r)\frac{d}{dr} J_m(\bar{\alpha} r) - J_m(\bar{\alpha} r)\frac{d}{dr} J_m(\alpha r)\right\}$$

Assuming that if

$$\frac{d}{dr} J_m(\alpha r) = 0 \qquad (A.16)$$

then

$$\frac{d}{dr} J_m(\bar{\alpha} r) = 0 \qquad (A.17)$$

also, we have in this situation

$$\int_r^r J_m(\alpha r) J_m(\bar{\alpha} r)\, dr = \int_r^r J_m(\alpha r)\, \overline{J_m(\alpha r)} = 0$$

$$= \int_r^r J_m^2(\alpha r)\, dr \neq 0$$

(A.18)

Thus α cannot be complex. However, it may still be imaginary since the denominator of equation A.15 vanishes in this case. But, expanding J_m in an infinite series, gives

$$\frac{d}{dX} J_m(X) = \sum_{n=0}^{\infty} \frac{(-1)^n (X/2)^{2n+m-1}}{n!(n+m)!} \frac{2n+m}{2}$$

$$= \left(\frac{Y}{2}\right)^{m-1} (i)^{m-1} \sum_{n=0}^{\infty} \frac{(Y/2)^{2n}}{n!(n+m)!} \frac{2n+m}{2} \neq 0$$

$$(X = iY) \qquad (A.19)$$

so that α being neither complex nor purely imaginary must be real.

APPENDIX 2.2

Proof of the Equivalence of Several Criteria for Resonance at Sufficiently High Frequencies and the Effect of Higher Modes on the Measured Absorption Coefficient.

It will be shown that the same values of l at resonance are obtained when (a) $Z_G(l)$ is entirely real, (b) The real part of $Z_G(l)$ is greatest or (c) the power dissipated is greatest povided that the frequency is sufficiently high.

Condition (a)

From equation 2.2.24 it can be seen that this requires

$$\sum_m \sum_n G_{mn} X_{mn}(l) = 0 \qquad (A.20)$$

Now from equation 2.2.36

$$\sum_m \sum_n G_{mn} X_{mn}(l) =$$

$$\sum_m \sum_n G_{mn} \frac{\sin 2k_{mn} l}{\cosh 2\alpha_{mn} l - \cos 2k_{mn} l} \qquad (A.21)$$

But at high frequencies α_{mn} and k_{mn} are roughly constant for the first few values of m and n which are expected to correspond to those modes of high amplitude which are unlikely to be resolved. Thus we may for practical purposes cancel the denominators in equation A.21 to give

$$\sum_m \sum_n G_{mn} \sin 2k_{mn}\ell = 0 \qquad (A.22)$$

It will now be shown that this same criterion for resonance is obtained in cases (b) and (c).

Condition (b)

Again, equation 2.2.24 enables this condition to be interpreted into the following constraint on l:

$$\frac{d}{d\ell} \sum_m \sum_n G_{mn} R_{mn}(\ell) = \sum_m \sum_n G_{mn} \frac{dR_{mn}(\ell)}{d\ell} = 0 \qquad (A.23)$$

Now

$$\frac{d}{d\ell} R_{mn}(\ell) \doteq \frac{2\alpha_{mn}(\cosh 2\alpha_{mn}\ell - \cos 2k_{mn}\ell - 2k_{mn}\ell \sin 2k_{mn}\ell)}{(\cosh 2\alpha_{mn}\ell - \cos 2k_{mn}\ell)^2}$$

$$\pm \frac{4\alpha_{mn} k_{mn} \sin 2k_{mn}\ell}{(\cosh 2\alpha_{mn}\ell - \cos 2k_{mn}\ell)^2} \qquad (A.24)$$

where we have retained only terms of second order of smallness, there being none greater in the immediate vicinity of the resonance. As before the denominator can be cancelled together with the factor $4\alpha_{mn} k_{mn}$ which is also approximately constant with changing m and n for the same reasons. This leads to the same condition on ℓ at resonance as was obtained in the previous situation.

Condition (c)

It may immediately be seen from equation 2.2.40 that this condition leads to the same equation for ℓ at resonance as have the last two conditions.

At somewhat lower frequencies where α_{mn} and k_{mn} may no longer be considered to be exactly equal for the various different values of m and n, the conditions

$$\sum_m \sum_n G_{mn} \frac{\sin 2k_{mn}\ell}{\cosh 2d_{mn}\ell - \cos 2k_{mn}\ell} = 0 \qquad (A.25)$$

and

$$\sum_m \sum_n G_{mn} \frac{\sin 2k_{mn}\ell}{(\cosh 2d_{mn}\ell - \cos 2k_{mn}\ell)^2} = 0 \qquad (A.26)$$

are no longer equivalent. In such a case the denominators of equations 2.2.46 and 2.2.52 will no longer be raised to the power two if resonance is defined by criterion (a). It may easily be shown that the requirement for the equivalence of these criteria of resonance is, in fact, equation 2.2.47:

$$\Delta_{mn}^2 \doteq \Delta_{oo}^2 \gg (\ell - \ell_{mn})^2 \qquad (2.2.47)$$

stating that the mnth resonance is far from being resolved.

Higher Modes and the Measured Absorption Coefficient.

The effect of higher modes upon the measured absorption coefficient may also be calculated easily at frequencies high enough to satisfy equation 2.2.47. At the observed resonance

$$\dot{W}_q(l) = \sum_m \sum_n G_{mn} R_{mn} \left(\frac{N}{2} \frac{\sum_m \sum_n G_{mn} \lambda_{mn}}{\sum_m \sum_n G_{mn}} \right) \qquad (A.27)$$

But

$$R_{mn}(l) \doteq \frac{\alpha_{mn} l}{\alpha_{mn}^2 l^2 + k_{mn}^2 (l - l_{mn})^2} \doteq \frac{1}{\alpha_{oo} l_{oo}} \qquad (A.28)$$

under the approximations already used at these frequencies. Thus

$$\dot{W}_q(l) = \frac{\sum_m \sum_n G_{mn}}{\alpha_{oo} l_{oo}} \qquad (A.29)$$

At somewhat lower frequencies when equation 2.2.47 no longer holds good, but when the higher modes still remain unresolved, this becomes

$$\dot{W}_q(l) = \frac{\sum_m \sum_n G'_{mn}}{\alpha_{oo} l_{oo}} \qquad (A.30)$$

It might at first be supposed that both these expressions would lead to errors in the evaluation of the absorption coefficient since the

equivalent ideal expression would be

$$\dot{W}_q(\ell) = \frac{G_{00}}{\alpha_{00}\, l_{00}} \qquad (A.31)$$

However, in order to evaluate α_{00}, independent evaluation of their numerators is required. These values might be obtained from the corresponding values of $\dot{W}_G(l)$ at antiresonance which are

$$\dot{W}_q(\ell) = \sum_m \sum_n G_{mn}\, \alpha_{mn}\, \ell \doteq \alpha_{00}\, \ell \sum_m \sum_n G_{mn} \qquad (A.32)$$

for the first two cases where higher modes are present, or

$$\dot{W}_q(\ell) = G_{00}\, \alpha_{00}\, \ell \qquad (A.33)$$

in the ideal case. Thus a correct value of α_{00} may be calculated from measured values of $\sum_m \sum_n G_{mn}\, \alpha_{00}$ and $\sum_m \sum_n G_{mn} / \alpha_{00}$ at sufficiently high frequencies as for the ideal case. In the case of the lower frequencies, on the other hand, a fractional increase in α_{00} of

$$\left\{ \frac{\sum_m \sum_n G_{mn}}{\sum_m \sum_n G'_{mn}} \right\}^{\frac{1}{2}} - 1$$

will be found. This might betray the presence of higher modes if adequate data is available to enable a reliable value of the true absorption coefficient to be calculated from equation 2.1.16. For example, if we take the case of Table 2.5 where a/b=1 (i.e. a stiff driven diaphragm of the same diameter as the cavity) we may derive from equation 2.2.52 the following amplitudes G'_{mn} :

mn	G_{mn}	X_{mn}	G'_{mn}
00	1.00	0.00	0.94
01	0.66	7.01	0.56
02	0.04	10.17	0.01

Here we have assumed that the 02th mode is virtually resolved so that $\Delta_{00} \doteq l - l_{02}$. This occurs at a frequency of approximately 1MHz for a cavity of 2cm diameter filled with helium-4 gas at a temperature of 4.2K and a pressure of one atmosphere. Thus

$$\alpha = \left\{\frac{1.70}{1.51}\right\}^{\frac{1}{2}} \alpha_{00} = 1.06\,\alpha_{00}$$

showing a 6 per cent increase in the measured value of the absorption coefficient over the correct value. Unfortunately, however, much of the information on the transport coefficients of gases is of uncertain accuracy, and so an effect of this size may not be a sufficiently pronounced indication of the presence of higher modes to enable a definite conclusion to be reached. Furthermore, there is no guarantee that the spectrum of this example is relevant to any given practical case where, for example, one single higher mode may predominate thus leading to a change in the measured velocity, but to no visible change in the measured absorption coefficient at all. Consequently measured values of absorption coefficients cannot be relied upon to check on the absence of errors attributable to higher modes.

REFERENCES

1. Comite intern. poids et mesures, proces-verbaux des seances de 1948 21, T30 (1948)

2. Comite Consultatif de Thermometrie, 8e session, 1967, Annexe 2.

3. Metrologia, 5, 2 (1969).

4. "The International Practical Temperature Scale of 1968" (English version of the official French text) HMSO (1969).

5. R.E. Bedford, M. Durieux, R. Muijlwijk and C.R. Barber. Metrologia 5, 2 (1969).

6. Comite Consultatif de Thermometrie, 5e session, 1958 p.t192.

7. F.G. Brickwedde, J. Research Natl. Bur. Standards, 64A, 1 (1960).

8. Comite Consultatif de Thermometrie, 6e session, 1962, p.184

9. J. Research Natl. Bur. Standards, 68A, 547,559,567,579, (1964).

10. L.G. Rubin, Cryogenics 11, 1 (1970).

11. A.C. Anderson, "Temperature, its Measurement and Control in Science and Industry" (Proceedings of the Fifth Symposium on Temperature, Washington (1971) - to be published).

12. Collins and Kemp. See ref.11.

13. T.C. Cetas and C.A. Swenson. See Ref. 11.

14. C. van Rijn and M. Durieux. See Ref. 11.

15. A. Van Itterbeek and G. Forrez, Physica 20, 767 (1954).

16. A. Van Itterbeek, J. Acoust. Soc. Am. 29,584 (1957).

17. A. Van Itterbeek, Proceedings of the Fifth International Conference on Low Temperature Physics and Chemistry. Ed. J.R. Dillinger (University of Wisconsin Press, Madison, Wisconsin, 1958) p.206.

18. A. Van Itterbeek and J. De Laet, Physica 24,59 (1958).

19. J. De Laet, Verh. K. Vlaam. Acad. Wet. Klasse der Wetenschappen (Brussels) 66,22(1960) - translation available from A.R. Colclough.

20. A.D. Brodsky, V.P. Kremlevsky and A.V. Savateev, Compt. rend. Comite. Intern. Poids et Mesures, Comite Consultat. Thermometrie, 6e session (1962), Annexe 27.

21. G. Cataland, M. Edlow and H. Plumb, Temperature, its Measurement and Control in Science and Industry. Ed. C.M. Herzfeld (Reinhold Publishing Corporation, New York, 1962) Vol.III, Pt.1, p. 129.

22. G. Cataland and H. Plumb, Proceedings of the Eighth International Conference on Low Temperature Physics, Ed. R.O. Davies (Butterworth Scientific Publications Ltd., London, 1963) p.439.

23. H. Plumb and G. Cataland, J. Research Natl. Bur. Standards 69A,375 (1965).

24. H. Plumb and G. Cataland, Metrologia 2,4 (1966).

25. D.T. Grimsrud and James H. Werntz. Jr. Phys. Rev. 157,1 (1967).

26. J.C. Hubbard, Phys. Rev. 38,1011 (1931).

27. J.C. Hubbard, Phys. Rev. 41,523 (1932).

28. Karl F. Herzfeld, Phys. Rev. 38,1011 (1931).

29. H. Helmholtz, Verhandlungen des Naturhistorisch-medecinischen Veriens zu Heidelberg 3, 16 (1863).

30. G. Kirchoff, Ann. Phys. Lpz. 134,177 (1868).

31. Jordan J. Markham, Robert T. Beyer and R.B. Lindsay, Rev. Mod. Phys. 23,4 (1951).

32. W.H. Pielemeier, Phys. Rev. 37,1682 (1931).

33. W.H. Pielemeier, J. Acoust. Soc. Amer. 9,212 (1938).

34. J.F.W. Bell, Proc. Phys. Soc. B63, 958 (1950).

35. P.E. Krasnooshkin, Phys. Rev. 65, 190 (1944).

36. D. E. Weston, Proc. Phys. Sos. B66, 695, (1953)

37. F. Douglas Shields, K. P. Lee and W. J. Wiley, J. Acoust. Soc.

Amer. 37,4(1965)

38. P. S. Henry, Proc. Phys. Soc. 43,340 (1931).

39. M. Thiesen, Ann. Phys. Lpz. 24,401(1907).

40. L. Fritche, Acustica,10,4(1960).

41. H.Schneebeli, Ann. Phys. Lpz., 136,296(1869).

42. Ad. Seebeck, Ann. Phys. Lpz., 139,104(1870). Ibid., 52,333(1917).

44. D. H. Smith and R. G. Harlow, Brit. J. App. Phys., 14,102(1963).

45. R. W. B. Stephens and A. E. Bate, Acoustic and Vibrational Physics, 479, 2nd Edn. (1966), Edward Arnold (Publishers) Ltd., London.

46. V. A. Del Grosso, U. S. Naval Res. Lab. Report No. 6133 Pt. II, 12(1965).

47. M. A. Breazeale and Laszlo Adler, Conf. on Non Linear Acoustics, Univ. Texas, Austin, Texas, USA (1970).

48. G. Cataland and H. H. Plumb, Meeting of the CCT, 8e session, (1967) Document 27.

49. R. Muijlwijk, M. Durieux and H. Van Dijk, Physica, 43, 622(1969).

50. J. S. Rogers, R. J. Tainsh, M. S. Anderson and C. A. Swenson, Metrologia, 4, 2 (1968).

51. W. H. Keesom, Helium, 49, Amsterdam, Elsevier Publishing Corpn. (1942).

52. J. E. Kilpatrick, W. E. Keller and E. F. Hammel, Phys. Rev., 102, 304 (1956).

SUPPLEMENTARY MATERIAL I.

This report was submitted to the Ninth Meeting of the CCT of the CIPM in Paris (1971). It was also read to the Fifth International Symposium on Temperature held in Washington DC, USA in the same year.

A low frequency acoustic thermometer for the range 2 - 20 K.

by

A.R. Colclough, National Physical Laboratory,

Teddington, Middlesex, United Kingdom.

Abstract

A low frequency acoustic thermometer for the liquid helium range is described which incorporates several novel features designed to eliminate the difficulties commonly encountered with this technique. Boundary layer errors which are particularly troublesome at low frequencies have been corrected for experimentally rather than by using the apparently unreliable corrections of Kirchhoff, Helmholtz et al. Increased sensitivity has been achieved with a method of detecting the resonances which is independent of the purely electrical impedance of the transducer used to excite the interferometer cavity. Acoustic paths are measured with an optical interferometer operating under isothermal conditions inside the cryostat.

Acoustic isotherms at the normal boiling points of helium-4 and equilibrium hydrogen have been plotted to yield thermodynamic temperatures which are in fair agreement with the high frequency work of Plumb and Cataland.

A low frequency acoustic thermometer for the range 2 - 20 K

by

A. R. Colclough

National Physical Laboratory, Teddington, Middlesex, United Kingdom

Introduction

In recent years a number of interferometric investigations into the propagation of sound in helium gas have been made with a view to measuring thermodynamic temperatures in the range 2 - 20 K.[1-12] Two methods seem to have emerged: the use of high frequencies with the attendant risk of an ill-defined wave field[1,2,7-11] and low frequency methods[3-5,12] where this problem is avoided at the expense of incurring difficulties with boundary layer effects for which reliable theoretical corrections may not easily be made. At the moment, however, there seems to be no detailed low frequency temperature scale to compare with the high frequency scale of Plumb and Cataland.[10] It was in answer to this need that the National Physical Laboratory designed and constructed a low frequency acoustic thermometer and undertook an examination of the systematic errors characteristic of low frequency acoustic interferometry. The degree of self-consistency achieved in the measurements made so far leads us to believe that the systematic errors have been successfully corrected for and the agreement reached between our preliminary results and the aforementioned ultrasonic work tends to support this view.

1. The design of the instrument

The instrument which is to be described more fully elsewhere[13] is essentially a variable-path cylindrical acoustic interferometer (Fig. 1) operated at some constant frequency below its first characteristic cut-off frequency so that only plane waves may propagate in the cavity.[14,15] As a result of the low frequencies used, the boundary layer causes a sizable decrease in the measured velocity of sound relative to the value in the unbounded fluid.[16-20] There is also an increase in the acoustic absorption coefficient brought about by the same mechanism. By measuring the acoustic absorption coefficient, however, it is possible to calculate the correction to the velocity. This enables one to avoid the use of the theoretical corrections of Kirchhoff, Helmholtz, Thiesen et al. which have often been found to be unreliable.

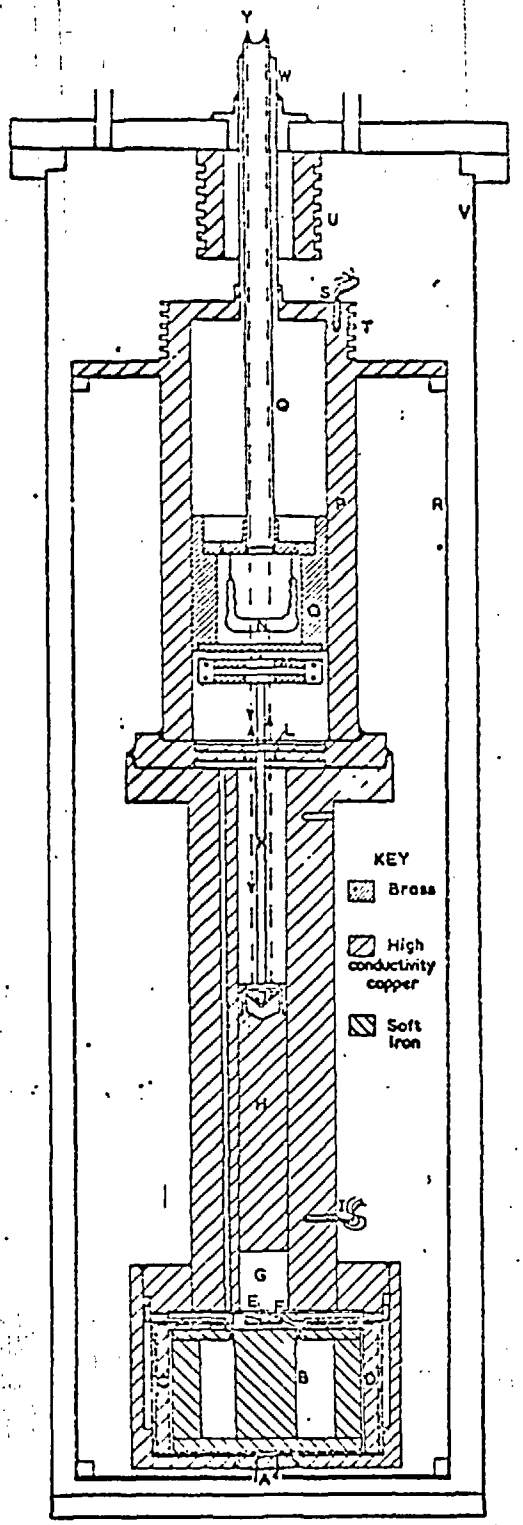

Figure 1

The Acoustic Interferometer.

A - Stycast Seals, B - Permanent Magnet Assembly, C & D - Electrical Lead Screens, E - PZT Accelerometer, F - Transducer Diaphragm, G - Acoustic Cavity, H - Piston Reflector, I - Germanium Resistance Thermometers, J - Cube-Corner Reflector, K - Pushrods, L - Beam Splitter, M - Gimbals, N - Optical Window, O - Bearing, P - Upper Chamber, Q - Moving Tube, R - Radiation Shield, S - Temperature Controlling Sensor, T - Thermal Anchoring Grooves (with heater), U - 4.2K Thermal Anchoring Grooves, V - Vacuum Can, W - Central Supporting Tube, Y - Laser Beams.

Conventionally resonance in the interferometer cavity is detected either by using a microphone to monitor the acoustic pressure or by measuring the electrical impedance of the transducer used to excite the cavity which is modified by the mechanical loading of the gas.[21-24] The latter method has the advantage of simplicity, but the mechanical impedance of the system may not be coupled very strongly to the electrical impedance of the device and will, in any case, be masked to some extent by that constituent of the electrical impedance which is purely electrical in origin. For this reason it was decided to measure the mechanical impedance of the loaded transducer directly.

A small lead zirconate.titanate (PZT) piezoelectric accelerometer was attached to the rear face of the moving coil driven diaphragm which served as the transducer. At constant frequency the amplitude of the voltage from the accelerometer gave the velocity amplitude of the diaphragm in arbitrary units. By dividing the driving force of the diaphragm by this quantity the mechanical impedance of the system is obtained. Since the driving force is constant at constant current, the impedance in arbitrary units may be obtained simply by taking the reciprocal of the voltage amplitude. This method enabled sound velocities to be measured at considerably lower pressures than would otherwise be possible.

The separation of the various positions of resonance from which the acoustic wavelength is calculated (and hence the velocity of sound) was measured using a laser interferometer situated within the acoustic interferometer unit itself. The wavelength of sound is therefore measured in terms of the accurately known wavelength of light from a laser. This has the advantage over the conventional pushrod and micrometer method where acoustic paths are measured from outside the cryostat in that it does not suffer from the indeterminate thermal contractions in the pushrod.

2. Experimental procedure

The normal boiling points of equilibrium hydrogen and helium-4 were realised by controlling the temperature of the interferometer at values which closely reproduced the calibrated boiling point resistances on three germanium resistance thermometers which were in thermal contact with it. Subsequent corrections of the measured velocities to their exact boiling point values were made from a rough prior calibration of these thermometers. It was estimated that the final value of velocity which was calculated corresponded to a temperature within $\pm$ 1.1 mK of the boiling point of helium-4 or within $\pm$ 4 mK at the hydrogen point. In quoting our final results these errors have been taken to be equal to three standard errors.

The interferometer was suspended in a vacuum can immersed in the liquid helium bath of a conventional liquid helium cryostat. For the 4.2 K isotherm the liquid coolant was pumped to a temperature slightly below its normal boiling point so that the interferometer itself could be brought to the exact boiling point by means of an electrical heater. It was, of course, unnecessary to pump the bath at the higher isotherm temperature. The heater current was controlled using an equal ratio a.c. Wheatstone bridge one arm of which was a two lead germanium sensor mounted close to the heater on the interferometer. Using this controller temperatures were held constant to within $\pm$ 0.5 mK at the lower point and seldom varied by more than $\pm$ 2 mK at the hydrogen point.

The pressure of the thermometric gas was controlled by a pressure controller from Texas Instruments Ltd. This device functioned by bleeding helium in or out of the interferometer through servo-operated needle valves. These were driven by an out-of-balance signal from a quartz spiral bourdon gauge supplied by the same manufacturer. Pressures could be held constant to within $\pm$ 5 N m^{-2} for the duration of a measurement (about three hours) and were measured and constantly monitored with a recently calibrated Kew pattern mercury barometer. The accuracy achieved in the measurement was about $\pm$ 5 N m^{-2} which represented an entirely negligible error in the final values of isotherm temperature.

At the highest frequency which could be used without exceeding the first cut-off frequency it was possible to accommodate five resonances in the cavity when fully extended. The resonances were scanned and about four hundred readings of the accelerometer voltage (and hence impedance) were taken at various points, together with the corresponding readings of acoustic path from the optical interferometer. This resonance curve was subsequently analysed by plotting impedance circles for each resonance which enabled the exact points of resonance to be determined to within several parts in 10^4 of the acoustic cut-off wavelength (approximately 3.4 cm with a cavity radius of 1 cm). All other things being equal, temperatures may be calculated to twice the fractional error in the final value obtained for the velocity or wavelength of sound.

It is also possible to calculate from the resonance curve the reflection coefficients for the ends of the cavity and the acoustic absorption coefficient, α, which is almost entirely attributable to the boundary layer at these frequencies. Thus, taking the fractional error in the measured velocity, v, to be $\alpha v/\omega$ where ω is the angular frequency of the sound, it is then possible to make a measured correction to the velocity

for the effect of the boundary layer. The validity of this correction depends on the assumption that the absorption coefficient is directly proportional to the square root of the frequency whilst the velocity correction varies inversely with it. Tests made at two frequencies at the helium point indicate that this is in fact the case. The ratio of the two measured absorption coefficients was equal to the square root of the ratio of the corresponding frequencies within the limits of accuracy achieved. Furthermore, the corrected velocities were equal to within the general reproducibility of velocity measurements made at the same frequency.* No such tests were made at 20 K, but the corrected velocities were found to lie randomly about a straight line whereas the uncorrected velocities showed a distinct curvature. We feel confident, therefore, that the systematic errors attributable to the boundary layer have been correctly assessed.

3. Experimental results

The values of the normal boiling points of helium-4 and equilibrium hydrogen which are presented are to be regarded as provisional pending the accumulation of sufficient data to define the shape of the isotherms more closely. Nevertheless, it is already clear from the results now available that their self-consistency is of a high enough order to justify confidence in the instrument.

Measured and corrected values of the velocity of sound at the normal boiling point of helium-4 are given in Table I together with the measured absorption coefficients and the frequencies at which they were obtained. The isotherm is plotted in fig. 2 where uncorrected values of the velocity are also included to show the general effect of the boundary layer on measured temperature. The two lowest points on the isotherm were the points taken at the two frequencies as described above. It can be seen that the point taken at the lower frequency has a correspondingly higher boundary layer correction as expected.

Straight line, quadratic and cubic polynomial representations of the data were tried and it was found that the quadratic fit was best, but not greatly superior to the linear fit. Details of the straight line and quadratic fits are given in Table II. It can be seen that the two answers for the boiling point differ by 4.6 mK - a difference easily covered by twice the sum of the purely statistical standard errors in the individual answers. Unfortunately, however, it is impossible to make a rational choice of one value in preference to the other. The improvement observed on raising the order of fit to two might be attributable to a curvature in the points brought about by the

---

* See Addendum

TABLE I

Showing Results at the Normal Boiling Point of Helium-4

Pressure Nm^{-2}	Measured Velocity ms^{-1}	Frequency kHz	Measured Absorption Coefficient m^{-1}	Corrected Velocity ms^{-1}	Square of Corrected Velocity $m^2 s^{-2}$
8470	119.592	3.3	.1850	119.720	14332.9
8480	119.486	1.5	.1220	119.671	14321.1
10700	119.274	3.3	.1430	119.372	14249.7
12520	119.018	3.3	.1460	119.118	14189.1
15930	118.517	3.3	.1270	118.603	14066.7
19700	117.961	3.3	.1190	118.041	13933.7
23290	117.401	3.3	.1170	117.479	13801.3
26630	116.880	3.3	.1380	116.971	13682.2

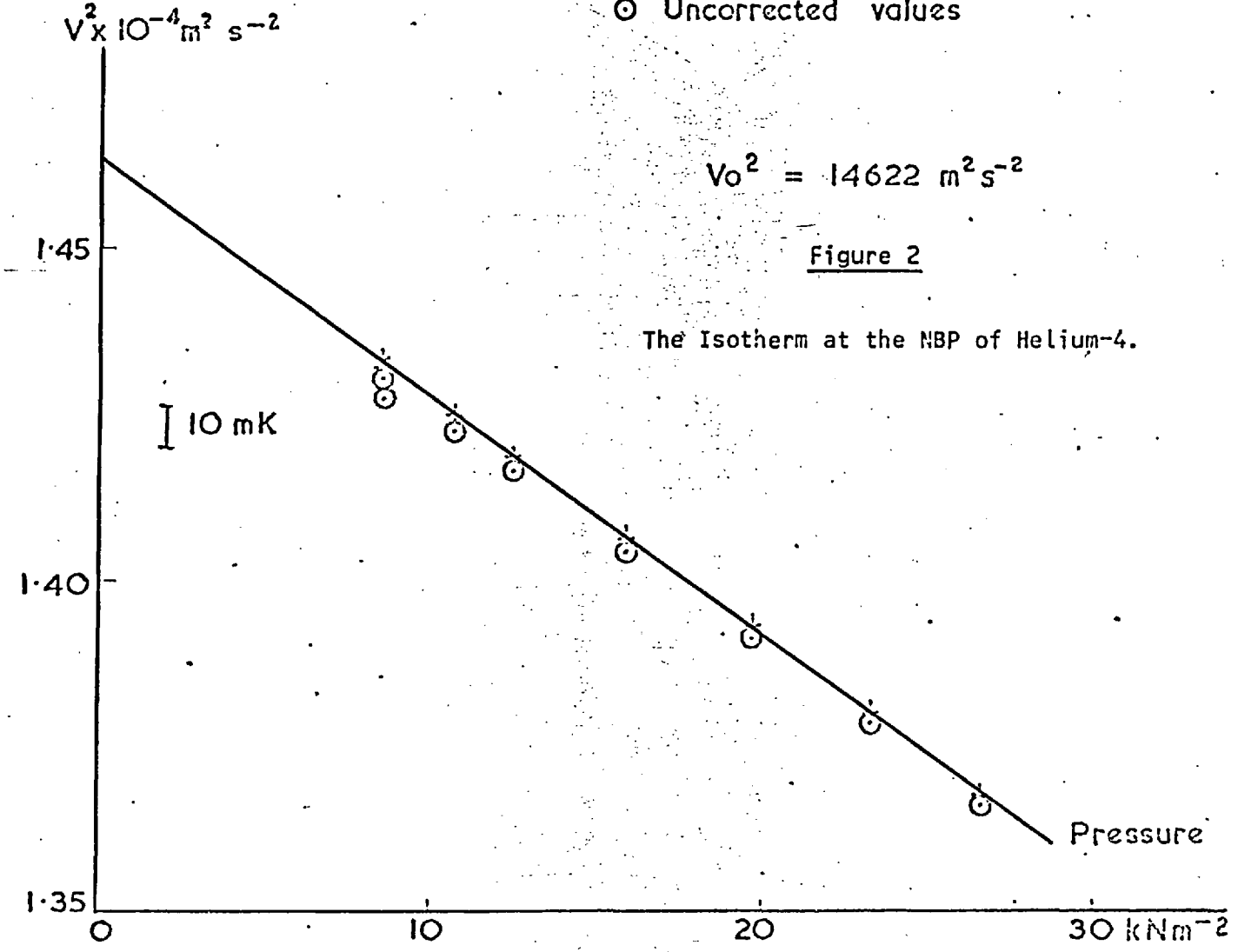

Figure 2

The Isotherm at the NBP of Helium-4.

TABLE II *

Showing Details of the fit to the Isotherm

at the Normal Boiling Point of Helium-4

$V_o^2 = \frac{\sigma R}{M} T$ where R is the gas constant (8.3143×10^3), $\sigma = C_p/C_V = 5/3$ and M is the molecular weight of He-4 (4.00260)	$V^2 = V_o^2 + ap$	$V^2 = V_o^2 + ap + bp^2$
RMS deviation of V^2 m^2 s^{-2}	3.7	3.1
Equivalent temperature mK	1.1	0.9
$V_o^2 \pm$ standard error m^2 s^{-2}	14630 ± 4	14614 ± 11
Equivalent temperature $\pm$ standard error K	4.2258 ± 0.0011	4.2212 ± 0.0033
a	- .0035525	- .0033276
b		$- 6.5988 \times 10^{-8}$
Mean value of two boiling points $\pm$ standard error K	$4.2235 \pm .0018$	

* See Addendum

physical properties of the thermometric gas. Or - equally likely on the present evidence - it could be brought about by the random distribution of points about what may transpire to be a straight line on further investigation. Accordingly the mean of the two answers has been adopted until the question can be settled. The compounded standard error in the mean is 1.8 mK. To this statistical error must be added any other source of systematic error which has not been accounted for, in particular the error due to the uncertainty in the reproduction of the boiling point and that due to the uncertainty in the gas constant. The former is taken to be $\pm$ 0.4 mK and the standard error in the gas constant 45 parts in 10^6 which is equivalent to $\pm$ 0.2 mK in the final answer. Thus for the normal boiling point of helium-4 we have:

$$T(\text{n. b. p. helium-4}) = 4.2235 \text{ K} \pm 1.9 \text{ mK}^*$$

where we have quoted the total estimated standard error.

The experimental results for the normal boiling point of equilibrium hydrogen are given in Table III and the isotherm is plotted in fig. 3. It can be seen that the boundary layer corrections are considerably greater in this isotherm than in the previous one due to the lower gas densities at the higher temperature. However, in terms of a fractional error they are roughly comparable. For this isotherm no improvement was observed on increasing the order of fit to two, and so a linear representation of the data could be unambiguously chosen. Assessing the errors in the same way as before we find

$$T(\text{n. b. p. e-hydrogen}) = 20.263 \text{ K} \pm 5 \text{ mK}.$$

Full details of the linear fit to the data are given in table IV.

4. Conclusions

A thermodynamic temperature of 4.2235 K for the normal boiling point of helium-4 indicates that the helium-4 vapour pressure scale, T_{58}, assigns it a value (4.215 K) which is too low by 8.5 mK. This is almost equal to the discrepancy o 10 mK found by Plumb and Cataland using their high frequency instrument.[10]

An early estimate of theirs[8] of the normal boiling point of equilibrium hydrogen gave the value as 20.265 K with a reproducibility equivalent to $\pm$ 7 mK in the measured velocities. Later measurements[10] at the slightly lower temperature of 20.0 K indicated that their acoustic temperature exceeded temperatures measured on the scale NBS-55[33] (defined only to $\pm$ 10 mK) by approximately 3 mK. This scale yields a value of 20.271[25] for the normal boiling point of equilibrium hydrogen indicating a rough value only of 20.274 K for the acoustic estimate which must be considered entirely compatible with the earlier measurement.

---

* See Addendum

TABLE III

Showing the Results at the Normal Boiling Point of Equilibrium Hydrogen

Pressure Nm^{-2}	Measured Velocity ms^{-1}	Frequency kHz	Measured Absorption Coefficient m^{-1}	Corrected Velocity ms^{-1}	Square of Corrected Velocity $m^2 s^{-2}$
10170	264.294	7.25	.4072	264.921	70183.1
20240	264.679	7.25	.3059	265.150	70304.5
30020	264.822	7.25	.2541	265.212	70337.4
40330	264.942	7.25	.2091	265.253	70359.2
49740	265.091	7.25	.1633	265.343	70406.9
50040	265.102	7.25	.1874	265.391	70432.4
60030	265.212	7.25	.1470	265.439	70457.9
69920	265.340	7.25	.1570	265.583	70534.3
80090	265.437	7.25	.1287	265.636	70562.5
97790	265.695	7.25	.1330	265.901	70703.3

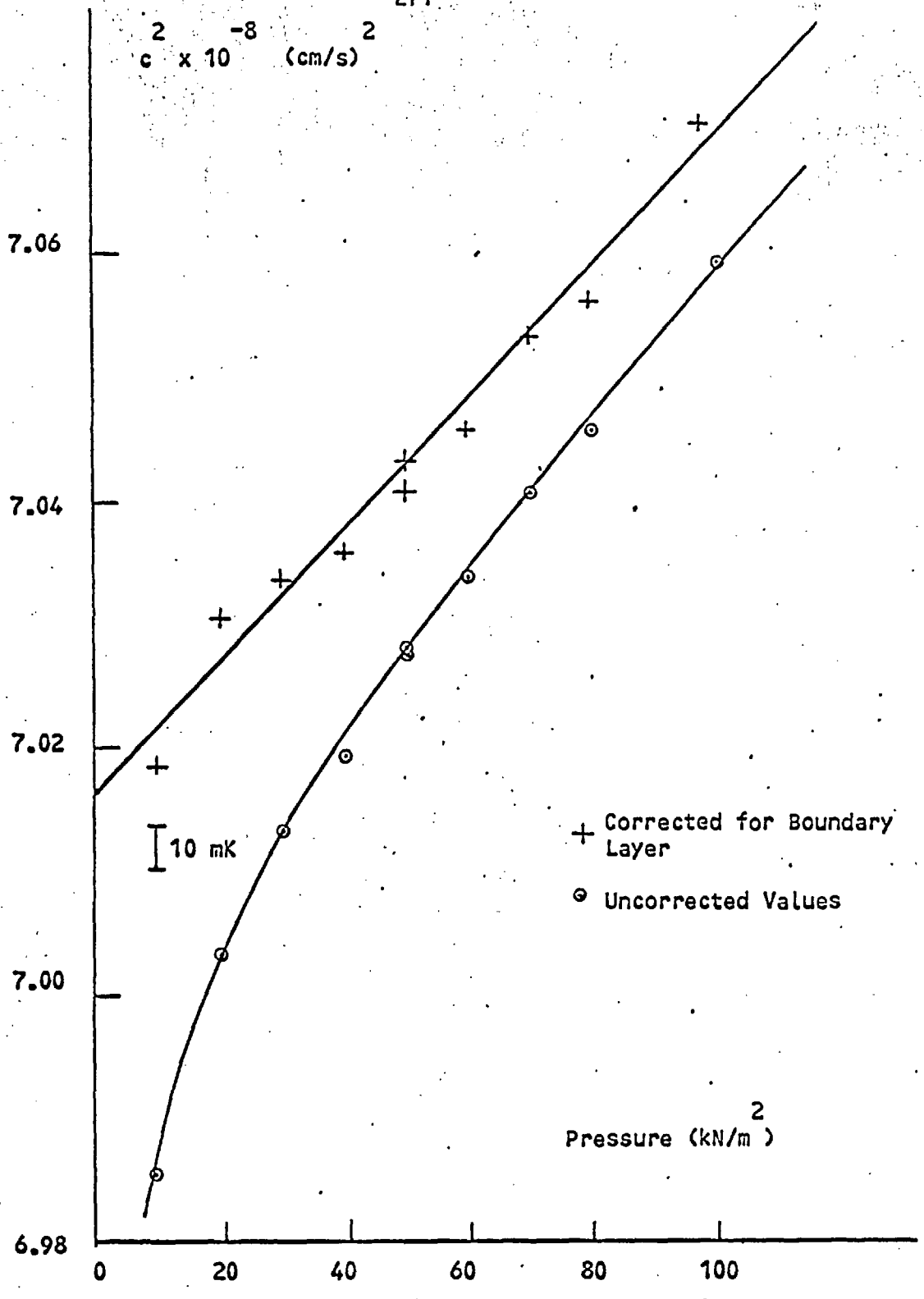

Figure 3

The Isotherm at the NBP of Equilibrium Hydrogen.

TABLE IV

Showing Details of the Fit to the Isotherm at the Normal Boiling Point of Equilibrium Hydrogen

$V_o^2 = \frac{\sigma R}{M} T$ where R is the gas constant (8.31434×10^3), $\sigma = C_p/C_V = 5/3$ and M is the molecular weight of He-4 (4.00260)	Linear Fit $V^2 = V_o^2 + ap$
RMS deviation of V^2 m^2 s^{-2}	21.7
Equivalent temperature mK	6.3
V_o^2 ± standard error m^2 s^{-2}	70156.3 ± 17.0
Equivalent temperature ± standard error K	20.2643 ± 0.0049
a	0.00534730

A small correction of 1.7 mK is subtracted from the value 20.2643 K to allow for a calibration error of the germanium resistance thermometers at this point. Thus we have 20.2626 K ± 4.9 mK for the NBP of e-hydrogen.

A second exact determination was reported in 1967 giving a value of 20.285 K.[26,27] This value, in company with values arrived at by other workers using gas thermometry, was used in the determination of the value, 20.28 K adopted for the corresponding primary fixed point on the International Practical Temperature Scale (1968).[28,29] It is, unfortunately, impossible to say whether or not this most recent result is compatible with our own value since it lies outside our three standard error bar and we are unaware of its associated error, knowledge of which is necessary to resolve the matter.

It is felt that the tests carried out on the boundary layer at 4.2 K together with the excellent agreement reached with the high frequency work of Plumb and Cataland lends considerable support to our claim to have measured the true thermodynamic boiling point of helium-4.

A similar conclusion follows for the normal boiling point of equilibrium hydrogen. Whilst no tests on the boundary layer corrections have been made at this temperature there is no reason to suppose that any new problems would arise which are not visible at the lower temperature. Furthermore, it can be seen from the isotherm that the corrected velocities are linear whilst the uncorrected velocities lie on a distinct curve which, as expected, falls away increasingly rapidly at the lower gas pressures.

References

1. A. Van Itterbeek and G. Forrez, Physica 20, 767 (1954).
2. A. Van Itterbeek, J. Acoust. Soc. Am. 29, 584 (1957).
3. A. Van Itterbeek, Proceedings of the Fifth International Conference on Low Temperature Physics and Chemistry. Ed. J.R. Dillinger (University of Wisconsin Press, Madison, Wisconsin, 1958) p. 206.
4. A. Van Itterbeek and J. De Laet, Physica 24, 59 (1958).
5. J. De Laet, Verh. K. Vlaam. Acad. Wet. Klasse der Wetenschappen (Brussels) 66, 22 (1960).
6. A.D. Brodsky, V.P. Kremlevsky and A.V. Savateev, Compt. Rend. Comite Intern. Poids Mesures, Comite Consultat. Thermometrie, 6^{e} Session (1962), annexe 27.
7. G. Cataland, M. Edlow and H. Plumb, Temperature, its Measurement and Control in Science and Industry. Ed. C.M. Herzfeld (Reinhold Publishing Corporation, New York, 1962) Vol. III, Pt. 1, p. 129.
8. G. Cataland and H. Plumb, Proceedings of the Eighth International Conference on Low Temperature Physics. Ed. R.O. Davies (Butterworth Scientific Publications Ltd., London, 1963) p. 439.
9. H. Plumb and G. Cataland, J. Research Natl. Bur. Standards 69A, 375 (1965).
10. H. Plumb and G. Cataland, Metrologia 2, 4 (1966).
11. G. Cataland and H.H. Plumb, Meeting of the CCT, 8^{e} Session, (1967), Document 27.
12. D.T. Grimsrud and James H. Werntz, Jr., Phys. Rev. 157, 1 (1967).
13. To be published in a metrological journal in the near future.
14. P.E. Krasnooshkin, Phys. Rev. 65,5, 6 (1944).
15. A.R. Colclough, Acustica 23, 2 (1970).
16. H. Helmholtz, Verhandlungen des Naturhistorisch-medecinischen Vereins zu Heidelberg 3, 16 (1863).
17. G. Kirchhoff, Ann. Phys. Lpz. 134, 177 (1868).
18. M. Thiesen, Ann. Phys. Lpz. 24, 401 (1907).
19. D.E. Weston, Proc. Phys. Soc. B66, 695 (1953).
20. L. Fritche, Acustica 10, 4 (1960).
21. D.H. Smith and R.G. Harlow, Brit. J. Appl. Phys. 14, 102 (1963).
22. R.D. Fay and W.M. Hall, J. Acoust. Soc. Am. 5, 46 (1933).
23. R.D. Fay, J. Acoust. Soc. Am. 15, 32 (1943).
24. J.E. White, J. Acoust. Soc. Am. 18, 155 (1946).

25. R.E. Bedford, M. Durieux, R. Muijlwijk and C.R. Barber, Metrologia, 5, 2 (1969).

26. G. Cataland and H.H. Plumb, Meeting of the Comite Consultat. Thermometrie, 8e session, (1967) Document 27. (Unpublished)

27. R. Muijlwijk, M. Durieux and H. Van Dijk, Physica, 43, 622 (1969).

28. Metrologia, 5, 2 (1969).

29. J.A. Hall, Rapport au Comite International des Poids et Mesures, Meeting of the Comite Consultat. Thermometrie, 8e session (1967).

ADDENDUM

Further measurements have been made at the NBP of helium-4 since this paper was submitted to the Symposium making a present total of 13 isotherm points in all. A definite curvature has become visible above a pressure of about 18 kN/m^2. Fitting a straight line to the lower (linear) part of the isotherm has produced an improved value of 4.2218 K $\pm$ 2.5 mK (standard error). A compatible answer was obtained by fitting a quadratic polynomial to the whole isotherm.

In addition a value of 13.8033 K $\pm$ 1.7 mK (standard error) has been obtained for the triple point of hydrogen. This was obtained from a linear fit to nine isotherm points between 10 and 70 N/m^2.

Very full investigations have now been carried out on the boundary layer effect at 4.2 K, and it has been found to behave exactly as predicted theoretically both qualitatively and quantitatively.

Summarising our best current values we have, therefore,

NBP of Helium-4 = 4.2218 K $\pm$ 2.5 mK (standard error)

Triple Point of Hydrogen = 13.8033 $\pm$ 1.7 mK (standard error)

NBP of Equilibrium Hydrogen = 20.263 $\pm$ 5 mK (standard error)

Further work is to be carried out on these isotherms and so these results are still to be regarded as being preliminary.

SUPPLEMENTARY MATERIAL II.

"Higher Modes in Acoustic Interferometry." A. R. Colclough, Acustica, 23, 93 (1970).

ACUSTICA
S. HIRZEL VERLAG · STUTTGART
Vol. 23 1970 Heft 2

Higher Modes in Acoustic Interferometry

by A. R. COLCLOUGH

National Physical Laboratory, Teddington, Middlesex

Summary

The form of the high order modes in a cylindrical acoustic interferometer is deduced, together with equations relating their amplitudes to the way in which the transducer vibrates. It is then possible to calculate the shape and shift in position of the resonance peaks in the interferometer, and the resulting error in a velocity of sound or absorption coefficient measurement. The theory is illustrated by an analysis of the likely performance of a common type of instrument, and its general bearing on interferometer design is discussed.

Modes plus élevés en interférométrie acoustique

Sommaire

On donne la forme des modes d'ordre élevé dans un interféromètre acoustique cylindrique en même temps que des équations établissant le rapport de leurs amplitudes suivant la façon dont vibre le transducteur. Il est alors possible de calculer la forme et la variation en position des pointes de résonance dans l'interféromètre et l'erreur résultante dans la vitesse du son ou la mesure du coefficient d'absorption. La théorie est illustrée par l'analyse d'une performance vraisemblable d'un type commun d'instrument et on discute son comportement général sur le dispositif interférométrique.

Höhere Moden bei akustischer Interferometrie

Zusammenfassung

Es wurden die Form der Moden höherer Ordnung in einem zylindrischen akustischen Interferometer und Gleichungen für ihre Amplituden, wie sie der Wandler produziert, abgeleitet. Es ist dann möglich, die Gestalt und die Verschiebung der Resonanzpeaks im Interferometer und den sich daraus ergebenden Fehler bei Schallgeschwindigkeits- und Absorptionskoeffizientenmessungen zu berechnen. Die Theorie wird an Hand einer Analyse der wahrscheinlichen Arbeitsweise eines üblichen Instrumententyps dargestellt. Ferner wird ihre allgemeine Bedeutung für die Interferometerkonstruktion diskutiert.

1. Introduction

It is well known that apart from plane wave modes more complicated acoustic modes can be propagated down cylindrical tubes. Each of these higher modes can be shown to have a unique phase velocity which is higher than that of the plane wave mode, and a characteristic cut-off frequency below which it is severely attenuated. Often workers with the acoustic interferometer have used frequencies well above many of these cut-off frequencies, and have observed "satellite" peaks corresponding to resonances of the higher modes (BELL [1]). When unresolved these parasitic resonances can lead to errors in measuring the velocity of sound due to the increased phase velocities of their parent modes. Measured values of absorption coefficients are also too high because of interference between the plane wave resonance peak and those of the higher modes (KRASNOOSHKIN [2], BELL [1]).

The purpose of this paper is to show how the amplitudes of the higher modes may be calculated from a knowledge of the way in which the transducer in the interferometer vibrates. Knowing this, it is possible to predict the shape of the resonance peaks and to assess the error in the positions of their maxima. This theory enables the likely performances of alternative transducer designs to be compared, and might be used to correct experimental results when other methods of dealing with the problem are not applicable.

2. The form of the high order modes

In order to establish the form of the high order modes we follow a method similar to that used by KRASNOOSHKIN [2], except that we shall allow for the angular dependence of the modes as well as for their radial dependence. It is assumed that a velocity potential

$$\Phi'(r, \vartheta, z, t) = \Phi(r, \vartheta, z)\, e^{i\omega t} \qquad (1)$$

exists such that

$$\nabla^2 \Phi(r, \vartheta, z) + a_{00}^2\, \Phi(r, \vartheta, z) = 0 \qquad (2)$$

where $a_{00} = k_{00} - i\alpha_{00}$ is the complex wavenumber for propagation in the unbounded medium at an angular frequency, ω. Thus α_{00} is the free gas absorption coefficient of sound whilst $i = (-1)^{\frac{1}{2}}$.

The relevant boundary conditions for an interferometer of radius b and length l (Fig. 1) are:

$$\left.\frac{\partial \Phi}{\partial z}\right|_{z=0} = 0, \tag{3}$$

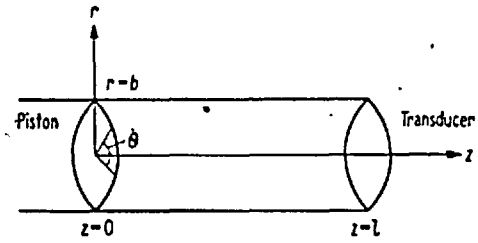

Fig. 1. The acoustic interferometer. The length of the cavity, l, may be changed by moving the piston.

$$\Phi(r, \vartheta, z) = \Phi(r, \vartheta + 2\pi, z), \tag{4}$$

$$\left.\frac{\partial \Phi}{\partial r}\right|_{r=b} = 0, \tag{5}$$

$\Phi(r, \vartheta, z)$ must not be infinite (6)

and

$$\left.\frac{-\partial \Phi'}{\partial z}\right|_{z=l} = \frac{\partial (F(r, \vartheta)\, e^{i\omega t})}{\partial t} \tag{7}$$

where $F(r, \vartheta)$ is the amplitude distribution over the face of the transducer. Using the first four of these boundary conditions and assuming a solution of the form:

$$\Phi(r, \vartheta, z) = R(r)\, \Theta(\vartheta)\, Z(z) \tag{8}$$

for eq. (2), its solution separates to give the following expression for the $m\,n$-th mode:

$$\Phi_{mn}(r, \vartheta, z) = J_m(X_{mn}\, r/b) \times \\ \times (A_{mn} \cos m\,\vartheta + B_{mn} \sin m\,\vartheta) \cos a_{mn}\, z \tag{9}$$

where m, $n = 0, 1, 2, \ldots$ and A_{mn} and B_{mn} are constants determining the amplitude of the $m\,n$-th mode. X_{mn} is the $(n+1)$-th root (always real) of:

$$\left.\frac{dJ_m(X)}{dX}\right|_{X = b(a_{00}^2 - a^2)^{\frac{1}{2}}} = 0 \tag{10}$$

where J_m is a BESSEL function of order m of the first kind and $-a^2$ and $-m^2$ are the respective z and ϑ separation constants of eq. (2). From eq. (10) it can be seen that for every value of X_{mn} there is a unique value of a, a_{mn}, which is to be interpreted as the complex wavenumber of the $m\,n$-th mode. Some values of X_{mn} are given in Table I, and the corresponding values of a a_{mn} are obtainable from:

$$a_{mn}^2 = a_{00}^2 - (X_{mn}/b)^2 \tag{11}$$

whose real and imaginary parts, k_{mn} and $-\alpha_{mn}$ respectively, are given by:

$$k_{mn}^2 = \tfrac{1}{2}(k_{00}^2 - \alpha_{00}^2 - (X_{mn}/b)^2 + ((k_{00}^2 - \\ - \alpha_{00}^2 - (X_{mn}/b)^2)^2 + 4\,\alpha_{00}^2\, k_{00}^2)^{1/2}) \tag{12}$$

Table I.
Values of X_{mn}.

m	n					
	0	1	2	3	4	5
0	0	3.83	7.01	10.17	13.32	16.47
1	1.84	5.33	8.54	11.71		
2	3.05	6.70	9.97	13.17		
3	4.20	8.01	11.37	14.54		

and $$\alpha_{mn} = \alpha_{00}\, k_{00}/k_{mn}. \tag{13}$$

Values of k_{0n} and α_{0n} are plotted in Fig. 2 for a plane wave mode wavelength of 0.1 cm with $\alpha_{00} = 0.1$ and $b = 1$ cm. The phase velocity, v_{mn}, of the $m\,n$-th mode is given by:

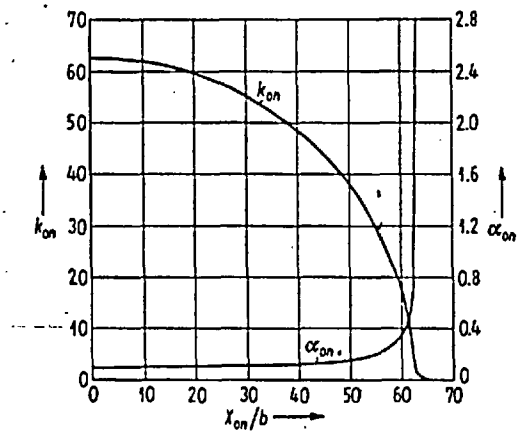

Fig. 2. Variation of k_{0n} and α_{0n} with X_{0n}/b ($\alpha_{00} = 0.1$, $k_{00} = 62.83$).

$$v_{mn} = \omega/k_{mn} = \omega\, \lambda_{mn}/2\pi \tag{14}$$

where λ_{mn} is the wavelength of the $m\,n$-th mode. The cut-off frequency, f_{mn}, of the $m\,n$-th mode is the frequency at which the wavenumber, a_{mn}, would become purely imaginary if $\alpha_{00} = 0$. It is given by:

$$f_{mn} = v_{00}\, X_{mn}/2\pi\, b. \tag{15}$$

3. The general solution and the amplitudes of the high order modes

The general solution of eq. (2) will be a linear superposition of the $m\,n$-th modes. At the face of the transducer it is given by:

$$\Phi(r, \vartheta, l) = \sum_m \sum_n J_m(X_{mn}\, r/b)\, (A_{mn} \cos m\,\vartheta + \\ + B_{mn} \sin m\,\vartheta) \cos a_{mn}\, l. \tag{16}$$

Applying the last boundary condition, eq. (7), we obtain:

$$F(r, \vartheta) = \frac{1}{i\,\omega} \sum_m \sum_n a_{mn}\, J_m(X_{mn}\, r/b)\, (A_{mn} \cos m\,\vartheta + \\ + B_{mn} \sin m\,\vartheta) \sin a_{mn}\, l. \tag{17}$$

On integrating this with respect to ϑ from 0 to 2π it becomes:

$$\int_0^{2\pi} F(r,\vartheta)\,\mathrm{d}\vartheta = \frac{2\pi}{\mathrm{i}\omega}\sum_n a_{0n} J_0(X_{0n} r/b)\, A_{0n} \sin a_{0n} l\,. \tag{18}$$

Now multiplying by $r J_0(X_{0k} r/b)$ where $k=0, 1, 2, \ldots$ and integrating with respect to r from 0 to b we have:

$$\int_0^b \int_0^{2\pi} r J_0(X_{0k} r/b)\, F(r,\vartheta)\,\mathrm{d}r\,\mathrm{d}\vartheta = \tag{19}$$
$$= \frac{2\pi}{\mathrm{i}\omega}\sum_n a_{0n} A_{0n} \sin a_{0n} l \int_0^b r J_0(X_{0k} r/b) J_0(X_{0n} r/b)\,\mathrm{d}r$$

which after applying the following orthogonality relations:

$$I = \int_0^b r J_0(X_{0k} r/b)\, J_0(X_{0n} r/b)\,\mathrm{d}r = 0 \text{ if } n \neq k \tag{20}$$

and

$$I = \int_0^b r J_0^2(X_{0k} r/b)\,\mathrm{d}r = \frac{b^2}{2} J_0^2(X_{0k}) \text{ if } n = k \tag{21}$$

becomes:

$$A_{0n} = \frac{\mathrm{i}\omega}{\pi b^2 a_{0n} J_0^2(X_{0n}) \sin a_{0n} l} \times$$
$$\times \int_0^b \int_0^{2\pi} r J_0(X_{0n} r/b) F(r,\vartheta)\,\mathrm{d}r\,\mathrm{d}\vartheta \tag{22}$$

after rearranging and changing the subscript k to n. The amplitude of the $0n$-th mode is given by $|A_{0n}|$ and, in particular, the amplitude of the plane wave (00-th) mode is given by $|A_{00}|$ for which

$$J_0^2(X_{0n}) = 1\,.$$

In order to find A_{mn} (where it is understood that $m>0$) eq. (17) is multiplied by $\cos j\vartheta$ with $j=0, 1, 2, \ldots$ and integrated with respect to ϑ from 0 to 2π:

$$\int_0^{2\pi} \cos j\vartheta\, F(r,\vartheta)\,\mathrm{d}\vartheta = .$$
$$= \frac{\pi}{\mathrm{i}\omega}\sum_n a_{jn} J_j(X_{jn} r/b)\, A_{jn} \sin a_{jn} l\,. \tag{23}$$

Multiplying eq. (23) by $r J(X_{jk} r/b)$ with $k=0, 1, 2, \ldots$ and integrating with respect to r from 0 to b it becomes:

$$\int_0^b \int_0^{2\pi} r J_j(X_{jk} r/b) \cos j\vartheta\, F(r,\vartheta)\,\mathrm{d}r\,\mathrm{d}\vartheta = \tag{24}$$
$$= \frac{\pi}{\mathrm{i}\omega}\sum_n a_{jn} A_{jn} \sin a_{jn} l \int_0^b r J_j(X_{jk} r/b) J_j(X_{jn} r/b)\,\mathrm{d}r$$

which on applying the following orthogonality relations:

$$K = \int_0^b r J_j(X_{jk} r/b)\, J_j(X_{jn} r/b)\,\mathrm{d}r = 0 \text{ if } n \neq k \tag{25}$$

and

$$K = \int_0^b r J_j^2(X_{jk} r/b)\,\mathrm{d}r = \tag{26}$$
$$= \frac{b^2}{2}(1 - j^2/X_{jk}^2) J_j^2(X_{jk}) \quad \text{if } n = k$$

gives:

$$A_{mn} = \frac{2\,\mathrm{i}\omega}{\pi b^2 a_{mn}(1 - m^2/X_{mn}^2) J_m^2(X_{mn}) \sin a_{mn} l} \times$$
$$\times \int_0^b \int_0^{2\pi} r J_m(X_{mn} r/b) \cos m\vartheta\, F(r,\vartheta)\,\mathrm{d}r\,\mathrm{d}\vartheta \tag{27}$$

after rearranging and changing the subscripts j and k to m and n respectively.

Similarly, it can be shown that:

$$B_{mn} = \frac{2\,\mathrm{i}\omega}{\pi b^2 a_{mn}(1 - m^2/X_{mn}^2) J_m^2(X_{mn}) \sin a_{mn} l} \times$$
$$\times \int_0^b \int_0^{2\pi} r J_m(X_{mn} r/b) \sin m\vartheta\, F(r,\vartheta)\,\mathrm{d}r\,\mathrm{d}\vartheta\,. \tag{28}$$

So that if $F(r,\vartheta)$ is known the amplitude of the mn-th mode may be calculated from

$$|A_{mn} + B_{mn}|\,.$$

From eqs. (16), (22), (27) and (28) it is now possible to write a completely defined expression for the velocity potential at the face of the transducer. In its preferred form it becomes:

$$\Phi(r,\vartheta,l) = \sum_m \sum_n (k_{mn} + \mathrm{i}\,\alpha_{mn})\, J_m(X_{mn} r/b) \times \tag{29}$$
$$\times (C_{mn} \cos m\vartheta + D_{mn} \sin m\vartheta) \coth(\alpha_{mn} + \mathrm{i}\,k_{mn})\, l$$

where

$$C_{0n} = \frac{\omega}{\pi b^2 (k_{0n}^2 + a_{0n}^2) J_0^2(X_{0n})} \times$$
$$\times \int_0^b \int_0^{2\pi} r J_0(X_{0n} r/b)\, F(r,\vartheta)\,\mathrm{d}r\,\mathrm{d}\vartheta\,, \tag{30}$$

$$C_{mn} = \frac{2\,\omega}{\pi b^2 (k_{mn}^2 + a_{mn}^2)(1 - m^2/X_{mn}^2) J_m^2(X_{mn})} \times$$
$$\times \int_0^b \int_0^{2\pi} r J_m(X_{mn} r/b) \cos m\vartheta\, F(r,\vartheta)\,\mathrm{d}r\,\mathrm{d}\vartheta \tag{31}$$

and

$$D_{mn} = \frac{2\,\omega}{\pi b^2 (k_{mn}^2 + a_{mn}^2)(1 - m^2/X_{mn}^2) J_m^2(X_{mn})} \times$$
$$\times \int_0^b \int_0^{2\pi} r J_m(X_{mn} r/b) \sin m\vartheta\, F(r,\vartheta)\,\mathrm{d}r\,\mathrm{d}\vartheta\,. \tag{32}$$

4. The shape of the resonance peaks

Eqs. (29) to (32) enable the shape of the resonance peaks to be determined in terms of the power dissipated in the cavity. The power, $W(l)$,

is given by:

$$W(l) = \int_0^b \int_0^{2\pi} r \,\mathrm{Re}(\dot{\xi}(l))\,\mathrm{Re}(p(l))\,\mathrm{d}r\,\mathrm{d}\vartheta \qquad (33)$$

where $\dot{\xi}(l)$ and $p(l)$ are respectively the particle velocity and the excess pressure at the face of the transducer. From the definition of $F(r,\vartheta)$:

$$\dot{\xi}(l) = \mathrm{i}\,\omega\,F(r,\vartheta)\,\mathrm{e}^{\mathrm{i}\omega t} \qquad (34)$$

so that

$$\mathrm{Re}(\dot{\xi}(l)) = -\omega\,F(r,\vartheta)\sin\omega t. \qquad (35)$$

The pressure at the transducer may be obtained from:

$$p(l) = \varrho\,\frac{\partial}{\partial t}(\Phi(r,\vartheta,l)\,\mathrm{e}^{\mathrm{i}\omega t}) \qquad (36)$$

so that, since $\alpha_{mn} \ll k_{mn}$ for all cases of practical interest,

$$\mathrm{Re}(p(l)) = -\varrho\,\omega \sum_m \sum_n k_{mn} J_m(X_{mn} r/b) \times \times (C_{mn}\cos\vartheta + D_{mn}\sin m\vartheta)\,(P_{mn}(l)\sin\omega t + + Q_{mn}(l)\cos\omega t) \qquad (37)$$

where $P_{mn}(l)$ and $Q_{mn}(l)$ are respectively the real and imaginary parts of $\coth(\alpha_{mn}+\mathrm{i}\,k_{mn})\,l$ given by:

$$P_{mn}(l) = \frac{\sinh 2\alpha_{mn} l}{\cosh 2\alpha_{mn} l - \cos 2 k_{mn} l} \qquad (38)$$

and

$$Q_{mn}(l) = \frac{\sin 2 k_{mn} l}{\cosh 2\alpha_{mn} l - \cos 2 k_{mn} l}. \qquad (39)$$

So, substituting eqs. (35) and (37) in eq. (33) and performing a time average:

$$W(l) = \sum_m \sum_n F_{mn} P_{mn}(l) \qquad (40)$$

where, if α_{mn} is again taken to be small in comparison with k_{mn},

$$F_{mn} = \frac{\varrho\, v_{mn}\,\omega^2}{\pi b^2 (1 - m^2/X_{mn}^2)\, J_m^2(X_{mn})} \times \qquad (41)$$

$$\times \left(\left(\int_0^b \int_0^{2\pi} r J_m(X_{mn} r/b) \cos m\vartheta\, F(r,\vartheta)\,\mathrm{d}r\,\mathrm{d}\vartheta \right)^2 + + \left(\int_0^b \int_0^{2\pi} r J_m(X_{mn} r/b) \sin m\vartheta\, F(r,\vartheta)\,\mathrm{d}r\,\mathrm{d}\vartheta \right)^2 \right)$$

when $m > 0$, and

$$F_{0n} = \tfrac{1}{2} F_{mn} \text{ as defined above when } m = 0. \qquad (42)$$

In order to illustrate the use of eqs. (40) to (42), the peak shapes for an ideal transducer executing perfect piston-like vibrations will be derived and compared with those produced by a stiff diaphragm driven, say, by a moving coil. Often transducers of the latter type have a diameter larger than that of the cavity in order to approximate to the ideal by diminishing the curvature of the diaphragm at the extreme positions of its vibration.

For the ideal case we put:

$$F(r,\vartheta) = \xi_0$$

where ξ_0 is a constant. All the amplitudes, F_{mn}, for which $m > 0$ are zero since the ϑ integrals of eq. (42) vanish. Similarly F_{0n} is zero when $n > 0$ because of the r integral in eq. (41). So, as would be expected, only the plane wave amplitude, F_{00}, is finite. In units of $\pi\varrho\,\omega^3\,\xi_0^2 b^2/2 k_{00}$ it is given by:

$$F_{00} = 1. \qquad (44)$$

The peak shapes for this case are shown in Fig. 3 where α_{00} has been taken to be 0.1. Since no high order modes have been excited the peak maxima always fall on a position for which $l = s\,\lambda_{00}/2$ where $s = 0, 1, 2, \ldots$.

To approximate to the amplitude distribution of the stiff diaphragm we choose:

$$F(r,\vartheta) = \xi_0\,\mathrm{e}^{-r^4/(a^4-r^4)} \quad \text{for} \quad 0 \leqq r \leqq a \qquad (45)$$

where a is the radius of the diaphragm. This ensures that $F(r,\vartheta)$ is zero at the edge of the diaphragm where it is clamped and that $\partial F(r,\vartheta)/\partial r|_{r=a}$ is also zero to allow for the stiffness of the diaphragm. In order to consider how the performance of the instrument is affected by changing the diameter of the diaphragm, peak shapes will be calculated for

$$a/b = 1 \quad \text{and} \quad a/b = 4.$$

The two cases are shown in Fig. 4.

For the same reason that was given in the ideal case, F_{mn} vanishes when $m > 0$. But now the ampli-

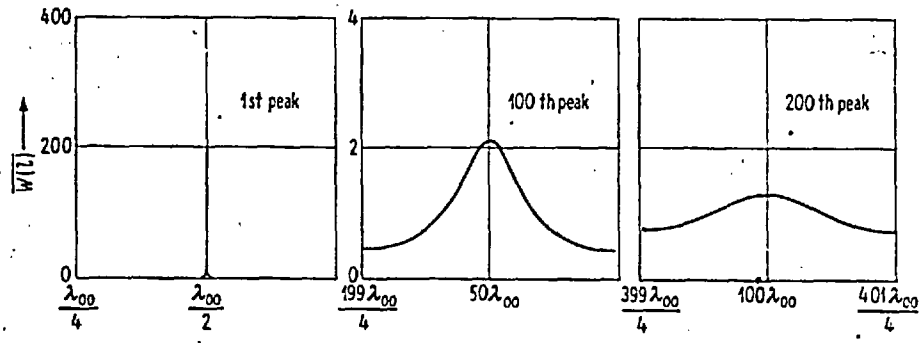

Fig. 3. Peak profiles for ideal transducer.

ACUSTICA
Vol. 23 (1970)

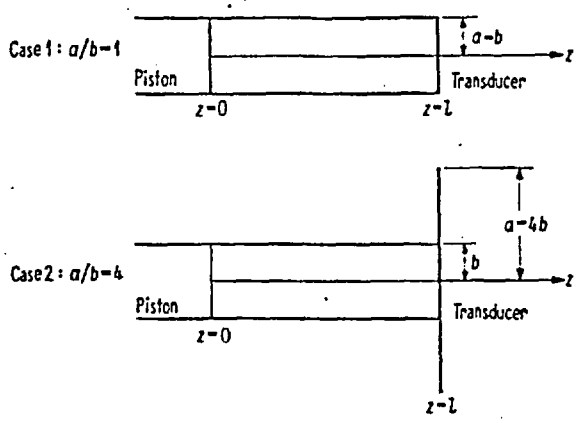

Fig. 4. The interferometers are shown with small and large diaphragms. The latter may be expected to approximate to the ideal.

Table II.
Amplitudes of the $0n$ th modes for a stiff diaphragm.

n	a/b	F_{0n}
0	4	5.752
1	4	0.002
2	4	0.000
3	4	0.000
4	4	0.000
5	4	0.000
0	1	1.000
1	1	0.658
2	1	0.043
3	1	0.02
4	1	0.000
5	1	0.000

tudes, F_{0n}, are no longer generally zero as may be seen from Table II where they are expressed in units of F_{00} when $a=b$. The resulting peak shapes are shown in Figs. 5 and 6 for cases 1 and 2 respectively. It can be seen that the case where $a/b=4$ approximates so well to the ideal case that there is no discernible difference in the peak shapes (the change in scale merely reflecting the change in units). The case for which $a/b=1$, however, has two parasitic modes, the 01-th and the 02-th, which cause severe distortion of the peaks. A marked asymmetry can be seen by the 100-th peak and by the 200-th peak the 01-th mode is virtually resolved. In practice, though, it is unlikely that a transducer could be made which would be sensitive enough to respond to these distortions so that the presence of the higher modes might go unsuspected. This would result in an error of several parts in 10 000 in a velocity of sound measurement and about 7% in α_{00}.

In the cases considered there has been no ϑ dependence in the amplitude of vibration of the transducer. Consequently F_{mn} has always vanished when $m>0$. But were this not the case the peaks could be further complicated by the presence of m-th modes. Furthermore, the functions chosen for $F(r,\vartheta)$ have been concisely expressible, whereas in practice it may well have to be expanded as a series of orthogonal functions of r and ϑ (preferably the mn-th modes).

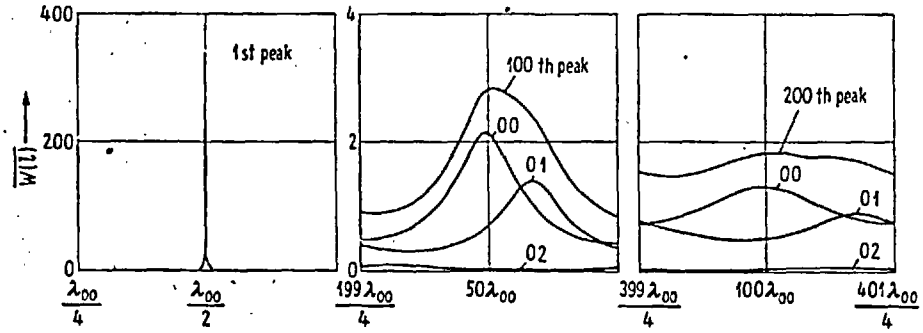

Fig. 5. Peak profiles for $a/b=1$.

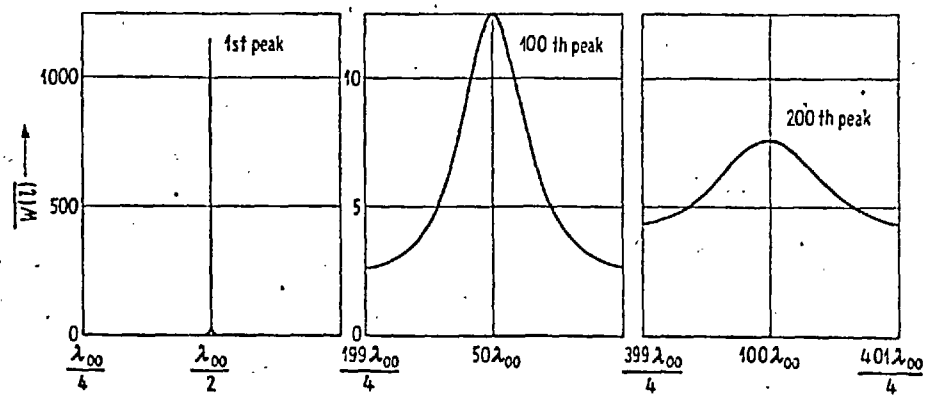

Fig. 6. Peak profiles for $a/b=4$.

5. Higher modes and interferometer design

It is clear from the last example that if accurate acoustic measurements are to be made, it is necessary to know what effect high order modes are having on the performance of one's instrument.

Of several ways of dealing with the problem, the simplest and most effective is to work below the cut-off frequency of the 01-th mode. Since only the plane wave mode can then be propagated it will be certain that all resonances are pure plane wave resonances. This is a satisfactory method if velocities alone are to be measured. But, in order to examine enough peaks to enable absorption coefficients to be measured, a very long interferometer might be required. A sufficient number of peaks must be traversed to enable a measurable decrease in their height to be observed. So quite apart from the increase in wavelength brought about by operating at low frequencies, allowance must be made for the diminished rate of decrease in peak height brought about by the dependence of α_{00} on the square of the frequency. Thus at low frequencies there are two factor working to increase the length of the cavity required. And as a consequence problems of temperature uniformity in the tube and mechanical alignment of the transducer and piston may become troublesome.

Secondly an attempt could be made to detect the presence of unwanted modes by using an intermediate frequency and a cavity of sufficient length to resolve a significant 01-th mode resonance (and therefore any other significant resonance). But, apart from any problems of temperature uniformity and mechanical alignment which might arise, there remains the problem of designing a sufficiently sensitive transducer capable of responding to deformities in the smallest peaks. In practice this is likely to require the use of a quartz crystal since other electromechanical devices, even when driven on resonance, have too large an impedance compared to the small changes in gas impedance which are to be measured.

Thirdly, a measurement might be made of $F(r, \vartheta)$ with a view to applying the preceding theory to correct the positions and heights of the resonance peaks. Such a measurement would have to be done in situ if it was to be of any value since transducers tend to be sensitive to the smallest changes in their immediate environment. This would almost certainly involve an optical experiment on the transducer so that its amplitude of vibration would have to be large compared to the wavelength of light. The amplitude would be limited by the maximum tolerable power input to the cavity. But, since the power radiated into the cavity is proportional to the squares of the amplitude and frequency of the transducer, this implies a maximum frequency for any given amplitude. For some interferometers it might be the case that, in order to obtain a measurable amplitude of vibration, the driving frequency of the transducer would have to be lowered to a value which again introduces problems in the measurement of absorption coefficients.

There is also another problem associated with the precise application of the preceding theory arising out of the "tube effect". When measured in tubes, velocities are found to be less than the free gas velocities of sound at the same frequency, and absorption coefficients are in excess of their free gas values too. This arises out of wall effects due to the viscosity of the gas and the relatively high thermal conductivity of the walls of the cavity. Unfortunately to try and take them into account from first principles produces a mathematically intractable problem, but there do exist corrections to allow for them. The corrections, given by the KIRCHHOFF-HELMHOLTZ equations, are fully discussed in a paper by WESTON [3], but it suffices to say here that they are large at low frequencies and in cavities of small bore, and small at high frequencies and in cavities of large bore. The difficulty arises because they are only relevant to the plane wave mode, so that it is not possible to tell exactly to what extent the phase velocities of the higher modes are altered by wall effects. It may be supposed, however, that the tube effect becomes increasingly unimportant for all modes as frequency and cavity bore increase, so the preceding theory may be expected to apply under these conditions. And, even at low frequencies, an optical experiment could provide useful confirmation that a well designed transducer was approximating to the ideal in which case the question of the phase velocities of the higher modes would not arise.

A more practical solution to the problem would seem to be to design a transducer which, according to the above theory, would be unlikely to excite unwanted modes and then to operate it below the first cut-off frequency. If it is then necessary to observe a larger number of peaks (to measure absorption coefficients) the frequency may be increased and a check made that velocities measured at the new frequency are compatible with those measured below the first cut-off frequency. This procedure should be quite satisfactory so long as all measurements are carried out at low enough frequencies to avoid problems associated with velocity dispersion.

Acknowledgements

The author would like to thank Dr. R. W. B. STEPHENS of Imperial College, University of London,

Dr. T. J. QUINN and Mr. A. J. BURTON both of the National Physical Laboratory for their assistance in the preparation of this paper, which relates to work carried out as part of the research programme of the National Physical Laboratory.

(Received September 5th, 1969.)

References

[1] BELL, J. F. W., Proc. Phys. Soc. B 63 [1950], 958.
[2] KRASNOOSHKIN, P. E., Phys. Rev. 65 [1944], 190.
[3] WESTON, D. E., Proc. Phys. Soc. B 66 [1953], 695.

ACKNOWLEDGEMENTS

The author would like to express his gratitude to all those at NPL and Imperial College who have made this mutual collaboration possible both by giving their permission for it to take place, and by generous material help.

Special thanks are also due to my supervisor, Dr. R.W.B. Stephens, of Imperial College and to Dr. T.J. Quinn of NPL. Dr. Stephens has given us his constant help and advice from the beginning notwithstanding our somewhat remote location at NPL, whilst Dr. Quinn's experience and understanding of the American work has enabled us to see the general problems of the technique much more clearly than we otherwise would. Credit for the inception of this project must go, of course, to the late C.R. Barber who was my director of studies at the NPL until his untimely death last Summer.

NOTATIONAL GLOSSARY

a p21; a figs.2.6 and 2.7; a pp125,136; $\underline{a}$ p87; a p91;

$\underline{A}^n$ pp46,84; area of transducer face; $\underline{A}^n$ p88; A' p85; A_{mn} p50; A_{n} p101; A_0, A_1, A_2, A'_0, ... acoustic virial coeffts. pp15,16;

b p21; b fig. 2.1; b pp125,135; b p91;

B_n, B' virial coeffts. p19; B_S adiabtc. blk. modls.; B_T isothl. blk. modls.; B_{mn} p50; B_n p102;

c velocity of sound; c_p, c_v principal specfc. hts./unit mass; c_{mn} p50; C_p, C_v principal specfc. hts./mole; C_n p102;

d p22;

D p102;

e p22;

f frequency;

F p111;

G subscript signifying gas in cavity; G_n p150; G_k p104;

i imaginary unit;

J Bessel function of first kind;

k wavenumber;

K thermal conductivity; modified Bessel function of second kind;

l length of acoustic cavity;

m subscript for mnth mode ($-m^2$ is separation const. for azimuthal variable p45);

M molecular weight;

n subscript for mnth mode (see equn. 2.2.19); n number of moles;

N order of resonance;

p acoustic (excess) pressure;

P pressure;

q complex wavenumber of mnth mode ($-q^2$ is axial separation constant q_{mn} p45); q_v, q_t p92; q_{1n} p101; q_{2n}, q_{3n} p102;

r radial cyl. coord.;

R gas const., resistance or real refln. coefft., p44;

t p126;

T thdc. temp., subscript signifying transducer;

$\underline{v}$ particle velocity;

$\overline{V}$ voltage; $\underline{V}$ p88;

W power; $\underline{W}$ heat flux;

x Cartesian coord.;

X reactance; X_n p101; X_{mn} p47;

y Cartesian coord.;
Y Bessel function of second kind; Y_n p102;

z Cartesian or axial cyl. coord.; z_R, z_T p74;

Z p44; Z_n p102;

α absorption coefft./unit length
β p124;
γ complex acoustic refln. coefft.;
δ Kronecker δ ; p110;
Δ_{mn} half width of mnth resonance;
ε p77;

ζ bulk viscosity;
η , η_1 layer viscosity; η_2 pp86,87;
θ azimuthal cyl. coord.; p79;
Θ p44,89;
λ acoustic wavelength;
μ refractive index;
ν , ν_1 kinematic layer viscosity; ν_2 p88; ν_3 thermal diffusivity, p89;
ξ particle displacement;
ρ density;
σ ratio of principal specfc. hts., c_p/c_v ;
φ velocity potential;
Φ p51;
χ p79;
Ψ p91;
ω angular frequency;